INSTITUT POLYTECHNIQUE DE PARIS

ÉCOLE POLYTECHNIQUE

IP PARIS

Thèse de doctorat

From spectra to total energy: beyond the GW approximation designing effective interactions

Thèse de doctorat de l'Institut Polytechnique de Paris
préparée à École Polytechnique

École doctorale n°626 École doctorale de l'Institut Polytechnique de Paris (EDIPP)
Spécialité de doctorat : Physique

Thèse présentée et soutenue à Palaiseau, le 26/01/2024, par

ABDALLAH EL SAHILI

Composition du Jury :

Fabien Bruneval
Directeur de recherche CEA, Université Paris–Saclay, CEA-Saclay   Président

Pina Romaniello
Directrice de recherche, (UMR 5152) Université Paul Sabatier,
Toulouse.   Rapporteure

Mark Van Schilfgaarde
Professeur, National Renewable Energy Laboratory, Golden CO
(USA)   Rapporteur

Roberta Poloni
Chargée de recherche CNRS, (UMR 5266) Université Grenoble
Alpes   Examinatrice

Fabio Caruso
Professeur, Christian-Albrechts-Universität zu Kiel (Germany)   Examinateur

Lucia Reining
Directrice de recherche CNRS, (UMR 7642) École Polytechnique,
Palaiseau   Directrice de thèse

Francesco Sottile
Ingénieur de recherche, (UMR 7642) École Polytechnique, Palaiseau   Co-directeur de thèse

Contents

Acknowledgments

I want to express my gratitude to those who stood by me throughout my thesis.

First, I would like to extend my sincere gratitude to my exceptional supervisors, Lucia Reining and Francesco Sottile. Their kindness and support throughout this journey have been invaluable. Under their guidance, I never felt like a student, but rather a valued colleague collaborating with them. I am deeply thankful for the trust and confidence they placed in me. In addition to their professionalism, they were incredibly approachable on a personal level. Whenever I encountered any difficulties, they were always available and willing to help.

Second, I want to thank Michèle Raynaud, the director of the Laboratoire des Solides Irradiés, as well as Elodie Dubois and Marylène Raclot for their invaluable assistance with administrative matters. I extend my thanks to Andrea Cucca for consistently offering support with technical issues. I am grateful to all the permanent members of the LSI for their contributions. Additionally, I appreciate the pleasant and amicable relationships I have developed with the non-permanent members.

Third, I want to thank the members of the jury, Fabien Bruneval, Pina Romaniello, Mark Van Schilfgaarde, Roberta Poloni, and Fabio Caruso for having accepted to examine my manuscript and my defense. I acknowledge the fruitful discussions with Steffen Backes, Fabien Bruneval, Kieron Burke, and Steven Crisostomo.

Finally, I would like to express my heartfelt gratitude to my family, who have been my unwavering support system throughout this journey. A special thank you goes to my beloved partner, Yara, who traveled all the way from Lebanon to stand by my side during my defense and for being always an essential source of motivation in my life.

Preface

In recent years, significant progress in research has elevated our understanding of condensed matter to unprecedented levels, leading to a new era with more advanced technology. With the rich diversity of chemical elements and their combinations, technological advancements have been made thanks to the comprehension and research in various domains, including physics, materials science, and chemistry. Electronic structure, a crucial field in this continuum, has witnessed a surge in publications, underscoring its significant impact. Many theories have been proposed and rigorously examined within the electronic structure field, translated into practical calculations through computer codes that are now indispensable.

This thesis delves into a specific part within electronic structure, aiming to enhance total energy calculations for the electronic ground-state using Green's functions. While Green's functions approaches are commonly favored for band structure calculations, with a certain number of approximations, density-functional theory is often thought to be designed for exploring the ground-state properties of interacting-electron systems. However, the ignorance of functionals in terms of the density poses a challenge for density-functional theory. Hence, investigations concerning the ground-state total energy using Green's functions become crucial, offering a more direct, or at least alternative, route for development compared to density-functional theory. Recognizing the potential synergy between these two approaches, it is also promising to search for combinations toward a unified pursuit of the same observable, which is the ground-state total energy. In this thesis, we start with a motivating introduction that highlights the importance of the total energy calculations. We then provide a foundational overview of mean field, density-functional and many-body Green's function theories in the theoretical background part, offering an introduction to the subject. In the theoretical developments part, various methods aimed at improving ground-state total energy calculations beyond the state-of-the-art are proposed, discussed, and investigated. For illustrations, we use the symmetric Hubbard dimer model.

In presenting this thesis, we aspire to contribute, albeit modestly, to the vast realm of research.

Notation

Coordinates, orbitals and operators

r	electron position
σ	electron spin projection
x	combined space/spin coordinates (r,σ)
1	combined space/spin/time coordinates (x_1, t_1)
$\hat{c}, \hat{c}^\dagger$	annihilation and creation operators for fermions
$\hat{\Psi}, \hat{\Psi}^\dagger$	field operators for fermions
$\phi_{i\sigma}(x) = \varphi_{i\sigma}(r)\chi_\sigma(s)$	single-particle "spin orbital"

Most used acronyms

HF	Hartree-Fock
DFT	density functional theory
TDDFT	time-dependent density functional theory
HK	Hohenberg-Kohn
KS	Kohn-Sham
LDA	local density approximation
GGA	generalized gradient approximation
ALDA	adiabatic local density approximation
MBPT	many-body perturbation theory
GWA	GW approximation
RPA	random phase approximation
QP	quasi-particle
xc	exchange-correlation
GM	Galitskii-Migdal
TCTC	test-charge test-charge
TCTE	test-charge test-electron
LDE	linearized dyson equation
AC	adiabatic connection
HOMO	highest occupied molecular orbital
LUMO	lowest unoccupied molecular orbital
SCD	self-consistency diagram

General physical quantities

$\hat{H}$ many-body hamiltonian

Ψ many-body wavefunction

Φ_{H} Hartree wavefunction

Φ_{HF} Hartree-Fock wavefunction

E_0 ground-state total energy

v_{c} bare Coulomb interaction

v_{ext} external potential

v_{H} Hartree potential

n one-body density

E_{HF} Hartree-Fock total energy

E_{H} Hartree energy

E_{x} exchange energy

v_{x} exchange potential

E_{KS} Kohn-Sham total energy

E_{xc} exchange-correlation energy

v_{KS} Kohn-Sham potential

v_{xc} exchange-correlation potential

f_{xc} exchange-correlation kernel

1-GF   one-body Green's function

γ one-body density matrix

A spectral function

2-GF   two-body Green's function

3-GF   three-body Green's function

G_0 non-interacting 1-GF

G_{H} Hartree 1-GF

Σ_{xc} exchange-correlation self-energy

v_{cl} total classical potential: Hartree + external potentials

W test-charge test-charge screened Coulomb interaction

χ reducible polarizability

L four-point reducible polarizability

P irreducible polarizability

P_0 non-interacting irreducible polarizability

χ_0 non-interacting reducible polarizability, equal to P_0 when the same framework is used

$\tilde{\Gamma}$ irreducible vertex function

$\tilde{W}$ test-charge test-electron screened Coulomb interaction

$v_{\mathrm{eff}}, \bar{v}$ effective potential

W_{eff} effective Coulomb interaction making the first-order self-energy exact

$\bar{W}$ effective screened Coulomb interaction

Introduction

Interacting particles

The world around us consists of interacting many-particle systems, making it essential to comprehend these systems in order to understand the nature of our reality, and therefore transforming this understanding into beneficial applications for a better life. This necessity has led to the division of human efforts into various disciplines, including physics and chemistry, which are further subdivided into specialized fields. For example, material science includes areas such as atomic, molecular, condensed matter, and nuclear physics, all of which attempt to describe the diverse behaviors of these systems. These studies, which have been made throughout human history, are directly linked to the technological advancements that shape our modern lives. In particular, the comprehension of interacting electrons systems, which is the focus of this thesis, holds significant importance for our daily lives. It underlies numerous practical applications and meets essential needs for individuals and communities around the world. Electrons are governed by "quantum physics", which was developed in the early

Figure I: Our earth from outside. This is to illustrate that everything is built with interacting many-particle systems. This photo is taken from Pixabay.

20th century to describe the behavior of particles at the atomic and subatomic scales. Its birth is often attributed to some key contributors, but its development was a collaborative effort involving many scientists over more than two decades. The literature is full of descriptions of the birth of quantum mechanics, from different points of view. A nice historical one is the compendium book on the Solvay 1927 Conference [1], that is also available on arXiv [2].

The electronic structure problem

To understand the behavior of electrons in many-body interacting systems, it is necessary to delve into the quantum level. From a theoretical perspective, this can in principle be accomplished by solving the Schrödinger equation, which is the fundamental equation in quantum mechanics governing the evolution of the system's wavefunction.

$$\hat{H} \left| \Psi(t) \right\rangle = i\hbar \frac{\partial}{\partial t} \left| \Psi(t) \right\rangle , \tag{1}$$

where $\Psi(r_1\sigma_1, r_2\sigma_2, ..., r_N\sigma_N, t)$ is the many-body wavefunction. It contains all the electronic information about the system and describes the distribution of electrons in space r, spin σ and time t. The electronic hamiltonian operator, denoted as $\hat{H}$, *already includes the Born-Oppenheimer (adiabatic) approximation*[3]. This approximation assumes that the motion of atomic nuclei is much slower compared to the motion of electrons, allowing for the separation of electronic and nuclear degrees of freedom. The electronic hamiltonian is written as follows,

$$\hat{H} = \underbrace{-\frac{\hbar^2}{2m_e} \sum_i \nabla_i^2}_{\hat{T}} \underbrace{- \sum_{i,I} \frac{Z_I e^2}{|r_i - R_I|}}_{\hat{V}_{\text{ext}}} + \underbrace{\frac{1}{2} \sum_{i \neq j} \frac{e^2}{|r_i - r_j|}}_{\hat{V}_{\text{ee}}} , \tag{2}$$

where electrons are denoted by lowercase subscripts and coordinates r_i and nuclei are denoted by uppercase subscripts and coordinates R_I. $\hat{T}$, $\hat{V}_{\text{ext}}$ and $\hat{V}_{\text{ee}}$ are the kinetic energy of electrons, electron-nuclei interaction and electron-electron interaction, respectively. In this thesis, we will use atomic units defined such that $\hbar = m_e = e = 4\pi/\epsilon_0 = 1$.

The Coulomb interaction V_{ee} indeed introduces significant complexity into the problem. Due to V_{ee}, Ψ can not be factorized into independent single-particle wavefunctions. As a result, the dimensionality of Ψ becomes immense and grows exponentially with the number of electrons in the system [4]. Therefore, the computation of the many-body wavefunction Ψ is restricted to systems with a small number of electrons, as storing and manipulating Ψ becomes impractical for larger systems. Additionally, since Ψ contains an immense amount of informations, it is often not necessary to explicitly calculate Ψ itself. Instead, the focus is on obtaining observables of interest from Ψ. Given these considerations, it becomes clear that exploring alternative approaches to solve the many-body problem is essential. Various theories that do not rely on Ψ to solve the many-body problem will be discussed later.

Why the ground-state total energy?

In this thesis, our main interest concerns the calculation of the ground-state total energy, which is the lowest energy E_0 of the static Schrödinger equation $\hat{H}\Psi = E\Psi$. But why we are interested in the total energy, and in general what practical applications does it have?

In nature, interacting particle systems tend to adopt configurations that minimize their energies, a principle governed by the laws of physics. This is beautifully exemplified by a water droplet on a surface, illustrated by the left-hand panel of Fig. II, which assumes an almost spherical shape. This

Figure II: These figures are presented to illustrate the energy minimization concept in nature. They are taken from Pixabay. Left-panel: the spherical form of a water droplet minimizes the energy in play (in this case, surface tension). Right-panel: the lake is created such that it minimizes the potential energy.

spherical form is the configuration that minimizes energy, and in this case the only "free" force field is the surface tension that tends to minimize the surface. The same holds for the lakes in the right-hand panel of Fig. II, where the lake is formed such that the water distribution minimizes the potential energy. *Thus, the concept of energy minimization provided by nature serves as a main motivation for our research.* For instance, total energy calculations are commonly employed in many domains of science, ranging from chemistry (predict chemical reaction or catalysis pathways) to biology (protein-ligand interaction, drug binding affinities), from environmental science (interaction pollutant-substances) to astrophysics (stellar formation, matter in extreme conditions). Very often in material science, and not surprisingly also in this thesis, the main use of the minimization principle is to study the existence and stability of a system, as a function of the atomic position of its constituents. Since nature presents a rich availability of chemical elements organized in a well-known periodic table, where each element is characterized by a specific electronic configuration, it is crucial to understand these elements and their combinations. For instance, hydrogen and oxygen naturally do not exist in isolation, but they are available as H_2 and O_2 molecules. This is due to the fact that the energy cost of forming chemical bonds is less than the energy required for dissociation. This phenomenon can be understood from the perspective of electronic configurations, for example, a hydrogen atom, with its single electron, tends to form a doubly occupied bond with another hydrogen atom for stability.

In practice, determining the existence of a chemical system, which is an interacting particle system, in the form A_xB_y involves examining the total energy as a function of the distance between the atoms. If a minimum is observed over a range of distances, from close proximity between atoms to dissociation, it implies the stability and existence of the chemical system. This is illustrated by the left-hand panel of Fig. III, where the hydrogen molecule exhibits a minimum, indicating the existence of the H_2 system. Therefore, the left-hand panel of Fig. III illustrates the interest of total energy calculations.

The search as a function of the distance is not the only strategy. In order to make a connection

with the present thesis work, we show in the right panel of Fig. III the ground-state total energy of the symmetric Hubbard dimer (for more details about this model see Chap. 6) as a function of the hopping parameter t, which plays the role of the interatomic distance. Here, $t \to 0$ represents the dissociation limit and $t \to \infty$ represents the very short distance between the two atoms. We are using this exactly solvable model as a model system for our theoretical investigations.

Besides the question of the existence of a system using, total energy calculations can also determine details of geometry. For example, a water molecule H_2O has its specific geometry with 104.5 degrees as an angle for $H - O - H$. This is also defined by the total energy minimization concept.

In summary, any stochiometric combination, existence and geometrical structure of a system can in principle be investigated by total energy calculations.
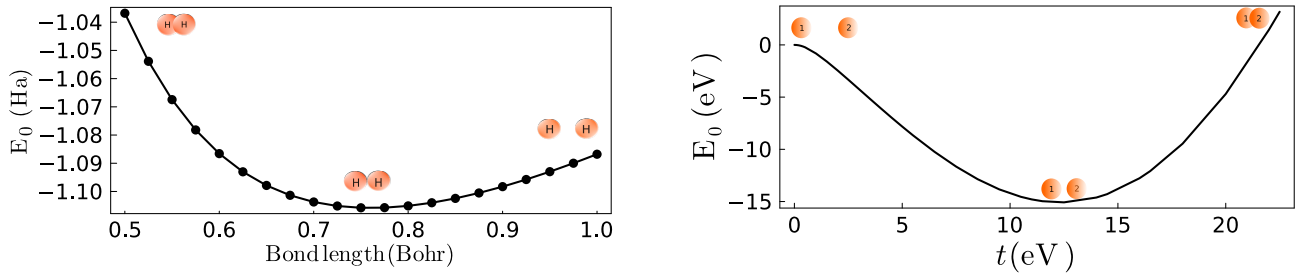
Figure III: Left panel: ground-state total energy E_0 of the hydrogen molecule as a function of the bond length. This result has been obtained using abinit [5, 6] within the density-functional theory formalism [7], where the exchange-correlation potential is approximated within the local-density approximation [8]. Right panel: ground-state total energy of the symmetric Hubbard dimer at half-filling as a function of the hopping parameter t, where the Coulomb interaction $U = 4$ eV. 1 and 2 refer to the first and second atom, respectively.

This thesis involves theoretical developments aimed at devising novel approaches to evaluate the ground-state total energy of a quantum many-body system of electrons. Calculations of total energies can, in principle, be addressed by solving the Schrödinger equation using the hamiltonian Eq.(2), and various quantum chemistry methods are available for this purpose [9]. Among the numerous approaches, some employ expansions of the many-body wavefunction in terms of Slater determinants built with one-particle wavefunctions (such as configuration interaction and coupled cluster [9]), while others rely on stochastic approaches to handle the multi-dimensional integrals involved (such as quantum monte carlo [10]). However, these methods suffer from unfavorable scaling and are typically applicable to systems with only a few electrons. Total energy calculations for real and complex materials are commonly performed within the framework of Density Functional Theory (DFT) [7, 11–13], which stands out as one of the most successful and widely used methods in physics [14]. This success arises from the good results achievable with very simple approximations. The time-dependent extension of DFT (TDDFT) can be also used, to evaluate total energies, via the use of the adiabatic connection fluctuation dissipation theorem [15–23]. Nevertheless, the drawback of the density functional approach lies in the challenge of systematically improving the approximations to yield more accurate results. Green's functions (GF) methods represent an intermediate approach, standing between the

complexity and reliability of wavefunction based methods and the ease and cost-effectiveness of DFT. The GF framework is recognized as state-of-the-art concerning spectral quantities related to various electronic excitation experiments, such as photoemission, absorption, or scattering spectroscopy. It usually operates on the premise of the self-energy concept, which constitutes a non-local, energy-dependent effective potential governing the behavior of (quasi) electrons. Developing approximations for the self-energy stands as the primary and most arduous task within this framework. The most widely used approximation is probably the GW approximation within many-body perturbation theory (MBPT) [24–26], so called because it formulates the self-energy as a product of a Green's function G times the screened Coulomb interaction W. This approximation has proven highly successful for the calculation of the quasi-particle (QP) part of electron addition and removal spectra in finite and extended systems [4, 26–33]. In addition, the functional derivative of GW yields an effective interaction kernel utilized in an equation known as the Bethe-Salpeter equation [34–39]. The solution of this equation gives us, among other quantities, the dielectric function, resulting in outstanding predictions for absorption spectra across a broad spectrum of materials [40–50]. However, while successful for spectra and band-gap for weakly to moderately correlated systems, the GW approximation often falls short in accurately predicting total energies [51–53]. Therefore, the primary goal of this thesis is to devise strategies to go beyond the GW approximation and systematically improve the results for the total energy calculation, within the framework of GF and MBPT.

By using the exactly solvable symmetric Hubbard dimer [54–58] as a reference tool and benchmark, our research has led to the development of three distinct strategies. Each strategy possesses its unique advantages and challenges, yet all of them enable both qualitative and quantitative enhancements beyond the limitations of the GW approximation. In the first strategy, we utilize linear response quantities to represent the exact total energy using a self-energy constructed from density-functional components [59–70]. We provide a computer code to illustrate and test this strategy, called "Symmetric Hubbard Dimer", it is available at the following address: https://gitlab.com/tsg1860938/symmetric-hubbard-dimer. The second strategy introduces an effective screened Coulomb interaction, denoted as W_{eff}, in a formula akin to GW but ensuring an exact exchange-correlation self-energy (Σ_{xc}). Notably, the approximations within this formulation ($\Sigma_{\text{xc}} = iGW_{\text{eff}}$) demonstrate significant improvements compared to the original GW approximation. Lastly, the third strategy involves expanding the self-energy to second order in W [71–81], where various interesting questions are discussed. All these strategies offer promising avenues for achieving improved accuracy in spectral features and total energy calculations of electronic system.

Part I

Theoretical Background

Chapter 1

Mean field theories

The many-body problem is an exponentially hard problem. Several strategies tackle this problem. Very often these strategies depend on the community working on it: quantum chemists, solid-state or nucler physicists. Here, we begin with the mean field approach, which will be used as a starting point for our strategy, based on many-body Green's functions.

1.1   Hartree approximation

The numerical solution to the Schrödinger equation was initially introduced by Douglas Hartree in 1928 [82, 83]. Hartree proposed an ansatz, known as the Hartree ansatz, which assumes that the total many-body wavefunction can be approximated as a simple product of single-particle orbitals:

$$\Phi_{\mathrm{H}}(r_1, r_2..., r_N) = \varphi_1(r_1).....\varphi_N(r_N) \,, \tag{1.1}$$

where $\varphi_i(r)$ is the single-particle orbital, with $r = (x, y, z)$ a 3-d vector and spin is neglected for the moment. The expectation value of the hamiltonian Eq.(2) using Φ_{H} is

$$\langle \Phi_{\mathrm{H}} | \hat{H} | \Phi_{\mathrm{H}} \rangle \tag{1.2}$$

$$= \langle \Phi_{\mathrm{H}} | \hat{T} + \hat{V}_{\mathrm{ext}} | \Phi_{\mathrm{H}} \rangle + \langle \Phi_{\mathrm{H}} | \hat{V}_{\mathrm{ee}} | \Phi_{\mathrm{H}} \rangle \tag{1.3}$$

$$= \sum_i \langle \varphi_i(r) | - \frac{\nabla_r^2}{2} + v_{\mathrm{ext}}(r) | \varphi_i(r) \rangle + \frac{1}{2} \sum_{i \neq j} \langle \varphi_i(r) \varphi_j(r') | v_{\mathrm{c}}(r, r') | \varphi_i(r) \varphi_j(r') \rangle \tag{1.4}$$

$$= \sum_i \int dr \, \varphi_i^*(r) \left[- \frac{\nabla_r^2}{2} + v_{\mathrm{ext}}(r) \right] \varphi_i(r) + \frac{1}{2} \sum_{i \neq j} \int dr dr' \, \varphi_i^*(r) \varphi_j^*(r') v_{\mathrm{c}}(r, r') \varphi_i(r) \varphi_j(r') \,, \tag{1.5}$$

where $v_{\mathrm{c}}(r, r') = \frac{1}{|r - r'|}$. To derive the Hartree equations, we utilize the concept of *total energy minimization* with respect to the single-particle orbitals. One approach is to employ the Lagrange multipliers method and the variational principle:

$$\frac{\delta}{\delta \varphi_i^*(r)} \left[\langle \Phi_{\mathrm{H}} | \hat{H} | \Phi_{\mathrm{H}} \rangle - \sum_j \epsilon_j \int dr' \, \varphi_j^*(r') \varphi_j(r') \right] = 0 \,, \tag{1.6}$$

where the Lagrangian multipliers ϵ_i in Eq.(1.6) arise from the constraint that the single-particle orbitals are normalized, *i.e*, $\int dr \varphi_j^*(r) \varphi_j(r) = 1$. This leads to the Hartree equations,

$$\left(-\frac{\nabla_r^2}{2} + v_{\text{ext}}(r) \right)\varphi_i(r) + \sum_{j,j\neq i} \int dr'\, \varphi_j^*(r')\varphi_j(r')v_{\text{c}}(r,r')\varphi_i(r) = \epsilon_i\varphi_i(r)\,, \qquad (1.7)$$

where i, j run over occupied orbitals, i.e, orbitals contained in the product Eq.(1.1). As a conclusion, in the Hartree approach, each electron, labeled by the quantum number i, interacts with the mean-field potential created by the other $N-1$ electrons. The Hartree term in Eq.(1.7) is not the same for all electrons, as it involves a summation over all orbitals except the one corresponding to the electron under consideration. As a result, each electron i experiences a different density $n_i(r') = \sum_{j\neq i} |\varphi_j(r')|$, as it is excluded from the density calculation based on its own orbital. The Hartree term can be interpreted as an effective classical interaction between charges, treating electrons as distinguishable particles and neglecting their quantum nature as fermions.[1] It is worth noting that today applications of Hartree equations do not use the orbital dependent density as Eq.(1.7), but a modified form that makes the potential term as a functional of the full density as,

$$\left(-\frac{\nabla_r^2}{2} + v_{\text{ext}}(r) \right)\varphi_i(r) + \int dr'\, n(r')v_{\text{c}}(r,r')\varphi_i(r) = \epsilon_i\varphi_i(r)\,, \qquad (1.8)$$

where one can define the Hartree potential as,

$$v_{\text{H}}(r) = \int dr'\, n(r')v_{\text{c}}(r,r')\,. \qquad (1.9)$$

Unlike Eq.(1.7), the new Eq.(1.8) contains a self-interaction error.

1.2 Hartree-Fock approximation

Since the Hartree wavefunction neglects the fermionic nature of electrons, it is necessary to go beyond and incorporate it into the description. The Hartree-Fock (HF) approximation [84, 85] is an extension that considers the fermionic nature of electrons. *In this approach, the many-body wavefunction is approximated as a single Slater determinant, which properly accounts for the antisymmetry requirement of fermions.* By using this ansatz, the interacting electrons system can be approximately described in terms of an effective single-particle problem, taking into consideration the fermionic statistics. In order to derive the HF effective potential and the HF equation, we evaluate the expectation value of the hamiltonian using the following HF wavefunction,

$$\Phi_{\text{HF}} = \begin{vmatrix} \phi_1(x_1) & \phi_1(x_2) & \phi_1(x_3) & ... \\ \phi_2(x_1) & \phi_2(x_2) & \phi_2(x_3) & ... \\ \phi_3(x_1) & \phi_3(x_2) & \phi_3(x_3) & ... \\ . & . & . & ... \\ . & . & . & ... \end{vmatrix}\,, \qquad (1.10)$$

---

[1]In practical Hartree calculations, one partially takes into account the fermionic nature, by filling the states with only 2 electrons, from the lowest energy level and moving upward.

where $\phi_1(x_1) = \varphi_{i\sigma_1}(r_1)\chi_{\sigma_1}(s_1)$ is the single-particle "spin-orbital", satisfying the following ortonormalization condition,

$$\langle \phi_i(x)|\phi_j(x)\rangle = \int dx \, \phi_i^*(x)\phi_j(x) \tag{1.11}$$

$$= \sum_s \chi_{\sigma_i}^*(s)\chi_{\sigma_j}(s) \int dr \, \varphi_{i\sigma_i}^*(r)\varphi_{j\sigma_j}(r) = \delta_{ij}\delta_{\sigma_i\sigma_j} \,. \tag{1.12}$$

To facilitate the calculation, we express the hamiltonian in second quantization formalism, which provides a more convenient mathematical framework for dealing with many-particle systems.

$$\hat{H} = \sum_{ij\sigma\sigma'} \langle i\sigma|\hat{h}|j\sigma'\rangle \, \hat{c}_{i\sigma}^\dagger \hat{c}_{j\sigma'} + \frac{1}{2}\sum_{ijkl}\sum_{\sigma_1\sigma_2\sigma_3\sigma_4} \langle i\sigma_1 j\sigma_2|\hat{v}_c|k\sigma_3 l\sigma_4\rangle \, \hat{c}_{i\sigma_1}^\dagger \hat{c}_{j\sigma_2}^\dagger \hat{c}_{l\sigma_4} \hat{c}_{k\sigma_3} \,, \tag{1.13}$$

where $\langle i\sigma|\hat{h}|j\sigma'\rangle = \int dx \, \phi_{i\sigma}^*(x)\left(-\frac{\nabla_r^2}{2}+v_{\text{ext}}(x)\right)\phi_{j\sigma'}(x)$ with $\hat{h}$ the one-body operator (kinetic energy and electron-nuclei interaction operators) and $\langle i\sigma_1 j\sigma_2|\hat{v}_c|k\sigma_3 l\sigma_4\rangle = \int\int dxdx'\phi_{i\sigma_1}^*(x)\phi_{j\sigma_2}^*(x')v_c(x,x')\phi_{l\sigma_4}(x)\phi_{k\sigma_3}(x')$ with $\hat{v}_c$ the two-body Coulomb interaction operator. The hamiltonian expectation value within Φ_{HF} is

$$\langle \Phi_{\text{HF}}|\hat{H}|\Phi_{\text{HF}}\rangle = \sum_{ij=1}^N \sum_{\sigma\sigma'} \langle i\sigma|\hat{h}|j\sigma'\rangle \langle \Phi_{\text{HF}}|\hat{c}_{i\sigma}^\dagger \hat{c}_{j\sigma'}|\Phi_{\text{HF}}\rangle$$

$$+ \frac{1}{2}\sum_{ijkl=1}^N \sum_{\sigma_1\sigma_2\sigma_3\sigma_4} \langle i\sigma_1 j\sigma_2|\hat{v}_c|k\sigma_3 l\sigma_4\rangle \langle \Phi_{\text{HF}}|\hat{c}_{i\sigma_1}^\dagger \hat{c}_{j\sigma_2}^\dagger \hat{c}_{l\sigma_4} \hat{c}_{k\sigma_3}|\Phi_{\text{HF}}\rangle \,, \tag{1.14}$$

where we will treat below each term separately. The one-body term becomes

$$\sum_{ij=1}^N \sum_{\sigma\sigma'} \langle i\sigma|\hat{h}|j\sigma'\rangle \langle \Phi_{\text{HF}}|\hat{c}_{i\sigma}^\dagger \hat{c}_{j\sigma'}|\Phi_{\text{HF}}\rangle = \sum_{ij=1}^N \sum_{\sigma\sigma'} \langle i\sigma|\hat{h}|j\sigma'\rangle \, \delta_{ij}\delta_{\sigma\sigma'} \tag{1.15}$$

$$= \sum_{i,\sigma}^N \langle i|\hat{h}|i\rangle = \sum_{i=1,\sigma} \int dx \, \phi_{i\sigma}^*(x)\left[-\frac{\nabla_r^2}{2}+v_{\text{ext}}(x)\right]\phi_{i\sigma}(x) \,. \tag{1.16}$$

Th two-body term is written as

$$\frac{1}{2}\sum_{ijkl=1}^N \sum_{\sigma_1\sigma_2\sigma_3\sigma_4} \langle i\sigma_1 j\sigma_2|\hat{v}_c|k\sigma_3 l\sigma_4\rangle \langle \Phi_{\text{HF}}|\hat{c}_{i\sigma_1}^\dagger \hat{c}_{j\sigma_2}^\dagger \hat{c}_{l\sigma_4} \hat{c}_{k\sigma_3}|\Phi_{\text{HF}}\rangle \,, \tag{1.17}$$

where it turns out that we must have either

1. $k = j$, $\sigma_3 = \sigma_2$ and $l = i$, $\sigma_1 = \sigma_4$ or

2. $k = i$, $\sigma_1 = \sigma_3$ and $l = j$, $\sigma_2 = \sigma_4$.

In this case, by using the anticommutation relations of fermions, we have

1.

$$\hat{c}_{i\sigma_1}^\dagger \hat{c}_{j\sigma_2}^\dagger \hat{c}_{l\sigma_4} \hat{c}_{k\sigma_3} |\Phi_{\text{HF}}\rangle = \hat{c}_{i\sigma_1}^\dagger \hat{c}_{j\sigma_2}^\dagger \hat{c}_{i\sigma_1} \hat{c}_{j\sigma_2} |\Phi_{\text{HF}}\rangle \tag{1.18}$$

$$= \delta_{ij}\delta_{\sigma_1\sigma_2}\hat{c}_{i\sigma_1}^\dagger \hat{c}_{i\sigma_1} |\Phi_{\text{HF}}\rangle - n_{i\sigma_1}n_{j\sigma_2} |\Phi_{\text{HF}}\rangle \,, \tag{1.19}$$

11

2.

$$\hat{c}_{i\sigma_1}^\dagger \hat{c}_{j\sigma_2}^\dagger \hat{c}_{l\sigma_4} \hat{c}_{k\sigma_3} |\Phi_{\text{HF}}\rangle = \hat{c}_{i\sigma_1}^\dagger \hat{c}_{j\sigma_2}^\dagger \hat{c}_{j\sigma_2} \hat{c}_{i\sigma_1} |\Phi_{\text{HF}}\rangle \tag{1.20}$$

$$= -\delta_{ij}\delta_{\sigma_1\sigma_2} n_{i\sigma_1} |\Phi_{\text{HF}}\rangle + n_{i\sigma_1} n_{j\sigma_2} |\Phi_{\text{HF}}\rangle , \tag{1.21}$$

where $n_{i\sigma} = \hat{c}_{i\sigma}^\dagger \hat{c}_{i\sigma}$ is the occupation number operator for a given spin. So, the two-body term of Eq.(1.17) becomes

$$\frac{1}{2}\sum_{ijkl=1}\sum_{\sigma_1\sigma_2\sigma_3\sigma_4} \langle i\sigma_1 j\sigma_2|\hat{v}_c|k\sigma_3 l\sigma_4\rangle \langle\Phi_{\text{HF}}|\hat{c}_{i\sigma_1}^\dagger \hat{c}_{j\sigma_2}^\dagger \hat{c}_{l\sigma_4} \hat{c}_{k\sigma_3}|\Phi_{\text{HF}}\rangle = \frac{1}{2}\sum_{ij}\sum_{\sigma_1\sigma_2} n_{i\sigma_1} n_{j\sigma_2} \bigg(\langle i\sigma_1 j\sigma_2|\hat{v}_c|i\sigma_1 j\sigma_2\rangle$$
$$- \langle i\sigma_1 j\sigma_2|\hat{v}_c|j\sigma_2 i\sigma_1\rangle \bigg) , \tag{1.22}$$

and the total energy can be finally written as,

$$\langle\Phi_{\text{HF}}|\hat{H}|\Phi_{\text{HF}}\rangle = \sum_{i\sigma} \int dx\, \phi_{i\sigma}^*(x)\left[-\frac{\nabla_r^2}{2} + v_{\text{ext}}(x)\right]\phi_{i\sigma}(x)$$
$$+ \frac{1}{2}\sum_{ij\sigma_1\sigma_2} \int dxdx'\, \phi_{i\sigma_1}^*(x)\phi_{j\sigma_2}^*(x')v_c(x,x')\phi_{i\sigma_1}(x)\phi_{j\sigma_2}(x')$$
$$- \frac{1}{2}\sum_{ij,\sigma_1\sigma_2} \int dxdx'\, \phi_{i\sigma_1}^*(x)\phi_{j\sigma_2}^*(x')v_c(x,x')\phi_{i\sigma_1}(x')\phi_{j\sigma_2}(x). \tag{1.23}$$

By writing explicitly the spins, Eq.(1.23) becomes

$$\langle\Phi_{\text{HF}}|\hat{H}|\Phi_{\text{HF}}\rangle = \sum_{i\sigma}\sum_s \chi_\sigma^*(s)\chi_\sigma(s) \int dr\, \varphi_{i\sigma}^*(r)\left[-\frac{\nabla_r^2}{2} + v_{\text{ext}}(x)\right]\varphi_{i\sigma}(r)$$
$$+ \frac{1}{2}\sum_{ij\sigma_1\sigma_2}\sum_s \chi_{\sigma_1}^*(s)\chi_{\sigma_1}(s)\sum_{s'} \chi_{\sigma_2}^*(s')\chi_{\sigma_2}(s') \int drdr'\, \varphi_{i\sigma_1}^*(r)\varphi_{j\sigma_2}^*(r')v_c(r,r')\varphi_{i\sigma_1}(r)\varphi_{j\sigma_2}(r')$$
$$- \frac{1}{2}\sum_{ij,\sigma_1\sigma_2}\sum_s \chi_{\sigma_1}^*(s)\chi_{\sigma_2}(s)\sum_{s'} \chi_{\sigma_2}^*(s')\chi_{\sigma_1}(s') \int drdr'\, \varphi_{i\sigma_1}^*(r)\varphi_{j\sigma_2}^*(r')v_c(r,r')\varphi_{i\sigma_1}(r')\varphi_{j\sigma_2}(r), \tag{1.24}$$

and by using $\sum_s \chi_{\sigma_1}^*(s)\chi_{\sigma_2}(s) = \delta_{\sigma_1\sigma_2}$, we obtain

$$\text{E}_{\text{HF}} = \langle\Phi_{\text{HF}}|\hat{H}|\Phi_{\text{HF}}\rangle = \sum_{i\sigma} \int dr\, \varphi_{i\sigma}^*(r)\left[-\frac{\nabla_r^2}{2} + v_{\text{ext}}(x)\right]\varphi_{i\sigma}(r)$$
$$+ \underbrace{\frac{1}{2}\sum_{ij\sigma_1\sigma_2} \int drdr'\, \varphi_{i\sigma_1}^*(r)\varphi_{j\sigma_2}^*(r')v_c(r,r')\varphi_{i\sigma_1}(r)\varphi_{j\sigma_2}(r')}_{\text{E}_{\text{H}}}$$
$$\underbrace{- \frac{1}{2}\sum_{ij,\sigma_1} \int drdr'\, \varphi_{i\sigma_1}^*(r)\varphi_{j\sigma_1}^*(r')v_c(r,r')\varphi_{i\sigma_1}(r')\varphi_{j\sigma_1}(r)}_{\text{E}_{\text{x}}}, \tag{1.25}$$

where E_{H} is the Hartree energy and E_{x} is the exchange energy. Given that the one-body density is defined as

$$n(r) = \sum_{i\sigma} \varphi_{i\sigma}^*(r)\varphi_{i\sigma}(r), \tag{1.26}$$

12

which describes the probability of finding an electron at r, the Hartree energy in terms of n is

$$E_H = \frac{1}{2} \int \int dr dr' \frac{n(r)n(r')}{|r - r'|} . \tag{1.27}$$

It is important to note that the E_H contains a self-interaction error within the HF context. This error arises because each electron, which contributes to the electron density, interacts with the overall density including itself. On the other hand, the one-body spin-resolved density-matrix is defined as

$$\gamma_\sigma(r, r') = \sum_i \varphi_{i\sigma}^*(r')\varphi_{i\sigma}(r) , \tag{1.28}$$

so, the exchange energy is

$$E_x = -\sum_\sigma \frac{1}{2} \int \int dr dr' \frac{\gamma_\sigma(r, r')\gamma_\sigma(r', r)}{|r - r'|} . \tag{1.29}$$

Interestingly, the Hartree self-interaction error is corrected by the exchange term when $i = j$ in Eq.(1.25) . To derive the HF equation, we use the same principle as in the Hartree equation in the previous section,

$$\frac{\delta}{\delta \varphi_{i\sigma}^*(r)} \left[\langle \Phi_{HF} | \hat{H} | \Phi_{HF} \rangle - \sum_{j\sigma'} \epsilon_{j\sigma'} \int dr \varphi_{j\sigma'}^*(r')\varphi_{i\sigma}(r') \right] = 0 . \tag{1.30}$$

Hence, we obtain the HF equation as follows,

$$\left(-\frac{1}{2}\nabla_r^2 + v_{ext}(r) + \sum_{j\sigma'} \int dr' \varphi_{j\sigma'}^*(r')\varphi_{j\sigma'}(r')v_c(r, r') \right) \varphi_{i\sigma}(r) - \sum_j \int dr' \varphi_{j\sigma}^*(r')\varphi_{j\sigma}(r)v_c(r, r')\varphi_{i\sigma}(r')$$
$$= \epsilon_{i\sigma}\varphi_{i\sigma}(r) . \tag{1.31}$$

From Eq.(1.31), we obtain the Hartree potential as previously defined in Eq.(1.9) and

$$v_x(r, r') = \sum_j \int dr' \varphi_{j\sigma}^*(r')\varphi_{j\sigma}(r)\varphi_{i\sigma}(r')v_c(r, r') , \tag{1.32}$$

which is the exchange Fock potential. It accounts for the effect of the Pauli exclusion principle, which states that two electrons with the same spin cannot occupy the same spatial location. The exchange term in the HF equation reflects this principle. *The exchange interaction only occurs between electrons with parallel spins, and there is no sum over spin in the exchange term.* When $i = j$ in the HF equation, the exchange term cancels out the self-interaction error present in the Hartree potential, effectively solving this problem. It ensures that each electron does not interact with itself, leading to an improved description of the electronic interactions. It is important to note that in the HF equation, the motions of fermions with equal spin are correlated, meaning that their behavior is influenced by each other. However, there are no such restrictions for particles with different spins, and their motions are uncorrelated in the HF approximation. *The difference between the exact ground-state energy and the HF ground-state energy is known as the "correlation energy". It captures the additional electronic correlations beyond the HF approximation.*[2]

---

[2]The many-body wavefunction could be seen as a superposition of an infinite sum over Slater determinants. So, the HF is a useful approximation of the full many-body wavefunction.

Chapter 2

Density Functional Theory

Density Functional Theory (DFT), introduced by Hohenberg and Kohn in 1964 [7], has gained immense popularity and is now one of the most widely employed theories globally. In its essence, DFT is an exact theory for describing "at least" the ground state of interacting many-body systems. It acts in contrast to the straightforward procedure, which relies on starting from the Schrödinger equation for the system of interest and find the desired observable from the wavefunction. The wavefunction contains vastly more information than one would care to know about, unless one would like to calculate all possible observables, which is usually not the case. DFT instead simplifies the electronic problem by focusing on a much easier quantity: "the electron density n", which, as will be shown, contains enough information to determine all we need for any system.

2.1 The Hohenberg-Kohn theorems

The hamiltonian of an interacting many-electron system can be divided into a universal part that includes the electronic kinetic energy and Coulomb interaction between electrons and an external part that represents the effect of an external potential v_{ext} due to the nuclei and other sources,

$$\hat{H} = \hat{T} + \hat{V}_{\mathrm{ee}} + \hat{V}_{\mathrm{ext}} \,, \tag{2.1}$$

where $\hat{T}$ and $\hat{V}_{\mathrm{ee}}$ are the kinetic energy and Coulomb interaction operators, respectively. The only component that varies between different systems is the external potential v_{ext}, while $\hat{T} + \hat{V}_{\mathrm{ee}}$ can be considered universal because it is the same for any electronic system. As a result, it is the external potential that defines the hamiltonian and, consequently, the ground-state many-body wavefunction, denoted as Ψ_0. This means that Ψ_0 depends on v_{ext}. Consequently Ψ_0 can be expressed as a functional of v_{ext}. The question that we should adress now is: *is this relation unique? Or in mathematical terms, can we consider the relation between v_{ext} and Ψ_0 as a bijective relation?* If yes, we would able, in principle, to express each observable of the ground-state as a unique functional of the external potential as follows,

$$O = O[v_{\mathrm{ext}}] = \langle \Psi_0[v_{\mathrm{ext}}] | \, \hat{O} \, | \Psi_0[v_{\mathrm{ext}}] \rangle \,. \tag{2.2}$$

This would be represented by the right-panel of Fig. 2.1. While this may seem self-evident, it can
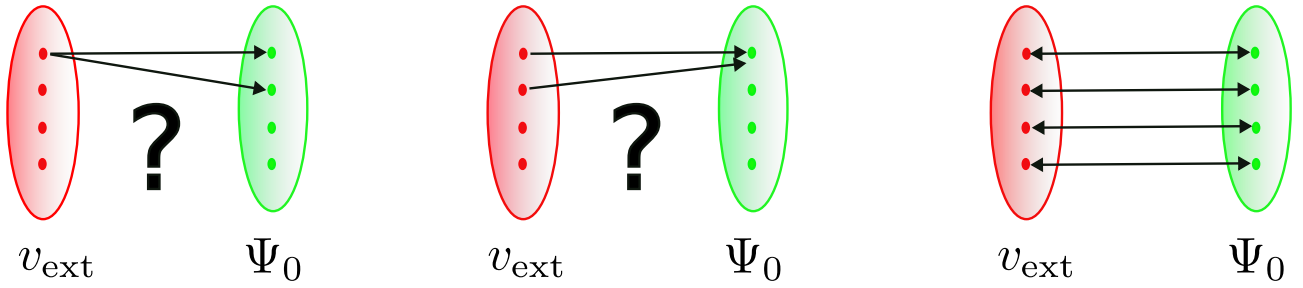
Figure 2.1: One-to-one correspondence between v_{ext} and Ψ_0

be formally proven by establishing a one-to-one correspondence between v_{ext} and Ψ_0. To exclude the scenario on the left-panel of Fig. 2.1, we just exclude the case in which the ground-state is degenerate. In order to address the scenario of the central-panel of Fig. 2.1, we assume that two different potentials (that differ by more than a constant) can lead to the same Ψ_0. Therefore, the derivation takes the following form,

$$v_{\text{ext}}^{(1)} \neq v_{\text{ext}}^{(2)} + constant, \tag{2.3}$$

meaning that we have two different hamiltonians,

$$\hat{H}_1 = \hat{T} + \hat{V}_{\text{ee}} + \hat{V}_{\text{ext}}^{(1)}, \tag{2.4}$$

and,

$$\hat{H}_2 = \hat{T} + \hat{V}_{\text{ee}} + \hat{V}_{\text{ext}}^{(2)}. \tag{2.5}$$

Using these two different hamiltonians, since they have the same Ψ_0, we obtain

$$\hat{H}_1 \left| \Psi_0 \right\rangle - \hat{H}_2 \left| \Psi_0 \right\rangle = \hat{V}_{\text{ext}}^{(1)} \left| \Psi_0 \right\rangle - \hat{V}_{\text{ext}}^{(2)} \left| \Psi_0 \right\rangle \tag{2.6}$$

$$= V_{\text{ext}}^{(1)} \left| \Psi_0 \right\rangle - V_{\text{ext}}^{(2)} \left| \Psi_0 \right\rangle \tag{2.7}$$

$$= \text{E}_1 - \text{E}_2 \left| \Psi_0 \right\rangle, \tag{2.8}$$

which is a contradiction with our initial assumption where the two selected external potentials differ by more than a constant. Thus, we conclude that there is a one-to-one correspondence between v_{ext} and Ψ_0, which is represented by the right side of Fig. 2.1. Consequently, *every observable in the ground-state is a unique functional of v_{ext}.*

The next question is: "is there a one-to-one correspondence between the v_{ext} and the ground-state density n_0?".

If yes, there should be a one-to-one correspondence between Ψ_0 and n_0. Let us consider that two different ground-states with their one-to-one correspondence external potentials yield the same density as represented in the left-hand subfigure of Fig. 2.2. So, we have two hamiltonians,

$$\hat{H}_1 = \hat{T} + \hat{V}_{\text{ee}} + \hat{V}_{\text{ext}}^{(1)}, \tag{2.9}$$

with Ψ_1 as the ground-state wavefunction and,

15
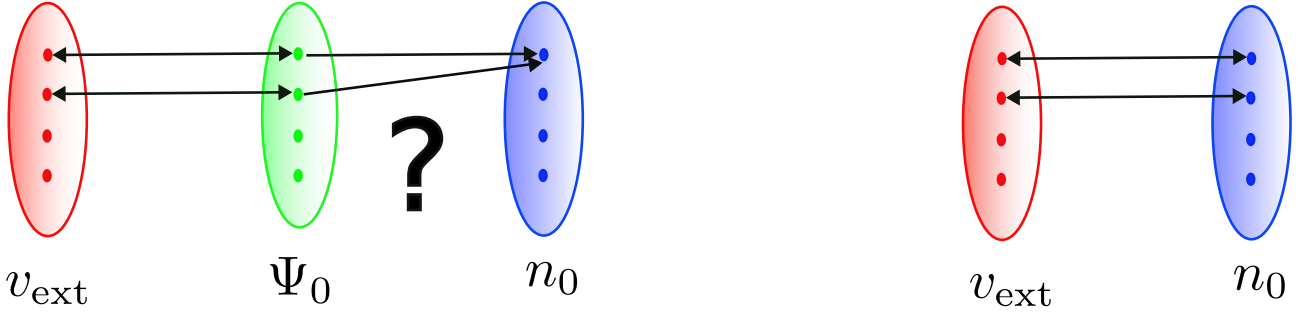
Figure 2.2: One-to-one correspondence between v_{ext} and n_0

$$\hat{H}_2 = \hat{T} + \hat{V}_{\text{ee}} + \hat{V}_{\text{ext}}^{(2)}\,, \tag{2.10}$$

with Ψ_2 as the ground-state wavefunction. Then, the ground-state energy for H_1, called E_1 evaluated with Ψ_1 is the minimum among all possible wavefunctions[1]. So, we have

$$E_1 = \langle\Psi_1|\,\hat{H}_1\,|\Psi_1\rangle < \langle\Psi_2|\,\hat{H}_1\,|\Psi_2\rangle = \langle\Psi_2|\,\hat{H}_1 + \hat{H}_2 - \hat{H}_2\,|\Psi_2\rangle \tag{2.11}$$

$$= E_2 + \langle\Psi_2|\,\hat{V}_{\text{ext}}^{(1)} - \hat{V}_{\text{ext}}^{(2)}\,|\Psi_2\rangle \tag{2.12}$$

$$= E_2 + \int dr\,\big(v_{\text{ext}}^{(1)}(r) - v_{\text{ext}}^{(2)}(r)\big)n_2(r)\,, \tag{2.13}$$

where $n_2(r)$ is the density obtained using Ψ_2 (to understand the transition to the last equation from the one before see Subsec. 2.2). We repeat exactly the same steps, by exchanging the role of system 1 and 2. This leads to,

$$E_2 = \langle\Psi_2|\,\hat{H}_2\,|\Psi_2\rangle < \langle\Psi_1|\,\hat{H}_2\,|\Psi_1\rangle = \langle\Psi_1|\,\hat{H}_2 + \hat{H}_1 - \hat{H}_1\,|\Psi_1\rangle \tag{2.14}$$

$$= E_1 + \langle\Psi_1|\,\hat{V}_{\text{ext}}^{(2)} - \hat{V}_{\text{ext}}^{(1)}\,|\Psi_1\rangle \tag{2.15}$$

$$= E_1 + \int dr\,\big(v_{\text{ext}}^{(2)}(r) - v_{\text{ext}}^{(1)}(r)\big)n_1(r)\,, \tag{2.16}$$

where $n_1(r)$ is the density built by Ψ_1, knowing that our initial assumption was to consider that $n_1 = n_2$. So, by adding the Eq.(2.13) to Eq.(2.16), we obtain the following contradiction,

$$E_1 + E_2 < E_1 + E_2\,. \tag{2.17}$$

In conculsion, *there is a one-to-one correspondence between v_{ext} and n_0 as shown in the right-hand panel of Fig. 2.2. Consequently, every observable is a functional of the ground-state density. This is the first HK theorem.* So, the first HK theorem shows that the ground-state total energy, which is an observable, can be written as a functional of the density,

$$E_{\text{HK}}[n] = F_{\text{HK}}[n] + \int dr\,v_{\text{ext}}(r)n(r)\,, \tag{2.18}$$

where $F_{\text{HK}}[n] = \langle\hat{T}\rangle + \langle\hat{V}_{\text{ee}}\rangle$ is a universal functional of the density, which is the same for any many-electron system.

---

[1] The extension to degenerate ground-states is possible [86].

The theory continues with a second HK theorem that establishes the variational property of the total energy,

$$E = E[n] = \langle \Psi_0[n] | \hat{H} | \Psi_0[n] \rangle, \tag{2.19}$$

with respect to the density. So, the ground-state total energy can be found by varying the density to minimize the energy,

$$E_0 = \min_{n \to n_0} E[n]. \tag{2.20}$$

As a summary, DFT has three essential messages: (1) there is one-to-one correspondence between the external potential and the ground-state density, meaning that the ground-state properties are functional of the ground-state density. (2) The total energy has also a variational character in terms of the density. (3) The universality of $F_{HK}[n]$.

2.2   Difficulty to find a density functional

We can notice that the external potential observable can be expressed in terms of the density, as indicated in Eq.(2.18). Below, we present the justification for this relationship, where any observable can be defined in terms of the full many-body wavefunction.

$$\langle \hat{V}_{ext} \rangle = \int dr_1...dr_N \, \Psi^*(r_1, ..., r_N) \sum_i v_{ext}(r_i) \Psi(r_1, ...r_N) \tag{2.21}$$

$$= \int dr_1...dr_N \, \Psi^*(r_1, ..., r_N) v_{ext}(r_1) \Psi(r_1, ..., r_N) + ... + \int dr_1...dr_N \, \Psi^*(r_1, ..., r_N) v_{ext}(r_N)$$
$$\Psi(r_1, ..., r_N). \tag{2.22}$$

Since the electrons are indistinguishable particles, the integrals above are the same. So,

$$\langle \hat{V}_{ext} \rangle = N \int dr_1...dr_N \, \Psi^*(r_1, ..., r_N) v_{ext}(r_1) \Psi(r_1, ...r_N) \tag{2.23}$$

$$= \int dr_1 \, v_{ext}(r_1) \underbrace{N \int dr_2...dr_N \, \Psi^*(r_1, ..., r_N) \Psi(r_1, ...r_N)}_{n(r_1)} \tag{2.24}$$

$$= \int dr_1 \, v_{ext}(r_1) n(r_1), \tag{2.25}$$

where $n(r_1)$ is the electron density at position r_1.

For the kinetic energy operator, we do the same,

$$\langle \hat{T} \rangle = \int dr_1...dr_N\, \Psi^*(r_1,...,r_N)\left(-\sum_i \frac{\nabla_{r_i}^2}{2}\right)\Psi(r_1,...,r_N) \tag{2.26}$$

$$= \int dr_1...dr_N\, \Psi^*(r_1,...,r_N)\left(-\frac{\nabla_{r_1}^2}{2}\right)\Psi(r_1,...,r_N) + ... \tag{2.27}$$

$$+ \int dr_1...dr_N \Psi^*(r_1,...,r_N)\left(-\frac{\nabla_{r_N}^2}{2}\right)\Psi(r_1,...,r_N)$$

$$= N \int dr_1...dr_N\, \Psi^*(r_1,...,r_N)\left(-\frac{\nabla_{r_1}^2}{2}\right)\Psi(r_1,...,r_N) \tag{2.28}$$

$$= \int dr_1 \lim_{r_1 \to r}\left(-\frac{\nabla_r^2}{2}\right)\underbrace{N \int dr_2...dr_N \Psi^*(r_1,...,r_N)\Psi(r,...r_N)}_{\gamma(r_1,r)} \tag{2.29}$$

$$= \int dr_1 \lim_{r_1 \to r}\left(-\frac{\nabla_r^2}{2}\right)\gamma(r_1,r)\,, \tag{2.30}$$

where $\gamma(r_1,r)$ is the one-body density matrix. The remaining observable is the two-body Coulomb interaction energy, derived as follows,

$$\langle \hat{V}_{ee} \rangle = \int dr_1...dr_N\, \Psi^*(r_1,...,r_N)\frac{1}{2}\sum_{i \neq j}\frac{1}{|r_i - r_j|}\Psi(r_1,...,r_N) \tag{2.31}$$

$$= N\left(\int dr_1...dr_N\, \Psi^*(r_1,...,r_N)\frac{1}{2}\frac{1}{|r_1 - r_2|}\Psi(r_1,...,r_N)\right. \tag{2.32}$$

$$+ \int dr_1...dr_N\, \Psi^*(r_1,...,r_N)\frac{1}{2}\frac{1}{|r_1 - r_3|}\Psi(r_1,...,r_N) + ...$$

$$\left.+ \int dr_1...dr_N\, \Psi^*(r_1,...,r_N)\frac{1}{2}\frac{1}{|r_1 - r_N|}\Psi(r_1,...,r_N)\right),$$

where the last equation is multiplied by N due to the double summation. So, we obtain

$$\langle \hat{V}_{ee} \rangle = \frac{1}{2}\int dr_1 dr_2 \frac{1}{|r_1 - r_2|}\underbrace{N(N-1)\int dr_3...dr_N\, \Psi^*(r_1,...,r_N)\Psi(r_1,...,r_N)}_{n^{(2)}(r_1,r_2)} \tag{2.33}$$

$$= \frac{1}{2}\int dr_1 dr_2 \frac{1}{|r_1 - r_2|}n^{(2)}(r_1,r_2)\,, \tag{2.34}$$

where $n^{(2)}(r_1,r_2)$ is the two-body density. So, among the three terms in the hamiltonian, only the external potential energy can be written as an explicit functional of the density, while $F_{HK}[n]$ is an unknown functional of the density.

2.3   The Kohn-Sham auxiliary system

The HK theorem, despite its intriguing concept, did not initially provide a practical computational method for real systems. The difficulty to develop such a computational method is mainly related to the electron-electron Coulomb interaction. However, Kohn and Sham [8] addressed this issue by

introducing an auxiliary system known today as the "Kohn-Sham (KS) system," which made DFT a practical computational approach. *The KS ansatz involves replacing the original interacting system with a non-interacting one, constructed such that the two densities coincide.* Within the KS scheme, the role of the Coulomb interaction is taken by the Hartree, exchange and correlations potentials. By using the non-interacting auxiliary system, and by adding and subtracting the kinetic energy of an independent-particle system and the Hartree energy, the total energy can be written in the KS form as

$$E_{KS}[n] = T_s[s] + \int dr \, v_{ext}(r)n(r) + E_H[n] + E_{xc}[n] \,, \tag{2.35}$$

where T_s is the kinetic energy for the independent-particle system, E_H is the Hartree energy and E_{xc} is the exchange-correlation contribution, defined as

$$E_{xc}[n] = \langle \hat{T} \rangle - T_s[n] + \langle \hat{V}_{ee} \rangle - E_H[n] \,, \tag{2.36}$$

where $\langle \hat{T} \rangle + \langle \hat{V}_{ee} \rangle = F_{HK}[n]$. The KS single-particle equations are derived through the application of the variational principle. This involves minimizing the ground-state energy, denoted as $E_{KS}[n]$, with respect to the one-particle wavefunctions of the non-interacting auxiliary system, with the condition of normalization of the single-particle wavefunctions $\int dr \, \varphi_i^*(r)\varphi_i(r) = 1$,

$$\frac{\delta}{\delta \varphi_i^*(r)} \left(E_{KS}[n] - \sum_i \epsilon_i \int dr \, \varphi_i^*(r)\varphi_i(r) \right) = 0 \,. \tag{2.37}$$

The KS equations are then obtained by using the chain-rule $\frac{\delta}{\delta \varphi} = \frac{\delta}{\delta n}\frac{\delta n}{\delta \varphi}$ with the density in Eq.(2.37), which yields

$$\left(-\frac{1}{2}\nabla_r^2 + v_{KS}(r) \right)\varphi_i(r) = \epsilon_i \varphi_i(r) \,, \tag{2.38}$$

where

$$v_{KS}(r) = v_{ext}(r) + v_H([n], r) + v_{xc}([n], r) \tag{2.39}$$

$$= v_{ext}(r) + \frac{\delta E_H[n]}{\delta n(r)} + \frac{\delta E_{xc}[n]}{\delta n(r)} \,. \tag{2.40}$$

The KS equations must be solved in a self-consistent scheme. The resulting KS density matches the interacting density. However, the lack of knowledge regarding the exact expression for the exchange-correlation potential in terms of the density makes the theory only exact in principle. Approximations are needed to be able to obtain results for real systems.

2.4   Approximate exchange-correlation functional

As the exchange-correlation (xc) energy remains unknown in DFT, it necessitates approximation. The quest for suitable approximations has been and still is a prominent focus in DFT research, yielding numerous proposals and investigations. In this section, we delve into some of these approximations, assessing their effectiveness and limitations.

The Local Density Approximation (LDA), introduced by Kohn and Sham [8], is indeed one of the earliest approximations for the xc energy in DFT. This approximation is based on the hypothesis

that the xc energy depends locally on the electron density, and it assumes that the xc energy can be approximated using the xc energy of the homogeneous electron gas (HEG) at that density as

$$E_{xc}^{LDA}[n] = \int dr\, n(r) \epsilon_{xc}^{HEG}(n(r)), \qquad (2.41)$$

where $\epsilon_{xc}^{HEG}(n(r))$ is the xc energy per particle for the HEG [14]. LDA has found successful applications in inhomogeneous systems , particularly in cases where electrons are highly delocalized, but it does have its limitations. One significant limitation is its applicability primarily to low-density systems, where electrons are localized. Additionally, LDA is not entirely free from self-interaction errors. This is because the exchange energy, which is intended to correct errors in the Hartree term as we have seen in Chap. 1, is not exact within the LDA framework.

One approach to extend beyond the LDA is to introduce a density gradient dependence into the functional. Various generalized gradient approximations (GGA) [87] have been proposed, and they often yield improved results compared to LDA. However, it is important to note that GGA, like LDA, is not entirely free from self-interaction errors.

2.5   Is the band gap energy a functional of the density?

As discussed earlier, observables can be expressed as functionals of the ground-state density within the framework of DFT. However, when it comes to observables like the energy gap (E_g), which involves changes in the number of electrons, we need to be more careful when using DFT. Another strategy to treat this can be ensemble DFT [88]. The definition of E_g is typically expressed in terms of energy differences as

$$E_g = (E_0^{N+1} - E_0^{N}) - (E_0^{N} - E_0^{N-1}), \qquad (2.42)$$

where all of the energies are ground-state energies but for different particle number. In principle, ground-state DFT has the potential to yield the exact ground-state energy, *and one might expect that by performing three ground-state DFT calculations for systems with $N-1$, N, and $N+1$ electrons, we should obtain the exact E_g.* However, *in practice, this is most often not the case.* This is the so-called ΔSCF method. This method cannot be applied directly to a solid, where the effect of adding or removing one electron (out of the 10^{23} electrons) is difficult to capture. Good results can be instead obtained for molecules. For solids, people often rely on the KS eigenvalues, which in principle do not carry the addition and removal energies meaning. In other words, they do not fulfill Koopmans' theorem.

Chapter 3

Time Dependent Density Functional Theory

While DFT has been extremely successful for ground-state properties, there are many important issues which extend beyond its reach. Most notably, time-dependent processes and excited state properties of electronic systems either are not included at all or are not easily accessible. This has motivated the development of time-dependent density functional theory (TDDFT). The formal foundation of TDDFT is the Runge–Gross (RG) theorem (1984) [89] - the time-dependent analogue of the Hohenberg-Kohn (HK) theorem. In the spirit of DFT, the TDDFT core idea is that the dynamics of any many-electron system is encoded in its time-dependent density, which makes the knowledge of the wavefunction unnecessary.

3.1   The Runge-Gross theorem

The hamiltonian of N interacting nonrelativistic electrons moving in a time-dependent external potential is given as

$$\hat{H}(t) = \hat{T} + \hat{V}_{\text{ee}} + \hat{V}_{\text{ext}}(t),\tag{3.1}$$

where $\hat{V}_{\text{ext}}(t) = \sum_{i=1}^{N} v_{\text{ext}}(r_i, t)$. The dynamic evolution of the system is governed by the time-dependent Schrödinger equation,

$$i\frac{\partial}{\partial t}\Psi(r_1, ..., r_N, t) = \hat{H}(t)\Psi(r_1, ..., r_N, t).\tag{3.2}$$

The time-dependent external potential defines the hamiltonian and produces a time-dependent wavefunction $\Psi(t)$ for a given initial state Ψ_0. Therefore, $\Psi(t)$ generates a time-dependent density $n(r, t)$. This can be illustrated in the following map,

$$v_{\text{ext}}(r, t) \xrightarrow{\ i\partial\Psi(t)/\hat{H}(t)\Psi(t)\ } \Psi(t) \xrightarrow{\ <\Psi(t)|\hat{n}|\Psi(t)>\ } n(r, t)$$

Figure 3.1: Map showing that the time dependent system is defined by the time dependent external potential.

To develop a TDDFT, one needs to establish an inversion of the map shown above. In the context of DFT, it was shown that the external potential uniquely determines the ground-state density and vice versa. In TDDFT, the goal is to demonstrate that the time-dependent density, denoted as $n(r,t)$, uniquely determines the dynamic behavior of the electronic system over time. In other words, we need to demonstrate that there is one-to-one correspondence between the time dependent densities and potentials. What we aim to demonstrate is that when we have two different potentials, both acting on a fixed initial quantum state denoted as Ψ_0, these two potentials will result in two distinct time-dependent electron densities. To clarify the concept of "different potentials", we consider that these potentials vary only by an additional time-dependent function added to one of them. In other words, they differ by a time-dependent additive term,

$$v_{\text{ext}}^{(1)}(t) = v_{\text{ext}}^{(2)}(t) + c(t), \tag{3.3}$$

where the corresponding wavefunctions differ by a phase factor $\Psi^{(1)}(t) = e^{-i\alpha t}\Psi^{(2)}(t)$, where $\frac{d\alpha}{dt} = c(t)$. In this case, the resulting two densities will be identical,

$$n^{(1)}(r,t) = \langle \Psi^{(1)}| \hat{n}(r) |\Psi^{(1)}(t)\rangle \tag{3.4}$$

$$= \langle \Psi^{(2)}| e^{i\alpha(t)}\hat{n}(r)e^{-i\alpha t} |\Psi^{(2)}(t)\rangle \tag{3.5}$$

$$= \langle \Psi^{(2)}| \hat{n}(r) |\Psi^{(2)}(t)\rangle \tag{3.6}$$

$$= n^{(2)}(r,t). \tag{3.7}$$

Thus, we need to consider two potentials that differ by more than a constant $v_{\text{ext}}^{(1)}(t) \neq v_{\text{ext}}^{(2)}(t) + c(t)$, which is the same as we do in DFT. The proof proceeds into two steps: we first prove the uniqueness of the current densities, then from there to the densities. The equation of motion for the current density j is given as follows,

$$i\frac{\partial}{\partial t}j(r,t) = \langle \Psi(t)| [\hat{j}(r), \hat{H}(t)] |\Psi(t)\rangle, \tag{3.8}$$

where

$$\hat{j}(r) = \frac{1}{2i}\sum_{j=1}^{N}\left[\nabla_j\delta(r-r_j) + \delta(r-r_j)\nabla_j\right]. \tag{3.9}$$

So, since the two different external potentials yield two different wavefunctions that evolve from the same initial state Ψ_0, we obtain

$$\frac{\partial}{\partial t}\left(j^{(1)}(r,t) - j^{(2)}(r,t)\right)\Big|_{t=t_0} = -i\langle \Psi_0| [\hat{j}(r), \hat{H}^{(1)}(t_0) - \hat{H}^{(2)}(t_0)] |\Psi_0\rangle \tag{3.10}$$

$$= -n(r,t_0)\nabla\left(v_{\text{ext}}^{(1)}(r,t_0) - v_{\text{ext}}^{(2)}(r,t_0)\right), \tag{3.11}$$

where if the two potentials are different by more a constant at t_0, then the derivative of the two current densities is different from zero. In other words, the two current densities $j^{(1)}$ and $j^{(2)}$ have a different time derivative at t_0, which means that they could be equivalent at t_0 but their time evolution will be different. But does that hold true if we have two different potentials, that are equal at t_0?

22

The two different potentials, if they are equivalent at t_0, would have different time derivative, i.e, $\frac{\partial v_{\text{ext}}^{(1)}(r,t_0)}{\partial t} \neq \frac{\partial v_{\text{ext}}^{(2)}(r,t_0)}{\partial t}$. So, the second derivative of the current densities,

$$\frac{\partial^2}{\partial t^2}\left(j^{(1)}(r,t) - j^{(2)}(r,t)\right)\bigg|_{t=t_0} = -n(r,t_0)\nabla\left(\frac{\partial v_{\text{ext}}^{(1)}(r,t_0)}{\partial t} - \frac{\partial v_{\text{ext}}^{(2)}(r,t_0)}{\partial t}\right)\bigg|_{t=t_0}, \tag{3.12}$$

will be different. Thus, the two current densities are different. However, what happens if the two different potentials have the same time derivative at t_0, or even the second time derivative? In fact, there must be a finite time derivative, which is different for the two potentials at t_0, otherwise $v_{\text{ext}}^{(1)}$ and $V_{\text{ext}}^{(2)}$ are equivalent. So, at some finite time derivative we have

$$\frac{\partial^{k+1}}{\partial t^{k+1}}\left(j^{(1)}(r,t) - j^{(2)}(r,t)\right)\bigg|_{t=t_0} = -n(r,t_0)\nabla\left(\frac{\partial^k v_{\text{ext}}^{(1)}(r,t_0)}{\partial t^k} - \frac{\partial^k v_{\text{ext}}^{(2)}(r,t_0)}{\partial t^k}\right)\bigg|_{t=t_0}, \tag{3.13}$$

meaning that the two current densities are different if the potentials differ by more than a constant.
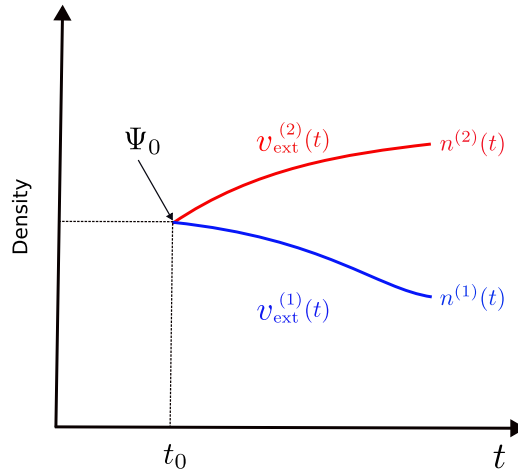
Figure 3.2: Runge-Gross theorem: two different external potential having the same ground-state at t_0, generate two different densities.

With this, we have demonstrated the first part of the Runge-Gross theorem. The second part consists in showing that having different current densities means that the densities themselves are different. To do that, we need a relation between the density and the current density, which is given by the continuity equation,

$$\frac{\partial}{\partial t}n(r,t) = -\nabla.j(r,t), \tag{3.14}$$

which leads to

$$\frac{\partial^{k+2}}{\partial t^{k+2}}\left(n^{(1)}(r,t) - n^{(2)}(r,t)\right)\bigg|_{t=t_0} = -\nabla.\frac{\partial^{k+1}}{\partial t^{k+1}}\left(j^{(1)}(r,t) - j^{(2)}(r,t)\right)\bigg|_{t=t_0} \tag{3.15}$$

$$= \nabla.\left[n(r,t_0)\nabla\left(\frac{\partial^k v_{\text{ext}}^{(1)}(r,t_0)}{\partial t^k} - \frac{\partial^k v_{\text{ext}}^{(2)}(r,t_0)}{\partial t^k}\right)\bigg|_{t=t_0}\right]. \tag{3.16}$$

So, two different potentials will generate two different densities, meaning that *there is a one-to-one correspondence between the external potential and the density, given in the initial state. Thus, the map in Fig. 3.1 is invertible and the Runge-Gross theorem is demonstrated.*[1]

---
[1] This demonstration holds if the divergence in Eq.(3.16) is different from zero [90].

3.2 The time-dependent KS scheme

The Runge-Gross theorem asserts that given the initial state, any time-dependent observable can be expressed as a unique functional of the time-dependent density. However, like in the case of DFT, the exact functionals are generally unknown. Consequently, a Kohn-Sham (KS) scheme has been introduced to render TDDFT computationally feasible and practical [90]. The TDDFT KS equation is given as follows:

$$\left(-\frac{\nabla^2}{2} + v_{\mathrm{KS}}[n](r,t) \right) \varphi_i^{\mathrm{KS}}(r,t) = i\frac{\partial}{\partial t} \varphi_i^{\mathrm{KS}}(r,t) \,, \tag{3.17}$$

where the time-dependent KS orbitals construct the time-dependent density,

$$n(r,t) = \sum_{i=\mathrm{occ}} |\varphi_i^{\mathrm{KS}}(r,t)|^2 \,. \tag{3.18}$$

The time-dependent KS potential $v_{\mathrm{KS}}(r,t)$ is

$$v_{\mathrm{KS}}[n](r,t) = v_{\mathrm{ext}}[n](r,t) + v_{\mathrm{H}}[n](r,t) + v_{\mathrm{xc}}[n](r,t) \,, \tag{3.19}$$

where

$$v_{\mathrm{H}}[n](r,t) = \int dr' \, \frac{n(r',t)}{|r-r'|} \,, \tag{3.20}$$

and $v_{\mathrm{xc}}[n](r,t)$ is, like in the DFT case, an unknown potential. It is in principle much more complicated than its static equivalent $v_{\mathrm{xc}}[n](r)$, because its dependence is in terms of the densities at all previous times, and in terms of the initial many-body and KS states.

This thesis does not involve TDDFT calculations in real time. However, some ingredients of linear response TDDFT will be used in Chap. 7. We will therefore move directly to the linear response formalism.

3.3 Time-dependent density functional theory in linear response

The linear response polarizability, often denoted as χ, is a vital quantity that encapsulates essential informations about electronic systems, in particular about their optical properties. It contains details about the system's excitation energies and can be used to compute absorption and electron energy loss spectra. In principle, it can be calculated exactly within the TDDFT framework. χ is defined as the linear relation between an external applied potential and the variation of the density,

$$\chi(r_1,t_1; r_2,t_2) = \frac{\delta n(r_1,t_1)}{\delta v_{\mathrm{ext}}(r_2,t_2)} \tag{3.21}$$

$$= \int dr_3 dt_3 \, \frac{\delta n(r_1,t_1)}{\delta v_{\mathrm{KS}}(r_3,t_3)} \frac{\delta v_{\mathrm{KS}}(r_3,t_3)}{\delta v_{\mathrm{ext}}(r_2,t_2)} \,. \tag{3.22}$$

$$\tag{3.23}$$

By using the v_{KS} expression of Eq.(3.19), we obtain

$$\chi(r_1,t_1;r_2,t_2) = \int dr_3 dt_3\, \chi_0^{\text{KS}}(r_1,t_1;r_3,t_3)\bigg(\delta(r_3-r_2)\delta(t_3-t_2) + \int dr_4 dt_4\, v_{\text{c}}(r_3,r_4)\frac{\delta n(r_4,t_4)}{\delta v_{\text{ext}}(r_2,t_2)}$$
$$+ \frac{\delta v_{\text{xc}}[n](r_3,t_3)}{\delta v_{\text{ext}}(r_2,t_2)}\bigg) \tag{3.24}$$

$$= \chi_0^{\text{KS}}(r_1,t_1;r_2,t_2) + \int dr_3 dt_3 dr_4 dt_4\, \chi_0^{\text{KS}}(r_1,t_1;r_3,t_3)\bigg(v_{\text{c}}(r_3,r_4)\chi(r_4,t_4;r_2,t_2)$$
$$+ \frac{\delta v_{\text{xc}}[n](r_3,t_3)}{\delta n(r_4,t_4)}\frac{\delta n(r_4,t_4)}{\delta v_{\text{ext}}(r_2,t_2)}\bigg) \tag{3.25}$$

$$= \chi_0^{\text{KS}}(r_1,t_1;r_2,t_2) + \int dr_3 dt_3 dr_4 dt_4\, \chi_0^{\text{KS}}(r_1,t_1;r_3,t_3)\bigg(v_{\text{c}}(r_3,r_4) \tag{3.26}$$
$$+ f_{\text{xc}}(r_3,t_3;r_4,t_4)\bigg)\chi(r_4,t_4;r_2,t_2)\,,$$

where $\chi_0^{\text{KS}} = \frac{\delta n}{\delta v_{\text{KS}}}$ is the KS non-interacting polarizability and $f_{\text{xc}} = \frac{\delta v_{\text{xc}}}{\delta n}$ is called the exchange-correlation kernel. In a static system χ_0, χ and f_{xc} depend only on a time difference. In frequency space Eq.(3.26) reads

$$\chi(r_1,r_2;\omega) = \chi_0(r_1,r_2;\omega) + \int dr_3 dr_4\, \chi_0(r_1,r_3,)\big(v_{\text{c}}(r_3,r_4) + f_{\text{xc}}(r_3,r_4;\omega)\big)\chi(x_4,x_2;\omega)\,. \tag{3.27}$$

From the polarizability χ, one obtains the inverse dielectric function ϵ^{-1}, defined as

$$\epsilon^{-1}(r_1,r_2;\omega) = \delta(r_1-r_2) + \int dr_3\, v_{\text{c}}(r_1,r_3)\chi(r_3,r_2;\omega)\,, \tag{3.28}$$

which is a key quantity for spectroscopy and in MBPT. The inverse dielectric function also screens the Coulomb interaction, yielding the screened interaction $W = \epsilon^{-1}v_{\text{c}}$.

3.4 f_{xc} kernel in practice

The f_{xc} kernel is a critical quantity of interest, because its knowledge enables the calculation of χ. However, since the exact v_{xc} functionals are unknown, so the f_{xc} is unknown, and approximations are necessary, which leads to approximated χ. The simplest approximation for χ is to use $\chi \approx \chi_0^{\text{KS}}$, relying on independent electronic transitions between the KS orbitals. Unfortunately, this method has shown significant errors when compared to experimental results [4]. Taking a step beyond the independent particle approximation, one can set $f_{\text{xc}} = 0$, resulting in the well-known Random Phase Approximation (RPA), which includes the variation of the Hartree potential upon excitations. However, the RPA is not an efficient method to describe optical properties of solids. Finding feasible and accurate approximations for f_{xc} has been and continues to be a significant challenge. Several approximations have been proposed, including the Adiabatic Local Density Approximation (ALDA), which eliminates frequency dependence and long-range effects [91]. While ALDA provides improvements beyond the

RPA in some cases, it still has limitations, as the long-range effects and frequency dependence are important factors that need to be addressed [49].

While in this thesis we will not propose new f_{xc} for TDDFT, we will propose a link between time-dependent density functional theory and Green's function theory for the determination of total energies. This will be discussed in Chap. 7.

Chapter 4

Many-Body Green's function methods

As pointed out in the previous chapters, in theoretical condensed matter physics, the focus is often on obtaining observables and properties of materials without relying on the explicit knowledge of the full many-body wavefunction. This is because the wavefunction becomes prohibitively large and difficult to handle for systems with a large number of particles [92]. Therefore, the challenge lies in finding alternative methods that can provide accurate and reliable predictions for observables and properties using more tractable quantities. One such approach is to work within the framework of Density Functional Theory (DFT) (see Chap. 2) and its time-dependent extension (TDDFT) (see Chap. 3), which use instead of the full many-body wavefunction the electron one-body density as the central quantity, defined below in terms of the field operators at zero-temperature T $= 0$ K and in equilibrium:

$$n(x) = \langle N_0 | \hat{\psi}^\dagger(x) \psi(x) | N_0 \rangle \, , \tag{4.1}$$

where $|N_0\rangle$ is the many-body wavefunction in the ground-state for N electrons. x stands for position r and spin σ. $\hat{\psi}$ and $\hat{\psi}^\dagger$ are the annihilation and creation field operators, respectively. They can be expanded in a single-particle basis $\phi_i(x)$,

$$\hat{\Psi}(x) = \sum_i \phi_i(x) \hat{c}_i \, , \tag{4.2}$$

and

$$\hat{\Psi}^\dagger(x) = \sum_i \phi_i^*(x) \hat{c}_i^\dagger \, . \tag{4.3}$$

It is important to note that these operators satisfy the same commutation relations as the operators $\hat{c}_i^\dagger$ and $\hat{c}_i$, so we have

$$\left\{ \hat{\Psi}(x), \hat{\Psi}(x') \right\} = 0 \, , \tag{4.4}$$

$$\left\{ \hat{\Psi}^\dagger(x), \hat{\Psi}^\dagger(x') \right\} = 0 \, , \tag{4.5}$$

$$\left\{ \hat{\Psi}(x), \hat{\Psi}^\dagger(x') \right\} = \delta(x - x') \, . \tag{4.6}$$

As discussed in Chap.2, DFT has been successful in describing ground-state properties of materials by approximating the unknown exchange-correlation energy functional. However, developments in DFT

are often difficult due to our ignorance of the exchange-correlation potential (v_{xc}) as well as the lack of knowledge about how some observables or other important quantities can be written in terms of the density. For instance, we do not know how the exchange energy can be written in terms of the density. Therefore, we need to move on and define other objects than can be used as central quantities to find observables. Another possible object is the spin-resolved one-body density-matrix defined as follows,

$$\gamma(x, x') = \langle N_0 | \hat{\psi}^\dagger(x') \psi(x) | N_0 \rangle \ , \tag{4.7}$$

which is non-local in space and spin coordinates. It is possible to write explicitly the exchange energy in terms of γ. However, the quantities n and γ are static quantities (local in time and time independent in equilibrium) that do not capture the internal time-dependent behavior of the system. It is therefore difficult to describe quantities that depend on the internal temporal evolution or frequency-dependent properties, in particular spectra. *Thus, the need for a time non-local object that incorporates temporal aspects of a system is obvious.*

4.1 Why are Green's functions important?

The object that we are looking for, which besides the non-locality in space and spin is non-local in time, is the time-ordered one-body Green's function (1-GF), defined at T $= 0$ K as

$$G(1, 2) = -i \langle N_0 | \hat{T} \big[\hat{\psi}(1) \hat{\psi}^\dagger(2) \big] | N_0 \rangle \tag{4.8}$$

$$= -i\theta(t_1 - t_2) \langle N_0 | \hat{\psi}(1) \hat{\psi}^\dagger(2) | N_0 \rangle + i\theta(t_2 - t_1) \langle N_0 | \hat{\psi}^\dagger(2) \hat{\psi}(1) | N_0 \rangle \ , \tag{4.9}$$

where $1 = x_1, t_1$ and $2 = x_2, t_2$. $\hat{T}$ is the time-ordering operator and θ is the heaviside function. The 1-GF, which is non-local in space, spin and time, describes the propagation of an electron (or hole) from a space-spin-time point to another. At equilibrium, the 1-GF depends only on the time difference $t_1 - t_2$. Its frequency Fourier transform reads

$$G(x, x'; \omega) = \sum_s \left[\frac{\langle N_0 | \hat{\Psi}^\dagger(x') | N-1 \rangle_s \langle N-1 |_s \hat{\Psi}(x) | N_0 \rangle}{\omega - (\text{E}_0^N - \text{E}_s^{N-1}) - i\eta} + \frac{\langle N_0 | \hat{\Psi}(x) | N+1 \rangle_s \langle N+1 |_s \hat{\Psi}^\dagger(x') | N_0 | \rangle}{\omega - (\text{E}_s^{N+1} - \text{E}_0^N) + i\eta} \right] , \tag{4.10}$$

where $|N-1\rangle_s$ and $|N+1\rangle_s$ are the many-body states for $N-1$ and $N+1$ electrons, respectively. The $\sum_s$ stands for the sum over all possible states, including ground and excited states, whereas $|N_0\rangle$ remains the ground-state wavefunction since T $= 0$ K. The poles of the 1-GF in Eq.(4.10) have a significant implication. These poles correspond to the energy differences between systems with N and $N-1$ electrons, as well as between systems with N and $N+1$ electrons. These energies are directly related to the measured energies in the photoemission spectrum. It establishes a direct connection between experiment and the integrated spectral function of the 1-GF expressed as

$$A(\omega) = \frac{1}{\pi}|\int dx \, \text{Im}\big(G(x,x;\omega)\big)| \tag{4.11}$$

$$= \sum_s \langle N_0|\hat{\Psi}^\dagger(x')\,|N-1\rangle_s \,\langle N-1|_s\,\hat{\Psi}(x)|N_0\rangle\, \delta(\omega - (\text{E}_0^N - \text{E}_s^{N-1})) \tag{4.12}$$

$$+ \sum_s \langle N_0|\hat{\Psi}(x)\,|N+1\rangle_s \,\langle N+1|_s\hat{\Psi}^\dagger(x')|N_0|\rangle\, \delta(\omega - (\text{E}_s^{N+1} - \text{E}_0^N))\,.$$

In practice one of the main purposes of using the 1-GF is to access the band structure informations of materials [93]. However, many more observables can be written in terms of the 1-GF, such as the one-body density $n(x) = -iG(x,t;x,t^+)$, density-matrix $\gamma(x,x') = -iG(x,t;x',t^+)$ and total energy. The main interest of this thesis is ground-state total energy (E_0) calculations using Green's functions. Among the different possibilities that link E_0 with the 1-GF, we use the Galitskii-Migdal [94] expression, written as the following,

$$\text{E}_0 = \frac{1}{2} \lim_{x'\to x, t'\to t^+} \int dx \left(\frac{\partial}{\partial t} - ih(x)\right) G(x,t;x',t')\,, \tag{4.13}$$

where h is the one-body hamiltonian including the kinetic energy and the external potential. Another way to write E_0 in terms of the 1-GF with explicitly appearing self-energy (the self-energy will be discussed in the next chapter) is also used in this thesis, particularly in Chap. 7. Both expressions of E_0 are derived in App. C.

The significance of the 1-GF is due to its ability to provide a wealth of observables. However, this relies on the knowledge of the 1-GF, which itself relies on the knowledge of the many-body wavefunctions $|N-1\rangle$, $|N_0\rangle$ and $|N+1\rangle$ as shown in Eq.(4.10). This is absolutely useless, since it does not avoid the many-body wavefunction calculations: it even requires calculations for many many-body wavefunctions including a set of excited states. Hence, alternative methods are necessary to calculate the 1-GF, making it essential to address the question: how do we get the 1-GF, by avoiding the many-body wavefunctions? This question will be discussed in Sec. 4.2.

4.2 The equation of motion for the Green's function

The way to make the 1-GF calculation independent from the many-body wavefunctions, *is via deriving an equation of motion for the 1-GF*. In this section, we derive in detail the 1-GF equation of motion. So, we begin by introducing the second quantization version of the exact hamiltonian in terms of field operators:

$$\hat{H} = \underbrace{\int dx \, \hat{\Psi}^\dagger(x)h(x)\hat{\Psi}(x)}_{\hat{H}_1} + \underbrace{\frac{1}{2}\int dxdx' \, \hat{\Psi}^\dagger(x)\hat{\Psi}^\dagger(x')v_\text{c}(x,x')\hat{\Psi}(x')\hat{\Psi}(x)}_{\hat{H}_2}\,, \tag{4.14}$$

where $\hat{H}_1$ and $\hat{H}_2$ are the one-body and two-body operators, respectively. We derive the 1-GF expression defined in Eq.(4.9) with respect to the time t,

$$\frac{\partial G(x,t;x',t')}{\partial t} = -i\langle N_0|\frac{\partial \hat{\Psi}(x,t)}{\partial t}\hat{\Psi}^\dagger(x',t')|N_0\rangle\,\theta(t-t') - i\langle N_0|\hat{\Psi}(x,t)\hat{\Psi}^\dagger(x',t')|N_0\rangle\,\frac{\partial\theta(t-t')}{\partial t}$$
$$+ i\langle N_0|\hat{\Psi}^\dagger(x',t')\frac{\partial\hat{\Psi}(x,t)}{\partial t}|N_0\rangle\,\theta(t'-t) + i\langle N_0|\hat{\Psi}^\dagger(x',t')\hat{\Psi}(x,t)|N_0\rangle\,\frac{\partial\theta(t'-t)}{\partial t}\,. \quad (4.15)$$

By using the following definition of the field operator evolution within the Heisenberg scheme,

$$\frac{\partial\hat{\Psi}(x,t)}{\partial t} = ie^{i\hat{H}t}\big[\hat{H},\hat{\Psi}(x)\big]e^{-i\hat{H}t} \quad (4.16)$$
$$= i\big[\hat{H},\hat{\Psi}^\dagger(x,t)\big] \quad (4.17)$$
$$= -ie^{i\hat{H}t}\big[\hat{\Psi}(x),\hat{H}\big]e^{-i\hat{H}t}\,, \quad (4.18)$$

where

$$\hat{\Psi}(x,t) = e^{i\hat{H}t}\hat{\Psi}(x)e^{-i\hat{H}t}\,, \quad (4.19)$$

we obtain

$$\frac{\partial G(x,t;x',t')}{\partial t} = -\langle N_0|\big[\hat{\Psi}(x,t),\hat{H}\big]\hat{\Psi}^\dagger(x',t')|N_0\rangle\,\theta(t-t') - i\langle N_0|\hat{\Psi}(x)\hat{\Psi}^\dagger(x')|N_0\rangle\,\delta(t-t')$$
$$+ \langle N_0|\hat{\Psi}^\dagger(x',t')\big[\hat{\Psi}(x,t),\hat{H}\big]|N_0\rangle\,\theta(t'-t) - i\langle N_0|\hat{\Psi}^\dagger(x')\hat{\Psi}(x)|N_0\rangle\,\delta(t-t')\,. \quad (4.20)$$

Then, by using the anticommutation relations, defined in Eq.(4.6), in the last term in Eq.(4.20), we obtain

$$\frac{\partial G(x,t,x',t')}{\partial t} = -i\delta(x-x')\delta(t-t') - \langle N_0|\big[\hat{\Psi}(x,t),\hat{H}\big]\hat{\Psi}^\dagger(x',t')|N_0\rangle\,\theta(t-t')$$
$$+ \langle N_0|\hat{\Psi}^\dagger(x',t')\big[\hat{\Psi}(x,t),\hat{H}\big]|N_0\rangle\,\theta(t'-t)\,. \quad (4.21)$$

Now, we divide the calculation of the hamiltonian Eq.(4.14) and the field operator commutators into two steps. We first start with the $\hat{H}_1$ part of Eq.(4.14)

$$\big[\hat{\Psi}(x),\hat{H}_1\big] = \int dy\,\hat{\Psi}(x)\hat{\Psi}^\dagger(y)h(y)\hat{\Psi}(y) - \int dy\,\hat{\Psi}^\dagger(y)h(y)\hat{\Psi}(y)\hat{\Psi}(x) \quad (4.22)$$
$$= \int dy\,h(y)\hat{\Psi}(y)\delta(x-y) - \int dy\,\hat{\Psi}^\dagger(y)\hat{\Psi}(x)h(y)\hat{\Psi}(y) + \int dy\,\hat{\Psi}^\dagger(y)h(y)\hat{\Psi}(x)\hat{\Psi}(y) \quad (4.23)$$
$$= h(x)\hat{\Psi}(x) - \underbrace{\int dy\,\hat{\Psi}^\dagger(y)\big[\hat{\Psi}(x),h(y)\big]\hat{\Psi}(y)}_{0}\,, \quad (4.24)$$

and,

$$\big[\hat{\Psi}(x),\hat{H}_2\big] = \int dy\,\hat{\Psi}^\dagger(y)v_{\rm c}(x,y)\hat{\Psi}(y)\hat{\Psi}(x) + \underbrace{\frac{1}{2}\int dydz\,\hat{\Psi}^\dagger(z)\hat{\Psi}^\dagger(y)[\hat{\Psi}(x),v_{\rm c}(y,z)]\hat{\Psi}(y)\hat{\Psi}(z)}_{0}\,. \quad (4.25)$$

Thus, we obtain

$$\big[\hat{\Psi}(x),\hat{H}\big] = h(x)\hat{\Psi}(x) + \int dy\,\hat{\Psi}^\dagger(y)v_{\rm c}(x,y)\hat{\Psi}(y)\hat{\Psi}(x)\,. \quad (4.26)$$

So, with this, Eq.(4.21) becomes

$$\frac{\partial G(x,t;x',t')}{\partial t} = -i\delta(x-x')\delta(t-t') - \langle N_0 | e^{i\hat{H}t} \left[h(x) + \int dy\, \hat{\Psi}^\dagger(y) v_c(x,y) \hat{\Psi}(y) \right]$$

$$\hat{\Psi}(x) e^{-i\hat{H}t} \hat{\Psi}^\dagger(x',t') |N_0\rangle\, \theta(t-t')$$

$$+ \langle N_0 | \hat{\Psi}^\dagger(x',t') e^{i\hat{H}t} \left[h(x) + \int dy\, \hat{\Psi}^\dagger(y) v_c(x,y) \hat{\Psi}(y) \right] \hat{\Psi}(x) e^{-i\hat{H}t} |N_0\rangle\, \theta(t'-t)\,, \quad (4.27)$$

which can be written as

$$\frac{\partial G(x,t,x',t')}{\partial t} = -i\delta(x-x')\delta(t-t') - \langle N_0 | \hat{\Psi}(x,t) h(x) \hat{\Psi}^\dagger(x',t') |N_0\rangle\, \theta(t-t')$$

$$+ \langle N_0 | \hat{\Psi}^\dagger(x',t') \hat{\Psi}(x,t) \hat{h}(x) |N_0\rangle\, \theta(t'-t)$$

$$- \int dy\, v_c(x,y) \Bigg[\langle N_0 | e^{i\hat{H}t} \hat{\Psi}^\dagger(y) \hat{\Psi}(y) \hat{\Psi}(x) e^{-i\hat{H}t} \hat{\Psi}^\dagger(x',t') |N_0\rangle\, \theta(t-t') -$$

$$\langle N_0 | \hat{\Psi}^\dagger(x',t') e^{i\hat{H}t} \hat{\Psi}^\dagger(y) \hat{\Psi}(y) \hat{\Psi}(x) e^{-i\hat{H}t} |N_0\rangle\, \theta(t'-t) \Bigg]. \quad (4.28)$$

By using Eq.(4.19) in Eq.(4.28), we obtain

$$\frac{\partial G(x,t,x',t')}{\partial t} = -i\delta(x-x')\delta(t-t') + h(x) \Bigg[-\langle N_0 | \hat{\Psi}(x,t) \hat{\Psi}^\dagger(x',t') |N_0\rangle\, \theta(t-t')$$

$$+ \langle N_0 | \hat{\Psi}^\dagger(x',t') \hat{\Psi}(x,t) |N_0\rangle\, \theta(t'-t) \Bigg]$$

$$- \int dy\, v_c(x,y) \Bigg[\langle N_0 | \hat{\Psi}^\dagger(y,t) \hat{\Psi}(y,t) \hat{\Psi}(x,t) \hat{\Psi}^\dagger(x',t') |N_0\rangle\, \theta(t-t')$$

$$- \langle N_0 | \hat{\Psi}^\dagger(x',t') \hat{\Psi}^\dagger(y,t) \hat{\Psi}(y,t) \hat{\Psi}(x,t) |N_0\rangle\, \theta(t'-t) \Bigg]. \quad (4.29)$$

Finally, we obtain the equation of motion for the 1-GF as

$$\frac{\partial G(x,t,x',t')}{\partial t} = -i\delta(x-x')\delta(t-t') - ih(x)G(x,t,x',t') - \int dy\, v_c(x,y) G_2(x,t,y,t^+;x',t',y,t^{++})\,,$$
$$(4.30)$$

where $t^+ = t + \eta$ and $\eta \longrightarrow 0$. G_2 is two-body Green's function (2-GF), defined as follows:

$$G_2(x_1,t_1,x_2,t_2;x_3,t_3,x_4,t_4) = (-i^2) \langle N | \hat{T} \big[\hat{\Psi}(x_1,t_1) \hat{\Psi}(x_2,t_2) \hat{\Psi}^\dagger(x_4,t_4) \hat{\Psi}^\dagger(x_3,t_3) | N \rangle\,. \quad (4.31)$$

In a more compact notation, we write

$$\left(\frac{\partial}{\partial t_1} - h(1) \right) G(1,2) + i \int d3\, v_c(1,3) G_2(1,3^+;2,3^{++}) = \delta(1,2)\,, \quad (4.32)$$

where $1 = x_1, t_1$ and $v_c(1,3) = v_c(x_1,x_3)\delta(t_1-t_3)$. *The equation of motion for the 1-GF derived in this section, as shown in Eq.(4.32), cannot be solved directly due to the appearance of the 2-GF. If we attempt to write an equation of motion for the 2-GF, it would involve the three-body Green's function (3-GF), leading to a series of equations called Martin-Schwinger hierarchy [95] with no analytical solution.* In the next chapter, we discuss how to overcome this.

On the other hand, it is worth noting that for small systems, one can use exact diagonalization (ED), where it is possible to calculate the many-body states. This is what we do for the Hubbard dimer model Chap. 6. For still relatively simple systems, and on the imaginary frequency axis at non-vanishing temperature, one can use quantum Monte Carlo (QMC) [96]. Another way is to use dynamical mean field theory (DMFT) that uses high-level approaches such as ED or QMC for a small model system, and that then uses the result to reconstruct the 1-GF of more complex systems [97]. In this thesis, the framework of choice is instead many-body perturbation theory (MBPT).

Chapter 5

Many-Body Perturbation Theory and GW approximation

As discussed in the previous chapter, the equation of motion for the 1-GF does not have an analytical solution due to the appearance of the 2-GF, which arises from the Coulomb interaction coupling. This presents a challenge in solving the electronic problem directly. To address this challenge, in this thesis we employ the many-body perturbation theory (MBPT) approach, which *involves starting from an independent-particle problem and treating the Coulomb interaction as a perturbation.* The usual way is to expand the time evolution operator in the interaction picture in terms of the Coulomb interaction. Here, we follow an approach based on functional derivatives. The idea is to describe a system by probing its reaction to an external perturbation [95, 98, 99]. So, we define below the interaction hamiltonian that depends on external potential (which will be taken to zero at the end) and which will be added to the many-body hamiltonian in Eq.(4.14),

$$\hat{H}'(t) = \int dx dx' \, \hat{\Psi}^\dagger(x) v_{\text{ext}}(x,t) \hat{\Psi}(x') \,. \tag{5.1}$$

Since the time-dependent field operators are given in Heisenberg scheme as Eq.(4.19), we similarly can write the interaction hamiltonian as follows:

$$\hat{H}'_I(t) = e^{i\hat{H}t} \hat{H}'(t) e^{-i\hat{H}t} = \int dx dx' \, \hat{\Psi}^\dagger(x,t^+) v_{\text{ext}}(x,t) \hat{\Psi}(x',t) \,. \tag{5.2}$$

When a time-dependent external potential is applied and the system is therefore out of equilibirium [100], the 1-GF will be defined as the following,

$$G(x,t;x',t') = -i \frac{\langle N_0 | \hat{T} \left[\hat{S} \hat{\Psi}(x,t) \hat{\Psi}^\dagger(x',t') \right] | N_0 \rangle}{\langle N_0 | \hat{T}[\hat{S}] | N_0 \rangle} \,, \tag{5.3}$$

where $\hat{S}$ is the operator that takes the system from the ground-state to the perturbed one due to external potential. $\hat{S}$ reads

$$\hat{S} = e^{-i \int_{-\infty}^{+\infty} dt \hat{H}'_I(t)} \,. \tag{5.4}$$

In the following sections, we will present two different derivations within MBPT, one involving a local external potential and the other a non-local external potential. This is because, during this

thesis, the time non-locality of the external potential was a crucial factor, especially when dealing with total energy calculations. In such cases, considering infinitesimal time differences, such as t^+, and t^{++}, becomes highly important as this can influence the results by altering the contour of integration. Therefore, we emphasize the presentation of both derivations. We aim to provide a comprehensive account of this journey in detail. The subtleties of using a time non-local external potential are discussed in [101].

5.1 Derivation of many-body perturbation theory in terms of a local external potential

We start by deriving the 1-GF with respect to the local external potential. So, the 1-GF derivative is proportional to the operator $\hat{S}$ derivative as follows:

$$\frac{\delta G(x,t;x',t')}{\delta v_{\text{ext}}(y,t'')} \longrightarrow \frac{\delta \hat{S}}{\delta v_{\text{ext}}(y,t'')} \longrightarrow \int_{t_1}^{t_2} d\tau \int dz\, \delta(\tau - t'')\delta(y-z)\frac{\partial}{\partial v_{\text{ext}}(z,\tau)}\big[\hat{\Psi}^\dagger(z,\tau)v_{\text{ext}}(z,\tau)$$
$$\hat{\Psi}(z,\tau)\big]\hat{S} \longrightarrow \hat{\Psi}^\dagger(y,t''^+)\hat{\Psi}(y,t'')\hat{S}\,. \quad (5.5)$$

Therefore, we obtain

$$\frac{\delta G(x,t;x',t')}{\delta v_{\text{ext}}(y,t'')} = -i\frac{\langle N_0|\hat{T}\big[\frac{\delta\hat{S}}{\delta v_{\text{ext}}(y,t'')}\hat{\Psi}(x,t)\hat{\Psi}^\dagger(x',t')\big]|N_0\rangle}{\langle N_0|\hat{T}[\hat{S}]|N_0\rangle}$$
$$+ i\frac{\langle N_0|\hat{T}\frac{\delta\hat{S}}{\delta v_{\text{ext}}(y,t'')}|N_0\rangle \langle N_0|\hat{T}\big[\hat{S}\hat{\Psi}(x,t)\hat{\Psi}^\dagger(x',t')\big]|N\rangle}{\langle N_0|\hat{T}[\hat{S}]|N_0\rangle}\,, \quad (5.6)$$

where by using Eq.(5.5), we obtain

$$\frac{\delta G(x,t;x',t')}{\delta v_{\text{ext}}(y,t'')} = -i\frac{\langle N_0|\hat{T}\big[-i\hat{\Psi}^\dagger(y,t''^+)\hat{\Psi}(y,t'')\hat{S}\hat{\Psi}(x,t)\hat{\Psi}^\dagger(x',t')\big]|N_0\rangle}{\langle N_0|\hat{T}[\hat{S}]|N_0\rangle}$$
$$+ i\frac{\langle N_0|\hat{T}\big[-i\hat{\Psi}^\dagger(y,t''^+)\hat{\Psi}(y,t'')\hat{S}\big]|N_0\rangle \langle N_0|\hat{T}\big[\hat{S}\hat{\Psi}(x,t)\hat{\Psi}^\dagger(x',t')\big]|N_0\rangle}{\langle N_0|\hat{T}[\hat{S}]|N_0\rangle^2}\,. \quad (5.7)$$

By taking the external potential to zero, $\hat{S} \to 1$, and we have

$$\frac{\delta G(x,t;x',t')}{\delta v_{\text{ext}}(y,t'')} = (-i)^2\,\langle N_0|\hat{T}\big[\hat{\Psi}^\dagger(y,t''^+)\hat{\Psi}(y,t'')\hat{\Psi}(x,t)\hat{\Psi}^\dagger(x',t')\big]|N_0\rangle$$
$$+ i\,\langle N_0|\hat{T}\big[-i\hat{\Psi}^\dagger(y,t''^+)\hat{\Psi}(y,t'')\big]|N_0\rangle \langle N_0|\hat{T}\big[\hat{\Psi}(x,t)\hat{\Psi}^\dagger(x',t')\big]|N_0\rangle\,. \quad (5.8)$$

So, finally we obtain

$$\frac{\delta G(x,t;x',t')}{\delta v_{\text{ext}}(y,t^+)} = -G_2(y,t^+,x,t;y,t^{++},x',t') + G(x,x';t,t')G(y,t^+;y,t^{++})\,, \quad (5.9)$$

which is a direct relation between the 1-GF and the 2-GF. This can be used in Eq.(4.32) to obtain an equation of motion that depends only on the 1-GF. It reads

$$\frac{\partial G(x,t;x',t')}{\partial t} = -i\delta(x-x')\delta(t-t') - iG(x,t,x',t')h(x) + \int dy\, v_{\mathrm{c}}(x,y)\frac{\delta G(x,t;x',t')}{\delta v_{\mathrm{ext}}(y,t^+)}$$

$$- \int dy\, v_{\mathrm{c}}(x,y)G(y,t^+;y,t^{++})G(x,t;x',t'). \quad (5.10)$$

We can already recognize the last term in Eq.(5.10), which is the Hartree potential v_{H} since, as pointed out in Chap. 4, the 1-GF $G(1,2)$ at equal time $t_2 \to t_1^+$ is proportional to the density. Therefore, we have

$$\left(i\frac{\partial}{\partial t} - h(x,t) - v_{\mathrm{H}}(x,t) - i\int dy\, v_{\mathrm{c}}(x,y)\frac{\delta}{\delta v_{\mathrm{ext}}(y,t^+)}\right)G(1,2) = \delta(1,2)\,. \quad (5.11)$$

5.1.1 The exchange-correlation self-energy

We write down again Eq.(5.11) by changing arguments,

$$\left(i\frac{\partial}{\partial t} - h(1) - v_{\mathrm{H}}(1)\right)G(1,2) - i\int dx_3 dt_3\, v_{\mathrm{c}}(x_1,x_3)\delta(t_1^+ - t_3)\frac{\delta G(1,2)}{\delta v_{\mathrm{ext}}(3)} = \delta(1,2) \quad (5.12)$$

$$\left(i\frac{\partial}{\partial t} - h(1) - v_{\mathrm{H}}(1)\right)G(1,2) - i\int d3\, v_{\mathrm{c}}(1^+,3)\frac{\delta G(1,2)}{\delta v_{\mathrm{ext}}(3)} = \delta(1,2)\,. \quad (5.13)$$

In order to find an expression for $\frac{\delta G(1,2)}{\delta v_{\mathrm{ext}}(3)}$ in terms of G^{-1}, we do the following:

$$\frac{\delta G(1,2)}{\delta v_{\mathrm{ext}}(3)} = \int d(4)\frac{\delta G(1,4)}{\delta v_{\mathrm{ext}}(3)}\delta(4,2)\,, \quad (5.14)$$

where by using

$$\int d3\, G^{-1}(1,3)G(3,2) = \int d3\, G(1,3)G^{-1}(3,2) = \delta(1,2)\,, \quad (5.15)$$

we have

$$\frac{\delta G(1,2)}{\delta v_{\mathrm{ext}}(3)} = \int d4\, \frac{\delta G(1,4)}{\delta v_{\mathrm{ext}}(3)}\delta(4,2) \quad (5.16)$$

$$= \int d(45)\, \frac{\delta G(1,4)}{\delta v_{\mathrm{ext}}(3)}G^{-1}(4,5)G(5,2) \quad (5.17)$$

$$= -\int d(45)\, G(1,4)\frac{\delta G^{-1}(4,5)}{\delta v_{\mathrm{ext}}(3)}G(5,2)\,. \quad (5.18)$$

This yields the equation of motion,

$$\left(i\frac{\partial}{\partial t_1} - h(1) - v_{\mathrm{H}}(1)\right)G(1,2) + i\int d(345)\, v_{\mathrm{c}}(1^+,3)G(1,4)\frac{\delta G^{-1}(4,5)}{\delta v_{\mathrm{ext}}(3)}G(5,2) = \delta(1,2)\,. \quad (5.19)$$

The advantage of transforming $\frac{\delta G}{\delta v_{\mathrm{ext}}}$ to $\frac{\delta G^{-1}}{\delta v_{\mathrm{ext}}}$ in the equation of motion is the fact that this introduces direct derivations of the effective potential contained in G^{-1} with respect to v_{ext}, since G^{-1} is

$$G^{-1}(1,2) = \left(i\frac{\partial}{\partial t_1} + \frac{\nabla_{r_1}^2}{2} - v_{\mathrm{ext}}(1,2)\delta(1,2) - v_{\mathrm{H}}(1,2)\delta(1,2)\right) - \Sigma_{\mathrm{xc}}(1,2)\,, \quad (5.20)$$

where Σ_{xc} is the exchange-correlation self-energy that contains all the many-body quantum effects acting on the motion of a particle (electron or hole). Σ_{xc} is defined as

$$\Sigma_{xc}(1,5) = -i \int d(34) \, v_{\text{c}}(1^+,3) G(1,4) \frac{\delta G^{-1}(4,5)}{\delta v_{\text{ext}}(3)} \,. \tag{5.21}$$

Hence, the equation of motion in terms of Σ_{xc} is

$$\left(i\frac{\partial}{\partial t_1} - h(1) - v_{\text{H}}(1) \right) G(1,2) - \int d3 \, \Sigma_{\text{xc}}(1,3) G(3,2) = \delta(1,2) \,. \tag{5.22}$$

5.1.2 The Dyson equation

In the following, we will derive the Dyson equation, which provides an alternative formulation of the equation of motion for the 1-GF in a simpler and more practical form. So, starting from Eq.(5.22), the derivation proceeds as follows:

$$\int d3 \, \delta(1,3) \left(i\frac{\partial}{\partial t_3} - h(3) \right) G(3,2) - \int d3 \left(v_{\text{H}}(1,3)\delta(1,3) + \Sigma_{\text{xc}}(1,3) \right) G(3,2) = \delta(1,2) \tag{5.23}$$

$$\int d3 \left(G_0^{-1}(1,3) - \Sigma(1,3) \right) G(3,2) = \delta(1,2) \tag{5.24}$$

$$\int d(23) \left(G_0^{-1}(1,3) - \Sigma(1,3) \right) G(3,2) G^{-1}(2,4) = \int d2 \, \delta(1,2) G^{-1}(2,4) \tag{5.25}$$

$$G_0^{-1}(1,4) - \Sigma(1,4) = G^{-1}(1,4) \,, \tag{5.26}$$

where $\Sigma = v_{\text{H}} + \Sigma_{\text{xc}}$ and G_0 is the non-interacting 1-GF with G_0^{-1} defined as

$$G_0^{-1}(1,3) = \delta(1,3) \left(i\frac{\partial}{\partial t_3} - h(3) \right) \,. \tag{5.27}$$

Then, we complete the derivation starting from Eq.(5.26) as

$$\int d1 \, G_0(2,1) G_0^{-1}(1,4) - \int d1 \, G_0(2,1) \Sigma(1,4) = \int d1 \, G_0(2,1) G^{-1}(1,4) \tag{5.28}$$

$$\delta(2,4) - \int d1 \, G_0(2,1) \Sigma(1,4) = \int d1 \, G_0(2,1) G^{-1}(1,4) \tag{5.29}$$

$$\int d4 \, \delta(2,4) G(4,3) - \int d(14) \, G_0(2,1) \Sigma(1,4) G(4,3) = \int d(14) \, G_0(2,1) G^{-1}(1,4) G(4,3) \tag{5.30}$$

$$G(2,3) - \int d(14) \, G_0(2,1) \Sigma(1,4) G(4,3) = G_0(2,3) \,, \tag{5.31}$$

So, finally the Dyson equation is

$$G(1,2) = G_0(1,2) + \int d(34) \, G_0(1,3) \Sigma(3,4) G(4,2) \,. \tag{5.32}$$

It provides a direct relation between the non-interacting 1-GF and the interacting one.

5.2 Derivation of many-body perturbation theory in terms of a non-local external potential

Up to here, in this chapter we have only transformed expressions involving the 1-GF. However, in this thesis response functions play a crucial role. They are based on the 2-GF. In order to include the full 2-GF, which contains 4 space-spin-time arguments, a space and time non-local potential is needed.

5.2.1 The non-locality in the Hartree potential

Using a non-local external potential in the hamiltonian, the relation in Eq.(5.9) becomes

$$L(1,2,3,4) = G(1,3)G(2,4) - G_2(1,2,3,4), \tag{5.33}$$

where $L(1,2,3,4) = \frac{\delta G(1,3)}{v_{\text{ext}}(4,2)}$. *This generalization has important consequences. During this thesis, we have found that taking this properly into account is necessary in order to derive the expressions for the total energy in a clean way. One can appreciate this by deriving the Dyson equation of the reducible polarizability $\chi(1,2)$ that yields the density change due to a local external potential, and that can, for example, be calculated in TDDFT (see Chap. 3), from the Green's function framework:*

$$\chi(1,2) = \frac{\delta n(1)}{\delta v_{\text{ext}}(2)} \tag{5.34}$$

$$= \int d3 \, \frac{\delta n(1)}{\delta v_{\text{cl}}(3)} \frac{\delta v_{\text{cl}}(3)}{\delta v_{\text{ext}}(2)} \tag{5.35}$$

$$= \int d3 \, \frac{\delta n(1)}{\delta v_{\text{cl}}(3)} \frac{\delta}{\delta v_{\text{ext}}(2)} \left(v_{\text{ext}}(3) + v_{\text{H}}(3) \right) \tag{5.36}$$

$$= P(1,2) + \int d(34) \, P(1,3) v_{\text{c}}(3,4)\chi(4,2), \tag{5.37}$$

where $v_{\text{cl}} = v_{\text{ext}} + v_{\text{H}}$ is the total classical potential and P is the irreducible polarizability $\frac{\delta n}{\delta v_{\text{cl}}}$. To find a similar equation in the Green's function framework, we use the link between the density and the 1-GF,

$$\chi(1,2) = -i\frac{\delta G(1,1^+)}{\delta v_{\text{ext}}(2^+,2)} \tag{5.38}$$

$$= -i \int d(34) \, \frac{\delta G(1,1^+)}{v_{\text{cl}}(3,4)} \frac{\delta v_{\text{cl}}(3,4)}{\delta v_{\text{ext}}(2^+,2)} \tag{5.39}$$

$$= -i \int d(34) \, \frac{\delta G(1,1^+)}{\delta v_{\text{cl}}(34)}\delta(3,2^+)\delta(2,4) - i \int d(34) \, \frac{\delta G(1,1^+)}{\delta v_{\text{cl}}(3,4)} \frac{\delta v_{\text{H}}(34)}{v_{\text{ext}}(2^+,2)} \tag{5.40}$$

$$= -i\frac{\delta G(1,1^+)}{\delta v_{\text{cl}}(2^+,2)} - i \int d(34) \, \frac{\delta G(1,1^+)}{\delta v_{\text{cl}}(3,4)} \frac{\delta v_{\text{H}}(3,4)}{v_{\text{ext}}(2^+,2)}. \tag{5.41}$$

Here for consistency, we have to suppose that all potentials, including v_H, are non-local. The correct Dyson equation for χ is obtained if the generalized v_H is defined as

$$v_\mathrm{H}(3,4) = -i \int d5 \, \delta(3,4^+) v_\mathrm{c}(4,5) G(5,5^+) \tag{5.42}$$

$$= -i \int d(56) \, \delta(3,4^+) v_\mathrm{c}(4,6) \delta(6,5^+) G(5^+,5^{++}) \tag{5.43}$$

$$= -i \int d(56) \, V(3,4,6,5) G(5^+,5^{++}) \,. \tag{5.44}$$

With this, we have

$$\chi(1,2) = P(1,2) - i \int d(345) \frac{\delta G(1,1^+)}{\delta v_\mathrm{cl}(3,4)} \delta(3,4^+) v_\mathrm{c}(4,5) \frac{-i\delta G(5,5^+)}{\delta v_\mathrm{ext}(2^+,2)} \tag{5.45}$$

$$= P(1,2) + \int d(45) \, P(1,4) v_\mathrm{c}(4,5) \chi(5,2) \,, \tag{5.46}$$

which is the same as Eq.(5.37). As one can see from Eq.(5.44), we have to introduce the generalized Coulomb interaction

$$V(3,4,6,5) = \delta(3,4^+) v_\mathrm{c}(4,6) \delta(6,5^+) \,. \tag{5.47}$$

Otherwise, Eq.(5.46) will not be equal to Eq.(5.37).

5.2.2 The Dyson equation of the Green's function

The equation of motion of the 1-GF derived in the previous Chapter in Eq.(4.32), using the generalized interaction V in terms of G_2, reads [4]

$$G(1,2) = G_0(1,2) - i \int d(34) \, G_0(1,3) v_\mathrm{c}(3,4) G_2(3,4^+,2,4^{++}) \,, \tag{5.48}$$

This equation, however, was derived for a time-local potential and has to be changed for our purpose. Such a 4-argument Coulomb interaction has already been introduced in Ref. [101] in conjunction with time non-local potentials. Indeed, let us first derive the Hartree potential expression from the Dyson equation in Eq.(5.48) by using the relation between G_2 and L in Eq.(5.33):

$$G_\mathrm{H}(1,2) = G_0(1,2) - i \int d(34) \, G_0(1,3) v_\mathrm{c}(3,4) G_2^H(3,4^+,2,4^{++}) \tag{5.49}$$

$$= G_0(1,2) - i \int d(34) \, G_0(1,3) v_\mathrm{c}(3,4) G(4^+,4^{++}) G(3,2) \tag{5.50}$$

$$= G_0(1,2) + \int d3 \, G_0(1,3) \int d4(-i) v_\mathrm{c}(3,4) G(4^+,4^{++}) G(3,2) \,, \tag{5.51}$$

where G_2^H is the Hartree approximation for G_2, which relies on neglecting L in Eq.(5.33). Thus, the v_H defined in the equation of motion (5.48) is

$$v_\mathrm{H}(3) = -i \int d4 \, v_\mathrm{c}(3,4) G(4^+,4^{++}) \,, \tag{5.52}$$

which is local and not compatible with Eq.(5.44). Instead, we have to replace v_c in the equation of motion the generalized interaction V, which yields the desired non-local Hartree potential. The Hartree Dyson equation becomes

$$G_H(1,2) = G_0(1,2) + \int d(34)\, G_0(1,3)v_H(3,4)G_H(4,2) \tag{5.53}$$

$$= G_0(1,2) + \int d(3456)\, G_0(1,3)\delta(3,4^+)v_c(4,6)\delta(6,5^+)G(5^+,5^{++})G_H(4,2) \tag{5.54}$$

$$= G_0(1,2) - i \int d(345)\, G_0(1,3)\delta(3,4^+)v_c(4,5^+)G(5^+,5^{++})G_H(4,2) \tag{5.55}$$

$$= G_0(1,2) - i \int d(45)\, G_0(1,4^+)v_c(4,5)G(5,5^+)G_H(4,2) \tag{5.56}$$

$$= G_0(1,2) - i \int d(34)\, G_0(1,3^+)v_c(3,4)G(4,4^+)G_H(3,2)\,, \tag{5.57}$$

and the general equation of motion reads

$$G(1,2) = G_0(1,2) - i \int d(34)\, G_0(1,3^+)v_c(3,4)\Big(G(3,2)G(4,4^+) - L(3,4,2,4^+)\Big). \tag{5.58}$$

This differs from Eq.(5.48) by some "simple" $+$, which are actually essential in order to be able to obtain the correct Dyson equation for χ in a consistent way and therefore, for example, to obtain the same result for the total energy using the Dyson equation for χ or the Bethe-Salpeter equation (BSE) for L [34, 37].

5.2.3 The exchange-correlation self-energy

Given that the Dyson equation of the 1-GF should be in the form of Eq.(5.58), we can find the expression for Σ_{xc}. Starting by approximating $L \approx L_0$, we get the exchange self-energy,

$$G_{HF}(1,2) = G_H(1,2) + i \int d(34)\, G_H(1,3^+)v_c(3,4)L_0(3,4,2,4^+) \tag{5.59}$$

$$= G_H(1,2) + i \int d(34)\, G_H(1,3^+)v_c(3,4)G(3,4^+)G(4,2) \tag{5.60}$$

$$= G_H(1,2) + i \int d(34)\, G_H(1,3)v_c(3,4^+)G(3^-,4^+)G(4,2) \tag{5.61}$$

$$= G_H(1,2) + i \int d(34)\, G_H(1,3)\Sigma_x(3,4)G(4,2)\,, \tag{5.62}$$

where $\Sigma_x(3,4) = iG(3^-,4^+)v_c(3,4^+)$. To go beyond, we write the BSE for L [34, 37], which can be done as follows:

$$L(1,2,3,4) = \frac{\delta G(1,3)}{\delta v_{ext}(4,2)} \tag{5.63}$$

$$= \int d5\, \frac{\delta G(1,5)}{\delta v_{ext}(4,2)}\delta(5,3) \tag{5.64}$$

$$= \int d(56)\, \frac{\delta G(1,5)}{\delta v_{ext}(4,2)}G^{-1}(5,6)G(6,3) \tag{5.65}$$

$$= -\int d(56)\, G(1,5)\frac{\delta G^{-1}(5,6)}{\delta v_{ext}(4,2)}G(6,3)\,, \tag{5.66}$$

where

$$G^{-1}(5,6) = G_0^{-1}(5,6) - v_{\text{ext}}(5,6) - v_{\text{H}}(5,6) - \Sigma_{\text{xc}}(5,6) \,. \tag{5.67}$$

So,

$$L(1,2,3,4) = \int d(56) \, G(1,5)\delta(5,4)\delta(2,6)G(6,3) + \int d(56) \, G(1,5)\frac{\delta v_{\text{H}}(5,6)}{\delta v_{\text{ext}}(4,2)}G(6,3) \tag{5.68}$$
$$+ \int d(56) \, G(1,5)\frac{\delta \Sigma_{\text{xc}}(5,6)}{\delta v_{\text{ext}}(4,2)}G(6,3) \,.$$

Before proceeding, we can again see the importance of the generalized Coulomb interaction. From the BSE for L given in Eq.(5.68), we can conclude the Dyson equation for χ, which is defined as $\chi(1,2) = -iL(1,2,1^+,2^+)$. So, at the RPA level, we have

$$\chi(1,2) = \chi_0(1,2) - i \int d(56) \, G(1,5)\frac{\delta v_{\text{H}}(5,6)}{\delta v_{\text{ext}}(2^+,2)}G(6,1^+) \tag{5.69}$$

$$= \chi_0(1,2) - i \int d(567) \, G(1,5)\delta(5,6^+)v_{\text{c}}(6,7^+)\frac{-i\delta G(7^+,7^{++})}{\delta v_{\text{ext}}(2^+,2)}G(6,1^+) \tag{5.70}$$

$$= \chi_0(1,2) - i \int d(67) \, G(1,6^+)G(6,1^+)v_{\text{c}}(6,7)\chi(7,2) \tag{5.71}$$

$$= \chi_0(1,2) + \int d(67) \, \chi_0(1,6)v_{\text{c}}(6,7)\chi(7,2) \,, \tag{5.72}$$

which is the same equation for χ that we obtained in the previous subsection. This highlights the importance of the generalized Coulomb interaction to make everything consistent.

Then, the L used in the Dyson equation (5.58) becomes

$$L(3,4,2,4^+) = L_0(3,4,2,4^+) + \int d(56) \, G(3,5)\frac{\delta v_{\text{H}}(5,6)}{\delta v_{\text{ext}}(4^+,4)}G(6,2) \tag{5.73}$$
$$+ \int d(56) \, G(3,5)\frac{\delta \Sigma_{\text{xc}}(5,6)}{\delta v_{\text{ext}}(4^+,4)}G(6,2) \,.$$

The random phase approximate (RPA) for L consists in neglecting $\frac{\Sigma_{\text{xc}}}{\delta v_{\text{ext}}}$, this leads to the GW approximation as a first step beyond HF [24]: Using L^{RPA} in Eq.(5.58) we obtain

$$G^{GW}(1,2) = G_{\text{HF}}(1,2) + i \int d(34) \, G_{\text{HF}}(1,3^+)v_{\text{c}}(3,4) \int d(56)G(3,5)\frac{\delta v_{\text{H}}(5,6)}{\delta v_{\text{ext}}(4^+,4)}G(6,2) \tag{5.74}$$

$$= G_{\text{HF}}(1,2) + i \int d(34567) \, G_{\text{HF}}(1,3^+)v_{\text{c}}(3,4)G(3,5)\delta(5,6^+)v_{\text{c}}(6,7^+)\frac{-i\delta G(7^+,7^{++})}{\delta v_{\text{ext}}(4^+,4)}G(6,2) \tag{5.75}$$

$$= G_{\text{HF}}(1,2) + i \int d(3467) \, G_{\text{HF}}(1,3^+)v_{\text{c}}(3,4)G(3,6^+)v_{\text{c}}(6,7)\frac{-i\delta G(7,7^+)}{\delta v_{\text{ext}}(4^+,4)}G(6,2) \tag{5.76}$$

$$= G_{\text{HF}}(1,2) + i \int d(3467) \, G_{\text{HF}}(1,3^+)v_{\text{c}}(3,4)G(3,6^+)v_{\text{c}}(6,7)\chi(7,4)G(6,2) \tag{5.77}$$

$$= G_{\text{HF}}(1,2) + i \int d(36) \, G_{\text{HF}}(1,3^+)G(3,6^+) \int d(47)v_{\text{c}}(3,4)\chi(4,7)v_{\text{c}}(7,6)G(6,2) \tag{5.78}$$

$$= G_{\text{HF}}(1,2) + i \int d(36) \, G_{\text{HF}}(1,3)\Sigma_{\text{c}}^{GW}(3,6)G(6,2) \,. \tag{5.79}$$

This defines the correlation GW self-energy as

$$\Sigma_{\mathrm{c}}^{GW}(3,6) = iG(3^-, 6^+)W^P(3^-, 6),\tag{5.80}$$

with W^P, the polarization part of W, which is

$$W(1,2) = v_{\mathrm{c}}(1,2) + \int d(34)\, v_{\mathrm{c}}(1,3)\chi(3,4)v_{\mathrm{c}}(4,2),\tag{5.81}$$

where only time differences are important. In equilibirium, $\Sigma_{\mathrm{c}}^{GW}(3,6) = iG(3, 6^{++})W^P(3, 6^+)$. Thus, the exchange-correlation self-energy within the GW approximation is

$$\Sigma_{\mathrm{xc}}^{GW}(1,2) = \Sigma_{\mathrm{x}}(1,2) + \Sigma_{\mathrm{c}}^{GW}(1,2)\tag{5.82}$$

$$= iG(1, 2^{++})v_{\mathrm{c}}(1, 2^+) + G(1, 2^{++})W^P(1, 2^+)\tag{5.83}$$

$$= iG(1, 2^{++})W(1, 2^+).\tag{5.84}$$

Note that this expression for the xc self-energy is equivalent to the more familiar expression $\Sigma_{\mathrm{xc}}^{GW}(1,2) \to \Sigma_{\mathrm{xc}}(1^{++}, 2) = iG(1,2)W(1^+, 2)$ [35]. *The general expression for* Σ_{xc} *reads*

$$\Sigma_{\mathrm{xc}}(1,2) = -i \int d(34)\, G(1, 4^+)W(1, 3^+)\frac{\delta G^{-1}(4,2)}{\delta v_{\mathrm{cl}}(3^+, 3)},\tag{5.85}$$

as well as the Dyson equation,

$$G(1,2) = G_0(1,2) + \int d(34)\, G_0(1,3)\Big(v_{\mathrm{H}}(3,4) + \Sigma_{\mathrm{xc}}(3,4)\Big)G(4,2).\tag{5.86}$$

App. E gives expressions beyond this derivation by introducing the non-equilibirium concept, although these derivations are not be used in this thesis.

In the following, every definition will be based on the derivations of the current section 5.2. Moreover, we will use this extended derivation with the generalized Coulomb interaction V in Chap. 7, where we discovered its importance when deriving the total energy using the response functions. The rest of the theoretical developments will be based on the standard formulation, which does not lead to any changes in the final results in those cases.

5.2.4 Hedin's equations

We addressed, in the above, the challenge of solving the equation of motion for the 1-GF, which involved the 2-GF and posed difficulties for finding a direct solution. To tackle this problem, we employed the functional derivative approach, which allowed us to establish a direct relationship between the 1-GF and the 2-GF Eq.(5.33). We also derived the Dyson equation that relates the non-interacting 1-GF with the interacting one Eq.(5.86). However, this does not mean that we are able to solve the equation exactly and get the 1-GF. The exact solution of the Dyson equation relies on the exact Σ_{xc}, which is written in Eq.(5.85). *The Σ_{xc} plays a critical role as it is responsible for obtaining the exact 1-GF. However, to find the solution for Σ_{xc}, we need the knowledge of the 1-GF itself which creates a self-consistency loop, and we need the dependence of the 1-GF on the time non-local external potential. This*

makes it impossible to obtain the exact solution. Therefore, approximations and numerical methods are commonly employed to tackle this issue. Lars Hedin has proposed a set of self-consistent equations that highlight important physical contributions, in particular the *screened Coulomb interaction W*, introduced in Chap. 3, that appears at any level approximation [24]. The motivation for this is the fact that *the Coulomb interaction is strongly modified by the rearrangement of the charges in the system as a response to a perturbation, which is known as screening effects.* Therefore, the appearance of the weaker (often W is weaker than v_{c}), screened interaction instead of the bare one at any level of approximation is crucial, especially in the case of extended systems, where screening is important.
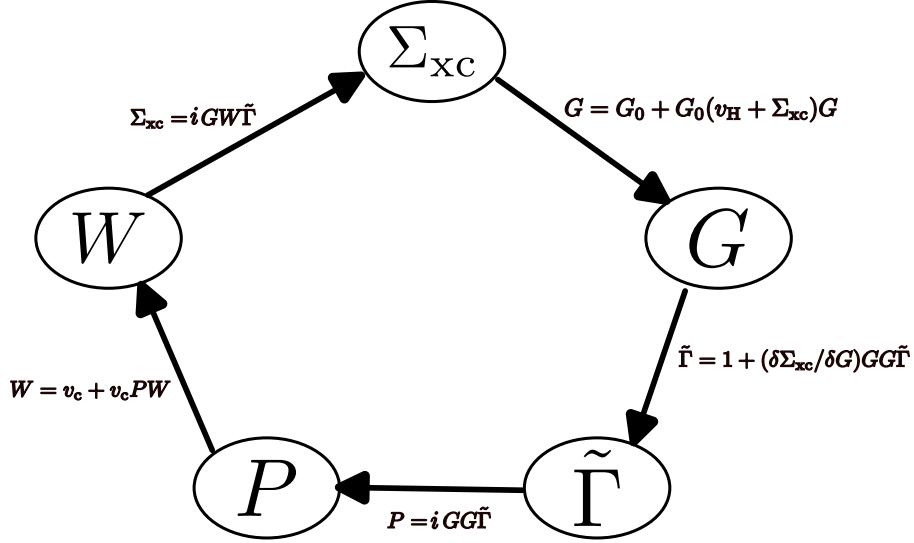
Figure 5.1: Hedin's Pentagon.

The functional derivative of G^{-1} in Eq.(5.85) defines the irreducible vertex function $\tilde{\Gamma}$,

$$\tilde{\Gamma}(1,2,3) = -\frac{\delta G^{-1}(1,2)}{\delta v_{\mathrm{cl}}(3^+,3)} \tag{5.87}$$

$$= -\frac{G_{\mathrm{H}}^{-1}(1,2)}{\delta v_{\mathrm{cl}}(3^+,3)} + \frac{\delta \Sigma_{\mathrm{xc}}(1,2)}{\delta v_{\mathrm{cl}}(3^+,3)} \tag{5.88}$$

$$= \delta(1,3^+)\delta(2,3) + \int d(456) \frac{\delta \Sigma_{\mathrm{xc}}(1,2)}{\delta G(4,6)} \frac{\delta G(4,6)}{\delta v_{\mathrm{cl}}(3^+,3)} \delta(6,5) \tag{5.89}$$

$$= \delta(1,3^+)\delta(2,3) + \int d(4567) \frac{\delta \Sigma_{\mathrm{xc}}(1,2)}{\delta G(4,6)} \frac{\delta G(4,6)}{\delta v_{\mathrm{cl}}(3^+,3)} G^{-1}(6,7)G(7,5) \tag{5.90}$$

$$= \delta(1,3^+)\delta(2,3) - \int d(4567) \frac{\delta \Sigma_{\mathrm{xc}}(1,2)}{\delta G(4,6)} G(4,6) \frac{\delta G^{-1}(6,7)}{\delta v_{\mathrm{cl}}(3^+,3)} G(7,5) \tag{5.91}$$

$$= \delta(1,3^+)\delta(2,3) + \int d(4567) \frac{\delta \Sigma_{\mathrm{xc}}(1,2)}{\delta G(4,6)} G(4,6)G(7,5)\tilde{\Gamma}(6,7,3)\,. \tag{5.92}$$

So, Hedin's equations are summarized in Fig. 5.1 as

1.

$$\Sigma_{\mathrm{xc}}(1,2) = i \int d(34)\, G(1,4^+)W(1,3^+)\tilde{\Gamma}(4,2,3)\,, \tag{5.93}$$

42

2.

$$G(1,2) = G_0(1,2) + \int d(34)\, G_0(1,3)\Big(v_{\mathrm{H}}(3,4) + \Sigma_{\mathrm{xc}}(3,4)\Big)G(4,2)\,, \qquad (5.94)$$

3.

$$\tilde{\Gamma}(1,2,3) = \delta(1,3^+)\delta(2,3) + \int d(4567)\, \frac{\delta\Sigma_{\mathrm{xc}}(1,2)}{\delta G(4,5)}G(4,6)G(7,5)\tilde{\Gamma}(6,7,3)\,, \qquad (5.95)$$

4.

$$P(1,2) = -i\int d(34)\, G(1,3)G(4,1^+)\tilde{\Gamma}(3,4,2)\,, \qquad (5.96)$$

where P is the irreducible polarizability, $P(1,2) = -i\frac{\delta G(1,1^+)}{\delta v_{\mathrm{cl}}(2^+,2)}$.

5.

$$W(1,2) = v_{\mathrm{c}}(1,2) + \int d(34)\, v_{\mathrm{c}}(1,3)P(3,4)W(4,2)\,. \qquad (5.97)$$

These equations are in principle exact, but difficult to solve. Therefore, one may think to approaching the solutions iteratively, as illustrated in Hedin's pentagon Fig. 5.1.

5.2.5 The GW approximation for the self-energy and the random phase approximation for the polarizability

Figure 5.2: Photos representing the difference between the bare and the screened Coulomb interactions. These photos are taken from Pixabay.

By neglecting the vertex corrections in $\tilde{\Gamma}$, i.e , $\tilde{\Gamma} \approx \delta$ in Eq.(5.95), Σ_{xc} Eq.(5.93) becomes

$$\Sigma_{\mathrm{xc}}^{GW}(1,2) = iG(1,2^{++})W(1,2^+)\,, \qquad (5.98)$$

the same as Eq.(5.84). The GW xc self-energy is the multiplication of the 1-GF and the screened Coulomb interaction W, hence the name "GW approximation" (GWA) [24]. It looks similar to the HF self-energy, but the bare interaction is replaced by the screened one. So, the difference between the HF and the GW self-energies is the screening, which is a long range correlation. Screening is an important feature, represented by "satellites" (explained in Subsec. 5.2.6) in the spectral function. It is important for total energies calculation as well as it allows for the van der Waals dispersion, which

is a major challenge for density functional theory functionals. On the other hand, Hedin suggested to approximate his equations consistently, so by using the approximate vertex function $\tilde{\Gamma} \approx \delta$, we obtain the Random Phase Approximation (RPA) for the irreducible polarizability in Eq.(5.96),

$$P^{\mathrm{RPA}}(1,2) = -iG(1,2^+)G(2,1^+)\,, \tag{5.99}$$

which is used to calculate W in Eq.(5.97).

The GW approximation, established in the 60's [24], was developed within an ab initio framework in the 80's [25, 26] and it has since become the state-of-the-art for the description of charged electronic excitations, [4, 53, 102–111], especially thanks to self-consistent approaches [52, 53, 112–119].

An illustrative way to understand the difference between the electron motion within the two contexts, HF and GW, is shown in Fig. 5.2 [93]. *In the HF framework, the electron moves through the system without experiencing any response from the other electrons.* This can be compared to a person skiing on the ice, where the person's movement is unaffected by the surrounding environment. *In contrast, within the GW framework, the electron's motion creates a perturbation in the system.* This perturbation induces a response from the other electrons (including itself, actually GW suffers from a self-screening error [54, 120]), resulting in screening effects. This can be linked to a boat moving on the sea, where the boat's motion causes ripples and waves in the water, and the water reacts by exerting forces on the boat.

Another way to grasp the additional capabilities of GW with respect to HF is by examining the spectral function. GW is able to exhibit the presence of *satellites* (which will be discussed in the next subsection 5.2.6), which are indicative of the dynamical correlations occurring within the electronic system.

5.2.6 What are the satellites?

One might wonder about the physical significance of satellites and how they come into existence. The simplest explanation is as follows: picture a single electron moving through a system containing N electrons. If we isolate this electron from the other electrons, and examine its spectral function (for simplicity we only consider the removal part), we would observe a narrow peak. On the other hand, when we take into account the interactions, we observe a broader peak with reduced intensity and the appearance of additional stucture called satellites. This is illustrated in Fig. 5.3, where we present the spectral function of the symmetric Hubbard dimer with two-electrons (this model is presented in detail in Chap. 6). As shown, the non-interacting spectral function does not exhibit satellites whereas the exact one does. So, it is the interactions that give rise to satellites. But which part of the interaction is responsible? In our context, the interaction potential can be divided into Hartree, exchange, and correlation potentials. It is the correlation potential, which is dynamic, that leads to the satellites. As a particle (electron or hole) moves through the system, it gives a portion of its energy to create neutral excitations. The neutral excitations are represented by the removal and addition satellites that appear when removing and adding an electron, respectively. In Fig. 5.3 we only show the removal

satellites. Moreover, it is noticeable that the intensity of the main peak, which is called quasi-particle (QP), decreases within the exact solution compared to the non-interacting one. This missing intensity goes to the satellite.

Furthermore, the intensities of these satellites, as they are generated by correlations, are contingent on the strength of these correlations. Stronger correlations result in more pronounced satellite peaks, while weaker correlations lead to less prominent ones (compare left and right panels of Fig. 5.3). This is why weakly correlated systems, where satellites are negligible, can be approximated as almost non-interacting systems. The right-panel of Fig. 5.3 represents strong correlation as the strength U/t becomes higher, and ideed one can notice that the satellite intensity becomes higher.
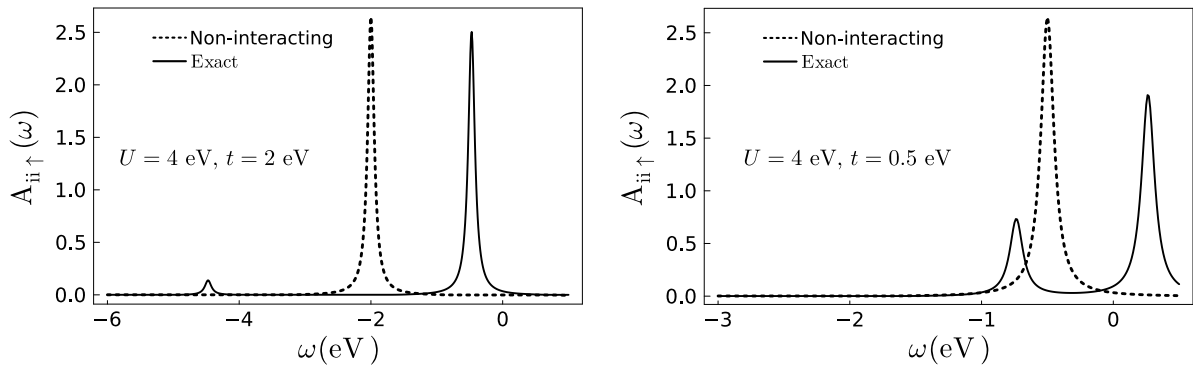
Figure 5.3: Non-interacting and exact spectral functions (removal part of the spin-up diagonal element) of the symmetric Hubbard dimer model with two electrons. The on-site interaction $U = 4$ eV and the the hopping t is 2 eV and 0.5 eV in the left and right figure, respectively.

5.2.7 How does the self-energy contribute to the generation of the spectral function?

In order to discuss in detail, the spectral function features introduced in the previous subsection, one can write the spectral function directly in terms of the self-energy. In the bonding (b) and anti-bonding (ab) basis, we have

$$A_{\text{b-b/ab-ab}}(\omega) = (1/\pi) \frac{\text{Im}\Sigma_{\text{b-b/ab-ab}}(\omega)}{\left(\omega - (\epsilon^0_{\text{b-b/ab-ab}}) - \text{Re}\Sigma_{\text{b-b/ab-ab}}(\omega)\right)^2 + \left(\text{Im}\Sigma_{\text{b-b/ab-ab}}(\omega)\right)^2} . \tag{5.100}$$

In Fig. 5.4, we illustrate the spectral function $A(\omega)$, the numerator of Eq.(5.100) and the first term of the denominator for the symmetric Hubbard dimer model at half-filling. From Eq.(5.100), we can comprehend the different components of the spectral function, namely satellites and QP. Generally, satellites are generated due to ImΣ, and the QP peaks emerge when $\omega - (\epsilon^0) - \text{Re}\Sigma(\omega) = 0$. This is often assumed for infinite systems. However, the situation is slightly more complicated for finite systems, as illustrated by the Hubbard dimer solutions in Fig. 5.4. The satellites appear almost at the same position as ImΣ in the upper panels when $t = 6\,\text{eV}$ and $t = 4\,\text{eV}$. However, this does not imply that these satellites are directly given by ImΣ. They are actually produced by an additional solution
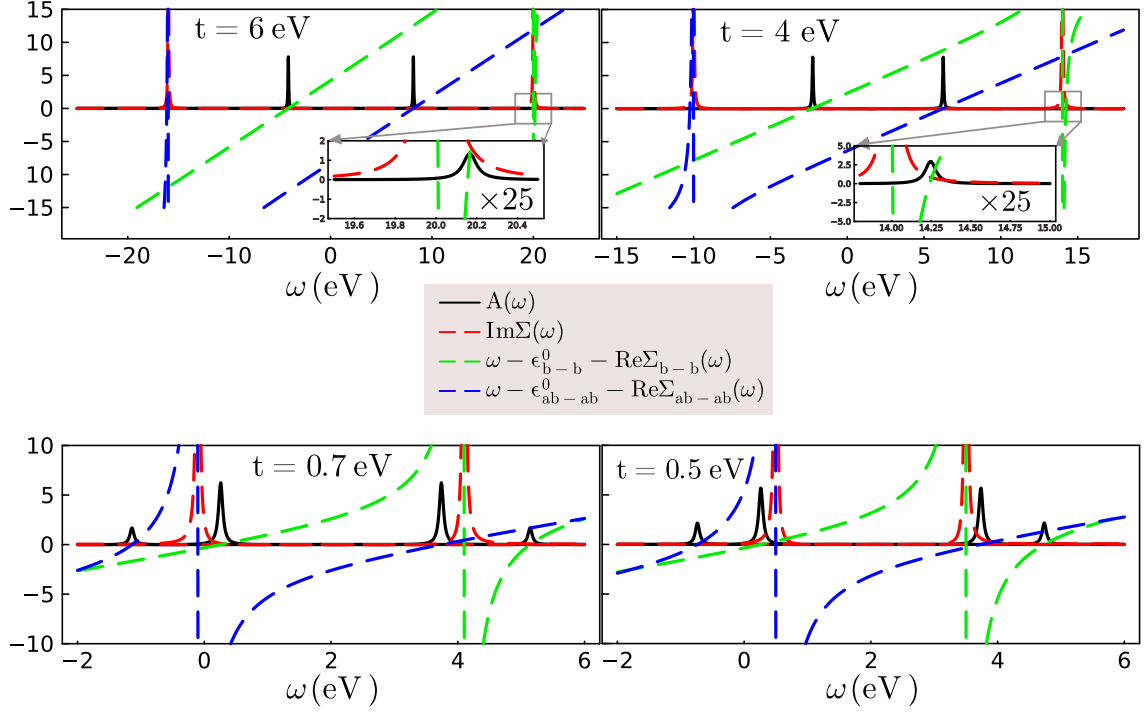
Figure 5.4: Spectral function features of the symmetric Hubbard dimer at half-filling for a given spin as a function of frequency, where $U = 4$ eV. The spectral function is shown in the black solid lines. The imaginary part of the self-energy is given by the red lines. The first term of the denominator in Eq.(5.100) for the bonding-bonding and antibonding-antibonding matrix elements is given in the dashed green and blue lines, respectively.

of $\omega - (\epsilon^0) - \text{Re}\Sigma(\omega) = 0$, as clearly shown in the insets. More evidently, this can be observed in the lower panels when t decreases, i.e when correlations increase. Here, the satellites are quite far from the position of the peak of ImΣ. *Note that this is unlikely to happen in infinite systems, where the broadening is very high* due to a continuum of states; therefore, $\omega - (\epsilon^0) - \text{Re}\Sigma(\omega) = 0$ does not yield satellites. Instead, these are formed at the peak of ImΣ.

Chapter 6

GW successes and failures: insights from the Hubbard dimer model

Exactly solvable models are crucial for theoretical investigations and illustrations. Having the exact result at hand, we are able to explore any approximation. As pointed out before, in the present thesis we use, for illustrations, the widely used Hubbard dimer model [54–58], which is made up of two equivalent sites, each has one single orbital and on-site Coulomb interaction U [121, 122] as illustrated by the left-hand and right-hand panels of Fig. 6.1, respectively. The orbitals are localized, since this model is performed initially to deal with strongly correlated physics. Therefore the electron can go to the nearest neighboor site with a hopping integral t, representing the kinetic energy as illustrated by the middle panel of Fig. 6.1.

On the other hand, besides the exact solution that the model provides, it also allows for exploring systems with different ranges of correlations such as, weakly, moderately and strong correlated systems. This is due to the fact that the Coulomb interaction and the kinetic energy are parameters that can be changed to change the correlations.
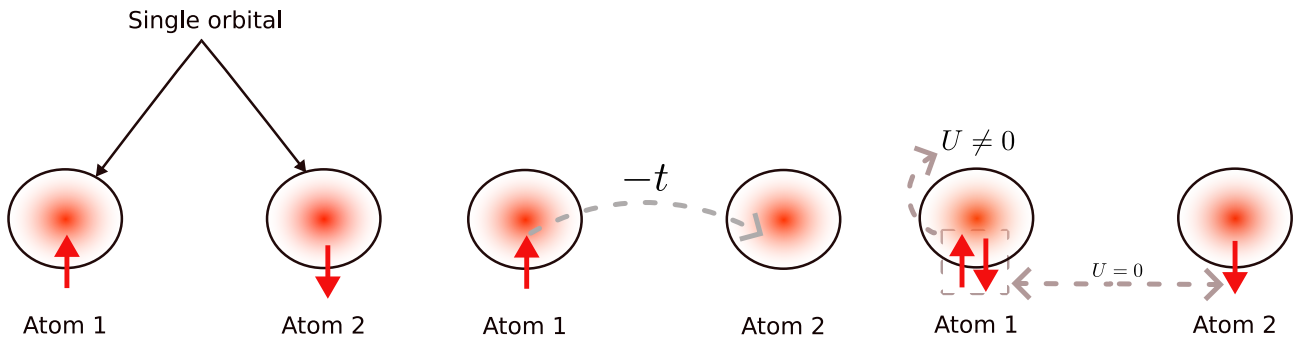
Figure 6.1: Left panel: the atom in this model has only one single orbital. Middle panel: the orbital localization imposes an electronic displacement to the nearest neighbor site. This approximation does not make sense in the case of the two-site model, but it will be meaningful if we want to extend the dimer. Right panel: the electrons are short-range interacting, they do not interact with each other unless they are on the same site.

6.1 Hubbard hamiltonian

Starting from the exact hamiltonian, written in second quantization in Eq.(1.13), the derivation of the Hubbard hamiltonian proceeds as follows, where we treat each part of the exact hamiltonian separately. We start with the external potential term,

$$\sum_{ij=1}^{\infty} \sum_{\sigma\sigma'} \int dx \, \phi_{i\sigma}^*(x) v_{\text{ext}}(x) \phi_{j\sigma'}(x) \hat{c}_{i\sigma}^\dagger \hat{c}_{j\sigma'} \tag{6.1}$$

$$= \sum_{ij=1}^{\infty} \sum_{\sigma\sigma'} \sum_s \chi_\sigma^*(s) \chi_{\sigma'}(s) \int dr \, \varphi_{i\sigma}^*(r) v_{\text{ext}}(r) \varphi_{j\sigma'}(r) \hat{c}_{i\sigma}^\dagger \hat{c}_{j\sigma'} \tag{6.2}$$

$$= \sum_{ij=1}^{\infty} \sum_{\sigma\sigma'} \delta_{\sigma\sigma'} \int dr \, \varphi_{i\sigma}^*(r) v_{\text{ext}}(r) \varphi_{j\sigma'}(r) \hat{c}_{i\sigma}^\dagger \hat{c}_{j\sigma'} \,, \tag{6.3}$$

where using the fact that the orbitals are localized, we obtain

$$\sum_{i=1}^{\infty} \sum_\sigma \int dr \, \varphi_{i\sigma}^*(r) v_{\text{ext}}(r) \varphi_{i\sigma}(r) \hat{c}_{i\sigma}^\dagger \hat{c}_{i\sigma} = \sum_{i=1,\sigma}^{\infty} v_{\text{ext},i\sigma} \hat{c}_{i\sigma}^\dagger \hat{c}_{i\sigma} \,. \tag{6.4}$$

For the kinetic energy operator, we have

$$\sum_{ij=1}^{\infty} \sum_{\sigma\sigma'} \int dx \, \phi_{i\sigma}^*(x) (-\frac{\nabla_r^2}{2}) \phi_{j\sigma'}(x) \hat{c}_{i\sigma}^\dagger \hat{c}_{j\sigma'} \tag{6.5}$$

$$= \sum_{<i,j>,i\neq j}^{\infty} \sum_{\sigma\sigma'} \sum_s \chi_\sigma^*(s) \chi_{\sigma'}(s) \int dr \, \varphi_{i\sigma}^*(r) (-\frac{\nabla_r^2}{2}) \varphi_{j\sigma'}(r) \hat{c}_{i\sigma}^\dagger \hat{c}_{j\sigma'} \,. \tag{6.6}$$

In this case, even though we have localized orbitals, we cannot consider that $i = j$ to avoid neglecting the kinetic energy. So, we obtain

$$\sum_{<i,j>,i\neq j}^{\infty} \sum_\sigma \int dr \, \varphi_{i\sigma}^*(r) (-\frac{\nabla_r^2}{2}) \varphi_{j\sigma}(r) \hat{c}_{i\sigma}^\dagger \hat{c}_{j\sigma} = - \sum_{<i,j>,i\neq j,\sigma}^{\infty} t_{ij} \hat{c}_{i\sigma}^\dagger \hat{c}_{j\sigma} \,, \tag{6.7}$$

where t_{ij} is called hopping integral and defined as,

$$t_{ij} = \int dr \varphi_{i\sigma}^*(r) \frac{\nabla_r^2}{2} \varphi_{j\sigma}(r) \,. \tag{6.8}$$

For the Coulomb interaction operator, we make two approximations, localization of orbitals and short range interactions. Thus, we have

$$\frac{1}{2} \sum_{ijkl=1}^{\infty} \sum_{\sigma_1\sigma_2\sigma_3\sigma_4} \int\int dx dx' \, \phi_{i\sigma_1}^*(x) \phi_{j\sigma_2}^*(x') v_{\text{c}}(x,x') \phi_{l\sigma_3}(x') \phi_{k\sigma_4}(x) \hat{c}_{i\sigma_1}^\dagger \hat{c}_{j\sigma_2}^\dagger \hat{c}_{l\sigma_3} \hat{c}_{k\sigma_4} \tag{6.9}$$

$$= \frac{1}{2} \sum_{ijkl=1}^{\infty} \sum_{\sigma_1\sigma_2\sigma_3\sigma_4} \sum_s \chi_{\sigma_1}^*(s) \chi_{\sigma_4}(s) \sum_{s'} \chi_{\sigma_2}^*(s') \chi_{\sigma_3}(s') \int\int dr dr' \, \varphi_{i\sigma_1}^*(r) \varphi_{j\sigma_2}^*(r') v_{\text{c}}(r,r') \varphi_{l\sigma_3}(r')$$
$$\varphi_{k\sigma_4}(r) \hat{c}_{i\sigma_1}^\dagger \hat{c}_{j\sigma_2}^\dagger \hat{c}_{l\sigma_3} \hat{c}_{k\sigma_4} \tag{6.10}$$

$$= \frac{1}{2} \sum_{ijkl=1}^{\infty} \sum_{\sigma_1\sigma_2} \int\int dr dr' \, \varphi_{i\sigma_1}^*(r) \varphi_{j\sigma_2}^*(r') v_{\text{c}}(r,r') \varphi_{l\sigma_2}(r') \varphi_{k\sigma_1}(r) \hat{c}_{i\sigma_1}^\dagger \hat{c}_{j\sigma_2}^\dagger \hat{c}_{l\sigma_2} \hat{c}_{k\sigma_1}, \tag{6.11}$$

which, by considering the localization of orbitals, becomes

$$\frac{1}{2}\sum_{ij=1}^{\infty}\sum_{\sigma_1\sigma_2}\int\int drdr'\varphi_{i\sigma_1}^*(r)\varphi_{j\sigma_2}^*(r')v_{\rm c}(r,r')\varphi_{j\sigma_2}(r')\varphi_{i\sigma_1}(r)\hat{c}_{i\sigma_1}^{\dagger}\hat{c}_{j\sigma_2}^{\dagger}\hat{c}_{j\sigma_2}\hat{c}_{i\sigma_1}\,. \qquad (6.12)$$

Then, since the two electrons can only interact if they are on the same site, we put $i = j$, meaning that in this case, the two electrons cannot have the same spin. Thus, we obtain

$$\frac{1}{2}\sum_{i=1}^{\infty}\sum_{\sigma_1\sigma_2,\sigma_1\neq\sigma_2}\int\int drdr'\varphi_i^*(r)\varphi_i^*(r')v_{\rm c}(r,r')\varphi_i(r)\varphi_i(r')\hat{c}_{i\sigma_1}^{\dagger}\hat{c}_{i\sigma_2}^{\dagger}\hat{c}_{i\sigma_2}\hat{c}_{i\sigma_1} \qquad (6.13)$$

$$=\frac{U}{2}\sum_{i=1}^{\infty}\sum_{\sigma_1\sigma_2,\sigma_1\neq\sigma_2}\hat{c}_{i\sigma_1}^{\dagger}\hat{c}_{i\sigma_2}^{\dagger}\hat{c}_{i\sigma_2}\hat{c}_{i\sigma_1}, \qquad (6.14)$$

where σ_1 and σ_2 are two opposite spins projections. Finally, we write down the symmetric Hubbard hamiltonian as

$$\hat{H} = \epsilon_0\sum_{i,\sigma}\hat{n}_{i\sigma} - \sum_{<i,j>,i\neq j,\sigma}t_{ij}\hat{c}_{i\sigma}^{\dagger}\hat{c}_{j\sigma} + U\sum_i\hat{n}_{i\uparrow}\hat{n}_{i\downarrow}, \qquad (6.15)$$

where for the dimer $i,j = 1,2$. The conventions are reminded here:

ϵ_0: external on-site potential.

t_{ij}: kinetic energy.

U: on-site Coulomb repulsion.

$\hat{n}_{i\sigma} = \hat{c}_{i\sigma}^{\dagger}\hat{c}_{i\sigma}$: particle number operator, where $\hat{c}^{\dagger}$ and $\hat{c}$ are creation and annihilation operators, respectively.

6.2 Illustrations within the quarter-filled case (one-electron system)

After deriving the symmetric Hubbard hamiltonian in the previous section, where exact and GW solutions are given in Sec. 6.5, we begin with the quarter-filled case (one-electron system) to represent successes and failures of GW.

6.2.1 Spectral function: the GW self-screening problem

The one-electron system provides a useful example to illustrate the self-screening error present in the GWA. As shown in Fig. 6.2, within the exact solution, the electron-electron interactions are absent, as the removed and added electrons do not interact with any other electrons. In the case of electron addition, this is due to the fact that the added spin-up electron must go to the empty site and the Hubbard U is an onsite interaction. However, the GW approximation introduces two satellites in the spectral function, which are indicative of screening correlations contributions. This indicates that when an electron is removed within GWA, it induces a reaction of the system density, which is effectively its own density. This issue is akin to the Hartree self-interaction error and is referred to as the self-screening error or variational self-interaction error [55]. The self-screening error arises due to
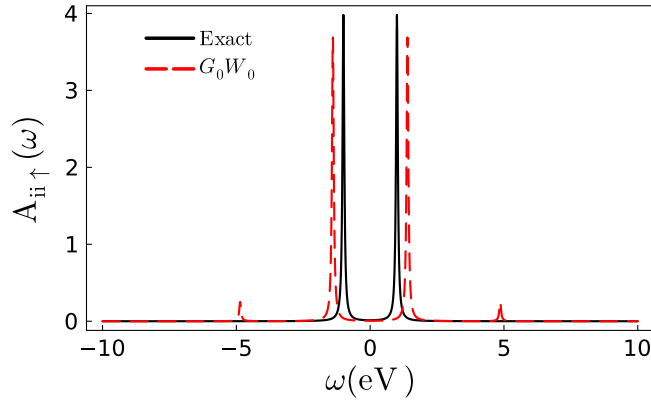
Figure 6.2: Spin-up spectral function of the symmetric two-site Hubbard model at quarter-filling: the exact result is represented by the black solid line and the G_0W_0 result is given in the dashed red line. $U = 4$ eV, $t = 1$ eV.

the limitation of using only the GW self-energy, which neglects the vertex corrections. As a result, the screened Coulomb interaction within GWA depends on the system density, including the density of the specific electron under consideration, leading to errors in the interaction description. Conversely, the satellite attached to the added spin-up electron (the satellite which is in the positive frequency range) is not directly due to the self-screening error because the additional electron interacts with the density of the other electron, not its own density. Nevertheless, in the case of the Hubbard short-range interaction, this interaction between the two electrons should not occur due to the Pauli principle, which prohibits two electrons from occupying the same site. Thus, this indicates another problem, related to the treatment of spins within the GW framework. Overall, these issues emphasize the need for improved treatments beyond GW to accurately capture the electronic interactions and correlations even in very simple systems.

6.2.2 Strong correlation limitations of GW
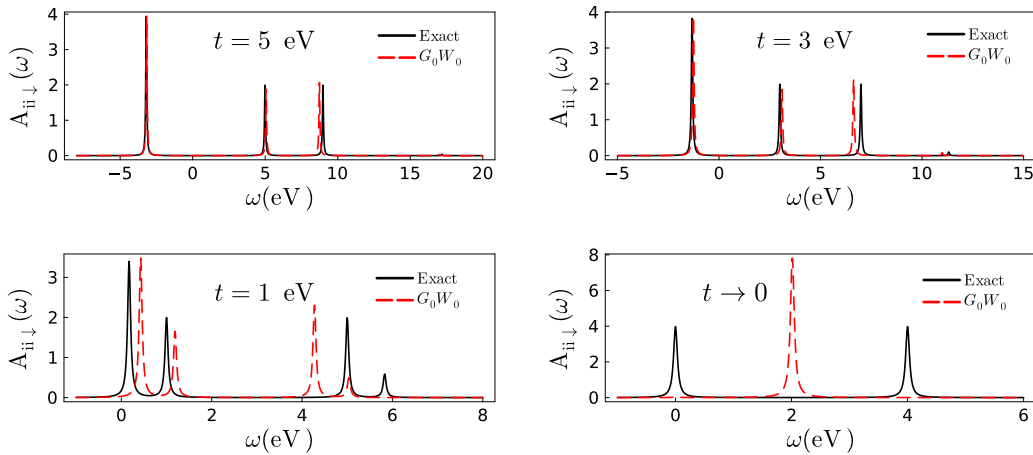
Figure 6.3: Spin-down spectral function as a function of frequency for different values of t, where $U = 4$ eV: the exact results are represented by the black solid lines and G_0W_0 results are given by the dashed red lines.

In the case of the spin-down spectral function, there are only addition parts since there is no spin-down electron to remove. In Fig. 6.3, we illustrate how the performance of the GW approximation changes with the correlation strength U/t. The smaller U/t, the weaker the correlations. For small U/t, GW shows a good performance, as shown in the upper panels. As U/t increases and correlations become more significant, the accuracy of the GW approximation decreases, leading to increasingly inaccurate results in the atomic limit where $t \to 0$, as depicted in the right-hand lower panel. Here, the exact result shows 2 peaks splitted by the U interaction. Instead, G_0W_0 yields a single peak at $U/2$. This is due to the fact that the average occupation of the sites in the ground-state is $1/2$. This highlights the sensitivity of the GW to the strength of electronic correlations, and the need for alternative methods when dealing with strongly correlated systems.

6.2.3 Violation of exact constraints
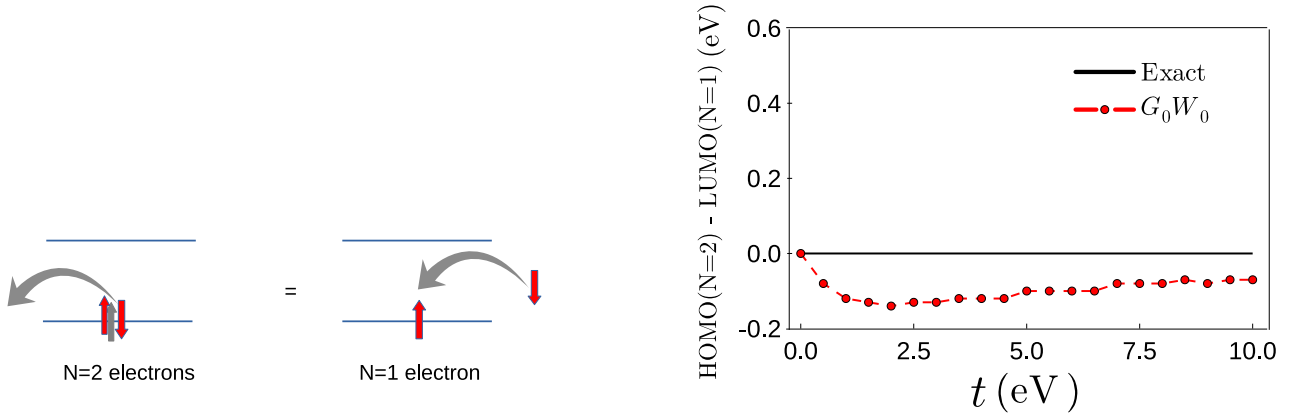
Figure 6.4: Difference between the highest occupied molecular orbital (HOMO) energy of the $N = 2$ electron system and the lowest unoccpied molecular orbital (LUMO) energy of the $N = 1$ electron as a function of t, where $U = 4$ eV. The exact result is given by the black solid line. The G_0W_0 result is shown in the red dashed line with dot markers.

The highest occupied molecular orbital (HOMO) for $N = 2$ is defined as the energy difference between the ground-state energies of the $N = 2$ and $N = 1$ electron systems, which can be expressed as $\epsilon_{HOMO}^{N=2} = E_0^{N=2} - E_0^{N=1}$. Similarly, the lowest unoccupied molecular orbital (LUMO) for $N = 1$ is defined as $\epsilon_{LUMO}^{N=1} = E_0^{N=2} - E_0^{N=1}$, and thus these two quantities should be equivalent.

However, in the GWA (G_0W_0 as shown in Fig. 6.4), this symmetry is violated. *The reason behind this discrepancy is due to the test-charge test-charge TCTC screened interaction of GW, that depends on the charge density of the system without taking into account that the charge is added or removed. This leads to two different screened interactions for $N = 2$ and $N = 1$, since the density of the two systems is different.* This reason is also the origin of the self-screening error.

6.2.4 Total energy

The exact ground-state total energy for the Hubbard dimer with one electron is calculated using exact diagonalization in Sec. 6.5. Here, we show the calculation using the exact 1-GF (which is, for the one

electron system, the non-interacting 1-GF) by solving the GM formula written in Eq.(C.12). It can be solved analytically, since we have the exact 1-GF.

$$\mathrm{E}_0 = -\frac{i}{4\pi}\sum_{i\sigma}\int_{-\infty}^{+\infty}d\omega\,\omega G_{ii\sigma}(\omega)e^{i\omega\eta} + \frac{it}{4\pi}\sum_{<i,j>,i\neq j,\sigma}\int_{-\infty}^{+\infty}d\omega\,G_{ij\sigma}(\omega)e^{i\omega\eta} - \frac{i\epsilon_0}{4\pi}\sum_{i\sigma}\int_{-\infty}^{+\infty}d\omega\,G_{ii\sigma}(\omega)e^{i\omega\eta}$$

(6.16)

$$= -\frac{i}{4\pi}\int_{-\infty}^{+\infty}d\omega\,\frac{\omega e^{i\omega\eta}}{\omega - (\epsilon_0 - t) - i\eta} + \frac{it}{4\pi}\int_{-\infty}^{+\infty}d\omega\,\frac{e^{i\omega\eta}}{\omega - (\epsilon_0 - t) - i\eta} - \frac{i\epsilon_0}{4\pi}\int_{-\infty}^{+\infty}d\omega\,\frac{e^{i\omega\eta}}{\omega - (\epsilon_0 - t) - i\eta},$$

(6.17)

where the integration should only be over occupied states of the 1-GF. Indeed, the presence of $e^{i\omega\eta}$ decides that the integration is over the upper contour, which contains the occupied poles. Physically speaking, to calculate the ground-state total energy, the additional energies coming from the additional electrons should be excluded. So, we obtain

$$\mathrm{E}_0 = \epsilon_0 - t\,,$$

(6.18)

which is the non-interacting total energy of the bonding-state. Similarly, by using the G_0W_0 1-GF given in Eq.(6.87), we have

$$\mathrm{E}_0^{G_0W_0} = \epsilon_0 - \frac{A}{4} + (\frac{2t+h}{4A})(h-2t)\,.$$

(6.19)

For $U = 0$, $\mathrm{E}_0^{G_0W_0}$ yields the non-interacting solution. *It is important to note that we do not plot the analytical solutions for total energies, as it is not always possible to have the analytical 1-GF. However, it is crucial to compare both solutions, numerical and analytical ones, when it is possible in order to create reliable codes.*
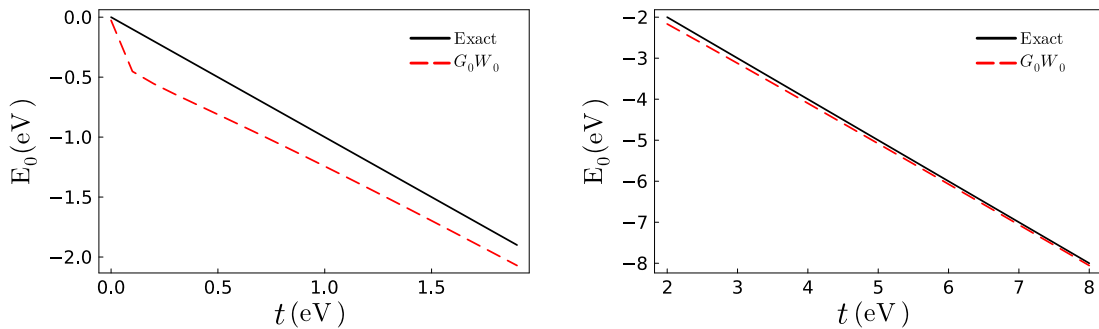
Figure 6.5: Ground-state total energy as a function of t, where $U = 4$ eV: the exact result is represented by the black solid line and the G_0W_0 result is given in the red dashed line. The left and right panels show different range of t.

In Fig. 6.5, we compare the G_0W_0 ground-state total energy with the exact result in different regimes of correlations. In the left-hand figure, we focus on the strong correlations regime, where G_0W_0 encounters more difficulties. Interestingly, the self-screening error does not affect the total energy in the atomic limit ($t \to 0$) because, in this case, the two atoms are isolated, and each atom

has only one single orbital. Therefore, the electron cannot be excited due to the lack of available orbitals. Consequently, there is no more screening, which was the origin of the G_0W_0 errors observed in this scenario.

In contrast, the right-hand figure illustrates a situation where correlations become progressively less important, and as a result, the G_0W_0 error decreases, indicating that the G_0W_0 approximation is more suitable for weakly to moderately correlated systems. It is also worth noting that the strong correlations problem observed when $t \to 0$ does not impact the G_0W_0 result, as the spin-down 1-GF is not included in the calculation due to its only having addition parts.

6.2.5 G_0W results

The GW calculations can be approached from different angles, involving choices in the utilized ingredients such as the 1-GF and the screened interaction. In our present discussion, we maintain the use of the 1-GF while modifying the screened interaction. Rather than relying on the RPA, we accurately calculate the screened interaction W. This alteration enables us to explore the impact of this change on our GW calculations. The exact W can be calculated from Eq.(5.81) using the exact reducible polarizability, which is equal to the non-interacting χ_0.

$$\chi_{0ij\uparrow}(\omega) = \frac{(-1)^{i-j}}{4} \left(\frac{1}{\omega - 2t + 2i\eta} - \frac{1}{\omega + 2t - 2i\eta} \right), \tag{6.20}$$

and $\chi_{0ij\downarrow} = 0$ since there is no spin-down to polarize. This exact polarizability can be used to calculate the exact screened interaction W by solving the following equation derived for the Hubbard model,

$$W_{ij}(\omega) = U\delta_{ij} + U^2 \sum_{\sigma\sigma'} \chi_{0ij\sigma\sigma'}(\omega). \tag{6.21}$$

This yields the exact screened Coulomb interaction matrix elements,

$$W_{ij}(\omega) = U\delta_{ij} + \frac{(-1)^{i-j}U^2}{4} \left(\frac{1}{\omega - 2t + 2i\eta} - \frac{1}{\omega + 2t - 2i\eta} \right). \tag{6.22}$$

It is crucial to emphasize that even though we have the exact W, this adjustment does not rectify the issues related to self-screening, constraint violations, and strong correlations. These challenges persist due to the nature of the GW approximation, which inherently involves approximations. Regardless of the choices that we make for the 1-GF and W, achieving an exact outcome is unattainable within the framework of GW. It is worth noting that W remains a classical TCTC interaction, intrinsically linked to the charge density of the system, not the electron under consideration.

The G_0W xc self-energy $\Sigma_{xc}^{G_0W}$ solutions are

$$\Sigma_{xc,ij\uparrow}(\omega) = -\frac{U}{2}\delta_{ij} + \frac{U^2}{8} \left(\frac{1}{\omega - (\epsilon_0 + 3t) + 3i\eta} + \frac{(-1)^{i-j}}{\omega - (\epsilon_0 - 3t) - 3i\eta} \right), \tag{6.23}$$

$$\Sigma_{xc,ij\downarrow}(\omega) = \frac{U^2}{8} \left(\frac{1}{\omega - (\epsilon_0 + 3t) + 3i\eta} + \frac{(-1)^{i-j}}{\omega - (\epsilon_0 + t) + 3i\eta} \right). \tag{6.24}$$

In Fig. 6.6, we engage in a comparative analysis of the spectral functions generated by the two GW variants, namely G_0W_0 and G_0W. Clearly, G_0W suffers from its own self-screening error (as depicted in
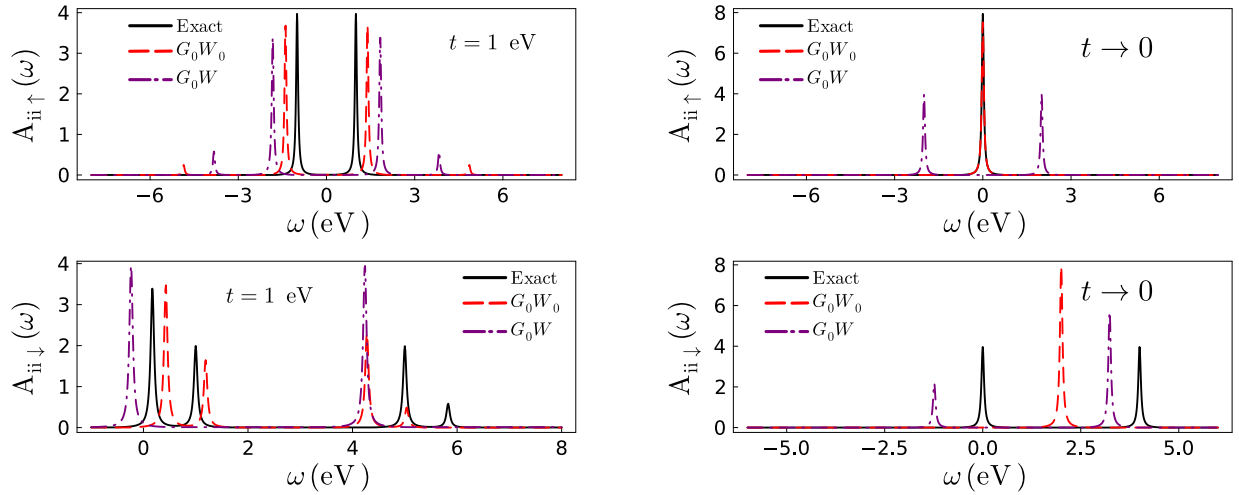
Figure 6.6: Spectral function as a function of frequency, where $U = 4$ eV. Spin-up and spin-down components are shown in the upper and lower panels, respectively. $t = 1$ eV and $t \to 0$ are given in the left and right-panels, respectively. The exact results are shown in the black solid lines. G_0W_0 and G_0W are represented by the red dashed and dot-dashed purple lines, respectively.

the upper left panel). This stems from its reliance on W, whose behavior hinges on the charge density of the system, irrespective of whether the underlying χ is exact or an approximation. In striking contrast to G_0W_0, the G_0W approach produces an erroneous spin-up spectral function (as shown in the upper right panel) in the atomic limit, a situation that deviates from physical expectations. Specifically, as $t \to 0$, the screening effects should subside, causing the correlation contribution of the self-energy Σ_c^{GW} to vanish. This, however, is not observed in the case of G_0W.

In the context of the spin-down component, it is apparent that G_0W manifests only two peaks, whereas G_0W_0 exhibits four, aligning more closely with the exact result (as seen in the lower right-panel). As we delve into the atomic limit, we find that both G_0W and G_0W_0 deviate from the exact outcome, albeit each manifesting its own distinct deviation.
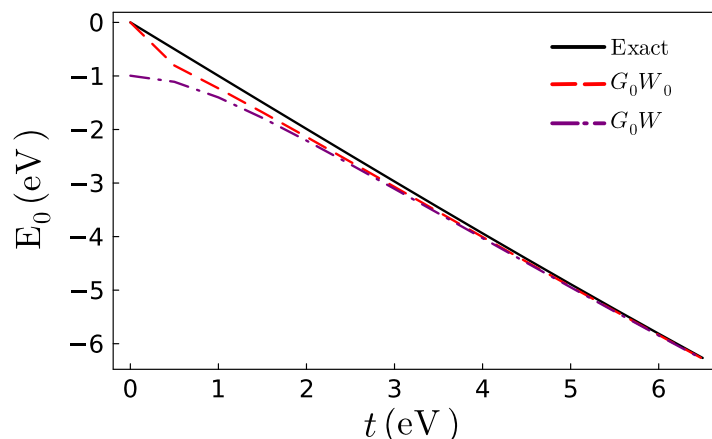
Figure 6.7: Ground-state total energy as a function of t. The exact result is given in the black solid line. G_0W_0 and G_0W are represented by the red dashed and dot-dashed purple lines, respectively.

In Fig. 6.7, we show the ground-state total energy comparison between G_0W_0 and G_0W with re-

spect to the exact result. G_0W_0 outperforms G_0W in the whole range of correlations. Moreover, G_0W does not yield the exact result when $t \to 0$.

6.3 Illustrations within the half-filled case (two-electron system)

In the two electron filling case, where the ground-state involves electron-electron interactions, the underlying physics becomes more complex and intricate. We present and discuss in this the section the GW solutions of this system in comparison with the exact results. We calculate self-energies within the same flavors of GW as used previously in the one-electron case, namely G_0W_0 and G_0W, where G_0 is the non-interacting 1-GF ($U = 0$). W and W_0 are the screened Coulomb interactions calculated using the exact polarizability and the one within the RPA, respectively. In the present section, we discuss the spectral function and total energy results within GWA in comparison with the exact ones.

6.3.1 Spectral function

The GW self-screening problem has been represented by an additional satellite, which should not exist in the case of the one-electron. In the two-electron case, there should be a satellite as shown by the exact result in Fig. 6.8. The GW self-screening problem is then represented by the big energy difference between the exact and the GW (both flavors). Indeed, this difference is lower in the case of G_0W since W contains the exact χ. The vertex corrections in χ decrease the neutral excitation energies, therefore the satellites are closer to the exact ones (except for the particular value $t = 1$ eV).
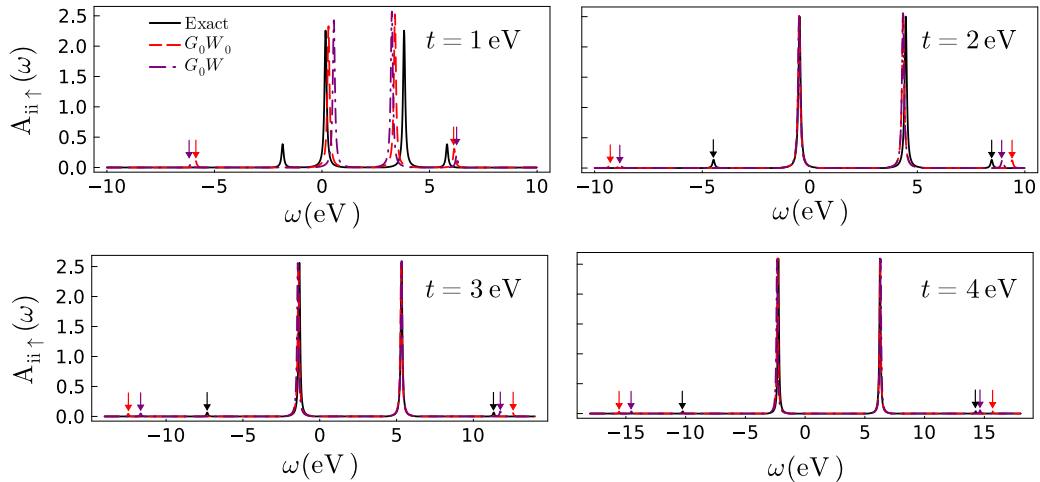
Figure 6.8: Spin-up diagonal spectral function matrix-element (the spin-down elements are equal to the spin-up ones) for the symmetric Hubbard dimer model at half-filling as a function of frequency, where different values of t are shown with $U = 4$ eV. The exact results are given in black solid lines. G_0W_0 and G_0W results are the red dashed and purple dot-dashed lines, respectively. The black, red and purple arrows indicate the presence of exact, G_0W_0 and G_0W satellites, respectively.

Although the G_0W satellites exhibit better agreement with the exact results compared to the G_0W_0

satellites, this does not hold true for the QP energies. As depicted in Fig. 6.9, the HOMO and LUMO energies are better described within G_0W_0, where the approximate screening is employed. This is similar to the observations in the one electron system.
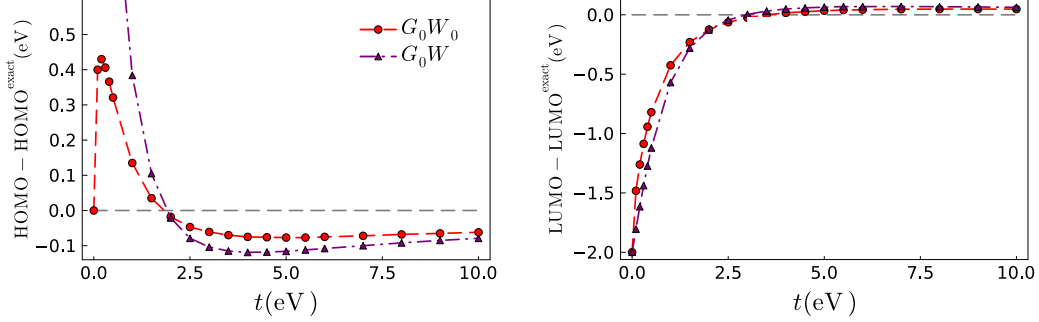
Figure 6.9: Error of the QP energy as a function of the hopping t, where $U = 4$ eV. The HOMO and LUMO energy errors are shown in the left and right panels, respectively. G_0W_0 and G_0W results are given in the red dashed and purple dot-dashed lines, respectively.

6.3.2 Ground-state total energy

In Fig. 6.10, we show the ground-state total energy errors with respect to the exact result for both the G_0W_0 and G_0W flavors. It is again noticed, as in the case of the QP results that the use of the RPA screening leads to a better performance of the total energy calculations. It is worth mentioning that G_0W_0 has the correct result in the atomic limit $t \to 0$ due to a problem in the electrons number that is shown in Fig. 6.11 and discussed below. In general and as in the one electron case, GW performs well when correlation is not strong, and becomes less accurate in the strong correlation ranges. This can be seen in Fig. 6.10, where the errors decrease in both GW flavors, when U/t decreases.
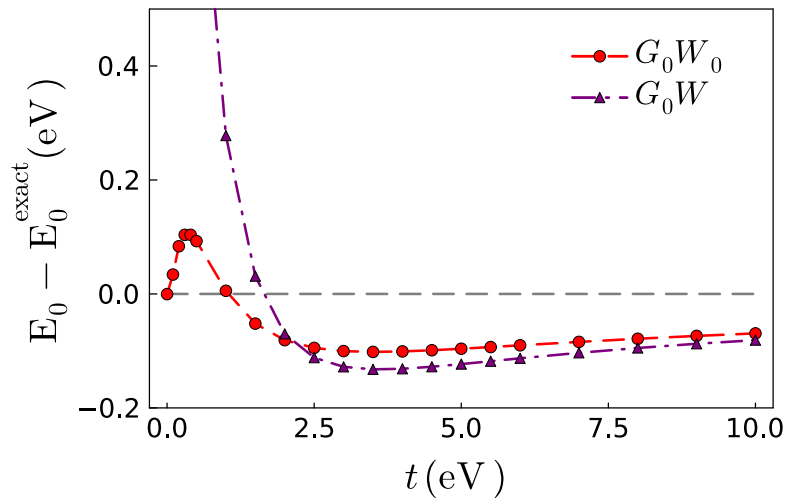
Figure 6.10: Error of the ground-state total energy as a function of the hopping t, where $U = 4$ eV. G_0W_0 and G_0W results are given in the red dashed and purple dot-dashed lines, respectively.

6.3.3   Electrons number

It is commonly known that the one-shot GW (G_0W_0) violates the electrons number [123]. This means that using the 1-GF resulting from the Dyson equation the integral $\int d\omega A(\omega)$ does not yield N. This is illustrated using the Hubbard dimer in Fig. 6.11. The problem is less severe when the exact W is used instead of the RPA one, where G_0W_0 yields zero electrons in the atomic limit. This explains using G_0W_0 why we get the exact HOMO and E_0 in this strong correlations regime where GW is supposed to fail. In both cases, the electrons number converge to the exact result in the range of weak correlations (U/t small).
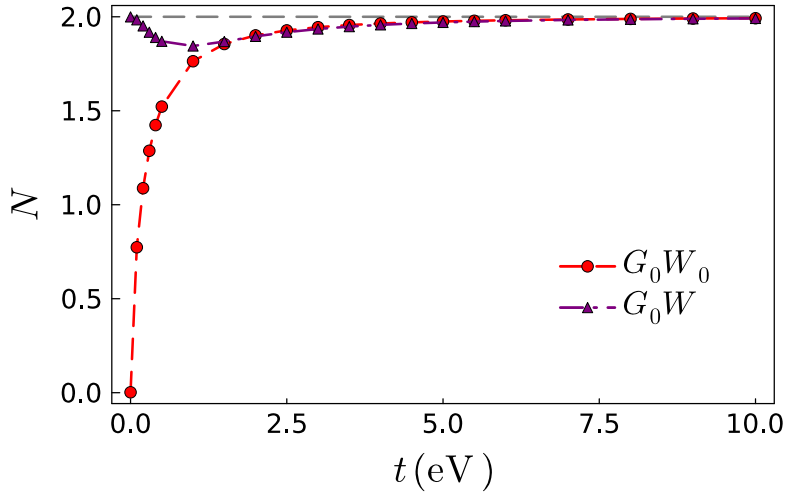
Figure 6.11: Electrons number N as a function of the hopping t, where $U = 4$ eV. G_0W_0 and G_0W results are given in the red dashed and purple dot-dashed lines, respectively.

6.4   Conclusions

After getting insights into the GW performance using two different screened interactions, namely the RPA and the exact ones, within the Hubbard dimer model at quarter and half-fillings, we summarize our findings about successes and failures of GWA, making a link with observations found in real systems.

- The GW method is capable of capturing spectral satellites, which are indicative of correlation effects and are important for total energies calculations. However, the GWA, besides giving a poor description of satellites, it is afflicted by a self-screening issue, particularly evident in the removal portions of the spectral function.

- There are instances where the GW approach violates exact constraints, notably the addition-removal symmetry and the electron number [55, 123].

- The accuracy of GW is most favorable for systems characterized by moderate to weak correlations. In such cases, it tends to yield reasonable results. For instance, in practice, the first and probably most well-known success of the GWA was to overcome the band gap underestimate

of Kohn-Sham eigenvalue differences in simple semiconductors [26, 64, 124, 125]. On the other hand, GW reduces the band gap overestimation by the HF since W is weaker than v_c. Moreover, the band structure or other properties such as effective masses and band widths have been calculated successfully for many other simple semiconductors and insulators [4, 102, 103].

However, its accuracy decreases significantly for systems exhibiting strong correlation, thereby limiting its applicability and reliability in these scenarios. For example, similarly to the failure describing the atomic limit of the symmetric Hubbard dimer, the GWA also fails in describing bulk NiO, predicting a metal character, where in reality the system is a paramagnetic insulator [126]. This is, therefore, a strong indication that GW falls down in describing systems with strong correlations.

- Using the exact TCTC screened Coulomb interaction W instead of the RPA W_0 does not improve, but rather worsens the results. The choice of the optimal screened Coulomb interaction is a question of interest that will be addressed in Chap. 9.

In conclusion, having introduced various approaches addressing the many-body electronic system, ranging from mean-field methods to many-body Green's functions, and having discussed the strengths and limitations of the GW approximation, the next part of this work introduces several strategies to go beyond GW.

6.5 Supporting informations: analytical solutions

In the present section, we provide the exact and approximate solutions for the Hubbard dimer model, where approximations are within the GW framework.

6.5.1 Exact solutions

Quarter-filling case: one electron system

We begin with the quarter-filling case of the symmetric Hubbard dimer model. It is a one-electron problem, where both choices of spin-up and down are equivalent. The hamiltonian becomes

$$\hat{H} = \epsilon_0 \sum_{i=1,2 \, \sigma=\uparrow\downarrow} \hat{n}_{i\sigma} - \sum_{<i,j>=1,2 \, i \neq j, \sigma} t_{ij} \hat{c}^{\dagger}_{i\sigma} \hat{c}_{j\sigma} \,. \tag{6.25}$$

Solving this one-electron hamiltonian analytically requires a basis-set of Slater determinants, denoted as $|1,2\rangle$ where 1 and 2 are the indices of the first and second atoms, respectively. Each atom can be occupied by $0, \uparrow, \downarrow$ and $\uparrow\downarrow$. So, for one-electron, the basis is: $\left[|\uparrow,0\rangle, |0,\uparrow\rangle, |\downarrow,0\rangle, |0,\downarrow\rangle \right]$. Thus, the hamiltonian is written as follows,

$$H = \begin{pmatrix} \langle\uparrow,0|\hat{H}|\uparrow,0\rangle & \langle\uparrow,0|\hat{H}|0,\uparrow\rangle & \langle\uparrow,0|\hat{H}|\downarrow,0\rangle & \langle\uparrow,0|\hat{H}|0,\downarrow\rangle \\ \langle0,\uparrow|\hat{H}|\uparrow,0\rangle & \langle0,\uparrow|\hat{H}|0,\uparrow\rangle & \langle0,\uparrow|\hat{H}|\downarrow,0\rangle & \langle0,\uparrow|\hat{H}|0,\downarrow\rangle \\ \langle0,\downarrow|\hat{H}|\uparrow,0\rangle & \langle0,\downarrow|\hat{H}|0,\uparrow\rangle & \langle0,\downarrow|\hat{H}|0,\downarrow\rangle & \langle0,\downarrow|\hat{H}|0,\downarrow\rangle \\ \langle\downarrow,0|\hat{H}|\uparrow,0\rangle & \langle\downarrow,0|\hat{H}|0,\uparrow\rangle & \langle\downarrow,0|\hat{H}|\downarrow,0\rangle & \langle\downarrow,0|\hat{H}|0,\downarrow\rangle \end{pmatrix}, \tag{6.26}$$

$$so, H = \begin{pmatrix} \epsilon_0 & -t & 0 & 0 \\ -t & \epsilon_0 & 0 & 0 \\ 0 & 0 & \epsilon_0 & -t \\ 0 & 0 & -t & \epsilon_0 \end{pmatrix}. \tag{6.27}$$

Eq.(6.27) can be written in the basis of eigenvectors, which are

$$\phi_1 = \frac{1}{\sqrt{2}} \begin{pmatrix} 1 \\ 1 \\ 0 \\ 0 \end{pmatrix}, \phi_2 = \frac{1}{\sqrt{2}} \begin{pmatrix} 0 \\ 0 \\ 1 \\ 1 \end{pmatrix}, \phi_3 = \frac{1}{\sqrt{2}} \begin{pmatrix} 1 \\ -1 \\ 0 \\ 0 \end{pmatrix}, \phi_4 = \frac{1}{\sqrt{2}} \begin{pmatrix} 0 \\ 0 \\ 1 \\ -1 \end{pmatrix}.$$ In this basis, a diagonal matrix

D can be obtained by using the following basis transformations,

$$D = P^{-1}HP, \tag{6.28}$$

where P is constructed by the eigenvectors

$$P = \frac{1}{\sqrt{2}} \begin{pmatrix} 1 & 0 & 1 & 0 \\ 1 & 0 & -1 & 0 \\ 0 & 1 & 0 & 1 \\ 0 & 1 & 0 & -1 \end{pmatrix}, \tag{6.29}$$

with P^{-1}, the inverse of P. By solving Eq.(6.28), we obtain the diagonal hamiltonian as,

$$D = \begin{pmatrix} \epsilon_0 - t & 0 & 0 & 0 \\ 0 & \epsilon_0 - t & 0 & 0 \\ 0 & 0 & \epsilon_0 + t & 0 \\ 0 & 0 & 0 & \epsilon_0 + t \end{pmatrix}. \tag{6.30}$$

In Tab. 6.1, we write the eigenvectors and eigenvalues for the one-electron system.

The ground-state for a one-electron system is the bonding-bonding molecular orbital, which is a constructive overlop between the atomic orbitals,

$$|N = 1\rangle = \frac{1}{\sqrt{2}} \left(|\uparrow, 0\rangle + |0, \uparrow\rangle \right), \tag{6.31}$$

with $\epsilon_0 - t$ the ground- state total energy. Regarding the ground-state, it is degenerate, meaning there are multiple states with the same energy. The ground-state can be a bonding state with a spin-up electron or a bonding state with a spin-down electron, or a linear combination. In reality, the choice of the ground-state for a one-electron system would be naturally the spin-up electron due to the presence of a magnetic field coming from earth. Following this, we select the spin-up electron as a ground-state for the quater-filling case.

Eigenvector	Eigenvalue
$\frac{1}{\sqrt{2}}\left(\left|\uparrow, 0\right\rangle + \left|0, \uparrow\right\rangle \right) = \frac{1}{\sqrt{2}}\begin{pmatrix} 1 \\ 1 \\ 0 \\ 0 \end{pmatrix}$	$\epsilon_0 - t$
$\frac{1}{\sqrt{2}}\left(\left|\downarrow, 0\right\rangle + \left|0, \downarrow\right\rangle \right) = \frac{1}{\sqrt{2}}\begin{pmatrix} 0 \\ 0 \\ 1 \\ 1 \end{pmatrix}$	$\epsilon_0 - t$
$\frac{1}{\sqrt{2}}\left(\left|\uparrow, 0\right\rangle - \left|0, \uparrow\right\rangle \right) = \frac{1}{\sqrt{2}}\begin{pmatrix} 1 \\ -1 \\ 0 \\ 0 \end{pmatrix}$	$\epsilon_0 + t$
$\frac{1}{\sqrt{2}}\left(\left|\downarrow, 0\right\rangle - \left|0, \downarrow\right\rangle \right) = \frac{1}{\sqrt{2}}\begin{pmatrix} 0 \\ 0 \\ 1 \\ -1 \end{pmatrix}$	$\epsilon_0 + t$

Table 6.1: Eigenvectors and eigenvalues of the symmetric two-site Hubbard modelat quarter-filling.

Half-filling case: two-electron system

In the case of a two-electron system, the basis of Slater determinants is $\left(\left|\uparrow, \uparrow\right\rangle, \left|\downarrow, \downarrow\right\rangle, \left|\uparrow, \downarrow\right\rangle, \left|\downarrow, \uparrow\right\rangle, \left|\uparrow\downarrow, 0\right\rangle, \left|0, \uparrow\downarrow\right\rangle \right)$. So, the hamiltonian becomes

$$H = \begin{pmatrix} 2\epsilon_0 & 0 & 0 & 0 & 0 & 0 \\ 0 & 2\epsilon_0 & 0 & 0 & 0 & 0 \\ 0 & 0 & 2\epsilon_0 & 0 & -t & -t \\ 0 & 0 & 0 & 2\epsilon_0 & t & t \\ 0 & 0 & -t & t & 2\epsilon_0 + U & 0 \\ 0 & 0 & -t & t & 0 & 2\epsilon_0 + U \end{pmatrix}. \tag{6.32}$$

In the diagonal basis, we have

$$D = \begin{pmatrix} 2\epsilon_0 & 0 & 0 & 0 & 0 & 0 \\ 0 & 2\epsilon_0 & 0 & 0 & 0 & 0 \\ 0 & 0 & 2\epsilon_0 & 0 & 0 & 0 \\ 0 & 0 & 0 & 2\epsilon_0 + U & 0 & 0 \\ 0 & 0 & 0 & 0 & 2\epsilon_0 + (U - c)/2 & 0 \\ 0 & 0 & 0 & 0 & 0 & 2\epsilon_0 + (U + c)/2 \end{pmatrix}, \tag{6.33}$$

where $c = \sqrt{16t^2 + U^2}$, $a = \sqrt{2((16t^2/(c - U)^2) + 1)}$ and $b = \sqrt{2((16t^2/(c + U)^2) + 1)}$.

The ground-state for $N = 2$ electrons system is

$$\left|N = 2\right\rangle = \frac{4t}{a(c - U)}\left(\left|\uparrow, \downarrow\right\rangle - \left|\downarrow, \uparrow\right\rangle \right) + \frac{1}{a}\left(\left|\uparrow\downarrow, 0\right\rangle + \left|0, \uparrow\downarrow\right\rangle \right), \tag{6.34}$$

where the ground-state energy E_0 is, $E_0 = 2\epsilon_0 + \frac{U - c}{2}$.

Eigenvector	Sector	Eigenvalue
$|\uparrow, \uparrow\rangle$	$\begin{pmatrix} 1 \\ 0 \\ 0 \\ 0 \\ 0 \\ 0 \end{pmatrix}$	$2\epsilon_0$
$|\downarrow, \downarrow\rangle$	$\begin{pmatrix} 0 \\ 1 \\ 0 \\ 0 \\ 0 \\ 0 \end{pmatrix}$	$2\epsilon_0$
$\frac{1}{\sqrt{2}}\left(|\uparrow, \downarrow\rangle + |\downarrow, \uparrow\rangle \right)$	$\frac{1}{\sqrt{2}}\begin{pmatrix} 0 \\ 0 \\ 1 \\ 1 \\ 0 \\ 0 \end{pmatrix}$	$2\epsilon_0$
$\frac{1}{\sqrt{2}}\left(|\uparrow\downarrow, 0\rangle - |0, \uparrow\downarrow\rangle \right)$	$\frac{1}{\sqrt{2}}\begin{pmatrix} 0 \\ 0 \\ 0 \\ 0 \\ 1 \\ -1 \end{pmatrix}$	$2\epsilon_0 + U$
$\frac{4t}{a(c-U)}\left(|\uparrow, \downarrow\rangle - |\downarrow, \uparrow\rangle \right) + 1/a\left(|\uparrow\downarrow, 0\rangle + |0, \uparrow\downarrow\rangle \right)$	$\begin{pmatrix} 0 \\ 0 \\ \frac{4t}{a(c-U)} \\ -\frac{4t}{a(c-U)} \\ 1/a \\ 1/a \end{pmatrix}$	$2\epsilon_0 + (U - c)/2$
$\frac{4t}{b(c+U)}\left(|\downarrow, \uparrow\rangle - |\uparrow, \downarrow\rangle \right) + 1/b\left(|\uparrow\downarrow, 0\rangle + |0, \uparrow\downarrow\rangle \right)$	$\begin{pmatrix} 0 \\ 0 \\ -\frac{4t}{b(c+U)} \\ \frac{4t}{b(c+U)} \\ 1/b \\ 1/b \end{pmatrix}$	$2\epsilon_0 + (U + c)/2$

Table 6.2: Eigenvectors and eigenvalues of the symmetric Hubbard dimer model at half-filling.

Three-electron system

For three-electron system, the basis of Slater determinants consists of: $\left(|\uparrow\downarrow, \uparrow\rangle, |\uparrow, \uparrow\downarrow\rangle, |\uparrow\downarrow, \downarrow\rangle, |\downarrow, \uparrow\downarrow\rangle \right)$. So, the hamiltonian is built as

$$H = \begin{pmatrix} \langle\uparrow\downarrow,\uparrow|\hat{H}|\uparrow\downarrow,\uparrow\rangle & \langle\uparrow\downarrow,\uparrow|\hat{H}|\uparrow,\uparrow\downarrow\rangle & \langle\uparrow\downarrow,\uparrow|\hat{H}|\uparrow\downarrow,\downarrow\rangle & \langle\uparrow\downarrow,\uparrow/\hat{H}/\downarrow,\uparrow\downarrow\rangle \\ \langle\uparrow,\downarrow\uparrow|\hat{H}|\uparrow\downarrow,\uparrow\rangle & \langle\uparrow,\uparrow\downarrow|\hat{H}|\uparrow,\uparrow\downarrow\rangle & \langle\uparrow,\uparrow\downarrow|\hat{H}|\uparrow\downarrow,\downarrow\rangle & \langle\uparrow,\uparrow\downarrow|\hat{H}|\downarrow,\uparrow\downarrow\rangle \\ \langle\uparrow\downarrow,\downarrow|\hat{H}|\uparrow\downarrow,\uparrow\rangle & \langle\uparrow\downarrow,\downarrow|\hat{H}|\uparrow,\uparrow\downarrow\rangle & \langle\uparrow\downarrow,\downarrow|\hat{H}|\uparrow\downarrow,\downarrow\rangle & \langle\uparrow\downarrow,\downarrow|\hat{H}|\downarrow,\uparrow\downarrow\rangle \\ \langle\downarrow,\uparrow\downarrow|\hat{H}|\uparrow\downarrow,\uparrow\rangle & \langle\downarrow,\uparrow\downarrow|\hat{H}|\uparrow,\uparrow\downarrow\rangle & \langle\downarrow,\uparrow\downarrow|\hat{H}|\uparrow\downarrow,\downarrow\rangle & \langle\downarrow,\uparrow\downarrow,|\hat{H}|\downarrow,\uparrow\downarrow\rangle \end{pmatrix} . \tag{6.35}$$

It is solved as

$$H = \begin{pmatrix} 3\epsilon_0 + U & -t & 0 & 0 \\ -t & 3\epsilon_0 + U & 0 & 0 \\ 0 & 0 & 3\epsilon_0 + U & -t \\ 0 & 0 & -t & 3\epsilon_0 + U \end{pmatrix} . \tag{6.36}$$

Eigenvector	Sector	Eigenvalue
$\frac{1}{\sqrt{2}}(|\uparrow\downarrow,\uparrow\rangle + |\uparrow,\uparrow\downarrow\rangle)$	$1/\sqrt{2} \begin{pmatrix} 1 \\ 1 \\ 0 \\ 0 \end{pmatrix}$	$-t + U + 3\epsilon_0$
$\frac{1}{\sqrt{2}}(|\uparrow\downarrow,\downarrow\rangle + |\downarrow,\uparrow\downarrow\rangle)$	$1/\sqrt{2} \begin{pmatrix} 0 \\ 0 \\ 1 \\ 1 \end{pmatrix}$	$-t + U + 3\epsilon_0$
$\frac{1}{\sqrt{2}}(|\uparrow\downarrow,\uparrow\rangle - |\uparrow,\uparrow\downarrow\rangle)$	$1/\sqrt{2} \begin{pmatrix} 1 \\ -1 \\ 0 \\ 0 \end{pmatrix}$	$t + U + 3\epsilon_0$
$\frac{1}{\sqrt{2}}(|\uparrow\downarrow,\downarrow\rangle - |\downarrow,\uparrow\downarrow\rangle)$	$1/\sqrt{2} \begin{pmatrix} 0 \\ 0 \\ 1 \\ -1 \end{pmatrix}$	$t + U + 3\epsilon_0$

Table 6.3: Eigenvectors and eigenvalues of the symmetric Hubbard dimer model with three-electron.

Exact Green's functions for the Hubbard model

The 1-GF in the discrete space is defined in Eq.(B.13). We derive its expression in frequency space as follows.

$$G_{ij\sigma\sigma'}(t - t') = -i\left[\theta(t - t')\langle N|\hat{c}_{i\sigma}(t)\hat{c}^\dagger_{j\sigma'}(t')|N\rangle - \theta(t' - t)\langle N|\hat{c}^\dagger_{j\sigma'}(t')\hat{c}_{i\sigma}(t)|N\rangle\right], \tag{6.37}$$

where $\theta(t)$ is the heaviside function, which is defined as,

$$\theta(t) = \begin{cases} 1 & \text{if } t > 0 \\ \frac{1}{2} & \text{if } t = 0 \\ 0 & \text{if } t < 0 . \end{cases}$$

Then, by using the following definition of the time dependent operators within the Heisenberg scheme,

$$\hat{c}(t) = e^{i\hat{H}t}\hat{c}e^{-i\hat{H}t} , \qquad (6.38)$$

we have

$$G_{ij\sigma\sigma'}(t - t') = -i\theta(t - t') \langle N|e^{i\hat{H}t}\hat{c}_{i\sigma}e^{-i\hat{H}t}e^{i\hat{H}t'}\hat{c}_{j\sigma'}^{\dagger}e^{-i\hat{H}t'}|N\rangle$$
$$+ i\theta(t' - t) \langle N|e^{i\hat{H}t'}\hat{c}_{j\sigma'}^{\dagger}e^{-i\hat{H}t'}e^{i\hat{H}t}\hat{c}_{i\sigma}e^{-i\hat{H}t}|N\rangle . \qquad (6.39)$$

Now, we insert the completeness relations for $N - 1$ and $N + 1$ electrons systems,

$$G_{ij\sigma\sigma'}(t, t') = -i\theta(t - t') \langle N_0|e^{i\hat{H}t}\hat{c}_{i\sigma}e^{-i\hat{H}t} \sum_s |N + 1\rangle_s \langle N + 1|_s e^{i\hat{H}t'}\hat{c}_{j\sigma'}^{\dagger}e^{-i\hat{H}t'}|N_0\rangle +$$
$$i\theta(t' - t) \langle N_0|e^{i\hat{H}t'}\hat{c}_{j\sigma'}^{\dagger}e^{-i\hat{H}t'} \sum_s |N - 1\rangle_s \langle N - 1|_s e^{i\hat{H}t}\hat{c}_{i\sigma}e^{-i\hat{H}t}|N_0\rangle , \qquad (6.40)$$

where $|N - 1\rangle$ and $|N + 1\rangle$ are the many-body wavefunctions for $N - 1$ and $N + 1$ electron systems. The $\sum_s$ is the sum over all the states, ground and excited states, with $|N_0\rangle$ is the ground-state for the N electrons system. So, we have

$$G_{ij\sigma\sigma'}(t - t') = -i\theta(t - t') \sum_s e^{iE_0^N t} \langle N_0|\hat{c}_{i\sigma}|N + 1\rangle_s e^{-iE_s^{N+1}t}e^{(iE_s^{N+1})t'} \langle N + 1|_s\hat{c}_{j\sigma'}^{\dagger}|N_0\rangle e^{-(iE_0^N)t'}$$
$$+ i\theta(t' - t) \sum_s e^{iE_0^N t'} \langle N_0|\hat{c}_{j\sigma'}^{\dagger}|N - 1\rangle_s e^{-iE_s^{N-1}t'}e^{iE_s^{N-1}t} \langle N - 1|_s\hat{c}_{i\sigma}|N_0\rangle e^{-iE_0^N t}$$

$$(6.41)$$

$$= -i\theta(t - t') \sum_s e^{i(E_0^N - E_s^{N+1})(t-t')} \langle N_0|\hat{c}_{i\sigma}|N + 1\rangle_s \langle N + 1|_s\hat{c}_{j\sigma'}^{\dagger}|N_0\rangle . \qquad (6.42)$$
$$+ i\theta(t' - t) \sum_s e^{i(E_s^{N-1} - E_0)(t-t')} \langle N_0|\hat{c}_{j\sigma'}^{\dagger}|N - 1\rangle_s \langle N - 1|_s\hat{c}_{i\sigma}|N_0\rangle$$

Now, we move to the frequency space, by using the inverse Fourier transform of the heaviside function,

$$\theta(t - t') = -\frac{1}{2\pi i} \int d\omega' \frac{e^{-i\omega'(t-t')}}{\omega' + i\eta} , \qquad (6.43)$$

so, this yields

$$G_{ij\sigma\sigma'}(t - t') = \sum_s \int \frac{d\omega'}{2\pi} \frac{e^{-i(E_s^{N+1} - E_0^N + \omega')(t-t')}}{\omega' + i\eta} \langle N_0|\hat{c}_{i\sigma}|N + 1\rangle_s \langle N + 1|_s\hat{c}_{j\sigma'}^{\dagger}|N_0\rangle$$
$$- \sum_s \int \frac{d\omega'}{2\pi} \frac{e^{-i(E_0^N - E_s^{N-1} - \omega')(t-t')}}{\omega' + i\eta} \langle N_0|\hat{c}_{j\sigma'}^{\dagger}|N - 1\rangle_s \langle N - 1|_s\hat{c}_{i\sigma}|N_0\rangle . \qquad (6.44)$$

Finally, we obtain the 1-GF definition in frequency and discrete space,

$$G_{ij\sigma\sigma'}(\omega) = \sum_s \left[\frac{\langle N_0|\hat{c}_{j\sigma'}^{\dagger}|N - 1\rangle_s \langle N - 1|_s\hat{c}_{i\sigma}|N_0\rangle}{\omega - (E_0^N - E_s^{N-1}) - i\eta} + \frac{\langle N_0|\hat{c}_{i\sigma}|N + 1\rangle_s \langle N + 1|_s\hat{c}_{j\sigma'}^{\dagger}|N_0|\rangle}{\omega + (E_0^N - E_s^{N+1}) + i\eta} \right] . \qquad (6.45)$$
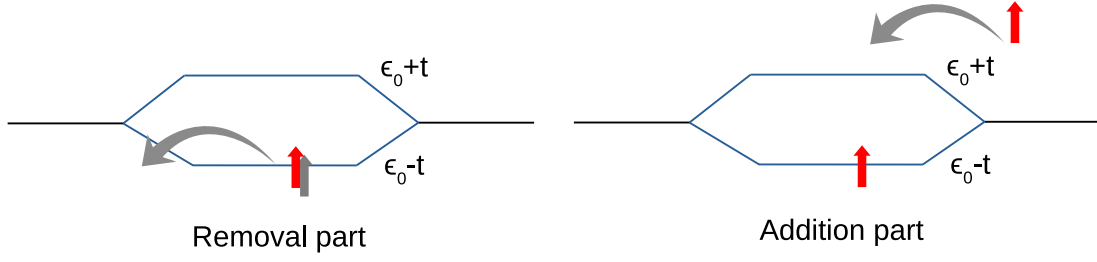
Figure 6.12: Removal (left panel) and addition (right panel) parts of the spin-up 1-GF for the symmetric two-site Hubbard model with one-electron. $\epsilon_0 - t$ and $\epsilon_0 + t$ are the bonding and antibonding energies, respectively.

By using Eq.(6.45) for the Hubbard model with different electron number, we calculate the 1-GF for the different systems. For $N = 1$, the exact 1-GF matrix ij elements are

$$G_{ij\uparrow}(\omega) = \frac{1}{2}\left[\frac{1}{\omega - (\epsilon_0 - t) - i\eta} + \frac{(-1)^{i-j}}{\omega - (\epsilon_0 + t) + i\eta}\right], \tag{6.46}$$

which is equivalent to the non-interacting 1-GF, because since the 1-GF describes the removal and addition of electron, the spin-up electron when it is removed has no other electrons to interact with. When we add a spin-up electron, it should be added to the unoccupied state, since another spin-up electron is in the ground-state. Therefore, the added electrob also does not interact with the other spin-up electron, because they occupy different sites. This is illustrated in Fig. 6.12.

On the other hand, the spin-down 1-GF involves interaction since the additional electron can occupy the same site as the spin-up electron. The matrix elements for the spin-down components are

$$G_{ij\downarrow}(\omega) = (-1)^{i-j}\frac{1}{4}\left(\frac{1}{\omega - (\epsilon_0 + t) + i\eta} + \frac{1}{\omega - (\epsilon_0 + t + U) + i\eta}\right) + \frac{\frac{1}{2a^2}\left(1 + 4t/(c - U)\right)^2}{\omega - (\epsilon_0 + t + (U - c)/2) + i\eta}$$

$$+ \frac{\frac{1}{2b^2}\left(1 - 4t/(c + U)\right)^2}{\omega - (\epsilon_0 + t + (U + c)/2) + i\eta}. \tag{6.47}$$

There are only addition parts, because there is no spin-down electron in the ground-state. For $N = 2$, the 1-GF matrix elements are

$$G_{ij\sigma}(\omega) = \frac{\frac{1}{2a^2}\left(1 + 4t/(c - U)\right)^2}{\omega - \left(\epsilon_0 + t - (c - U)/2\right) - i\eta} + \frac{\frac{(-1)^{i-j}}{2a^2}\left(1 - 4t/(c - U)\right)^2}{\omega - \left(\epsilon_0 - t - (c - U)/2\right) - i\eta} + \frac{\frac{(-1)^{i-j}}{2a^2}\left(1 + 4t/(c - U)\right)^2}{\omega - \left(\epsilon_0 - t + (c + U)/2\right) + i\eta}$$

$$+ \frac{\frac{1}{2a^2}\left(1 - 4t/(c - U)\right)^2}{\omega - \left(\epsilon_0 + t + (c + U)/2\right) + i\eta}, \tag{6.48}$$

where $G_{ij\uparrow} = G_{ij\downarrow}$.

64

6.5.2 *GW* solutions

Quarter-filling case: one-electron system

For illustration and discussion, we first present results for the dimer with one spin-up electron in the ground state. These results can be also found in literature, e.g, in Ref. [55].

The 1-GF solution within GWA (G^{GW}) can be obtained by solving the Dyson equation, which is written in matrix form in site basis and in frequency space as follows,

$$G^{GW}(\omega) = G_0(\omega) - v_{\mathrm{H}} - \Sigma_{\mathrm{xc}}^{GW}(\omega)\,, \tag{6.49}$$

where G_0 is the non-interacting 1-GF matrix, v_{H} is the Hartree potential matrix and Σ^{GW} is the exchange-correlation (xc) self-energy matrix within GWA. To obtain G, we need G_0, v_{H} and $\Sigma_{\mathrm{xc}}^{GW}$. The G_0 matrix elements are given below,

$$G_{0ij\uparrow}(\omega) = \frac{(-1)^{i-j}}{2}\left(\frac{(-1)^{i-j}}{\omega - (\epsilon_0 - t) - i\eta} + \frac{1}{\omega - (\epsilon_0 + t) + i\eta}\right), \tag{6.50}$$

and,

$$G_{0ij\downarrow}(\omega) = \frac{(-1)^{i-j}}{2}\left(\frac{(-1)^{i-j}}{\omega - (\epsilon_0 - t) + i\eta} + \frac{1}{\omega - (\epsilon_0 + t) + i\eta}\right), \tag{6.51}$$

where the G_0 matrix is

$$G_0(\omega) = \begin{pmatrix} G_{011\uparrow} & G_{012\uparrow} & 0 & 0 \\ G_{021\uparrow} & G_{022\uparrow} & 0 & 0 \\ 0 & 0 & G_{011\downarrow} & G_{012\downarrow} \\ 0 & 0 & G_{021\downarrow} & G_{022\downarrow} \end{pmatrix}. \tag{6.52}$$

The Hartree potential within the Hubbard dimer is

$$v_{\mathrm{H}(ij)}(\omega) = \sum_{\sigma_1} \langle N_0 | \hat{c}_{i\sigma_1}^{\dagger} \hat{c}_{j\sigma_1} | N_0 \rangle\, \delta_{ij} U\,. \tag{6.53}$$

Thus, the Hartree matrix becomes

$$v_{\mathrm{H}}(\omega) = \begin{pmatrix} \frac{U}{2} & 0 & 0 & 0 \\ 0 & \frac{U}{2} & 0 & 0 \\ 0 & 0 & \frac{U}{2} & 0 \\ 0 & 0 & 0 & \frac{U}{2} \end{pmatrix}. \tag{6.54}$$

By using the Hartree potential in the Dyson equation, one obtains the Hartree 1-GF matrix-elements,

$$G_{\mathrm{H}ij\uparrow}(\omega) = \frac{1}{2}\left(\frac{1}{\omega - (\epsilon_0 - t + U/2) - i\eta} + \frac{1}{\omega - (\epsilon_0 + t + U/2) + i\eta}\right), \tag{6.55}$$

and,

$$G_{\mathrm{H}ij\downarrow}(\omega) = \frac{1}{2}\left(\frac{1}{\omega - (\epsilon_0 - t + U/2) + i\eta} + \frac{1}{\omega - (\epsilon_0 + t + U/2) + i\eta}\right). \tag{6.56}$$

Now, we calculate Σ_{xc}^{GW} within one-shot calculations using G_0 and the screened Coulomb interaction within the RPA (W_0). Therefore, we would solve the following integral, written in the Hubbard site-basis,

$$\Sigma_{\text{xc}ij,\sigma}^{G_0 W_0}(\omega) = \frac{i}{2\pi} \int d\omega G_{0ij\sigma}(\omega) W_{0ji}(\omega) e^{i\omega\eta} , \tag{6.57}$$

where W_0 matrix-elements are obtained by using the Dyson equation,

$$W_{0,ij}(\omega) = U\delta_{ij} + U \sum_{k\sigma} P_{ik=1,2\sigma=\uparrow,\downarrow}^{\text{RPA}}(\omega) W_{0kj}(\omega) . \tag{6.58}$$

where P^{RPA} is the irreducible polarizability P within the RPA that can be calculated from

$$P_{ij\sigma}^{\text{RPA}}(\omega) = -i \int \frac{d\omega}{2\pi} G_{0ij\sigma}(\omega + \omega') G_{0ji\sigma}(\omega') e^{i\omega\eta} . \tag{6.59}$$

It has the following solutions,

$$P_{ij\uparrow}^{RPA}(\omega) = \frac{(-1)^{i-j}}{4} \left(\frac{1}{\omega - 2t + i\eta} - \frac{1}{\omega + 2t - i\eta} \right) , \tag{6.60}$$

and,

$$P_{ij\downarrow}^{RPA}(\omega) = 0 . \tag{6.61}$$

Since there is no spin-down electron to polarize, the spin-down matrix-elements are zero. Note that P^{RPA} describes the non-interacting electron excitations, where the pole $2t$ represents the bonding-antibonding energy difference. Using P^{RPA} in Eq.(6.58), we obtain

$$W_{011}(\omega) = U + U\left(P_{11\uparrow}(\omega)W_{11}(\omega) + P_{12\uparrow}(\omega)W_{21}(\omega) + P_{11\downarrow}(\omega)W_{11}(\omega) + P_{12\downarrow}(\omega)W_{21}(\omega) \right) \tag{6.62}$$

$$W_{011}(\omega)\left(1 - UP_{11\uparrow}(\omega) \right) = U + UP_{12\uparrow}(\omega)W_{21}(\omega) . \tag{6.63}$$

For the off-diagonal elements,

$$W_{021}(\omega) = 0 + U\left(P_{21\uparrow}(\omega)W_{011}(\omega) + P_{22\uparrow}(\omega)W_{021}(\omega) \right) \tag{6.64}$$

$$W_{021}(\omega) = \frac{UP_{21\uparrow}(\omega)}{W_{011}(\omega)1 - UP_{22\uparrow}(\omega)} . \tag{6.65}$$

So,

$$W_{011}(\omega)\Big(1 - UP_{11\uparrow}(\omega)\Big) = U + \frac{U^2 P_{12\uparrow}^2(\omega) W_{11}(\omega)}{1 - UP_{22\uparrow}(\omega)} \tag{6.66}$$

$$W_{011}(\omega)\Big(1 - UP_{11\uparrow}(\omega) - \frac{U^2 P_{12\uparrow}^2(\omega)}{1 - UP_{22\uparrow}(\omega)}\Big) = U \tag{6.67}$$

$$W_{011}(\omega)\Big((1 - UP_{11\uparrow}(\omega))^2 - U^2 P_{12\uparrow}^2(\omega)\Big) = U\Big(1 - UP_{22\uparrow}(\omega)\Big) \tag{6.68}$$

$$W_{011}(\omega)\Big(1 - 2UP_{11\uparrow}(\omega) + U^2 P_{11\uparrow}^2(\omega) - U^2 P_{12\uparrow}^2(\omega)\Big) = U\Big(1 - UP_{22\uparrow}(\omega)\Big) \tag{6.69}$$

$$W_{011}(\omega) = U\frac{1 - UP_{22\uparrow}(\omega)}{1 - 2UP_{11\uparrow}(\omega)} \tag{6.70}$$

$$W_{011}(\omega) = U\frac{1 - \frac{Ut}{\omega^2 - 4t^2 + i\eta}}{1 - \frac{2Ut}{\omega^2 - 4t^2 + i\eta}} \tag{6.71}$$

$$W_{011}(\omega) = U\frac{1 - \frac{Ut}{\omega^2 - 4t^2 + i\eta}}{1 - \frac{2Ut}{\omega^2 - 4t^2 + i\eta}} \tag{6.72}$$

$$W_{011}(\omega) = U\frac{1 - \frac{Ut}{\omega^2 - 4t^2 + i\eta}}{1 - \frac{2Ut}{\omega^2 - 4t^2 + i\eta}} \tag{6.73}$$

$$W_{011}(\omega) = U + \frac{U^2 t}{\omega^2 - 4t^2 - 2Ut + i\eta}. \tag{6.74}$$

Moreover,

$$W_{021}(\omega) = \frac{UP_{21\uparrow}}{1 - UP_{22\uparrow}(\omega)}W_{011}(\omega) \tag{6.75}$$

$$= \frac{-Ut}{\omega^2 - 4t^2 - Ut + i\eta}W_{011}(\omega) \tag{6.76}$$

$$W_{021}(\omega) = -\frac{U^2 t}{\omega^2 - 4t^2 - Ut + i\eta} - \frac{U^3 t^2}{(\omega^2 - 4t^2 - Ut + i\eta)(\omega^2 - 4t^2 - 2Ut + i\eta)} \tag{6.77}$$

$$W_{021}(w) = -\frac{U^2 t}{\omega^2 - 4t^2 - Ut + i\eta}\Big(1 + \frac{Ut}{\omega^2 - 4t^2 - 2Ut + i\eta}\Big) \tag{6.78}$$

$$W_{021}(\omega) = -\frac{U^2 t}{\omega^2 - 4t^2 - 2Ut + i\eta}. \tag{6.79}$$

So, the W_0 matrix-elements are

$$W_{0ij}(\omega) = U\delta_{ij} + (-1)^{i-j}\frac{U^2 t}{2h}\Big(\frac{1}{\omega - h + 2i\eta} - \frac{1}{\omega + h - 2i\eta}\Big), \tag{6.80}$$

where $h^2 = 4t^2 + 2Ut$. Now, the necessary ingredients are obtained to solve the *GW* integral 6.57, which can be done by using the Cauchy's residue theorem, which is

$$\oint_C dz f(z) = 2\pi i \sum_k Res_{z=a_k} f(z), \tag{6.81}$$

where $Res_{z=a_k}$ denotes the residue of the function f with respect to the pole k. For a simple pole,

$$Res_{z=a_k} f(z) = lim_{z \to a_k}(z - a_k)f(z). \tag{6.82}$$

For poles of ordre n,

$$Res_{z=a_k} f(z) = \frac{1}{(n-1)!} lim_{z \to a_k} \frac{d^{n-1}}{dz^{n-1}} \left[(z - a_k)^n f(z) \right]. \tag{6.83}$$

By using this theorem, we obtain the $\Sigma_{\text{xc}}^{G_0 W_0}$

$$\Sigma_{\text{xc}}^{G_0 W_0}(\omega) = \begin{pmatrix} \Sigma_{\text{xc},11\uparrow}^{G_0 W_0}(\omega) & \Sigma_{\text{xc},12\uparrow}^{G_0 W_0}(\omega) & 0 & 0 \\ \Sigma_{\text{xc},21\uparrow}^{G_0 W_0}(\omega) & \Sigma_{\text{xc},22\uparrow}^{G_0 W_0}(\omega) & 0 & 0 \\ 0 & 0 & \Sigma_{\text{xc},11\downarrow}^{G_0 W_0}(\omega) & \Sigma_{\text{xc},12\downarrow}^{G_0 W_0}(\omega) \\ 0 & 0 & \Sigma_{\text{xc},21\downarrow}^{G_0 W_0}(\omega) & \Sigma_{\text{xc},22\downarrow}^{G_0 W_0}(\omega) \end{pmatrix}, \tag{6.84}$$

where

$$\Sigma_{\text{xc},ij\uparrow}^{G_0 W_0}(\omega) = -\frac{U}{2}\delta_{ij} + \frac{U^2 t}{4h} \left(\frac{(-1)^{i-j}}{\omega - (\epsilon_0 - t - h) - 3i\eta} + \frac{1}{\omega - (\epsilon_0 + t + h) + 3i\eta} \right), \tag{6.85}$$

$$\Sigma_{\text{xc},ij\downarrow}^{G_0 W_0}(\omega) = \frac{U^2 t}{4h} \left(\frac{1}{\omega - (\epsilon_0 + t + h) + 3i\eta} + \frac{(-1)^{i-j}}{\omega - (\epsilon_0 - t + h) + 3i\eta} \right). \tag{6.86}$$

It is worth mentioning that the exchange spin-up self-energy $-\frac{U}{2}$ corrects the Hartree self-interaction. The remaining part of $\Sigma_{\text{xc}\uparrow}$ is the dynamical correlation that describes the screening. For the spin-down self-energy, there is no exchange term, since the exchange interaction occurs between electrons with parallel spins. Additionally, it is important to attract attention to the fact that we keep all the broadening accumulation $i\eta$, $2i\eta$, $3i\eta$... despite the fact that $\eta \to 0$, because numerically η has a finite value.

Thus the $G_0 W_0$ 1-GF can be obtained by solving the matrix equation 6.49, numerically or analytically, leading to the following analytic result,

$$G_{ij\uparrow}^{G_0 W_0}(\omega) = (-1)^{i-j} \frac{\frac{1}{4} + \frac{2t+h}{4A}}{\omega - \omega_1 + i\eta} + (-1)^{i-j} \frac{\frac{1}{4} - \frac{2t+h}{4A}}{\omega - \omega_2 - i\eta} + \frac{\frac{1}{4} - \frac{2t+h}{4A}}{\omega - \omega_3 + i\eta} + \frac{\frac{1}{4} + \frac{2t+h}{4A}}{\omega - \omega_4 - i\eta}, \tag{6.87}$$

where $A = \sqrt{(h+2t)^2 + \frac{2U^2 t}{h}}$, $\omega_1 = \frac{2\epsilon_0 - h + A}{2}$, $\omega_2 = \frac{2\epsilon_0 - h - A}{2}$, $\omega_3 = \frac{2\epsilon_0 + h + A}{2}$ and $\omega_4 = \frac{2\epsilon_0 + h - A}{2}$. And,

$$G_{ij\downarrow}^{G_0 W_0}(\omega) = (-1)^{i-j} \frac{\frac{1}{4} + \frac{2t-h+U/2}{4B}}{\omega - \omega_5 + i\eta} + (-1)^{i-j} \frac{\frac{1}{4} - \frac{2t-h+U/2}{4B}}{\omega - \omega_6 + i\eta} + \frac{\frac{1}{4} - \frac{2t+h-U/2}{4C}}{\omega - \omega_7 + i\eta} + \frac{\frac{1}{4} + \frac{2t+h-U/2}{4C}}{\omega - \omega_8 + i\eta}, \tag{6.88}$$

where $B = \sqrt{(h - 2t - U/2)^2 + \frac{2U^2 t}{h}}$ and $C = \sqrt{(h + 2t - U/2)^2 + \frac{2U^2 t}{h}}$. $\omega_5 = \frac{2\epsilon_0 + h + U/2 + B}{2}$, $\omega_6 = \frac{2\epsilon_0 + h + U/2 - B}{2}$, $\omega_7 = \frac{2\epsilon_0 + h + U/2 + C}{2}$ and $\omega_8 = \frac{2\epsilon_0 + h + U/2 - C}{2}$.

Half-filling case: two-electron system

The non-interacting 1-GF holds the same definition as the one electron system, where the only difference is that the spin-down element has a removal pole since it exists in the ground-state. So, we have

$$G_{0,ij\sigma}(\omega) = \frac{1}{2} \left(\frac{1}{\omega - (\epsilon_0 - t) - i\eta} + \frac{(-1)^{i-j}}{\omega - (\epsilon_0 + t) + i\eta} \right), \tag{6.89}$$

where $G_{0,ij\uparrow} = G_{0,ij\downarrow}$. The screened interaction within the RPA (W_0) is obtained from $P^{\mathrm{RPA}}(\omega)$, which still has the same definition as the one-electron case, but the difference is that the spin-down components exist. Thus, using the W definition derived in Eq.(6.58), we obtain

$$W_{0,ij}(\omega) = U\delta_{ij} + (-1)^{i-j}\frac{U^2 t}{h_2}\left(\frac{1}{\omega - h_2 + i\eta} - \frac{1}{\omega + h_2 - i\eta}\right), \tag{6.90}$$

where $h_2 = \sqrt{4t^2 + 4Ut}$. The exact W is calculated in Sec. 7.5 of Chap. 7, where the exact χ and its structure is discussed. Here, we use the final answer,

$$W_{ij}(\omega) = U\delta_{ij} + (-1)^{i-j}\frac{2U^2}{a^2}\left(\frac{1}{\omega - (c+U)/2 + i\eta} - \frac{1}{\omega + (c+U)/2 - i\eta}\right).$$

Using these two screened interactions together with G_0, we get the two different Σ_{xc} matrix elements,

$$\Sigma_{\mathrm{xc},ij\sigma}^{G_0 W_0}(\omega) = -\frac{U}{2}\delta_{ij} + \frac{U^2 t}{2h_2}\left(\frac{1}{\omega - (\epsilon_0 + t + h_2) + i\eta} + \frac{(-1)^{i-j}}{\omega - (\epsilon_0 - t - h_2) - i\eta}\right), \tag{6.91}$$

where $\Sigma_{\mathrm{xc},ij\uparrow}^{G_0 W_0} = \Sigma_{\mathrm{xc},ij\downarrow}^{G_0 W_0}$ and,

$$\Sigma_{\mathrm{xc},ij\sigma}^{G_0 W}(\omega) = -\frac{U}{2}\delta_{ij} + \frac{U^2}{a^2}\left(\frac{1}{\omega - (\epsilon_0 + t + \frac{c+U}{2}) + i\eta} + \frac{(-1)^{i-j}}{\omega - (\epsilon_0 - t - \frac{c+U}{2}) - i\eta}\right), \tag{6.92}$$

where $\Sigma_{\mathrm{xc},ij\uparrow}^{G_0 W} = \Sigma_{\mathrm{xc},ij\downarrow}^{G_0 W}$. In both cases, the exact Hartree potential v_H matrix elements that will be added to Σ_{xc} to solve the Dyson equation are $v_{\mathrm{H},ij} = U\delta_{ij}$.

Part II

Theoretical Development

Chapter 7

Total energy beyond GW using density-functional ingredients

Many important properties of materials are linked to observables that can be expressed in principle as expectation values in the many-body ground-state or in thermal equilibrium. In practice, the use of many-body wavefunctions is often avoided by rather describing the observables as functionals of more compact quantities, i.e., quantities that depend on less arguments, such as the density [7], one-body reduced density matrix [127–129], or one- or two-body Green's functions [4]. This represents a trade-off: often, one does not know the exact functional for an observable in terms of these quantities, and approximations have to be designed. One important example is the total energy: it can be straightforwardly formulated in terms of the one-body Green's function (1-GF) [94], whereas no exact explicit expression in terms of the density is known. The same holds for electron addition and removal spectral functions. Excitation spectra involving neutral excitations in linear response, instead, are easily expressed in terms of a two-body Green's function, but not in terms of the ground-state density or the one-body Green's function [4]. Even when the expressions are known, one faces another problem: while the use of the compact quantities carries the promise of reduced computational load, they are themselves only known explicitly as expectation values involving many-body wavefunctions. Therefore, nothing is gained, unless one finds ways to calculate them in a different way, which may be in principle exact, and in practice, require approximations. Typically, the density is obtained from the Kohn-Sham equations [8] with an approximate exchange-correlation (xc) potential, and the 1-GF, from a Dyson equation with an approximate xc self-energy Σ_{xc} [63]. It is therefore not always obvious which framework (Density Functional Theory (DFT), Green's Function Functional Theory (etc.) is the best choice to access a given observable. This holds in particular for the total ground-state energy E_0. While the Galitskii-Migdal formula [94] or functional expressions such as the Luttinger-Ward [130] or Klein [131] functionals yield an in principal exact and, in the latter two cases, even variational, form in terms of the 1-GF G, the need for approximations to the 1-GF itself strongly impacts the quality of the results. Together with a computational load far heavier than that of the most widely used density functionals, this explains why the vast majority of total energy calculations is performed using DFT, not Green's functions. Still, research concerning total energy calculations using Green's functions is active and important [51, 53, 117, 132].

Besides the - important - fact that in principle expressions for E_0 as functional of G and/or Σ_{xc} are known, the Green's functions framework benefits from the existence of powerful approximations. In particular, Many-Body Perturbation Theory (MBPT) [63] suggests a way to expand the self-energy in diagrams that carry physical meaning and that are therefore helpful to describe phenomena such as the van der Waals dispersion interaction [133]. For situations that show only weak to moderate interaction effects, MBPT is often considered to be a systematic way to proceed, although in practice renormalizations, such as screening of the Coulomb interaction, are needed. In particular, even the lowest order of an expansion of the self-energy in terms of the screened Coulomb interaction W, which is the widely used GW approximation [24], has been very successful for the calculation of the quasi-particle (QP) part of electron addition and removal spectra in finite and extended systems [4, 26–33].

However, there are many cases where the GW approximation is not sufficient. On one hand, the description of QP energies is not always good and certainly worsens in more strongly correlated systems [4, 54]. On the other hand, other quantities, such as satellite features in the electron addition and removal spectra, are often less well described, even in absence of strong correlation [134, 135]. Most importantly, GW does not necessarily yield total energies of better quality than currently used density functionals [51–53]. Research on total energies in terms of 1-GFs goes therefore hand in hand with research on approximations to the self-energy beyond GW. The most straightforward way to go would be to explore higher orders in W, and important research in this direction is ongoing [71–81]. In many cases it cannot, however, bring a practical solution, since the resulting expressions become quickly very cumbersome and costly, and since perturbation theory will diverge when the interaction is too strong. Therefore, it would be desirable to find an efficient way to terminate the series.

In the various possible ways to express the xc energy contribution to the total energy such as the adiabatic connection fluctuation dissipation theorem [136, 137], the polarizability plays a key role. This suggests to explore links to other frameworks that are used to access the polarizability, in particular, Time-Dependent DFT (TDDFT) [89]. Indeed, there is a long, and sometimes very successful, history of attempts to use TDDFT in order to go beyond GW in terms of vertex corrections based on the xc kernel f_{xc} [59–66, 68, 70], the functional derivative with respect to the density of the xc potential v_{xc} of TDDFT [138], or related linear response kernels that may be closer to the many-body Green's functions framework [139–142]. This kind of combination leads to the so-called $G\tilde{W}$ self-energy, where the Coulomb interaction is screened by a test charge-test electron (TCTE) dielectric function instead of the test charge-test charge (TCTC) one used in the GW approximation [143, 144]. Independently of the specific recipe that is used in the various $G\tilde{W}$ expressions, these approaches replace the complicated exact vertex function Γ that depends on three space, spin and time arguments by a two-arguments function $(1 - f_{xc}\chi_0)^{-1}$, where χ_0 is an independent-particle polarizability. Therefore, the resulting self-energy is always approximate [65]. Nevertheless, using a $G\tilde{W}$ self-energy instead of GW often improves the QP energies [59, 68, 70]. At the same time, the idea is much less explored when it comes to total energies. Moreover, to the best of our knowledge a systematic study for both total energy and spectra that would discern the effect of the replacement of the full Γ by a two-arguments vertex on one side, from the effect of approximations to the f_{xc} itself on the other side, is still missing.

The present chapter has a focus on the total xc energy, while making a link to other aspects of the 1-GF when interesting. It addresses the following questions: *Could a self-energy with a two-arguments vertex correction, and in particular, a TDDFT-derived one, yield in principle exact results? If yes, how do we have to build the corresponding expressions for the total xc energy? How do widely used approximations impact the results? And what happens to the kinetic energy and to spectra?* As we will show, there are indeed different possibilities to obtain in principle exact expressions for the total xc energy, which are moreover quite robust when widely used approximations are made. Consistent combination of ingredients is a key requirement for this to be true. With these self-energies, the kinetic energy is not exact in principle, but we examine the possibility to use the virial theorem in order to overcome this problem. This allows us moreover to make an interesting comparison to the widely used adiabatic connection approach, which also makes use of the polarizability, but without involving a self-energy. Spectra are also approximate in principle when a two-arguments vertex correction is used, but we find that the $G\tilde{W}$ results still exhibit improvements over GW.

Our investigation and discussion is general, and it is accompanied by an illustration using the exactly solvable symmetric Hubbard dimer at half-filling.

7.1 Brief theoretical background

It is important to present the following theoretical background derivations in this chapter to provide the necessary foundation for understanding our proposed derivations.

7.1.1 Total energy and spectral function in terms of the Green's function

The ground-state total energy E_0 can be expressed in terms of the time ordered GF [53, 94]

$$E_0 = \underbrace{-i \lim_{t_2 \to t_1^+} \int dx_1 \left[-\frac{\nabla_{r_1}^2}{2} + v_{\text{ext}}(x_1) \right] G(x_1, x_1; t_1 - t_2)}_{E_k + E_{\text{ext}}}$$

$$\underbrace{-\frac{i}{2} \lim_{t_2 \to t_1^+} \int dx_1 \, v_{\text{H}}(x_1) G(x_1, x_1; t_1 - t_2)}_{E_{\text{H}}}$$

$$\underbrace{-\frac{i}{2} \lim_{t_2 \to t_1} \int dx_1 dx_3 dt_3 \, \Sigma_{\text{xc}}(x_1, x_3; t_1 - t_3) G(x_3, x_1; t_3 - t_2)}_{E_{\text{xc}}}, \quad (7.1)$$

where $x = (r, \sigma)$ stands for position and spin [1]. Here, we have highlighted the different contributions to the total energy, namely the kinetic energy E_k, the contribution E_{ext} coming from the external potential v_{ext}, the Hartree energy E_{H} given in terms of the Hartree potential v_{H}, and the exchange-correlation energy E_{xc} expressed in terms of the exchange-correlation self-energy Σ_{xc}. The last two terms compose the interaction energy $E^{\text{inter}} \equiv E_{\text{H}} + E_{\text{xc}}$. Note that here, in the context of MBPT,

---

[1] In the publication [145, 146], in the last term of Eq.(7.1) $\lim_{t_2 \to t_1}$ is replaced by $\lim_{t_2 \to t_1^{++}}$ since we were using the usual expression for the GW Σ_{xc}, see the remark after (5.84)

E_{xc} refers specifically to the exchange-correlation energy of the Coulomb interaction, in contrast to the DFT framework where the xc energy also includes the correlation contribution from the kinetic energy. The specific form Eq.(7.1) of the Galitskii-Migdal equation is convenient in order to discuss separately the different contributions to the total energy, and to find specific improvements for each part. While such a strategy does not benefit from error canceling and therefore does not necessarily lead to globally improved results, it helps to obtain deeper insight, and eventually to arrive to the good result for the good reason.

7.1.2 Interaction energy in terms of the polarizability

Our focus is to find accurate expressions for the interaction energy E^{inter}. For this purpose, it is useful to express it in terms of the reducible polarizability χ [147].

For a system with N electrons in its ground-state, the interaction energy is given by the expectation value of the Coulomb interaction operator $\hat{V}$ in the many-body ground-state $|N_0\rangle$,

$$E^{inter} = \langle N_0|\hat{V}|N_0\rangle = \frac{1}{2}\int dx_1 dx_2\, v_{\rm c}(x_1, x_2)\,\langle N_0|\,\hat{\psi}^\dagger(x_2)\hat{\psi}^\dagger(x_1)\hat{\psi}(x_1)\hat{\psi}(x_2)\,|N_0\rangle \,, \qquad (7.2)$$

where $\hat{\psi}$ and $\hat{\psi}^\dagger$ are the annihilation and creation field operators, respectively. On the other hand, the reducible polarizability χ is defined as,

$$\chi(x_1, t_1; x_2, t_2) = -iG(x_1, t_1; x_1, t_1^+)G(x_2, t_2; x_2, t_2^+)$$
$$- i\,\langle N_0|\,\hat{T}\big[\hat{\psi}^\dagger(x_1, t_1^+)\hat{\psi}(x_1, t_1)\hat{\psi}^\dagger(x_2, t_2^+)\hat{\psi}(x_2, t_2)\big]\,|N_0\rangle \,. \quad (7.3)$$

In the limit $t_2 = t_1^{++}$,

$$\chi(x_1, t_1; x_2, t_1^{++}) = -iG(x_1, t_1; x_1, t_1^+)G(x_2, t_1^{++}; x_2, t_1^{+++})$$
$$- i\,\langle N_0|\hat{\psi}^\dagger(x_2)\hat{\psi}(x_1)|N_0\rangle\,\delta(x_2 - x_1) - i\,\langle N_0|\hat{\psi}^\dagger(x_2)\hat{\psi}^\dagger(x_1)\hat{\psi}(x_1)\hat{\psi}(x_2)|N_0\rangle$$
$$= i\,n(x_1)n(x_2) - i\,\gamma(x_1, x_2)\delta(x_2 - x_1) - i\,\langle N_0|\hat{\psi}^\dagger(x_2)\hat{\psi}^\dagger(x_1)\hat{\psi}(x_1)\hat{\psi}(x_2)|N_0\rangle \,, \quad (7.4)$$

where we used the anticommutation relation $\{\psi(x_2), \psi^\dagger(x_1)\} = \delta(x_2 - x_1)$, and where we introduced the one-body reduced density-matrix $\gamma(x_1, x_2) = \langle N_0|\,\hat{\psi}^\dagger(x_2)\hat{\psi}(x_1)\,|N_0\rangle = -iG(x_1, t, x_2, t^+)$, with the electron density $n(x_1) = \gamma(x_1, x_1)$. The last term in Eq.(7.4) enters the definition of the interaction energy in Eq.(7.2). The interaction energy can therefore be expressed in terms of the polarizability χ as

$$E^{inter} = \frac{1}{2}\int dx_1 dx_2\, v_{\rm c}(x_1, x_2)n(x_1)n(x_2)$$
$$+ \frac{i}{2}\int dx_1 dx_2\, v_{\rm c}(x_1, x_2)\chi(x_1, t_1; x_2, t_1^{++}) - \frac{1}{2}\int dx_1 dx_2 v_{\rm c}(x_1, x_2)\gamma(x_1, x_2)\delta(x_2 - x_1) \,, \quad (7.5)$$

where the first term is the Hartree energy and the last two terms are the exchange-correlation energy. This formulation of E_{xc} is not directly suitable for practical purposes, since it consists of terms containing a divergence that cancels in the sum. It is, however, a good starting point for the developments in the next section.

7.2 Diving into the topic

The preceding section served as our point of departure. In this section, we present our proposed theoretical developments.

7.2.1 A freedom of choice

In order to eliminate the problematic last term in Eq.(7.5), we introduce a generalized independent-particle polarizability defined as $\chi_0(1,2) \equiv -i\bar{G}(1,2^+)\bar{G}(\bar{2},1^+)$. Its time diagonal is

$$\chi_0(x_1,t,x_2,t^{++}) = -i\bar{G}(x_1,t;x_2,t^{+++})\bar{G}(x_2,t^{++};x_1,t^+) \tag{7.6}$$

$$= \bar{\gamma}(x_1,x_2)\left(-i\langle\bar{N}_0|\hat{\psi}(x_2)\hat{\psi}^\dagger(x_1)|\bar{N}_0\rangle \right) \tag{7.7}$$

$$= -i\bar{\gamma}(x_1,x_2)\langle\bar{N}_0|\delta(x_2-x_1) - \hat{\psi}^\dagger(x_1)\hat{\psi}(x_2)|\bar{N}_0\rangle \tag{7.8}$$

$$= -i\bar{\gamma}(x_1,x_2)\delta(x_2-x_1) + i\bar{\gamma}(x_1,x_2)\bar{\gamma}(x_2,x_1), \tag{7.9}$$

where $|\bar{N}_0\rangle$ is the many-body ground-state corresponding to a system that could be the true interacting system or an auxiliary interacting or non-interacting system. $\bar{G}$ and $\bar{\gamma}$ are the corresponding 1-GF and the corresponding density matrix, respectively.

In the last term of Eq.(7.5), only the diagonal of the density matrix is needed. In order to replace this term, we can therefore consider all systems that yield the exact density $\bar{\gamma}(x,x) = n(x)$, such as the true interacting system, or the Kohn-Sham auxiliary system. This leaves considerable freedom, which we can use to derive different exact expressions for E^{inter} and to design efficient approximations. Indeed, when $\bar{\gamma}(x,x) = n(x)$ we have, from Eq.(7.9)

$$n(x_1)\delta(x_2-x_1) = i\chi_0(x_1,t;x_2,t^{++}) + \bar{\gamma}(x_1,x_2)\bar{\gamma}(x_2,x_1), \tag{7.10}$$

which, replaced in Eq.(7.5), yields

$$E_{\text{xc}} = -\frac{1}{2}\int dx_1 dx_2\, v_{\text{c}}(x_1,x_2)\bar{\gamma}(x_1,x_2)\bar{\gamma}(x_2,x_1) \tag{7.11}$$

$$+ \frac{i}{2}\int dx_1 dx_2\, v_{\text{c}}(x_1,x_2)\left(\chi(x_1,t_1;x_2,t_1^{++}) - \chi_0(x_1,t_1;x_2,t_1^{++}) \right)$$

$$= \bar{E}_{\text{x}} + \bar{E}_{\text{c}} = \bar{E}_{\text{x}} + E_{\text{c}} + \left(E_{\text{x}} - \bar{E}_{\text{x}} \right). \tag{7.12}$$

The first term in Eq.(7.11) is $\bar{E}_{\text{x}}$, the exchange energy corresponding to $|\bar{N}_0\rangle$. Since the derivation shows that the sum of all terms is the exact exchange-correlation energy, the second term in Eq.(7.11) $\bar{E}_{\text{c}}$ contains the exact correlation energy plus a correction that compensates the error of $\bar{E}_{\text{x}}$ with respect to the exact exchange energy E_{x}. *It is crucial to note that one can use any system defined by a ground-state $|\bar{N}_0\rangle$, as long as this system yields the exact density: this will yield the exact Coulomb interaction energy, although $\bar{\gamma}$ is not the density matrix of the true interacting system.* Two most obvious choices are either the true many-body system with $\bar{G} = G$, which leads to $\chi_0^{\text{MB}} \equiv -iGG$ and $\bar{\gamma}(x_1,x_2) = \gamma(x_1,x_2)$ the true density matrix, or the Kohn-Sham (KS) system with $\chi_0 \to \chi_0^{\text{KS}} \equiv -iG^{\text{KS}}G^{\text{KS}}$ the independent-particle polarizability built with the Kohn-Sham Green's function, and $\bar{\gamma} \to \gamma^{\text{KS}}$ the KS density matrix.

7.2.2 Exact exchange-correlation energy from approximate self-energies

Our next goal is to make a self-energy appear in the expression of E_{xc}. To this aim, we rewrite Eq.(7.11) as

$$E_{xc} = \frac{1}{2} \int dx_1 d2 \, \bar{G}(1, 2^+)\bar{G}(2, 1^+)v_c(2, 1) + \frac{i}{2} \int dx_1 d3 \, v_c(3, 1) \left[\chi(1, 3^{++}) - \chi_0(1, 3^{++})\right] \quad (7.13)$$

$$= \frac{1}{2} \int dx_1 d2 \, \bar{G}(1, 2^+)\bar{G}(2, 1^+)v_c(2, 1) \quad (7.14)$$

$$+ \frac{i}{2} \int dx_1 d(234) \, \chi_0(1, 2) \left[v_c(2, 4) + \bar{f}_{xc}(2, 4)\right] \chi(4, 3^{++})v_c(3, 1) \,,$$

where we have introduced the generalized exchange-correlation kernel $\bar{f}_{xc}$ that, once a choice for χ_0 is made, is defined from the Dyson-like equation

$$\chi(1, 2) = \chi_0(1, 2) + \int d(34) \, \chi_0(1, 3)\left(v_c(3, 4) + \bar{f}_{xc}(3, 4)\right)\chi(4, 2) \,, \quad (7.15)$$

keeping in mind that χ is always the exact reducible polarizability. When χ_0 is chosen to be the KS independent particle polarizability, $\bar{f}_{xc} = f_{xc}$, the xc kernel of linear response TDDFT[138], but, as pointed out above, other choices are possible.[2] By using the definition of χ_0, given in the beginning of 7.2.1, Eq.(7.14) can be written as

$$E_{xc} = \int dx_1 d2 \, \bar{G}(1, 2^+)\bar{G}(2, 1^+)\left(v_c(2, 1) + \int d(34) \left(v_c(2, 4) + \bar{f}_{xc}(2, 4)\right)\chi(4, 3^{++})v_c(3, 1)\right) \quad (7.16)$$

$$= \int dx_1 d2 \, \bar{G}(1, 2)\bar{G}(2, 1^{++})\left(v_c(2, 1^+) + \int d(34) \left(v_c(2, 4) + \bar{f}_{xc}(2, 4)\right)\chi(4, 3^{++})v_c(3, 1^+)\right) \quad (7.17)$$

$$= \frac{1}{2} \int dx_1 d2 \, \bar{G}(1, 2)\bar{\bar{W}}(2, 1^+)\bar{G}(2, 1^{++}) = \frac{1}{2} \int dx_1 d2 \, \bar{G}(1, 2^{++})\tilde{W}(2^+, 1)\bar{G}(2, 1) \,, \quad (7.18)$$

where we have defined the generalized TCTE screened Coulomb interaction[3]

$$\bar{\bar{W}}(2, 1) = v_c(2, 1) + \int d(34) \left(v_c(2, 4) + \bar{f}_{xc}(1, 4)\right)\chi(4, 3^{++})v_c(3, 1) \,. \quad (7.19)$$

In this way, the *exact* exchange-correlation energy takes a form analogous to the last term in the Galitskii-Migdal expression Eq.(7.1):

$$E_{xc} = -\frac{i}{2} \int dx_1 d2 \, \bar{\Sigma}_{xc}(1, 2)\bar{G}(2, 1) \,, \quad (7.20)$$

with the exchange-correlation self-energy

$$\bar{\Sigma}_{xc}(1, 2) \equiv i\bar{G}(1, 2^{++})\bar{\bar{W}}(2^+, 1) \,. \quad (7.21)$$

This is the same form as Eq.(5.84). The important point to stress here is the fact that the *exact* E_{xc} is obtained with an *approximate* self-energy Eq.(7.21). This approximation is often called $G\tilde{W}$.

It is usually derived [59] by replacing $\Sigma_{xc}(4, 2)$ in the functional derivative in Eq.(5.85) with a local $\delta(4, 2)\bar{v}_{xc}(4)$. Most often, $\bar{v}_{xc} \equiv v_{xc}$, the KS xc potential of TDDFT, is chosen and the resulting f_{xc} is approximated, for example, in the adiabatic local density approximation. In our derivation, $\bar{f}_{xc}$ does not have to be a functional derivative, since it is defined by Eq.(7.15), which generalizes the definition of $\bar{\bar{W}}$. This gives a rigorous foundation to attempts to use $\bar{f}_{xc}$ other than approximate TDDFT ones in order to approximate vertex corrections to the self-energy, in particular, the so-called nanoquanta kernel and approximations to it:[60, 139–142, 148–152] the only requirement is that χ_0 corresponds to the correct density. It should, however, be noted that a $\bar{f}_{xc}$ fulfilling Eq.(7.15) does not necessarily exist for every χ_0. We will give an illustration below in the Hubbard dimer.

The important message of this section is that *the exact exchange-correlation energy can be obtained with an approximate self-energy $\bar{\Sigma}_{xc}$ and with an approximate Green's function $\bar{G}$ which is not the solution of the Dyson equation using $\bar{\Sigma}_{xc}$, but which has been chosen from the beginning. The two important requirements are consistency of the ingredients used in Eq.(7.20), and the fact that they stem from the real or from an auxiliary system yielding the exact density.* In the following, we will call this a *consistent scheme*, as opposed to a non-consistent scheme where different 1-GFs are used in $E_{xc}, \bar{\Sigma}_{xc}, \bar{\bar{W}}$. Here, we have shown that there is more than one possible consistent choice, which may help to design efficient approximations.

7.2.3 The kinetic energy

Virial theorem

The TCTE screened self-energy $\bar{\Sigma}_{xc}$ does in general not correspond to the exact self-energy, and therefore one does not have access to the exact 1-GF nor to the exact density matrix. As a consequence, the kinetic energy E_k cannot be computed exactly. However, with the exact Coulomb interaction energy E^{inter} at hand, this problem can in principle be overcome by using the virial theorem for the electron system [153, 154],

$$2E_k + E^{inter} = \int d^3r \, n(r)r \cdot \nabla v_{ext}(r) \equiv S_{VT} \,. \tag{7.22}$$

Using the virial theorem requires in principle to know the exact density. This is not an additional requirement here, since it was already assumed throughout the above derivations. Moreover, research in the framework of DFT shows that errors induced by approximate functionals are often predominantly due to the form of the functional, whereas in many cases errors due to an approximate density are small [155]. Therefore, the use of the virial theorem is a promising route to take when, as it is the case here, one can expect to access the interaction energy with good accuracy.

Linearized Dyson Equation

The key ingredient for the calculation of the kinetic energy is the density matrix. Its diagonal is the density. In our quest to add corrections in order to improve treatment of the kinetic energy, we try to enhance the density-matrix calculations. Recognizing that the one-shot G_0W method violates the

electron number conservation [123], a linearized form of the Dyson equation to rectify this violation has been introduced in Ref. [51]:

$$G^{\mathrm{LDE}}(1,2) \approx G_0(1,2) + \int d(34)\, G_0(1,3)\Big(v_{\mathrm{H}}(3,4)\delta(3,4) + \Sigma_{\mathrm{xc}}(3,4) - v_{\mathrm{xc}}(3,4)\Big)G_0(4,2)\,, \quad (7.23)$$

where the same G_0, which may already contain some xc effects through the potential v_{xc}, must be used in the Dyson equation and in $\Sigma_{\mathrm{xc}} = iG_0 W$. With this consistent choice for G_0, the resulting G^{LDE} has the correct number of electrons, while the non-linearized Dyson equation using the same self-energy may violate particle number conservation. This is an alternative to adjusting the electron number by shifting the chemical potential [156]. It is interesting to examine whether restoring the particle number by linearizing the Dyson equation not only improves the diagonal of the density matrix but also its off-diagonal parts, such leading to an improved kinetic energy. This can be analyzed as follows: the exact density matrix can be written as

$$n(x,x') = \sum_s f_s \phi_s(x)\phi_s^*(x')\,, \tag{7.24}$$

where f_s are occupation numbers and ϕ_s natural orbitals. As an approximation, we suppose that the natural orbitals equal the independent particle ones, and we replace the f_s by an average occupation number f_v for the states below the fermi energy and by another average f_c for states above, which is valid in the limit of weak correlation where $f_v = 1$ and $f_c = 0$. Then

$$n(x,x') = f_v \sum_s^{occ} \phi_s(x)\phi_s^*(x') + f_c \sum_s^{empty} \phi_s(x)\phi_s^*(x') \tag{7.25}$$

$$= (f_v - f_c) \sum_s^{occ} \phi_s(x)\phi_s^*(x') + f_c\delta(x,x')\,. \tag{7.26}$$

The second term does not contribute to the kinetic energy. The first term equals the independent particle density matrix, scaled by the difference of average occupation numbers. Therefore the kinetic energy is dominated by this difference, rather than by the particle number, which is dominated by the sum. For this reason, constraining the result by imposing particle number conservation may not be beneficial for the kinetic energy, and the use of the virial theorem remains more promising. However, this analysis also shows that it may be interesting to examine the occupation number difference, which is shown in Subsec. 7.3.3

7.2.4 Comparison to the adiabatic connection

Finally, it is interesting to compare our equations to the adiabatic connection (AC) approach [136, 137, 157]. In principle, this approach yields the exact full correlation energy, which encompasses correlations arising from both kinetic and Coulomb interaction energies, as well as the difference between the exchange energy calculated with the true and the KS density matrix, respectively. Also in this approach, the correlation energy is expressed in terms of χ and χ_0, but with an integration over a coupling constant λ that scales the Coulomb interaction and modifies v_{ext} such that the density remains constant,

$$\mathrm{E}_{\mathrm{c}}^{\mathrm{full}} = \frac{i}{2} \int_0^1 d\lambda \int dx_1 dx_2\, v_{\mathrm{c}}(x_1,x_2)\Big(\chi^\lambda(x_1,t_1;x_2,t_1^{++}) - \chi_0^{\mathrm{KS}}(x_1,t_1;x_2,t_1^{++})\Big)\,. \tag{7.27}$$

78

Since the structure of the expression is the same as that of Eq.(7.12) (apart from the exchange-energy), one can express also the AC result in terms of an effective self-energy,

$$E_c^{full} = -\frac{i}{2} \int dx_1 d3 \, \Sigma_c^{eff}(1,3) G^{KS}(3,1^{++}) \,, \tag{7.28}$$

where

$$\Sigma_c^{eff}(1,3) = iG^{KS}(1,3) \int_0^1 d\lambda \, \tilde{W}_{pol}^{\lambda}(3,1^+) \,, \tag{7.29}$$

with $\tilde{W}_{pol}^{\lambda}$ the polarization contribution to the λ-dependent KS TCTE screened interaction. Σ_c^{eff} is an effective correlation self-energy that contains kinetic and interaction contributions. Here, we have worked with the KS scheme, since the AC expression is often (though not always, see, e.g., [80]) used in the framework of KS-DFT. Analogous expressions are obtained for other allowed choices of χ_0, e.g., stemming from a generalized KS scheme. Of course, this self-energy yields the exact full correlation energy, while it is not meant to be used in a Dyson equation to yield the 1-GF.

It is interesting to compare the errors to be expected in practice from the AC approach on one side, with the errors of the approach discussed in this chapter, i.e., the combination of the calculation of E^{inter} plus the use of the virial theorem. For this estimate, we suppose the virial term S_{VT} in Eq.(7.22) to be known with an error that is negligible with respect to the error ΔE^{inter} stemming from approximations to χ. This is consistent with the fact that we suppose the density to be known with good accuracy. Using the virial theorem $2E_k + E^{inter} = S_{VT}$, the error in the kinetic energy will be $\Delta E_k = -\frac{\Delta E^{inter}}{2}$, leading to a total error of $\Delta E = +\frac{\Delta E^{inter}}{2}$. In the case of the adiabatic connection, the error is determined entirely by the integral over response functions Eq.(7.27). Since the non-interacting χ_0 is subtracted, it is reasonable to suppose that the dominant contribution is linear in λ. Evidence that this is true can be found for small systems in Ref. [158]. Assuming linearity in λ, one obtains the *same* error $\Delta E = +\frac{\Delta E^{inter}}{2}$ as in our alternative scheme. Whether higher orders in λ will rather reduce or increase this result depends on whether χ_λ is convex or concave. In any case, this discussion suggests that similar errors are to be expected, while the λ-integration is avoided in the approach using the virial theorem.

7.2.5 Shortcomings of the TCTE self-energy

While different flavors of the TCTE screened $G\tilde{W}$ self-energies yield the exact xc energy, they will in general not yield the correct spectral function calculated from the solution of the Dyson equation. One may expect some improvement with respect to the GW approximation for the quasiparticle (QP) energies, since the use of $\bar{f}_{xc}$, which is negative, reduces the polarization contribution and therefore approximates one important effect of the full vertex corrections, which is to reduce self-polarization [54]. However, one may expect that it will not be sufficient to bring significant correction to the satellites, which are in general poorly described by the GW approximation. The reason is the following: as can be seen in Eq.(4.10), the poles of the exact Green's function are the total energy differences $\pm(E_{N\pm1,s} - E_N)$, where N is the particle number and s labels a ground ($s = 0$) or excited state s. This can be written as $\pm(E_{N\pm1,s} - E_{N\pm1,0}) \pm (E_{N\pm1,0} - E_N)$, i.e., the excitation energy of the $N\pm1$-electron

system plus the chemical potential for electrons or holes. This means that satellites of the QP, which lies at the respective chemical potential, must be found at a distance equal to the excitation energies of the $N \pm 1$-electron system, and not, as it would be the case in the GW approximation for small systems with a discrete spectrum, at a distance close to the excitation energies of the N-electron system (plus differences in input and output QP energies when G is not calculated self-consistently). This shortcoming cannot be overcome by a $f_{xc}(\omega)$ that depends on a single frequency and multiplies $\chi(\omega)$ in frequency space: such a structure cannot shift the poles of $\chi(\omega)$. This could only be achieved by a frequency integration, as it is the case when the true three-times vertex correction is used. One should therefore at best expect corrections of the intensities of the satellites when moving from GW to $G\tilde{W}$.

7.3   Illustrations

In order to illustrate our main findings and suggestions, we will use the symmetric Hubbard dimer, which is detailed in Chap. 6. Using this simple model allows us to explore the full range of correlation, which can be quantified by the ratio U/t, and to have an unambiguous benchmark. We will use it at half filling, i.e., with two electrons as just mentioned, which yields non-trivial electron removal and addition features, and we will set $U = 4$ eV throughout the illustrations. One limitation of the model is the fact that the density is trivial and always exact in all methods that conserve symmetry and particle number. Since in the present work we suppose to know the exact KS ingredients, this is not a main drawback. Moreover, asymmetry in the potential removes degeneracy and therefore has a tendency to decrease correlation effects. The symmetric dimer is therefore the most critical test case. Exploring density-driven errors would be interesting, but beyond the scope of this work.

The exact analytical expressions for the time-ordered Green's function and self-energy are given in Sec. 7.5. For the approximate Green's functions we have solved the Dyson equation numerically. Our code uses retarded quantities [159, 160], which avoids interference between the regions of positive and negative energies that otherwise can cause problems when $t \to 0$. Computational details are given in Sec. 7.5.

As worked out in Subsec. 7.2.1, different choices for χ_0 are possible. The simplest choice is to build χ_0 with KS Green's functions. In this case, the corresponding xc kernel f_{xc}^{KS} is the one defined in TDDFT. In the symmetric Hubbard dimer the KS xc potential is a number that we set by constraining the highest occupied level (HOMO) energy of the KS system to yield the exact ionization potential. In this way we obtain the KS Green's function and χ_0^{KS}, and subsequently f_{xc}^{KS} by inversion of Eq.(7.15). This inversion is not unique in the symmetric Hubbard dimer, because both the exact χ and χ_0^{KS} have only one non-zero element, which is the antibonding/antiboding one. Therefore, as already pointed out in [57], only the antibonding/antibonding matrix element of the resulting f_{xc} is defined. The other elements are arbitrary, but their choice has no impact on the results, since f_{xc} appears only in the combination $\chi_0 f_{xc} \chi$.

Another natural choice would be to use the exact Green's function G to build χ_0, since it also yields the exact density, as required. However, interestingly there is no solution to the inversion of
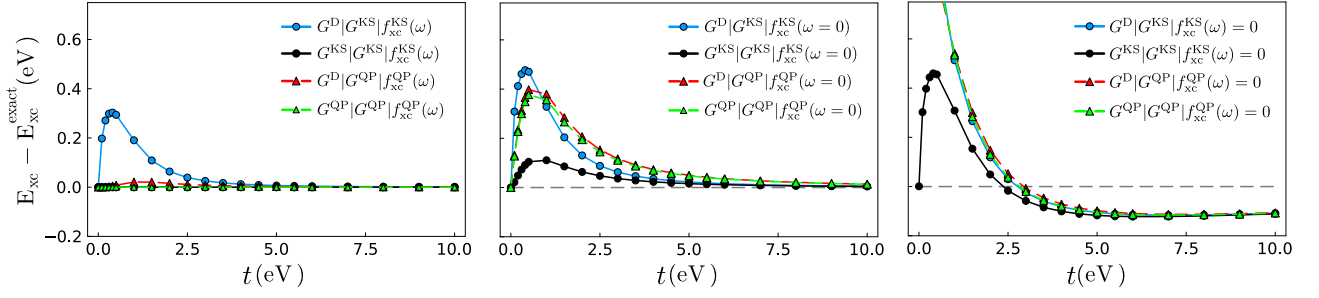
Figure 7.1: Symmetric Hubbard dimer at half filling and $U = 4$ eV: error of the exchange-correlation energy as a function of the hopping t. $\mathrm{E_{xc}}$ is obtained from $\mathrm{E_{xc}} = -\frac{i}{2} \int G^{\mathrm{out}} \Sigma_{\mathrm{xc}}[G^{\mathrm{in}}]$ for different $G^{\mathrm{in}}, G^{\mathrm{out}}$, which are, respectively, the input 1-GF used to build the self-energy, and the 1-GF that is usually the output of the Dyson equation, but for which we have more options here. Σ_{xc} is a $G\tilde{W}$ self-energy, built with G^{in} and using the consistently chosen xc kernel. For a compact notation, we denote this by $G^{\mathrm{out}}|G^{\mathrm{in}}|\bar{f}_{\mathrm{xc}}(\omega)$. The black and sky blue solid lines with dot markers result from a self-energy built with KS ingredients and integrated, respectively, consistently with $G^{\mathrm{out}} = G^{\mathrm{in}} = G^{\mathrm{KS}}$ or, inconsistently, with the $G^{\mathrm{out}} = G^{\mathrm{D}}$ resulting from the Dyson equation. The red and green dashed lines with triangle markers result from a self-energy built with QP ingredients and integrated, respectively, consistently with the $G^{\mathrm{out}} = G^{\mathrm{in}} = G^{\mathrm{QP}}$ or, inconsistently, with the $G^{\mathrm{out}} = G^{\mathrm{D}}$ resulting from the Dyson equation. Left panel: results using the exact consistent $\bar{f}_{\mathrm{xc}}(\omega)$. Middle panel: results using the adiabatic approximation $\omega = 0$ for $\bar{f}_{\mathrm{xc}}$. Right panel: results obtained by neglecting $\bar{f}_{\mathrm{xc}}$ completely, which corresponds to a GW_0 approximation, where W_0 is calculated in the RPA and $G = G^{\mathrm{in}}$.

Eq.(7.15) in this case. The reason is that also the bonding/bonding element of this $\chi_0 = -iGG$ is non-vanishing. Further analysis shows that this stems from the satellite contributions to G, which are not canceled by proper vertex corrections. This is a nice illustration for one of the problems of this ill-behaved polarizability which also, for example, does not fulfill the f-sum rule [161]. We will instead use $\chi_0^{\mathrm{QP}} \equiv -iG^{\mathrm{QP}}G^{\mathrm{QP}}$. It is built with the QP approximation G^{QP} to the exact G, where satellites are neglected and the remaining intensities normalized to 1. This can be seen as a realization of a generalized KS Green's function, stemming from a potential that is non-local in space but instantaneous in time. Such a potential can lead to accurate QP energies, but not to satellites. In a real material, the widely used hybrid functionals [162] fall into this class. It should again be stressed that both kernels, whether the one of the KS or the one of the QP scheme, can be called "exact", as long as they are used consistently in conjunction with χ_0 built with the corresponding Green's functions.

7.3.1 Results using exact xc kernels

In the following we will focus on the results obtained with the two kernels $f_{\mathrm{xc}}^{\mathrm{KS}}$ and $f_{\mathrm{xc}}^{\mathrm{QP}}$, without approximating them further. This will allow us to illustrate the effect of using an f_{xc} to simulate the full three-argument vertex of many-body perturbation theory, without further approximations.

Exchange-correlation energy

First, let us examine the xc contribution to the total energy, given by Eq.(7.20) $\mathrm{E_{xc}} = -\frac{i}{2} \int \bar{G} \bar{\Sigma}_{\mathrm{xc}}$. As pointed out above, here $\bar{G}$ should *not* be the exact Green's function nor the one resulting from

the Dyson equation with $\bar{\Sigma}_{\mathrm{xc}}$, which we will call G^{D} in the following, but $\bar{G}$, which is the one used to build the $G\tilde{W}$ self-energy $\bar{\Sigma}_{\mathrm{xc}}$. This point is important since in practical applications, using G^{D} would often seem to be a natural choice, being the best available Green's function, i.e. the one closest to the exact G. We will therefore compare these choices in the following, by evaluating $\mathrm{E}_{\mathrm{xc}} = \int G^{\mathrm{out}}\bar{\Sigma}_{\mathrm{xc}}[G^{\mathrm{in}}]$. Here, G^{in} is the input 1-GF used to build the $G\bar{\tilde{W}}$ self-energy $\bar{\Sigma}_{\mathrm{xc}}$, and the G^{out} is either the output of the corresponding Dyson equation G^{D}, or equal to G^{in}. In all cases, $\bar{\Sigma}_{\mathrm{xc}}$ is built with the xc kernel $\bar{f}_{\mathrm{xc}}$ that is consistent with G^{in}.

For a compact notation, we use $G^{\mathrm{out}}|G^{\mathrm{in}}|\bar{f}_{\mathrm{xc}}(\omega)$. For example, $G^{\mathrm{D}}|G^{\mathrm{KS}}|f_{\mathrm{xc}}^{\mathrm{KS}}(\omega)$ stands for $\mathrm{E}_{\mathrm{xc}} = -\frac{i}{2}\int G^{\mathrm{D}}\Sigma_{\mathrm{xc}}[G^{\mathrm{KS}}]$, where the $G\bar{\tilde{W}}$ self-energy is built using the KS Green's function and KS xc kernel. The Dyson equation is then solved using this self-energy, and the resulting Green's function G^{D} is used in the integral. Note that while G^{D} is not the same in the KS and QP frameworks, we do not highlight this difference in the notation, since it is clear from the context. Comparison of the various flavors allows us to illustrate the importance of the consistency requirement advocated in Sec. 7.2.2. For subsequent investigation, we also indicate by $|\bar{f}_{\mathrm{xc}}(\omega)$ whether the exact consistent $\bar{f}_{\mathrm{xc}}(\omega)$ is used or further approximations are made, e.g., $|\bar{f}_{\mathrm{xc}}(\omega = 0)$. Fig. 7.1 shows the difference to the exact xc energy E_{xc}. The results in the left panel were obtained using the exact consistent $\bar{f}_{\mathrm{xc}}(\omega)$. As predicted by Eq.(7.20), the two consistent calculations $G^{\mathrm{KS}}|G^{\mathrm{KS}}|f_{\mathrm{xc}}^{\mathrm{KS}}(\omega)$ and $G^{\mathrm{QP}}|G^{\mathrm{QP}}|f_{\mathrm{xc}}^{\mathrm{QP}}(\omega)$ both yield the exact result. Instead, when solution of the Dyson equation is used for G^{out} we obtain $G^{\mathrm{D}}|G^{\mathrm{KS}}|f_{\mathrm{xc}}^{\mathrm{KS}}(\omega)$ and $G^{\mathrm{D}}|G^{\mathrm{QP}}|f_{\mathrm{xc}}^{\mathrm{QP}}(\omega)$, which are both inconsistent and therefore not exact. The error of the former is larger than that of the latter. This can be understood, since the difference between G^{D} and the input Green's function is larger in the case of KS than in the case of the QP input. In all cases, errors are vanishing for large t, whereas they increase in the inconsistent calculations with decreasing t. Even closer to the atomic limit, all errors tend to zero. Nevertheless, the importance of consistency is nicely illustrated by this result.

Kinetic energy

While an approximate self-energy used in the consistent scheme yields exact results for E_{xc}, no such scheme exists for the kinetic energy. Instead, by definition the result of the Dyson equation G^{D} is used to determine the density matrix and hence, the kinetic energy. We will therefore examine the error introduced by various flavors of the self-energy, starting with those that can yield the exact E_{xc}.

The left panel of Fig. 7.2 shows the results for $G^{\mathrm{D}}|G^{\mathrm{KS}}|f_{\mathrm{xc}}^{\mathrm{KS}}(\omega)$ and $G^{\mathrm{D}}|G^{\mathrm{QP}}|f_{\mathrm{xc}}^{\mathrm{QP}}(\omega)$. Both exhibit errors that only vanish at large t and for $t \to 0$. The KS flavor converges more quickly to the exact result with increasing t than the QP version. This favors the use of the $G\tilde{W}$ self-energy built with KS, rather than QP, ingredients. Still, the error is significant. However, as noted in Subsec. 7.2.3, with an exact interaction energy one can, in principle, also obtain the exact kinetic energy by using the virial theorem. This allows one to overcome the problem of not knowing the exact density matrix.

Spectra

The situation is different for spectral properties: here, the shortcomings of an approximate Green's function cannot be overcome easily. As for the kinetic energy, the result of the Dyson equation is
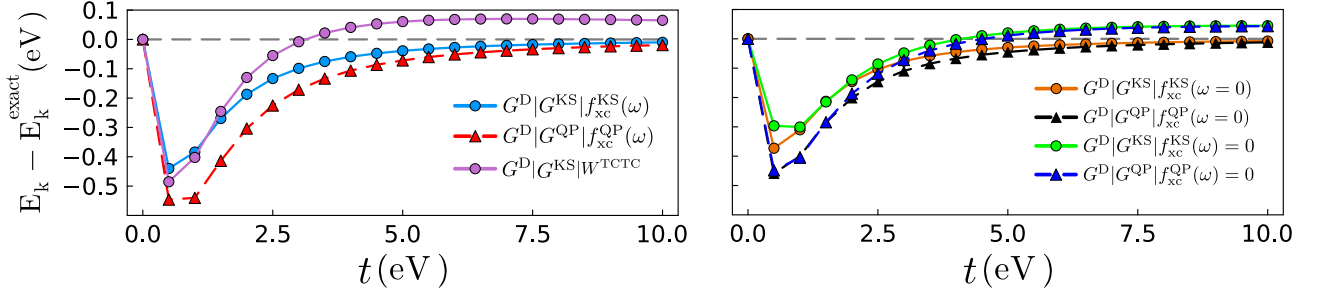
Figure 7.2: Kinetic energy errors as a function of the hopping parameter t. Left panel: E_k is calculated with the Green's function G^D resulting from the Dyson equation with a $G\tilde{W}$ self-energy (red with triangles and sky blue with dots) or with a GW^{TCTC} self-energy, where W^{TCTC} is the exact TCTC screened Coulomb interaction (violet with dots). The self-energy is built with KS ingredients (sky blue and violet) or QP ingredients (red). Right panel: f_{xc} is approximated adiabatically (orange with dots for KS ingredients, black with triangles for QP ingredients) or completely neglected (green with dots for KS ingredients, dark blue with triangles for QP ingredients).

used to calculate the spectra. We will explore which of the flavors of the self-energy that gives an in principle exact total energy will yield the best spectral properties, and what are the remaining problems.
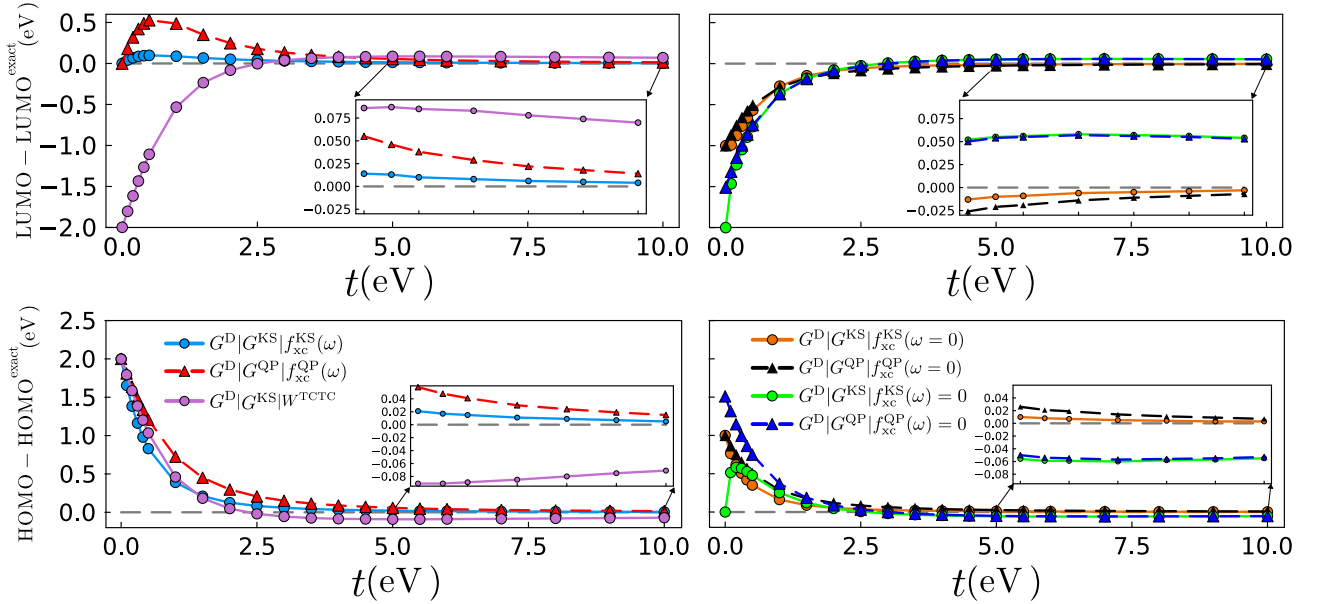

Figure 7.3: Error of the QP energies as a function of the hopping t. The LUMO and HOMO energy errors are shown in the upper and lower panels, respectively. Left column: The result of the Dyson equation with a $G\tilde{W}$ self-energy with KS ingredients (blue with dots) or QP ingredients (red with triangles), or with a GW self-energy using the exact TCTC screened Coulomb interaction (violet with dots) is shown. Right column: The result of the Dyson equation with a $G\tilde{W}$ self-energy with KS ingredients using a static $f_{\mathrm{xc}}(\omega = 0)$ (orange with dots) or neglecting f_{xc} (green with dots), or with QP ingredients using a static $f_{\mathrm{xc}}(\omega = 0)$ (black with triangles) or neglecting f_{xc} (blue with triangles) is shown.

Let us first look at the QP peaks of the spectral function Fig. 7.3 shows the error of the position

of the HOMO and of the lowest unoccupied state (LUMO) as a function of t. The two panels in the left column contain the HOMO (lower panel) and LUMO (upper panel) energy errors obtained with the exact KS or QP ingredients to build the $G\tilde{W}$ self-energy. While the KS and QP flavor perform very similarly for the HOMO, with small errors at larger t and a significant deviation from the exact result for small t that goes up to U/2 for $t \to 0$, the LUMO is relatively well described for all t, and the error vanishes for $t \to 0$. Results for the LUMO are particularly satisfying when KS ingredients are used, in which case the error does not exceed 0.1 eV for any t. For larger t, above 2.5 eV, the errors become small for both HOMO and LUMO, especially in the KS flavor, where they remain well below 0.1 eV and quickly move into the meV range (see insets).

Beyond the QP features, Fig. 7.4 shows the entire spectral functions for $t = 0.5$ eV. We will concentrate on the satellites. They are due to the peaks in the imaginary part of the self-energy, which are in turn determined by the peaks of $\tilde{W}$: the poles of Im $\bar{\Sigma}_{\mathrm{xc}}$ are situated at energies $\bar{\varepsilon}_i \pm \omega_j$, where $\bar{\varepsilon}_i$ is a removal/addition pole of the $G^{\mathrm{in}} = \bar{G}$ used to build the self-energy, and ω_j is a pole of χ. Not all poles are visible in all matrix elements: in the symmetric Hubbard dimer, the bonding (antibonding) matrix element of the self-energy is dominated by the addition (removal) part of G^{in}. The bonding (antibonding) matrix element satellites are therefore found at energies higher (lower) than the LUMO (HOMO). In many real materials, all parts of the Green's function contribute to all matrix elements of the self-energy, and for a given matrix element satellites are found on both sides of a QP. In this sense, the Hubbard dimer is an extreme case, where a given matrix element selects just one particular excitation, that may moreover not be the intuitively expected one. This does not influence our conclusions, but it is interesting to note.

The most obvious feature in Fig. 7.4 is that satellites are not well described in general when the exact $\bar{f}_{\mathrm{xc}}(\omega)$ is used. Their position at $\bar{\varepsilon}_i \pm \omega_j$ combines two errors: the fact that the excitation energy ω_j of the N electron system is used (see Subsec. 7.2.5), and the fact that $\bar{\varepsilon}_i$ can be different from the true QP energy. Since in our case the antibonding matrix element is dominated by the HOMO $\bar{\varepsilon}$, the exact QP energy is used in all cases and the error is entirely due to the difference between the (too high) excitation energy of the N electron system with respect to the $N - 1$ electron one. For the bonding matrix element, instead, the LUMO $\bar{\varepsilon}$ is used, which is exact when QP ingredients are used, but which is too low in the KS case. This adds to the error of the (too high) excitation energy of the N electron system with respect to the $N + 1$ electron one. Since the two errors are of opposite sign, the KS ingredients yield the best result for the bonding matrix element. The difference between the N and $N \pm 1$ excitation energies should be of particular importance in finite systems, but an analogous error might also impact results in infinite systems with localized electrons.[163] Note, however, that the problem discussed here is different from another issue in extended systems, where the satellite position can be spoiled by the appearance of a plasmaron, a spurious solution of the QP condition that is found at some distance from the peak in the imaginary part of the self-energy [164–166]. In a discrete system such as the Hubbard dimer, instead, for large enough t ,the satellites are always found close to the position of peaks of the imaginary part of the self-energy, and the point here is that this position is calculated with the wrong number of electrons.

The biggest effect of f_{xc} is to decrease screening, which remedies the self-screening problem for the
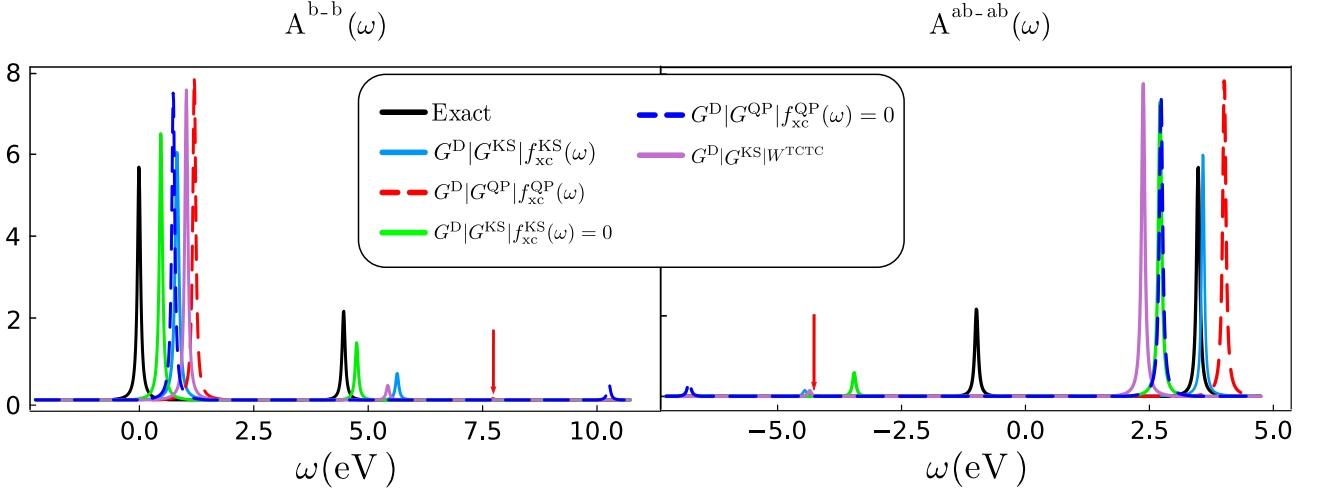
Figure 7.4: Bonding-bonding (left panel) and antibonding-antibonding (right panel) matrix elements of the spectral function for $U = 4$ eV and $t = 0.5$ eV. The continuous black curves are the exact result. The result of the Dyson equation using a $G\tilde{W}$ self-energy with KS ingredients and the exact $f_{\mathrm{xc}}^{\mathrm{KS}}$ is in sky blue or the vanishing $f_{\mathrm{xc}}^{\mathrm{KS}}(\omega) = 0$ is in green. The result of the Dyson equation using QP ingredients and the exact $f_{\mathrm{xc}}^{\mathrm{QP}}$ is in dashed red or the vanishing $f_{\mathrm{xc}}^{\mathrm{QP}}(\omega) = 0$ is in dashed blue. The red arrow indicates the position of the very weak satellite obtained when QP ingredients are used. Moreover, the result of the Dyson equation using a GW self-energy with the exact TCTC screening is shown in violet. The exact HOMO is situated at 0. Note that the corresponding satellites are found at higher energies, whereas the QP of the LUMO is situated at 3.5 eV, with satellites in the electron removal energy range.

QPs[54, 167, 168], but which also decreases the satellite intensity because, as can be seen in Fig. 7.5, f_{xc} is always negative. Indeed, the $G\tilde{W}$ satellites in Fig. 7.4 are of much too weak intensity. KS ingredients do a bit better than QP ones in this respect, since in this case a weaker $\bar{f}_{\mathrm{xc}}$ is used (see Fig. 7.5), which leads to a smaller decrease of the satellite intensities, but the result is still unsatisfactory. This dilemma cannot be solved with such a simple vertex correction that is multipicative in frequency. In other words and as expected, $G\tilde{W}$, even with exact KS or QP ingredients, cannot yield reliable satellites.

7.3.2 Impact of approximating f_{xc}

Understanding the impact of replacing the full vertex corrected self-energy with a $G\tilde{W}$ one is of fundamental interest. For practical applications, one also has to face the problem that the exact $f_{\mathrm{xc}}(\omega)$ is in general not known. Therefore, we also briefly examine the impact of two widely used approximations: either a complete neglect of f_{xc}, which brings us back to the GW approximation with an RPA $W = W_0$, or at least an adiabatic approximation where only $f_{\mathrm{xc}}(\omega = 0)$ is used, since the frequency dependence of $f_{\mathrm{xc}}(\omega)$ is notoriously difficult to approximate. As we will see, these approximations do not have the same impact according to the flavor (KS or QP) that is chosen, and according to the combination of ingredients.

Exchange-correlation energy: impact of approximations

Let us first look at the quantity that is obtained exactly when $G\tilde{W}$ is used consistently, namely, the xc contribution E_{xc} to the total energy. The middle panel of Fig. 7.1 compares results using the adiabatic approximation $\bar{f}_{xc}(\omega = 0)$ and combining the ingredients in a consistent or inconsistent way, respectively. Similarly, results in the right panel were obtained by completely neglecting f_{xc}. In all cases, the consistent results now show an error, but it is smaller than that of the corresponding inconsistent results, with a larger good impact for the KS flavor, which demonstrates that a consistent choice of ingredients remains essential to obtain good total energies. The best results are obtained using the consistent KS flavor. When the adiabatic approximation is used, the good performance of KS can be explained by the fact that the quadratic frequency dependence of the kernel, which is a universal feature of f_{xc} [169], is milder in the KS than in the QP case, as shown in Fig. 7.5. Although approximate, the benefit of using f_{xc} remains very important, as can be seen by comparing the middle panel and the right panel, where results on the GW level with an RPA W_0 are given. The GW_0 results tend to the exact result very slowly with increasing t, and a part from the consistent KS flavor, they deviate significantly from the exact result in the atomic limit towards. The $G^D|G^{KS}|f_{xc}(\omega) = 0$ flavor tends to $U/2$,while both consistent and non-consistent QP cases tend to $U/4$.
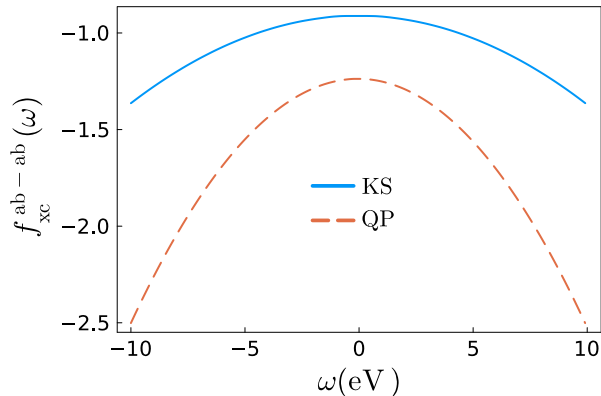

Figure 7.5: Antibonding matrix element of $f_{xc}(\omega)$ as a function of frequency for $U = 4$ eV and $t = 3$ eV. The light blue curve shows the xc kernel corresponding to the KS system, whereas the dashed orange result is the xc kernel that is consistent with QP ingredients.

Kinetic energy: impact of approximations

The kinetic energy is never exact in $G\tilde{W}$ unless the virial theorem is used, as explained above and as illustrated in Fig. 7.2. The right panel of Fig. 7.2 also shows the impact on the kinetic energy of approximations to f_{xc}. The adiabatic approximation $f_{xc}(\omega = 0)$ has a very moderate effect, with a tendency that is rather towards improving the results. The reason for this is the fact that the kinetic energy suffers from the underestimate of the satellite intensity discussed above, which is improved when f_{xc} is weaker. Neglecting the quadratic frequency-dependence of the kernel shown in Fig. 7.5 is therefore rather beneficial for the kinetic energy. A complete neglect of f_{xc}, instead, spoils results in the moderate to large t-range, while further slightly improving the small-t regime, where the satellites are important. Overall, KS flavors perform slightly better than QP ones. Finally, we also show in the left

panel the result of a GW^{TCTC} calculation, where the self-energy is of GW form using KS ingredients and the exact χ and therefore the exact W is used, but where the vertex $\Gamma = 1$ in the self-energy, i.e., the functional derivative in Eq.(5.85) is set to 1. This means that the so-called test-charge test-charge (TCTC) screening is used instead of the TCTE one that is used in the $G\tilde{W}$ approximation. Indeed, it would be tempting to think that a very good W used in GW could improve results. However, with respect to a standard GW_0 calculation using an RPA $W = W_0$, where $f_{\mathrm{xc}} = 0$ also in χ, the results are worsened, especially in the moderate to large-t regime. It has been pointed out that vertex corrections in the polarizability and in the self-energy tend to cancel partially[63, 170]: the present result is a good illustration.

Use of the adiabatic connection versus virial theorem

Finally, we can examine the quality of the result that can be obtained by using the virial theorem, instead of approximating the kinetic energy directly, and compare to the results obtained using the adiabatic connection (AC) fluctuation-dissipation theorem discussed in Sec. 7.2.4. Both approaches are in principle exact, but might react differently to approximations.

Fig. 7.6 gives the errors of the full correlation energy including interaction and kinetic contributions, obtained using an adiabatic kernel, $f_{\mathrm{xc}}(\omega = 0)$ and KS ingredients. In order to use the virial theorem, one has to determine the term S_{VT} in Eq.(7.22). We bypass the difficulty to adapt this equation to the Hubbard dimer by using the fact that here we work with the exact density in all cases, which allows us to use the exact S_{VT}, which we obtain from the exact solution as $S_{\mathrm{VT}} \equiv 2\mathrm{E_k} + \mathrm{E^{inter}}$ for all values of the hopping t. The resulting S_{VT} is then used in place of the right hand side of Eq.(7.22) in order to obtain $\mathrm{E_k} = (S_{\mathrm{VT}} - \mathrm{E^{inter}})/2$ for a given approximation to $\mathrm{E^{inter}}$. This procedure gives the light blue curve (VT) in Fig. 7.6. As predicted in Sec. 7.2.4, the error is similar to the one of the AC approach using the same approximation $f_{\mathrm{xc}}(\omega = 0)$. This is indeed due to the fact that the integrand of the full correlation energy depends approximately linearly on the coupling constant λ, as one can see in the inset of Fig. 7.6[4]. The difference of the correlation energy $\mathrm{E_c^{full}}$ is very small around $t = 3$ eV where the behaviour is almost exactly linear, while the deviation is larger at the smaller $t = 0.5$ eV, where a quadratic λ-dependence is clearly visible. In this small-t regime, where the function is convex, the approach using the virial theorem performs better, while also avoiding the need for the λ-integration.

Spectra

The fact that $G\tilde{W}$ does not yield the correct spectral properties cannot be overcome, but it is still interesting to examine the effect of approximations made in practice. This is done in the right panels of Fig. 7.3 for the QP energies, and in Fig. 7.4 for the satellites. For the LUMO position, both the adiabatic approximation and neglecting f_{xc} completely lead to significant worsening of the result in the small-t regime, the worst results being obtained with KS and QP GW_0, i.e, $f_{\mathrm{xc}} = 0$, which also slightly deteriorates results at larger t. It is interesting to note that keeping the exact $f_{\mathrm{xc}}(\omega)$ in W alone, i.e., using the exact W^{TCTC} instead of the RPA $W = W_0$, does not fix any of these

---

[4]The two insets show $\mathrm{E_c^\lambda}$, where $\mathrm{E_c^{full}} = \int_0^1 d\lambda \mathrm{E_c^\lambda}$
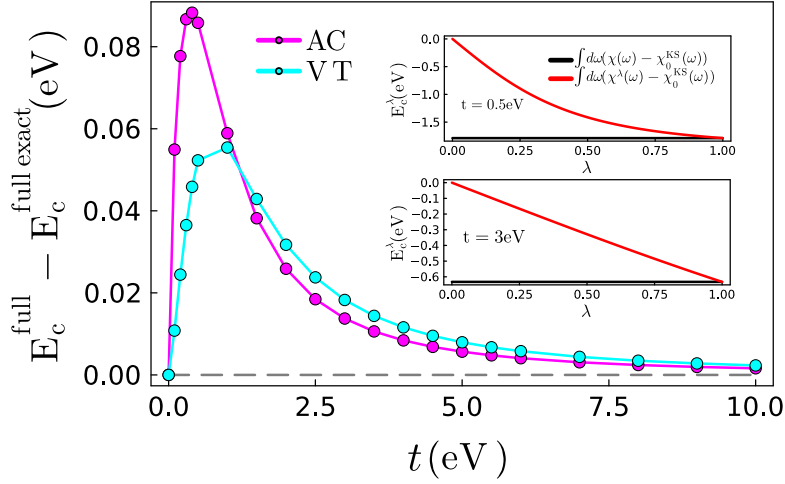
Figure 7.6: Error of the full correlation energy (kinetic and interaction contributions) as a function of the hopping t, when the adiabatic approximation $f_{xc}(\omega = 0)$ is made and KS ingredients are used: comparison of the adiabatic connection result (AC, in magenta) with the result obtained using the virial theorem (VT, in cyan). Insets: λ-resolved full correlation energy, based on the exact f_{xc} within the KS scheme, as a function of λ, for $t = 0.5$ eV (upper inset) and $t = 3$ eV (lower inset).

problems, as one can see in the left panel of Fig. 7.3 for the LUMO. The same is true also in the case of the HOMO. These findings are in line with observations on real systems [171]. Concerning the other approximations for the HOMO, shown in the lower right panel of Fig. 7.3, the observation concerning the GW approximation is similar to the LUMO for moderate to large t, whereas the adiabatic approximation is rather beneficial, especially for smaller t. Also a complete neglect of f_{xc}, i.e., the GW solution with RPA $W = W_0$, decreases the error for small t, and when KS ingredients are used, the GW_0 results even reaches the correct $t \to 0$ limit. However, in this case the improvement is limited to a very small range of t close to the atomic limit. The observed trends highlight the fact that the effect of including f_{xc} is beneficial for the LUMO at all t and for the HOMO at large t, but too strong for the HOMO at small t. Further analysis will be needed to eventually turn this observation into asystematic correction, which is beyond the scope of the present work.

Finally, Fig. 7.4 illustrates that including f_{xc} in W alone, i.e., performing a GW^{TCTC} calculation, rather worsens the satellites as compared to a GW result obtained with RPA W, which illustrates again the error canceling. Therefore, the best satellite results are obtained using the GW approximation with KS ingredients and a complete neglect of $\bar{f}_{xc}$, for both HOMO and LUMO.

7.3.3 Occupation numbers: the linearized vs full Dyson equations

As highlighted in Ref. [51] and as illustrated in Subsec. 7.2.3, the linearized Dyson equation (LDE) corrects the electron number, which is equal to the sum of occupation numbers, which is violated by the resulting 1-GF from the full Dyson equation (FDE) within the G_0W and $G_0\tilde{W}$ frameworks. This is illustrated in Fig. 7.7. In this comparison, we employ the KS flavors, i.e $G_0 \to G^{\mathrm{KS}}$, for which G_0W clearly violates particle number conservation. Especially when neglecting the f_{xc}, the $G^{\mathrm{KS}}W_0^{\mathrm{KS}}$ (represented by the solid green line with dot markers) particle number is very low for small t, whereas

it remains exact using the LDE, as predicted in [172]. Instead, the right panel of Fig. 7.7 shows the occupation number difference, which is proportional to the kinetic energy. This behavior is only reproduced by the full Dyson equation using $f_{xc} = 0$, which is the $G^{KS}W_0^{KS}$. This is due to the fact that $G^{KS}W_0^{KS}$ yields zero electron number when $t \to 0$.

On another note, the occupation numbers difference $(f_1 - f_2)$ almost remains unchanged for both GW (except when $t \to 0$) and $G\tilde{W}$, noting that the GW within the FDE yields the exact difference due to a problem of a vanishing electrons number. Therefore, this lack of improvement is not particularly advantageous for the kinetic energy, which is directly proportional to this difference.
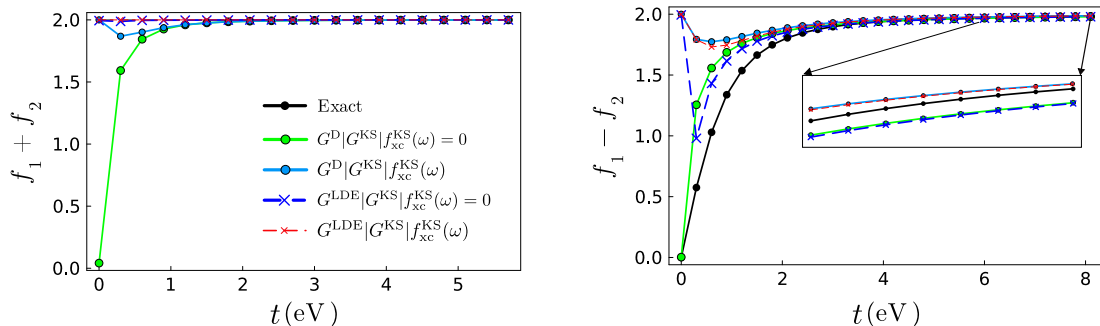

Figure 7.7: Errors of the occupation numbers f_1 and f_2 as a function of the hopping t Errors of the sum (left figure) and of the difference (right figure), where f_1 and f_2 are the occupation numbers of the bonding and anti-bonding state, respectively. In this figure, we compare the full with the linearized Dyson equation for a given approximation.

7.3.4 Spectral function features

As discussed above in this chapter, the f_{xc} kernel notably improves the LUMO, which is true for both the KS and QP flavors. In order to understand why, we look at the spectral function expression, written in terms of the self-energy in the bonding/antibonding basis as follows,

$$A(\omega) = \frac{1}{\pi} \sum_{b,ab} \frac{Im\Sigma_{b/ab}(\omega)}{\left(\omega - \epsilon_{b/ab} - Re\Sigma_{b/ab}(\omega)\right)^2 + \left(Im\Sigma_{b/ab}(\omega)\right)^2} . \tag{7.30}$$

The LUMO peak is determined by the ab matrix-element of the spectral function, which, in turn, is determined by the ab element of the self-energy. This particular element encompasses the "removal" part of its correlation contribution (as illustrated in Fig. 7.8). Given that the f_{xc} kernel is primarily designed to enhance this aspect of the self-energy, it becomes evident why the LUMO is accurately calculated.

7.4 Conclusions

In conclusion, the *exact* exchange-correlation contribution to the total interaction energy can be calculated using an *approximate* self-energy of the form $G\tilde{W}$. Here, $\tilde{W}$ is a test-charge test-electron screened Coulomb interaction, which replaces the RPA or the TCTC screened interaction that are
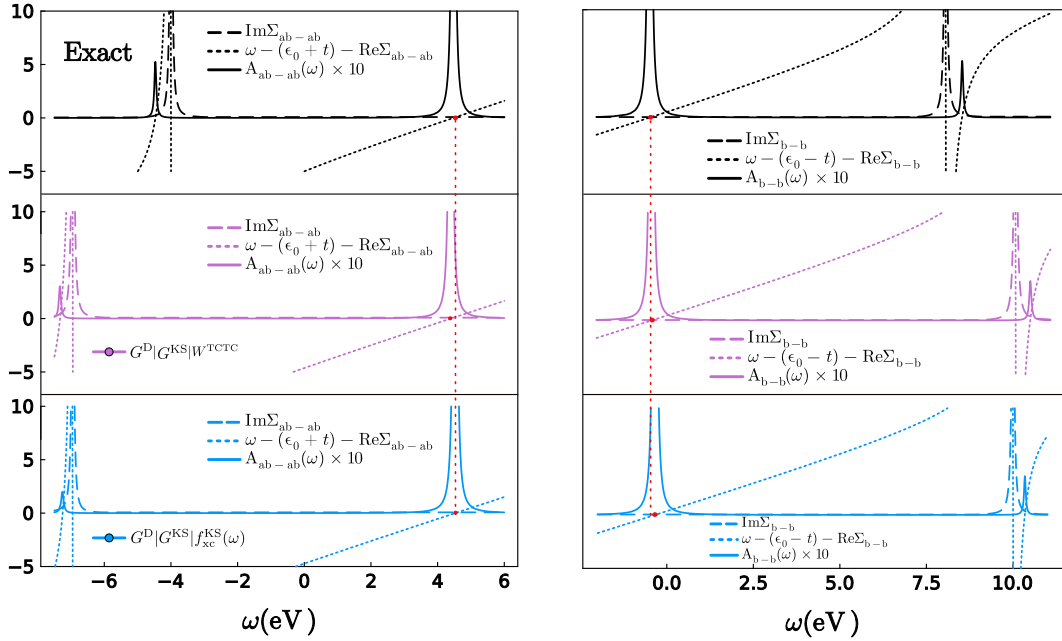
Figure 7.8: The figure shows ingredients of Eq.(7.30) for $U = 4$ eV and $t = 2$ eV. ab and b matrix-elements are shown in the left and right panels, respetively. The GW and $G\tilde{W}$ self-energies are chosen here within the KS flavors.

commonly used in the GW approximation. Different choices for $\tilde{W}$ are possible, one of them being the traditionally used KS scheme, which adds an xc kernel $f_{\mathrm{xc}}(\omega)$ from linear response TDDFT to the bare Coulomb interaction in the dielectric function. For all choices the condition is that the 1-GF and xc kernel used to build the self-energy are consistent and yield the correct density. On top of the KS choice, we have examined the case where the 1-GF is built with the exact QP energies. For all possible choices, it holds that the exact xc energy is obtained by integrating the approximate self-energy with the very same 1-GF that was used to build it. Instead, when the approximate self-energy is used in a Dyson equation and integrated with the resulting 1-GF, the results carry an error. The importance of consistency between the 1-GF used to build the self-energy and the 1-GF used for the integration may explain the success of self-consistent GW total energy calculations, which indeed fulfill the requirement that the self-energy is integrated with the 1-GF that is used to build it. Here, we show that one can obtain good quality results by being consistent without carrying out self-consistent calculations.

The exact correlation contribution to the kinetic energy cannot be accessed in the same way. Instead, we propose to use the virial theorem. We have studied the impact of widely used approximations to this approach, and compared with the use of the adiabatic connection fluctuation dissipation theorem. Our general derivation predicts that the final errors are similar, without the need of a coupling constant integration in the present approach.

Using the approximate self-energies in the Dyson equation leads to approximate 1-GFs and therefore, to approximate spectral functions. Still, $G\tilde{W}$ yields overall better QPs than GW, and since the computational difficulty is similar, it should be preferred. The satellite problem, instead, cannot be fixed in this way.

All statements have been illustrated for the symmetric half-filled Hubbard dimer, confirming our conjectures and highlighting the fact that results obtained using KS ingredients are overall superior and less impacted by additional approximations with respect to results obtained using QP ingredients. While the Hubbard dimer is a simple model, our findings rely on derivations that are valid for the general case, and they should open the way for interesting applications to more realistic systems.

7.5 Supporting informations: analytical results and numerical calculations

In this section, we provide the solutions for the model within the GW and $G\tilde{W}$ approximations using the KS and QP flavors. The exact solutions of the model, obtained by diagonalizing the hamiltonian, are given in Chap. 6.

7.5.1 GW solutions

The two needed ingredients to calculate Σ_{xc} at the GW level, are the 1-GF and the screened Coulomb interaction.

1. We examine two possibilities for the 1-GF the exact Kohn-Sham 1-GF and the exact Quasi-Particle (QP) 1-GF which, in the dimer sites basis read, respectively

$$G_{ij\sigma}^{\mathrm{KS}}(\omega) = \frac{1}{2}\left(\frac{1}{\omega - (\epsilon_0 + t - (c - U)/2) - i\eta} + \frac{(-1)^{i-j}}{\omega - (\epsilon_0 + 3t - (c - U)/2) + i\eta}\right), \quad (7.31)$$

$$G_{ij\sigma}^{\mathrm{QP}}(\omega) = \frac{1}{2}\left(\frac{1}{\omega - (\epsilon_0 + t - (c - U)/2) - i\eta} + \frac{(-1)^{i-j}}{\omega - (\epsilon_0 - t + (c + U)/2) + i\eta}\right), \quad (7.32)$$

where $c = \sqrt{16t^2 + U^2}$. The KS 1-GF (G^{KS}) is obtained by introducing an energy shift to the poles of the non-interacting 1-GF shift obtained such that HOMO energy becomes exact [173]. The QP 1-GF (G^{QP}) is built as the exact 1-GF, but it excludes the satellite contributions and sets the quasiparticle intensities to 1.

2. The screened Coulomb interaction W: in our study, we use both the exact W and approximations called W_0^{KS} or W_0^{QP}, depending on the choice of the 1-GF used to compute the polarizability. The W_0^{KS} and W_0^{QP} are calculated within the Random Phase Approximation (RPA), using the following irreducible polarizabilities,

$$P_{\mathrm{RPA}}^{\mathrm{KS}}(1, 2) = -iG^{\mathrm{KS}}(1, 2^+)G^{\mathrm{KS}}(2, 1^+), \quad (7.33)$$

and,

$$P_{\mathrm{RPA}}^{\mathrm{QP}}(1, 2) = -iG^{\mathrm{QP}}(1, 2^+)G^{\mathrm{QP}}(2, 1^+), \quad (7.34)$$

respectively for the KS and QP cases. They have the following analytical expressions,

$$P_{\mathrm{RPA},ij\sigma}^{\mathrm{KS}}(\omega) = \frac{(-1)^{i-j}}{4}\left(\frac{1}{\omega - 2t + i\eta} - \frac{1}{\omega + 2t - i\eta}\right), \quad (7.35)$$

$$P_{\text{RPA},ij\sigma}^{\text{QP}}(\omega) = \frac{(-1)^{i-j}}{4} \left(\frac{1}{\omega + (2t - c) + i\eta} - \frac{1}{\omega - (2t - c) - i\eta} \right). \tag{7.36}$$

For the exact W, we use the exact reducible polarizability χ, which is related to the 2-particle Green's Function (G_2),

$$\chi(1,2) = -iG(1,1^+)G(2,2^+) + iG_2(1,2,1^+,2^+), \tag{7.37}$$

where G_2 is the 2-GF. So, in the Hubbard dimer basis we have,

$$\chi_{ij\sigma_1\sigma_2}(\omega) = \sum_{s \neq 0} \left[\langle N_0 | \hat{c}_{i\sigma_1}^\dagger \hat{c}_{i\sigma_1} | N_s \rangle \langle N_s | \hat{c}_{j\sigma_2}^\dagger \hat{c}_{j\sigma_2} | N_0 \rangle \frac{1}{\omega + (E_0^N - E_s^N) + i\eta} \right.$$
$$\left. - \langle N_0 | \hat{c}_{j\sigma_2}^\dagger \hat{c}_{j\sigma_2} | N_s \rangle \langle N_s | \hat{c}_{i\sigma_1}^\dagger \hat{c}_{i\sigma_1} | N_0 \rangle \frac{1}{\omega - (E_0^N - E_s^N) - i\eta} \right], \tag{7.38}$$

which leads to the following solutions,

$$\chi_{ij\uparrow\uparrow}(\omega) = \frac{(-1)^{i-j}}{2a^2} \left(\frac{1}{\omega - (c + U)/2 + i\eta} - \frac{1}{\omega + (c + U)/2 - i\eta} \right)$$
$$+ (-1)^{i-j} \frac{16t^2}{2a^2(c - U)^2} \left(\frac{1}{\omega - (c - U)/2 + i\eta} - \frac{1}{\omega + (c - U)/2 - i\eta} \right), \tag{7.39}$$

$$\chi_{ij\uparrow\downarrow}(\omega) = \frac{(-1)^{i-j}}{2a^2} \left(\frac{1}{\omega - (c + U)/2 + i\eta} - \frac{1}{\omega + (c + U)/2 - i\eta} \right)$$
$$- (-1)^{i-j} \frac{16t^2}{2a^2(c - U)^2} \left(\frac{1}{\omega - (c - U)/2 + i\eta} - \frac{1}{\omega + (c - U)/2 - i\eta} \right), \tag{7.40}$$

where $a^2 = 2 \left(\frac{16t^2}{(c-U)^2} + 1 \right)$ and $\chi_{ij\uparrow\uparrow} = \chi_{ij\downarrow\downarrow}$, $\chi_{ij\uparrow\downarrow} = \chi_{ij\downarrow\uparrow}$.

The spin-independent χ matrix in the site basis (ij basis) is a sum over spins, i.e. $\chi_{ij}(\omega) = \chi_{ij\uparrow\uparrow} + \chi_{ij\uparrow\downarrow} + \chi_{ij\downarrow\uparrow} + \chi_{ij\downarrow\downarrow}$. In the bonding and antibonding basis χ is written as below,

$$\begin{pmatrix} 0 & 0 \\ 0 & 2\chi_{ii}(\omega) \end{pmatrix}, \tag{7.41}$$

where $\chi_{ii}(\omega) = \chi_{11}(\omega) + \chi_{22}(\omega)$ and the following non-interacting eigenvectors are used to make the basis transformation, $\frac{1}{\sqrt{2}} \begin{pmatrix} 1 \\ 1 \end{pmatrix}$, $\frac{1}{\sqrt{2}} \begin{pmatrix} 1 \\ -1 \end{pmatrix}$.

We can now write the screened Coulomb interaction W in the different flavors. We start with the exact χ,

$$W(1,2) = v_c(1,2) + \int d(34) v_c(1,3) P(3,4) W(4,2),$$

$$= v_c(1,2) + \int d(34) v_c(1,3) \chi(3,4) v_c(4,2),$$

or, in the site basis,

$$W_{ij}(\omega) = U\delta_{ij} + U\sum_{k\sigma} P_{ik\sigma}(\omega)W_{kj}(\omega),$$

$$= U\delta_{ij} + U^2 \sum_{\sigma\sigma'=\uparrow,\downarrow} \chi_{ij\sigma\sigma'}(\omega),$$

which leads to

$$W_{ij}(\omega) = U\delta_{ij} + (-1)^{i-j}\frac{2U^2}{a^2}\left(\frac{1}{\omega - (c+U)/2 + i\eta} - \frac{1}{\omega + (c+U)/2 - i\eta}\right).$$

By using Eq.s(7.35)(7.36), we find

$$W_{0,ij}^{\mathrm{KS}}(\omega) = U\delta_{ij} + (-1)^{i-j}\frac{U^2 t}{h}\left(\frac{1}{\omega - h + i\eta} - \frac{1}{\omega + h - i\eta}\right), \tag{7.42}$$

where $h = \sqrt{4t^2 + 4Ut}$, and

$$W_{0,ij}^{\mathrm{QP}}(\omega) = U\delta_{ij} + (-1)^{i-j}\frac{U^2(c/2 - t)}{h'}\left(\frac{1}{\omega - h' + i\eta} - \frac{1}{\omega + h' - i\eta}\right), \tag{7.43}$$

where $h' = \sqrt{(2t-c)^2 + 4U(c/2 - t)}$. Now, by using G^{KS}, G^{QP}, W_0^{KS}, W_0^{QP} and W we calculate the different flavors of Σ_{xc} by solving the following integration in the frequency space,

$$\Sigma_{\mathrm{xc},ij\sigma}(\omega) = \frac{i}{2\pi}\int d\omega'\, G_{0,ij\sigma}(\omega' + \omega)W_{0,ji}(\omega')e^{3i\omega'\eta}, \tag{7.44}$$

where G_0 can be G^{KS} or G^{QP}, and W_0 can be W_0^{KS}, W_0^{QP} or W.

The solutions of the different GW flavors are

$$\Sigma_{\mathrm{xc},ij\sigma}^{G^{\mathrm{KS}}W_0^{\mathrm{KS}}}(\omega) = -\frac{U}{2}\delta_{ij} + \frac{U^2 t}{2h}\left(\frac{1}{\omega - (\epsilon_0 + 3t - (c-U)/2 + h) + i\eta}\right.$$
$$\left. + \frac{(-1)^{i-j}e^{-3i\omega\eta}}{\omega - (\epsilon_0 + t - (c-U)/2 - h) - i\eta}\right), \tag{7.45}$$

$$\Sigma_{\mathrm{xc},ij\sigma}^{G^{\mathrm{KS}}W}(\omega) = -\frac{U}{2}\delta_{ij} + \frac{U^2}{a^2}\left(\frac{1}{\omega - (\epsilon_0 + 3t + U) + i\eta} + \frac{(-1)^{i-j}e^{-3i\omega\eta}}{\omega - (\epsilon_0 + t - c) - i\eta}\right), \tag{7.46}$$

$$\Sigma_{\mathrm{xc},ij\sigma}^{G^{\mathrm{QP}}W_0^{\mathrm{QP}}} = -\frac{U}{2}\delta_{ij} + \frac{U^2(\frac{c}{2} - t)}{2h'}\left(\frac{1}{\omega - (\epsilon_0 - t + (c+U)/2 + h') + i\eta}+\right.$$
$$\left. \frac{(-1)^{i-j}e^{-3i\omega\eta}}{\omega - (\epsilon_0 + t - (c-U)/2 - h') - i\eta}\right), \tag{7.47}$$

and

$$\Sigma_{\mathrm{xc},ij\sigma}^{G^{\mathrm{QP}}W} = -\frac{U}{2}\delta_{ij} + \frac{U^2}{a^2}\left(\frac{1}{\omega - (\epsilon_0 - t + c + U) + i\eta} + \frac{(-1)^{i-j}e^{-3i\omega\eta}}{\omega - (\epsilon_0 + t - c) - i\eta}\right). \tag{7.48}$$

It is worth noting that the non-interacting $\chi_0(1,2) = -iG(1,2)G(2,1^+)$ expression does not have the same structure as the exact χ for the Hubbard dimer, when G is the full exact 1-GF. In fact,

$$
\chi_{0,ij}^{GG}(\omega) = (-1)^{i-j} \frac{\left(1 + \frac{4t}{c-U}\right)^4}{2a^4} \times \left(\frac{1}{\omega + 2t - c + 2i\eta} - \frac{1}{\omega - 2t + c - 2i\eta} \right) +
$$
$$
\frac{\left(1 + \frac{4t}{c-U}\right)^2 \left(1 - \frac{4t}{c-U}\right)^2}{a^4} \times \left(\frac{1}{\omega - c + 2i\eta} - \frac{1}{\omega + c - 2i\eta} \right)
$$
$$
+ (-1)^{i-j} \frac{\left(1 - \frac{4t}{c-U}\right)^4}{2a^4} \times \left(\frac{1}{\omega - 2t - c + 2i\eta} - \frac{1}{\omega + 2t + c - 2i\eta} \right), \quad (7.49)
$$

or, in the bonding and anti-bonding basis as,

$$
\chi_0^{GG}(\omega) = \begin{pmatrix} 2C_2 & 0 \\ 0 & 2C_1 + 2C_3 \end{pmatrix}, \quad (7.50)
$$

where C_1, C_2 and C_3 correspond to the first, second and last term in Eq.(7.49), respectively. The fact that the bonding-bonding matrix element does not vanish, contratry to the exact interacting χ, explains why no f_{xc} can be found that would link χ_0^{GG} and χ in a Dyson equation.

7.5.2 $G\tilde{W}$ solutions

In our analysis, we analytically solve the $G\tilde{W}$ self-energy by considering both the exact and approximate f_{xc} kernels within the frameworks of TDDFT and MBPT (i.e. using KS or QP ingredients). This allows us to obtain explicit expressions for the self-energy and investigate the effects of different choices of the f_{xc} kernel on the system's electronic properties. The test-charge test-electron screened interaction is defined as,

$$
\tilde{W}(1,2) = v_c(1,2) + \int d(34) \Big(v_c(1,3) + f_{xc}(1,3) \Big) \chi(4,2) v_c(4,2). \quad (7.51)
$$

The two f_{xc} kernels that we used in this article are given by the matrix equations below,

$$
f_{xc}^{KS}(\omega) = \left[\chi_0^{KS}(\omega) \right]^{-1} - [\chi(\omega)]^{-1} - v_c, \quad (7.52)
$$

$$
f_{xc}^{QP}(\omega) = \left[\chi_0^{QP}(\omega) \right]^{-1} - [\chi(\omega)]^{-1} - v_c, \quad (7.53)
$$

where these equations are solved in the bonding-antibonding basis leading to the following equation,

$$
\begin{pmatrix} f_{xc}^{b\text{-}b}(\omega) & 0 \\ 0 & f_{xc}^{ab\text{-}ab}(\omega) \end{pmatrix} = \begin{pmatrix} 0 & 0 \\ 0 & 2\chi_{0,11}(\omega) \end{pmatrix}^{-1} - \begin{pmatrix} 0 & 0 \\ 0 & 2\chi_{11}(\omega) \end{pmatrix}^{-1} - \begin{pmatrix} U & 0 \\ 0 & U \end{pmatrix}, \quad (7.54)
$$

where $\chi_{0,11}^{KS}(\omega) = \chi_{0,11\uparrow}^{KS}(\omega) + \chi_{0,11\downarrow}^{KS}(\omega)$ and $\chi_{11}(\omega) = \chi_{11\uparrow\uparrow}(\omega) + \chi_{11\uparrow\downarrow}(\omega) + \chi_{11\downarrow\uparrow}(\omega) + \chi_{11\downarrow\downarrow}(\omega)$. $f_{xc}^{b\text{-}b}$ and $f_{xc}^{ab\text{-}ab}$ are the bonding-bonding and antibonding-antibonding elements of the f_{xc} matrix. This leads to

$$
f_{xc}^{KS,ab\text{-}ab}(\omega) = \omega^2 \left(\frac{1}{4t} - \frac{a^2}{4(c+U)} \right) - t + \frac{a^2(c+U)}{16} - U, \quad (7.55)
$$

and

$$f_{xc}^{QP,ab-ab}(\omega) = \omega^2 \left(\frac{1}{2c - 4t} - \frac{a^2}{4(c + U)} \right) + 2t - c + \frac{a^2(c + U)}{16} - U \,, \tag{7.56}$$

respectively, for the KS and QP cases. In the Hubbard dimer, the f_{xc} does not have poles. Its frequency dependence is quadratic. Comparison of Eq.(7.55) with Eq.(7.56) shows that, since $\frac{1}{2c - 4t} - \frac{a^2}{4(c + U)} > \frac{1}{4t} - \frac{a^2}{4(c + U)}$, f_{xc}^{QP} varies more than f_{xc}^{KS} with ω, as it is also shown in Fig. 7.5.

To calculate the self-energies based on these kernels, we solve the following integration written in the Hubbard basis,

$$\Sigma_{xc,ij\sigma}(\omega) = i \int \frac{d\omega_1}{2\pi} G_{ij\sigma}(\omega_1 + \omega) W_{ji}(\omega_1) e^{3i\omega_1\eta}$$

$$+ iU \sum_{m=1,2} \int \frac{d\omega_1}{2\pi} G_{ij\sigma}(\omega_1 + \omega) f_{xcjm}(\omega_1) \chi_{mi}(\omega_1) e^{3i\omega_1\eta} \tag{7.57}$$

whose solutions are

$$\Sigma_{xc,ij\sigma}^{G^{KS}\tilde{W}_{exact}^{KS}} = -\frac{U}{2}\delta_{ij} + (-1)^{i-j}\left(\frac{U}{4} - \frac{U(c + U)}{4ta^2} \right) e^{-3i\omega\eta} +$$

$$\frac{U}{4a^2} \times \frac{(c + U)^2/4 - 4t^2}{t} \left(\frac{1}{\omega - (\epsilon_0 + 3t + U) + i\eta} + \frac{(-1)^{i-j}e^{-3i\omega\eta}}{\omega - (\epsilon_0 + t - c) - i\eta} \right) , \tag{7.58}$$

$$\Sigma_{xc,ij\sigma}^{G^{QP}\tilde{W}_{exact}^{QP}}(\omega) = -\frac{U}{2}\delta_{ij} + (-1)^{i-j}\left(\frac{U}{4} - \frac{U(c + U)}{a^2(2c - 4t)} \right) e^{-3i\omega\eta}$$

$$+ \frac{U}{a^2} \times \frac{(c + U)^2/4 - (2t - c)^2}{(2c - 4t)} \left(\frac{1}{\omega + (\epsilon_0 - t + c + U) + i\eta} + \frac{(-1)^{i-j}e^{-3i\omega\eta}}{\omega - (\epsilon_0 + t - c) - i\eta} \right) , \tag{7.59}$$

in which $\tilde{W}_{exact}$ is the TCTE screened interaction based on the exact f_{xc} kernel and χ. From this, we can conclude the TCTE expressions

$$\tilde{W}_{exact,ij}^{KS} = U\delta_{ij} - (-1)^{i-j}\left(\frac{U}{2} - \frac{U(c + U)}{2ta^2} \right) +$$

$$(-1)^{i-j}\frac{U}{2a^2} \times \frac{(c + U)^2/4 - 4t^2}{t} \left(\frac{1}{\omega - (c + U)/2 + i\eta} - \frac{1}{\omega + (c + U)/2 - i\eta} \right) , \tag{7.60}$$

and

$$\tilde{W}_{exact,ij}^{QP} = U\delta_{ij} - (-1)^{i-j}\left(\frac{U}{2} - \frac{2U(c + U)}{a^2(2c - 4t)} \right)$$

$$+ (-1)^{i-j}\frac{2U}{a^2} \times \frac{(c + U)^2/4 - (2t - c)^2}{(2c - 4t)} \left(\frac{1}{\omega - (c + U)/2 + i\eta} - \frac{1}{\omega + (c + U)/2 - i\eta} \right) . \tag{7.61}$$

When we use the the adiabatic approximation for the f_{xc} kernel to evaluate χ and Σ_{xc}, the Dyson equation becomes

$$\chi_{adiab}(\omega) = \left(\chi_0^{-1}(\omega) - f_{xc}(\omega = 0) - v_c \right)^{-1} . \tag{7.62}$$

We calculate two different χ_{adiab} depending on the choice of χ_0 and $f_{\text{xc}}(\omega = 0)$. So, we have $\chi_{\text{adiab}}^{\text{KS}}$ and $\chi_{\text{adiab}}^{\text{QP}}$ when χ_0^{KS}, $f_{\text{xc}}^{\text{KS}}(\omega = 0)$ and χ_0^{QP}, $f_{\text{xc}}^{\text{QP}}(\omega = 0)$ are used, respectively in the equation above. This yields

$$
\Sigma_{\text{xc},ij\sigma}^{G^{\text{KS}}\tilde{W}_{\text{adiab}}^{\text{KS}}}(\omega = 0) = -\frac{U}{2}\delta_{ij} +
$$
$$
\frac{Ut}{2\omega_1}\left(\frac{1}{\omega - (\epsilon_0 + 3t - (c - U)/2 + \omega_1) + i\eta} + \frac{(-1)^{i-j}e^{-3i\omega\eta}}{\omega - (\epsilon_0 + t - (c - U/2) - \omega_1) - i\eta}\right), \quad (7.63)
$$

where $\omega_1 = \sqrt{4t^2 + 2tf_{\text{Hxc}}^{\text{KS}}(\omega = 0)}$, with $f_{\text{Hxc}}^{\text{KS}}(\omega = 0) = f_{\text{xc},11}^{\text{KS}}(\omega) - f_{\text{xc},12}^{\text{KS}}(\omega = 0) + 2U = -2t + \frac{a^2(c+U)}{8}$ is the difference between the diagonal and off-diagonal elements of the f_{xc} matrix defined in Eq.(7.52) but without $-v_{\text{c}}$. For the QP ingredients, we have, similarly

$$
\Sigma_{xc,ij\sigma}^{G^{\text{QP}}\tilde{W}_{\text{adiab}}^{\text{QP}}}(\omega = 0) = -\frac{U}{2}\delta_{ij} + \frac{U(2c - 4t)}{8\omega_2}
$$
$$
\times \left(\frac{1}{\omega - (\epsilon_0 - t + (c + U)/2 + \omega_2) + i\eta} + \frac{(-1)^{i-j}e^{-3i\omega\eta}}{\omega - (\epsilon_0 + t - (c - U/2) - \omega_2) - i\eta}\right), \quad (7.64)
$$

where $\omega_2 = \sqrt{(2t - c)^2 + (2c - 4t)f_{\text{Hxc}}^{\text{QP}}(\omega = 0)}$, with $f_{\text{Hxc}}^{\text{QP}}(\omega = 0) = \frac{2t-c}{2} + \frac{a^2(c+U)}{16}$. Note that $\tilde{W}_{\text{adiab}}$ is the TCTE screened interaction that includes $f_{\text{xc}}(\omega = 0)$ and $\chi_{\text{adiab}}(\omega)$ within the two different schemes.

7.5.3 Total energy contributions for the Hubbard dimer

The xc and kinetic energy contributions to the total energy, given in the Galitskii-Migdal formula in Eq.(7.1) are written in the site basis and frequency space of the Hubbard dimer respectively as follows,

$$
\text{E}_{\text{xc}} = -\frac{i}{2}\sum_{ij\sigma}\int_{-\infty}^{+\infty}\frac{d\omega}{2\pi}\Sigma_{\text{xc},ij\sigma}(\omega)G_{ij\sigma}(\omega)e^{2i\eta\omega}, \quad (7.65)
$$

$$
\text{E}_{\text{k}} = it\sum_{ij,i\neq j,\sigma}\int_{-\infty}^{+\infty}\frac{d\omega}{2\pi}G_{ij\sigma}(\omega)e^{i\omega\eta}. \quad (7.66)
$$

7.5.4 Computational details

The entire computational framework for this work has been developed from scratch in the present thesis, using the Julia programming language [174]. The numerical developments were done in a perspective of futur application to real systems.

For the purpose of performing the energy integrals, we use 'quadgk' library, that relies on Gauss-Kronod quadratures.[175] Additionally, to visualize our findings effectively, we rely on the 'Plots.jl' library,[176] coupled with the GR backend. As mentioned earlier, even though we provide the analytic solutions and equations within the time-ordered Green's function framework, the numerical calculations have been performed within the retarded Green's function framework to avoid any issues with poles interference in the small t-range. This only requires replacing $-i\eta$ with $+i\eta$ in the poles of the functions [159, 160]. The total energy contributions defined in Eq.(7.65) and Eq.(7.68) become

96

$$E_{xc} = -\frac{1}{2\pi} \sum_{ij\sigma} \int_{-\infty}^{\mu} d\omega \, \text{Im}(\Sigma_{xc,ij\sigma}^{R}(\omega) G_{ij\sigma}^{R}(\omega)), \qquad (7.67)$$

$$E_{k} = \frac{t}{\pi} \sum_{ij,i\neq j,\sigma} \int_{-\infty}^{\mu} d\omega \, \text{Im} G_{ij\sigma}^{R}(\omega), \qquad (7.68)$$

where μ is the chemical potential.

The code of this project, called Symmetric Hubbard dimer, is available at the following address: https://gitlab.com/tsg1860938/symmetric-hubbard-dimer

Chapter 8

Exact self-energy via an effective interaction

In Chap. 7, we observed the immense utility of a linear self-energy expression in terms of a test-charge test-electron interaction ($\tilde{W}$). This $\tilde{W}$, when consistently employed, provides the exact exchange-correlation energy contribution E_{xc} to the total energy. However, the self-energy itself remains approximated, causing the fact that the kinetic energy and spectra are not of equal accuracy as E_{xc}.

In this chapter, we explore the fact that in principle, it is possible to define a two-point effective interaction $\bar{W}_{eff}$ capable of producing the exact self-energy when appropriately multiplied by a certain Green's function $\bar{G}$. We introduce general theoretical developments for an exact equation that directly provides the exact $\bar{W}_{eff}$ for various choices of $\bar{G}$. We also suggest approximations that might be used in practice. As in the previous chapter, the Hubbard dimer is used for illustrations.

8.1 Theory

8.1.1 Exact self-energy from an effective interaction

Let us introduce a general effective potential v_{eff} that has a one-to-one linear relation with v_{ext}. Then, the xc self-energy can be rewritten in terms of any effective interaction as,

$$\Sigma_{xc}(1,2) = -i \int d(345)\, G(1,4) v_c(3,1^+) \frac{\delta G^{-1}(4,2)}{\delta v_{eff}(5^+,5)} \frac{\delta v_{eff}(5^+,5)}{\delta v_{ext}(3^+,3)} \tag{8.1}$$

$$= -i \int d(45)\, G(1,4) W_{eff}(5,1^+) \frac{\delta G^{-1}(4,2)}{\delta v_{eff}(5,5^+)}\,, \tag{8.2}$$

where

$$G^{-1} = G_0^{-1} - v_{eff} - \left(\Sigma_{xc} + v_{ext} + v_H - v_{eff} \right). \tag{8.3}$$

For instance, if $v_{eff} = v_{cl} = v_{ext} + v_H$, we obtain Σ_{xc} in terms of the test-charge test-charge screened interaction (TCTC) W

$$\Sigma_{xc}(1,2) = -i \int d(45)\, G(1,4) W(5,1^+) \frac{\delta G^{-1}(4,2)}{\delta v_{cl}(5^+,5)}\,, \tag{8.4}$$

98

or if $v_{\text{eff}} = v_{\text{KS}} = v_{\text{cl}} + v_{\text{xc}}$, we obtain Σ_{xc} in terms of the test-charge test-electron (TCTE) screened interaction $\tilde{W}$

$$\Sigma_{\text{xc}}(1,2) = -i \int d(45)\, G(1,4)\tilde{W}(5,1^+)\frac{\delta G^{-1}(4,2)}{\delta v_{\text{KS}}(5^+,5)}\,. \tag{8.5}$$

However, we do not know a local v_{eff} that is capable to generate a two-point W_{eff}, which yields the exact self-energy. On the other hand, there must be a two-point W_{eff} that can yield the exact self-energy

$$\Sigma_{\text{xc}}(1,2) = iG(1,2)W_{\text{eff}}(2,1^+)\,, \tag{8.6}$$

since by definition $W_{\text{eff}} = \Sigma_{\text{xc}}/G$. Even more interestingly, there must be a modified two-point $\bar{W}_{\text{eff}}$, that can yield the exact self-energy at the first order when multiplied by the corresponding $\bar{G}$, whether $\bar{G}$ is exact or not i.e

$$\Sigma_{\text{xc}}(1,2) = i\bar{G}(1,2)\bar{W}_{\text{eff}}(2,1^+)\,, \tag{8.7}$$

as long as $\bar{G} \neq 0$ when $\Sigma_{\text{xc}} \neq 0$. This exact formula is first-order in W_{eff}.

8.1.2 Approximations for the effective interaction

To give usefulness to the existence of a $\bar{W}_{\text{eff}}$ capable of yielding the exact self-energy in a first order expression, our goal is to derive an in-principle exact Dyson equation that leads to the exact $\bar{W}_{\text{eff}}$. While finding the kernel and solving such equations is typically challenging in reality, as it is the case with many Dyson equations, we will propose approximations to make the solution feasible in practice. The process unfolds as follows:

$$\Sigma_{\text{xc}}(1,2) = -i \int d(34)\, G(1,4)W(3,1^+)\frac{\delta G^{-1}(4,2)}{\delta v_{\text{cl}}(3^+,3)} \tag{8.8}$$

$$= iG(1,2)W(2,1^+) + i \int d(34)\, G(1,4)W(3,1^+)\frac{\delta\Sigma_{\text{xc}}(4,2)}{\delta v_{\text{cl}}(3^+,3)} \tag{8.9}$$

$$= iG(1,2)W(2,1^+) + i \int d(3456)\, G(1,4)W(3,1^+)\frac{\delta\Sigma_{\text{xc}}(4,2)}{\delta\bar{G}(5,6)}\frac{\delta\bar{G}(5,6)}{\delta v_{\text{cl}}(3^+,3)}\,. \tag{8.10}$$

By using the ansatz self-energy in Eq.(8.7), we obtain the following,

$$i\bar{G}(1,2)\bar{W}_{\text{eff}}(2,1^+) = iG(1,2)W(2,1^+) + i \int d(3456)\, G(1,4)W(3,1^+)\frac{\delta\big(i\bar{G}(4,2)\bar{W}_{\text{eff}}(2,4^+)\big)}{\delta\bar{G}(5,6)}\frac{\delta\bar{G}(5,6)}{\delta v_{\text{cl}}(3^+,3)}$$

$$\tag{8.11}$$

$$\bar{G}(1,2)\bar{W}_{\text{eff}}(2,1^+) = G(1,2)W(2,1^+) + i \int d(3456)\, G(1,4)W(3,1^+)\left(\frac{\delta\bar{G}(4,2)}{\delta\bar{G}(5,6)}\bar{W}_{\text{eff}}(2,4^+)\right. \tag{8.12}$$

$$\left. + \bar{G}(4,2)\frac{\delta\bar{W}_{\text{eff}}(2,4^+)}{\delta\bar{G}(5,6)}\right)\frac{\delta\bar{G}(5,6)}{\delta v_{\text{cl}}(3^+,3)}\,,$$

so,

$$\bar{W}_{\text{eff}}(2,1^+) = \frac{G(1,2)}{\bar{G}(1,2)}W(2,1^+) + i \int d(3456)\, \frac{G(1,4)}{\bar{G}(1,2)}W(3,1^+)\Big(\delta(4,5)\delta(2,6)\bar{W}_{\text{eff}}(2,4^+) \tag{8.13}$$

$$\left. + \bar{G}(4,2)\frac{\delta\bar{W}_{\text{eff}}(2,4^+)}{\delta\bar{G}(5,6)}\right)\frac{\delta\bar{G}(5,6)}{\delta v_{\text{cl}}(3^+,3)}\,,$$

which is in principle an exact equation that yields $\bar{W}_{eff}$. It is convenient to write it in the form of a Dyson equation,

$$\bar{W}_{\text{eff}}(2,1^+) = \frac{G(1,2)}{\bar{G}(1,2)} W(2,1^+) + i \int d(345678) \frac{G(1,4)}{\bar{G}(1,2)} W(3,1^+) \Big(\delta(4,5)\delta(2,6)\bar{W}_{\text{eff}}(2,4^+) \tag{8.14}$$
$$- \bar{G}(7,2)\bar{W}_{\text{eff}}(8,7^+)\frac{\delta\bar{W}_{\text{eff}}^{-1}(4,8)}{\delta\bar{G}(5,6)}\bar{W}_{\text{eff}}(2,4) \Big) \frac{\delta\bar{G}(5,6)}{\delta v_{\text{cl}}(3^+,3)} ,$$

where we have renamed the integration variables. The existence of W_{eff} in the second part of the kernel of Eq.(8.14) makes the problem difficult to solve. Hence, approximations are required. In practice one could, for example, use

$$-\int d(48) \frac{\delta\bar{W}_{\text{eff}}^{-1}(4,8)}{\delta\bar{G}(5,6)}\bar{W}_{\text{eff}}(8,7^+)\bar{W}_{\text{eff}}(2,4) = \int d(48) \frac{\delta\bar{P}_{\text{eff}}(4,8)}{\delta\bar{G}(5,6)}\bar{W}_{\text{eff}}(8,7^+)\bar{W}_{\text{eff}}(2,4) \tag{8.15}$$
$$\approx \int d(48) \frac{\delta\bar{P}_{\text{0eff}}(4,8)}{\delta\bar{G}(5,6)}\bar{W}_{\text{eff}}(8,7^+)\bar{W}_{\text{eff}}(2,4) , \tag{8.16}$$

where $\bar{W}_{\text{eff}}^{-1} = v_{\text{c}}^{-1} - \bar{P}_{\text{eff}}$ with $\bar{P}_{\text{eff}}$ the effective irreducible polarizability and where $\bar{P}_{\text{0eff}} = -i\bar{G}\bar{G}$ is $\bar{P}_{\text{eff}}$ within the Random Phase Approximation (RPA). In principle, this approximation could be tried, but $\frac{\delta W}{\delta G}$ is usually neglected in the Bethe-Salpeter equation (BSE) [34–39], where this approximation has shown a significant efficiency [40–50]. Here, we also neglect this term, so we obtain

$$\bar{W}_{\text{eff}}(2,1^+) \approx \frac{G(1,2)}{\bar{G}(1,2)} W(2,1^+) + i \int d(34) \frac{G(1,4)}{\bar{G}(1,2)} W(3,1^+) \frac{\delta\bar{G}(4,2)}{\delta v_{\text{cl}}(3^+,3)} \bar{W}_{\text{eff}}(2,4^+) . \tag{8.17}$$

This is a Dyson-like equation with a two-point kernel. The complication with respect to the usual Dyson equation is the fact that this kernel also depends on argument 2, i.e, the equation has a structure

$$W_{\text{eff}}(2,1) = W(2,1) + \int d4 \, F(2;14)W_{\text{eff}}(2,4) . \tag{8.18}$$

This means that the matrix $F(1,4)$ has to be inverted for every value of the argument 2. Still, this should be less costly than the inversion of a 4-point matrix in the BSE.

Now, we approximate $\frac{\delta\bar{G}(4,2)}{\delta v_{\text{cl}}(3^+,3)} \approx \bar{G}(4,3^+)\bar{G}(3,2)$ in Eq.(8.17). To assess the physics of this approximation, let us evaluate the latter term in three different situations (three different choices of $\bar{G}$). By using the chain rule, $\frac{\delta\bar{G}}{\delta v_{\text{cl}}}$ can be written as

$$\frac{\delta\bar{G}(4,2)}{\delta v_{\text{cl}}(3^+,3)} = \int d(5) \frac{\delta\bar{G}(4,2)}{\delta u(5^+,5)} \frac{\delta u(5^+,5)}{\delta v_{\text{cl}}(3^+,3)} , \tag{8.19}$$

where we distinguish the following three different cases:

1. For $u = v_{\text{ext}}$, $\bar{G} = G_0$ with G_0 the non-interacting 1-GF, we have

$$\frac{\delta \bar{G}(4,2)}{\delta v_{\text{cl}}(3^+,3)} = \int d5 \, \frac{\delta G_0(4,2)}{\delta v_{\text{ext}}(5^+,5)} \frac{\delta v_{\text{ext}}(5^+,5)}{\delta v_{\text{cl}}(3^+,3)} \tag{8.20}$$

$$= \int d(56) \, \frac{\delta G_0(4,6)}{\delta v_{\text{ext}}(5^+,5)} \delta(6,2) \epsilon^{\text{TCTC}}(5,3) \tag{8.21}$$

$$= \int d(567) \, \frac{\delta G_0(4,6)}{\delta v_{\text{ext}}(5^+,5)} G_0^{-1}(6,7) G_0(7,2) \epsilon^{\text{TCTC}}(5,3) \tag{8.22}$$

$$= -\int d(567) \, G_0(4,6) \frac{\delta G_0^{-1}(6,7)}{\delta v_{\text{ext}}(5^+,5)} G_0(7,2) \epsilon^{\text{TCTC}}(5,3) \tag{8.23}$$

$$= \int d(567) \, G_0(4,6) \delta(6,5^+) \delta(7,5) G_0(7,2) \epsilon^{\text{TCTC}}(5,3) \tag{8.24}$$

$$= \int d5 \, G_0(4,5^+) G_0(5,2) \epsilon^{\text{TCTC}}(5,3) \,, \tag{8.25}$$

where $G_0^{-1} = \left(i \frac{\partial}{\partial t} + \frac{\nabla^2}{2} \right) - v_{\text{ext}}$ and ϵ^{TCTC} is the TCTC dielectric function, which will unscreen W in Eq.(8.17). So, by considering $\frac{\delta \bar{G}(4,2)}{\delta v_{\text{cl}}(3^+,3)} = \bar{G}(4,3^+)\bar{G}(3,2)$ if $\bar{G} = G_0$, the approximation is to neglect $\epsilon^{\text{TCTC}}(5,3)$ in Eq.(8.25).

2. $\bar{G} = G_{\text{H}}$ and $u = v_{\text{cl}}$. In this case, we have

$$\frac{\delta \bar{G}(4,2)}{\delta v_{\text{cl}}(3^+,3)} = \int d5 \, \frac{\delta G_{\text{H}}(4,2)}{\delta v_{\text{cl}}(5^+,5)} \frac{\delta v_{\text{cl}}(5^+,5)}{\delta v_{\text{cl}}(3^+,3)} \tag{8.26}$$

$$= \int d(56) \, \frac{\delta G_{\text{H}}(4,6)}{\delta v_{\text{cl}}(5^+,5)} \delta(6,2) \delta(5,3) \tag{8.27}$$

$$= \int d(567) \, \frac{\delta G_{\text{H}}(4,6)}{\delta v_{\text{cl}}(5^+,5)} G_{\text{H}}^{-1}(6,7) G_{\text{H}}(7,2) \delta(5,3) \tag{8.28}$$

$$= -\int d(567) \, G_{\text{H}}(4,6) \frac{\delta G_{\text{H}}^{-1}(6,7)}{\delta v_{\text{cl}}(5^+,5)} G_{\text{H}}(7,2) \delta(5,3) \tag{8.29}$$

$$= \int d(567) \, G_{\text{H}}(4,6) \delta(6,5^+) \delta(7,5) G_{\text{H}}(7,2) \delta(5,3) \tag{8.30}$$

$$= G_{\text{H}}(4,3^+) G_{\text{H}}(3,2) \,, \tag{8.31}$$

where $G_{\text{H}}^{-1} = \left(i \frac{\partial}{\partial t} + \frac{\nabla^2}{2} \right) - v_{\text{ext}} - v_{\text{H}}$, with v_{H} the Hartree potential. So, when $\bar{G} = G_{\text{H}}$ $\frac{\delta \bar{G}}{v_{\text{cl}}}$ is not an approximation at all.

3. $\bar{G} = G_{\text{KS}}$ and $u = v_{\text{KS}}$. Thus,

$$\frac{\delta\bar{G}(4,2)}{\delta v_{\text{cl}}(3^+,3)} = \int d5 \, \frac{\delta G_{\text{KS}}(4,2)}{\delta v_{\text{KS}}(5^+,5)} \frac{\delta v_{\text{KS}}(5^+,5)}{\delta v_{\text{cl}}(3^+,3)} \tag{8.32}$$

$$= \int d(56) \, \frac{\delta G_{\text{KS}}(4,6)}{\delta v_{\text{KS}}(5^+,5)} \delta(6,2) \frac{\delta v_{\text{KS}}(5^+,5)}{\delta v_{\text{cl}}(3^+,3)} \tag{8.33}$$

$$= \int d(567) \, \frac{\delta G_{\text{KS}}(4,6)}{\delta v_{\text{KS}}(5^+,5)} G_{\text{KS}}^{-1}(6,7) G_{\text{KS}}(7,2) \frac{\delta v_{\text{KS}}(5^+,5)}{\delta v_{\text{cl}}(3^+,3)} \tag{8.34}$$

$$= -\int d(567) \, G_{\text{KS}}(4,6) \frac{\delta G_{\text{KS}}^{-1}(6,7)}{\delta v_{\text{KS}}(5^+,5)} G_{\text{KS}}(7,2) \frac{\delta v_{\text{KS}}(5^+,5)}{\delta v_{\text{cl}}(3^+,3)} \tag{8.35}$$

$$= \int d(567) \, G_{\text{KS}}(4,6) \delta(6,5^+) \delta(7,5) G_{\text{KS}}(7,2) \frac{\delta v_{\text{KS}}(5^+,5)}{\delta v_{\text{cl}}(3^+,3)} \tag{8.36}$$

$$= \int d5 \, G_{\text{KS}}(4,5^+) G_{\text{KS}}(5,2) \frac{\delta v_{\text{KS}}(5^+,5)}{\delta v_{\text{cl}}(3^+,3)} \tag{8.37}$$

$$= \int d(56) \, G_{\text{KS}}(4,5^+) G_{\text{KS}}(5,2) \frac{\delta v_{\text{KS}}(5^+,5)}{\delta v_{\text{ext}}(6^+,6)} \frac{v_{\text{ext}}(6^+,6)}{\delta v_{\text{cl}}(3^+,3)} \, , \tag{8.38}$$

$$= \int d(56) \, G_{\text{KS}}(4,5^+) G_{\text{KS}}(5,2) \epsilon^{-1,\text{TCTE}}(5,6) \epsilon^{\text{TCTC}}(6,3) \, , \tag{8.39}$$

where $G_{\text{H}}^{-1} = \left(\frac{\partial}{\partial t} + \frac{\nabla^2}{2}\right) - v_{\text{ext}} - v_{\text{H}} - v_{\text{KS}}$ and v_{KS} is the Kohn-Sham potential. $\epsilon^{-1,\text{TCTE}}$ is the TCTE inverse dielectric function that will screen in Eq.(8.17) W, which has been unscreened before by ϵ^{TCTC} that comes from Eq.(8.39). *So, to summarize,* $\frac{\delta\bar{G}(4,2)}{\delta v_{\text{cl}}(3^+,3)} \approx \bar{G}(4,3^+)\bar{G}(3,2)$ *is an approximation, except for* $\bar{G} = G_{\text{H}}$.

Thus, our approximation to Eq.(8.17) reads

$$\bar{W}_{\text{eff}}(2,1^+) \approx \frac{G(1,2)}{\bar{G}(1,2)} W(2,1^+) + i \int d(34) \, \frac{G(1,4)}{\bar{G}(1,2)} W(3,1^+) \bar{G}(4,3^+) \bar{G}(3,2) \bar{W}_{\text{eff}}(2,4^+) \, . \tag{8.40}$$

Let us now consider two extra approximations, given the fact that in real situations the exact G and W are not known. At first we consider $G \approx \bar{G}$ in Eq.(8.40). We, therefore, obtain

$$\bar{W}_{\text{eff}}(2,1^+) \approx W(2,1^+) + i \int d(34) \, \frac{\bar{G}(1,4)}{\bar{G}(1,2)} W(3,1^+) \bar{G}(4,3^+) \bar{G}(3,2) \bar{W}_{\text{eff}}(2,4^+) \, . \tag{8.41}$$

And now we approximate the exact TCTC screened interaction W in Eq.(8.41) by the RPA W_0. This yields the roughest approximation, i.e

$$\bar{W}_{\text{eff}}(2,1^+) \approx W_0(2,1^+) + i \int d(34) \, \frac{\bar{G}(1,4)}{\bar{G}(1,2)} W_0(3,1^+) \bar{G}(4,3^+) \bar{G}(3,2) \bar{W}_{\text{eff}}(2,4^+) \, . \tag{8.42}$$

In practice, one could do better, e.g, calculate G self-consistently and calculate the TCTC W using time-dependent density functional theory (TDDFT) that goes beyond the RPA with the available kernels. *It will be important to explore and investigate the different flavors of ingredients. Therefore, comparing the outcomes from Eq.(8.40), Eq.(8.41) and Eq.(8.42) will be extremely fruitful.*
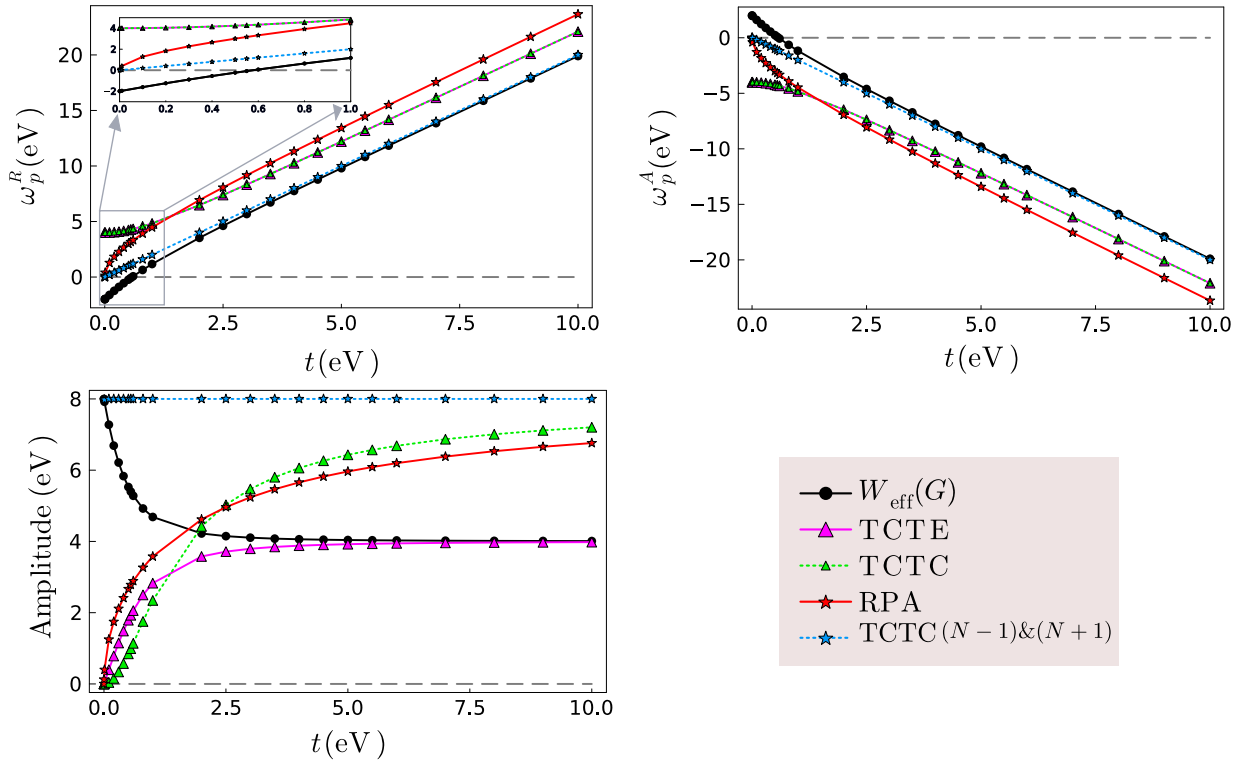
Figure 8.1: Symmetric Hubbard dimer at half-filling: resonant and anti-resonant poles (left and right upper panel, respectively) and amplitude (left-lower panel) of the screened Coulomb interaction as a function of t, where $U = 4$ eV. The solid black lines with dot markers represent $W_{\text{eff}}(G)$, the effective screened Coulomb interaction that yields the exact self-energy when multiplied by the exact 1-GF. The TCTE screened Coulomb interaction based on the TDDFT-derived f_{xc} kernel results are given in the magenta solid lines with triangle markers. The TCTC interaction based on the exact χ and the one within the RPA are represented by dot green lines with triangle markers and solid red lines with star markers, respectively. The dotted sky blue lines with star markers represent the screened interaction of the $N - 1$ and $N + 1$ electrons filling cases.

8.2 Illustration and analysis

In this section, we will explore our simplest approximations and show results and analysis for the two-point effective interaction W_{eff}. We will start by analyzing the W_{eff} that yields the exact self-energy, which is possible thanks to the use of our symmetric Hubbard dimer model. Next we will test the approximations proposed in Eqs.(8.41) (8.42).

8.2.1 Exact effective interaction: the case of $\bar{G} = G$

The exact Σ_{xc} of the Hubbard dimer can be obtained by inverting the Dyson equation, since the exact 1-GF is known (see the analytical formula in 8.4). Then, by using Eq.(8.7), we extract the $\bar{W}_{\text{eff}}$. For $\bar{G}$, we consider the following choices: G_0, G_{H}, G_{KS} and G. $\bar{W}_{\text{eff}}$ gives by construction the exact self-energy when multiplied by the corresponding 1-GF $\bar{G}$. Let us start our analysis of the W_{eff}, by considering the case in which $\bar{G} = G$, the exact Green's function. In Fig. 8.1, we show the resonant (top-left) and anti-resonant (top-right) poles of $W_{\text{eff}}(G)$, which is the exact effective interaction that

yields the exact xc self-energy when multiplied by G, as well as its amplitude, as a function of t and compare the results with well-known W, like TCTC, TCTE, RPA and TCTC(N-1) & (N+1). The latter, as explained in the caption of Fig. 8.1, is the exact TCTC screened interaction for the $N + 1$ and $N - 1$ electron systems, which is the same for both systems.

Let us initially analyze the characteristics of this W_{eff}. Regarding the resonant (left upper panel) and anti-resonant (right upper panel) poles, they exhibit symmetry in absolute value. Notably, the pole of W_{eff} demonstrates a well-behaved and nearly linear behavior with slight curvature within the small range of t. It crosses zero around $t = 0.5$ eV and reaches $-U/2$ ($U/2$ for the anti-resonant pole) as depicted in the inset in the upper left panel. This transition to a negative pole would be unphysical in the screened Coulomb interaction, implying a change in the ground-state leading to a phase transition. However, there is no such interpretation in the other W.

Examining its amplitude, presented in the left lower panel, it remains constant at 4 eV for moderate to large values of t. As t decreases, the amplitude starts increasing until it reaches 8 eV when $t \to 0$. *In summary, it is evident that W_{eff} exhibits a straightforward behavior that allows for easy extrapolation. This simplicity indicates a promising and uncomplicated behavior, at least in the context of the Hubbard dimer. Otherwise, if such an effective screened interaction displayed a complex behavior, extrapolation and approximation might be considerably challenging.*

After elucidating the behavior of $W_{\text{eff}}(G)$, it is crucial to compare it with well-known screened interactions. In the moderate to large range of t (approximately from $t = 4$ eV up to $t = 10$ eV), the pole of the screened interaction of the $N - 1$ or $N + 1$ system exhibits similar behavior to the pole of $W_{\text{eff}}(G)$. This is consistent with expectations, which is based on the anticipation that the effective interaction should depend on the neutral excitations of $N - 1/N + 1$ when an electron is removed/added (see Chap. 7). The pole of $W_{\text{eff}}(G)$ precisely mirrors this behavior. In contrast, the poles of TCTE, TCTC, and RPA do not follow the same pattern. They represent the neutral excitations of N electrons, whether an electron is removed or added. Importantly, their poles are overestimated compared to $W_{\text{eff}}(G)$, with a slightly better agreement for TCTE and TCTC. This difference arises because TCTE and TCTC incorporate the exact neutral excitations of the N electron system, which are reduced by vertex corrections compared to RPA.

It is noteworthy that the f_{xc} kernel in TCTE does not have a pole in the Hubbard dimer to modify the neutral excitations, leading TCTE and TCTC to share the same pole (see Chap. 7). As t decreases, approaching $t \to 0$, the pole of the exact TCTC for $N - 1$ and $N + 1$ goes linearly to zero, in contrast to W_{eff} which becomes negative, as discussed previously. TCTE and TCTC tend to U ($-U$ for the anti-resonant pole), while RPA goes to zero. Importantly, except for a part of $W_{\text{eff}}(G)$, none of the poles become negative, as they all hold physical significance.

Concerning the amplitude, as shown in the left-lower panel of Fig. 8.1, in the moderate to weak correlation regime, interestingly, the TCTE W exhibits a behavior similar to $W_{\text{eff}}(G)$ with an amplitude of 4 eV, emphasizing the importance of the TDDFT-derived vertex corrections in the self-energy when the correlations are not strong. The TCTC and RPA amplitudes are overestimated by approximately 2 eV, with a slightly better performance for the RPA. The TCTC for $N - 1$ and $N + 1$ have a fixed

amplitude of 8 eV. On the other hand, in the strong correlation range, the TCTE amplitude separates from the $W_{\text{eff}}(G)$ one and it goes to the opposite direction, towards zero for $t \to 0$. Similarly, the TCTC and RPA amplitude tend to zero.
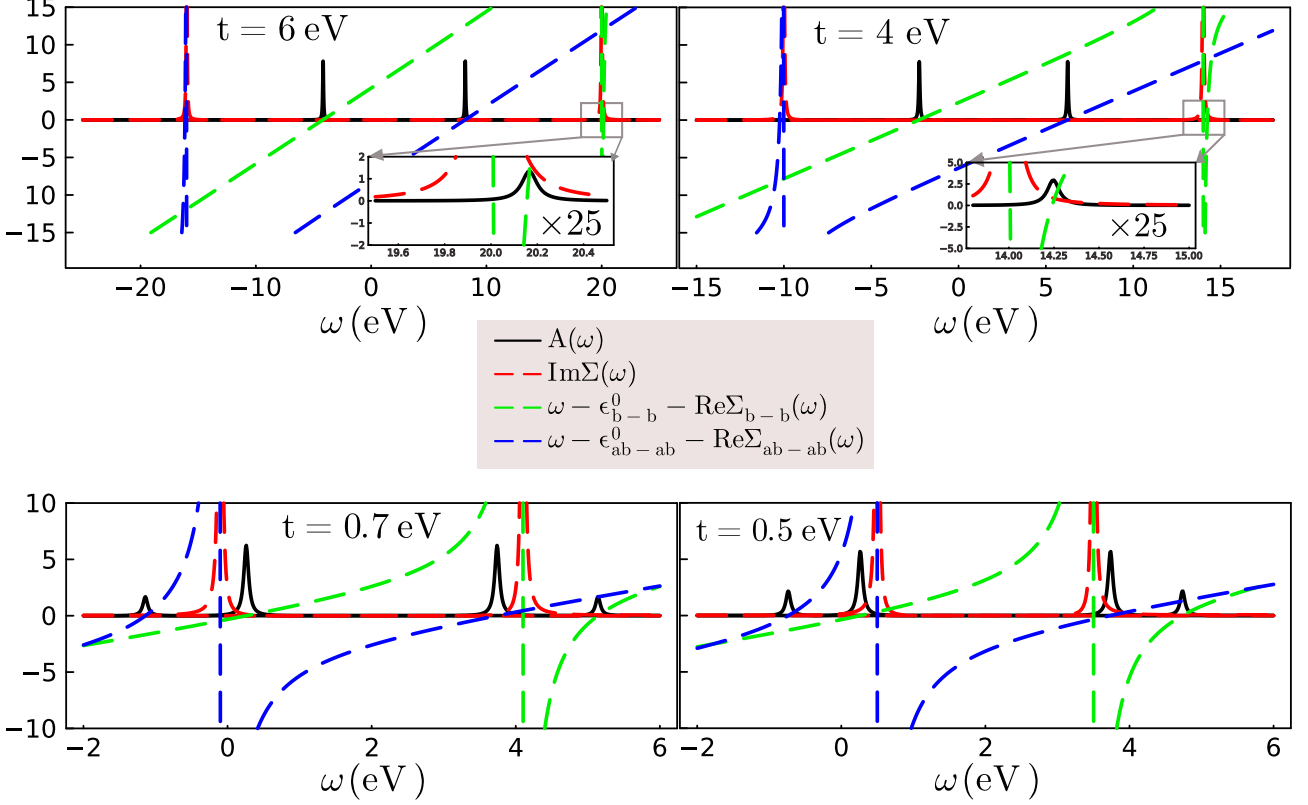

Figure 8.2: Spectral features related to the exact self-energy Σ as a function of frequency for different t values and $U = 4$ eV. The spectral function is given in solid black lines. The imaginary part of the self-energy is shown in dashed red lines. In dashed green and blue lines, the energies difference $\omega - \epsilon^0_{\text{b-b}} - \text{Re}\Sigma_{\text{b-b}}(\omega)$ and $\omega - \epsilon^0_{\text{ab-ab}} - \text{Re}\Sigma_{\text{ab-ab}}(\omega)$ are shown, where $\epsilon^0_{\text{b-b}}$ and $\epsilon^0_{\text{ab-ab}}$ are the poles of the bonding/antibonding elements of the non-interacting 1-GF.

8.2.2 Spectral features of the exact self-energy

In Fig. 8.2, we illustrate the spectral function and the different components of the self-energy that contribute in the generation of the spectral function. These observations are explained in Sec. 5.2.7. Our focus here is on the relation between these features and the zero crossing of the W_{eff} pole, as discussed and depicted in Fig. 8.1. The lower panels of Fig. 8.2 display the spectral features before ($t = 0.7$ eV) and after ($t = 0.5$ eV) the zero crossing of the W_{eff} pole. *It is noticeable that during this transition, the $Im\Sigma$ peaks go to the other side of the QP ones, which forces the pole of W_{eff} to become negative.* This is not in contradiction with principles of physics, since the satellites are always on the correct side of the QP.
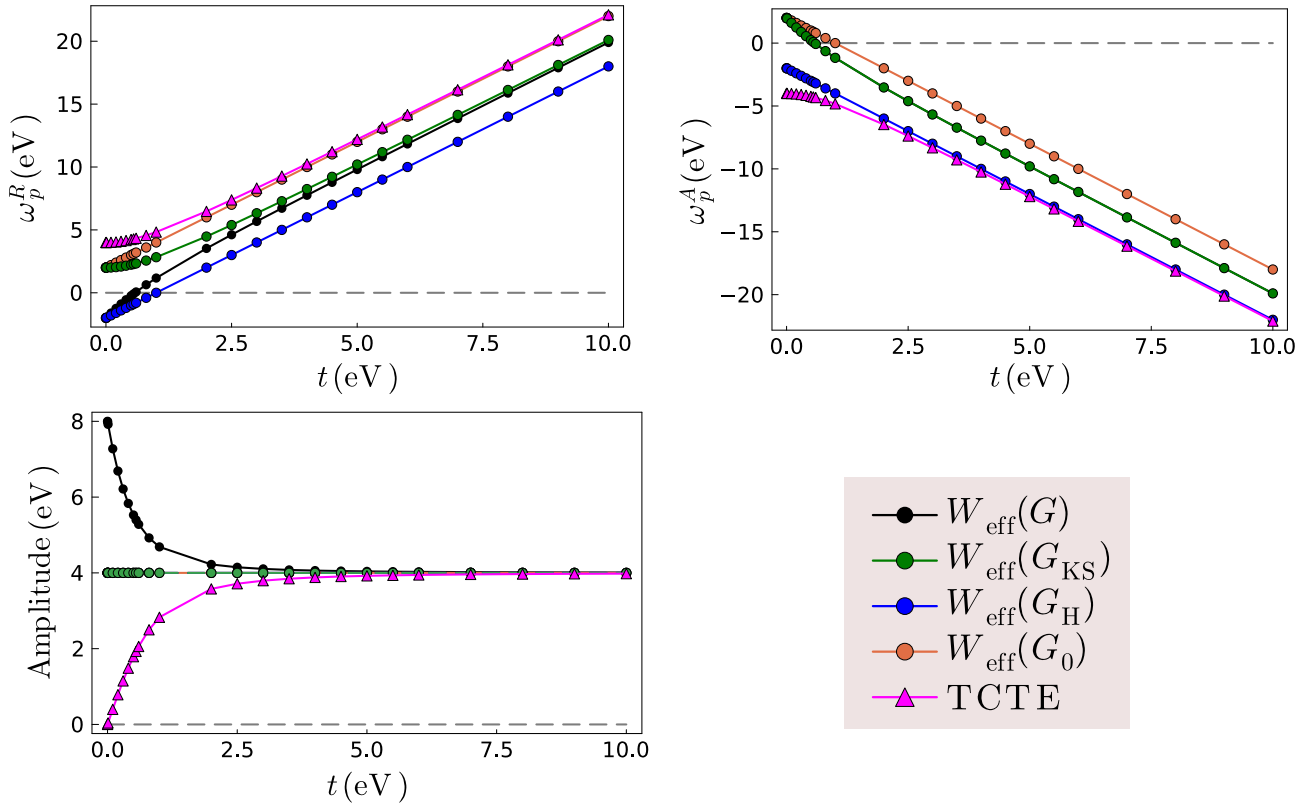
Figure 8.3: Resonant and anti-resonant poles (left and right-upper panel, respectively) and amplitude (left-lower panel) of the screened Coulomb interaction as a function of t, where $U = 4$ eV. Four different effective screened interactions that yield the exact self-energy when multiplied by the corresponding 1-GF (namely, G, G_{KS}, G_H and G_0 Green's functions) are shown, respectively, in solid black, green, blue and orange lines with dot markers. The TCTE W is shown in solid magenta line with triangle markers. Note that $W_{\text{eff}}(G)$ and $W_{\text{eff}}(G_{KS})$ are equal in the right-hand upper panel.

8.2.3 Different flavors of the effective interaction

So far, we have seen the results of W_{eff} associated to the exact 1-GF $W_{\text{eff}}(G)$. It is interesting to investigate the various options of W_{eff} that produce the exact self-energy when the corresponding 1-GF is used. In Fig. 8.3, we present a comparison among four different W_{eff}, based on the use of $\bar{G} = G, G_{KS}, G_H$ and G_0. The use of different 1-GF introduces a shift in the $W_{\text{eff}}(G)$ pole as shown in the left and right-hand panels. In contrast to $W_{\text{eff}}(G)$ and the other physical screened Coulomb interactions, the three effective interactions corresponding to G_{KS}, G_H and G_0 do not have the same resonant and anti-resonant pole in absolute value. $W_{\text{eff}}(G_{KS})$ is very similar to $W_{\text{eff}}(G)$ for the resonant pole, where a large difference appears only in the small range of t. $W_{\text{eff}}(G_{KS})$ does not cross zero, but it goes to $U/2$. For the anti-resonant pole, $W_{\text{eff}}(G_{KS})$ is equivalent to $W_{\text{eff}}(G)$, since G_{KS} has the exact highest occupied molecular orbital (HOMO) energy. The HOMO appears in the anti-resonant pole of $W_{\text{eff}}(G_{KS})$. For $W_{\text{eff}}(G_H)$, in blue line, the pole is shifted down compared to $W_{\text{eff}}(G)$. Its resonant part crosses zero, whereas the anti-resonant does not, showing a significative matching with the TCTE. $W_{\text{eff}}(G_0)$ shows the opposite tendency compared to $W_{\text{eff}}(G_H)$. The pole is shifted up compared to $W_{\text{eff}}(G)$, with crossing and non-crossing zero for the anti-resonant and resonant poles, respectively.

106

Concerning the amplitudes, $W_{\text{eff}}(G_{\text{KS}})$, $W_{\text{eff}}(G_{\text{H}})$ and $W_{\text{eff}}(G_0)$ take a constant value of 4 eV. *In conclusion, all of the studied W_{eff} exhibit a simple behavior in terms of poles and amplitude. Moreover, certain flavors are similar to known screened interactions over a wide range of t. This suggests that finding approximations for such an effective screened Coulomb interaction by making appropriate choices among the diversity of 1-GF might be not overly challenging, at least by extrapolating the findings from the Hubbard dimer model.*

8.2.4 Effective interaction from an approximate Dyson equation
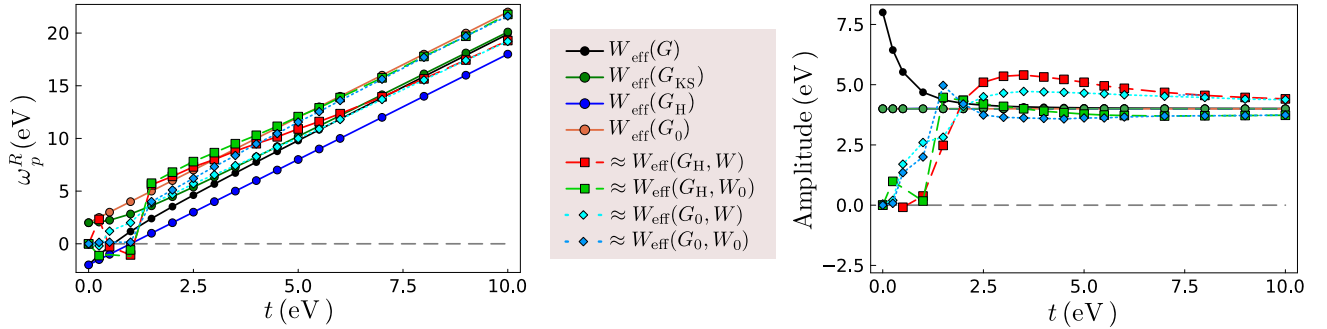
Figure 8.4: Resonant pole (left panel) and amplitude (right panel) of the effective screened Coulomb interaction as a function of t, where $U = 4$ eV. In addition to the exact W_{eff} results with different $\bar{G}$ that are already explained in Fig. 8.3, we add the approximate $W_{\text{eff}}(\bar{G})$ results obtained from the Dyson equation. $\approx W_{\text{eff}}(G_{\text{H}}, W)$ and $\approx W_{\text{eff}}(G_0, W)$, refer to the solutions of Eq.(8.41), where $\bar{G} = G_{\text{H}}$ and $\bar{G} = G_0$, respectively. In both cases, the exact TCTC screened interactions W is used in Eq.(8.41). $\approx W_{\text{eff}}(G_{\text{H}}, W_0)$ and $\approx W_{\text{eff}}(G_0, W_0)$, refer to the solutions of Eq.(8.42), where $\bar{G} = G_{\text{H}}$ and $\bar{G} = G_0$, respectively. In both cases, the RPA TCTC interaction W_0 is used in Eq.(8.42).

After having gained insight into the characteristics of various effective screened Coulomb interactions, calculated exactly when the exact self-energy is known, *it becomes crucial to compute $\bar{W}_{\text{eff}}$ by solving its Dyson equation within the approximate framework proposed in Eq.(8.41) and Eq.(8.42). This step is highly valuable as it enables the exploration of whether these approximate equations, whose solutions should be feasible in practice, yield promising results or not.*

To solve Eq.(8.41) and Eq.(8.42), we follow a procedure that is extensively explained in Sec.8.4. However, we summarize the main idea here: we multiply Eq.(8.41) (same for Eq.(8.42)) by $i\bar{G}(1,2)$, resulting in a $\bar{G}\bar{W}_{\text{eff}}$ self-energy on the left-hand side. The right-hand side involves $\bar{G}W$ and $\bar{G}W\bar{G}\bar{W}_{\text{eff}}\bar{G}$ contributions to the self-energy. These self-energies are then transformed to the Hubbard ij basis and expressed in frequency space, as detailed in Section 8.4. Subsequently, the integrals in frequency space, considering a given $\bar{G}$, are solved analytically. *It is crucial to note that for $\bar{W}_{\text{eff}}$, we introduce an ansatz assuming it has a single pole. This assumption is made despite the fact that $\bar{W}_{\text{eff}}$ can theoretically have multiple poles, as indicated by the structure of Eq.(8.41), where the right-hand side involves multiple poles. However, as an additional approximation, we assume a single-pole structure with a specific amplitude, and we solve the equation based on this assumption. The pole and amplitude of the approximate $\bar{W}_{\text{eff}}$ are varied until the left and right-hand sides of Eq.(8.41) are equal.* The detailed numerical and graphical strategies to solve Eq.(8.41) are given in Section 8.4.

In Fig. 8.4, we extend the previous results to extend the pole and amplitude of the approximate W_{eff} obtained from Eq.(8.41) and Eq.(8.42). Let us break down the analysis into two parts to facilitate comparisons. First, let us delve into the solutions of Eq.(8.41) and Eq.(8.42) with $\bar{G} = G_{\text{H}}$, depicted by the red and green lines with square markers, respectively. This exploration is crucial for understanding the implications of different screening choices while keeping $\bar{G}$ constant. As explained in 8.1, opting for G_{H} among all possible $\bar{G}$ in Eq.(8.41) and Eq.(8.42) minimizes the level of approximations. Naturally, one would expect that using the exact W, the interaction that should ideally be employed in Eq.(8.41), would yield better results. These expectations seem to hold for the pole, where the approximate $W_{\text{eff}}(G_{\text{H}}, W)$ represented by the red line with square markers is closer to the exact $W_{\text{eff}}(G_{\text{H}})$ than $W_{\text{eff}}(G_{\text{H}}, W_0)$, which is represented by the green line with square markers. However, this is not the case for the amplitude. Now, let us compare Eqs.(8.41) and 8.42 with $\bar{G} = G_0$, represented by the cyan and sky blue dotted lines with diamond markers. It is noteworthy that using the RPA W_0 proves to be a better choice than using W for both the pole and amplitude. This is a compelling indication of error cancellation.

Investigating the impact of different choices for $\bar{G}$ while maintaining fixed screening conditions is of equal importance. Therefore, we compare the same equation with different selections of $\bar{G}$. Specifically, for Eq.(8.41) with $\bar{G}$ set to G_{H} and G_0, this entails comparing $W_{\text{eff}}(G_{\text{H}}, W)$ with $W_{\text{eff}}(G_0, W)$. In terms of the pole, using G_{H} appears slightly more advantageous, especially in the larger range of t where the agreement between the approximate $W_{\text{eff}}(G_{\text{H}}, W)$ and the exact $W_{\text{eff}}(G_{\text{H}})$ is better than the agreement between the approximate $W_{\text{eff}}(G_0, W)$ and the exact $W_{\text{eff}}(G_0)$). *It is crucial to note that we are comparing the approximate W_{eff} with the exact one based on the same choice of $\bar{G}$.* Therefore, we are comparing the approximate W_{eff} using G_{H} to $W_{\text{eff}}(G_{\text{H}})$ and the approximate W_{eff} using G_0 to $W_{\text{eff}}(G_0)$. This holds also true when W_0 is used. Hence, we compare the approximate $W_{\text{eff}}(G_{\text{H}}, W_0)$ and the approximate $W_{\text{eff}}(G_0, W_0)$ refering to the exact $W_{\text{eff}}(G_{\text{H}})$ and $W_{\text{eff}}(G_0)$, respectively. It is evident that for Eq.(8.42), using G_0 would be a better choice, as the agreement between the approximate $W_{\text{eff}}(G_0, W_0)$ and the exact $W_{\text{eff}}(G_0)$ is better than the agreement between the approximate $W_{\text{eff}}(G_{\text{H}}, W_0)$ and the exact $W_{\text{eff}}(G_{\text{H}})$. Altogether, the outcomes are highly promising, as the approximate W_{eff} demonstrates significant agreement with the exact result, especially when solving Eq.(8.42) with the couple $\bar{G} = G_0$ and W_0, which is represented by the sky blue dotted lines with diamond markers. The quality of the result in terms of pole and amplitude is comparable to the results of the TCTE screened Coulomb interaction that have been shown in Fig. 8.1. It is important to note that for small values of t, there is some instability, particularly noticeable in the amplitude in the right panel where it approaches zero. Additionally, we underline that the assumption of a single pole for $W_{\text{eff}}(\bar{G})$ was made for simplicity, recognizing that, in principle, it could have multiple poles.

After analyzing the different approximate W_{eff}, we will use them to investigate the spectral function and total energy. In Fig. 8.5, we present the imaginary parts of the self-energy and the spectral function. The $W_{\text{eff}}(G_0)$ yields by definition the exact self-energy when multiplied by G_0, as shown in the orange dashed line. As approximation, we show the $\approx W_{\text{eff}}(G_0, W_0)$ mutiplied with G_0, which shows an improvement with respect to $G_0 W_0$. It also shows better agreement with the exact result
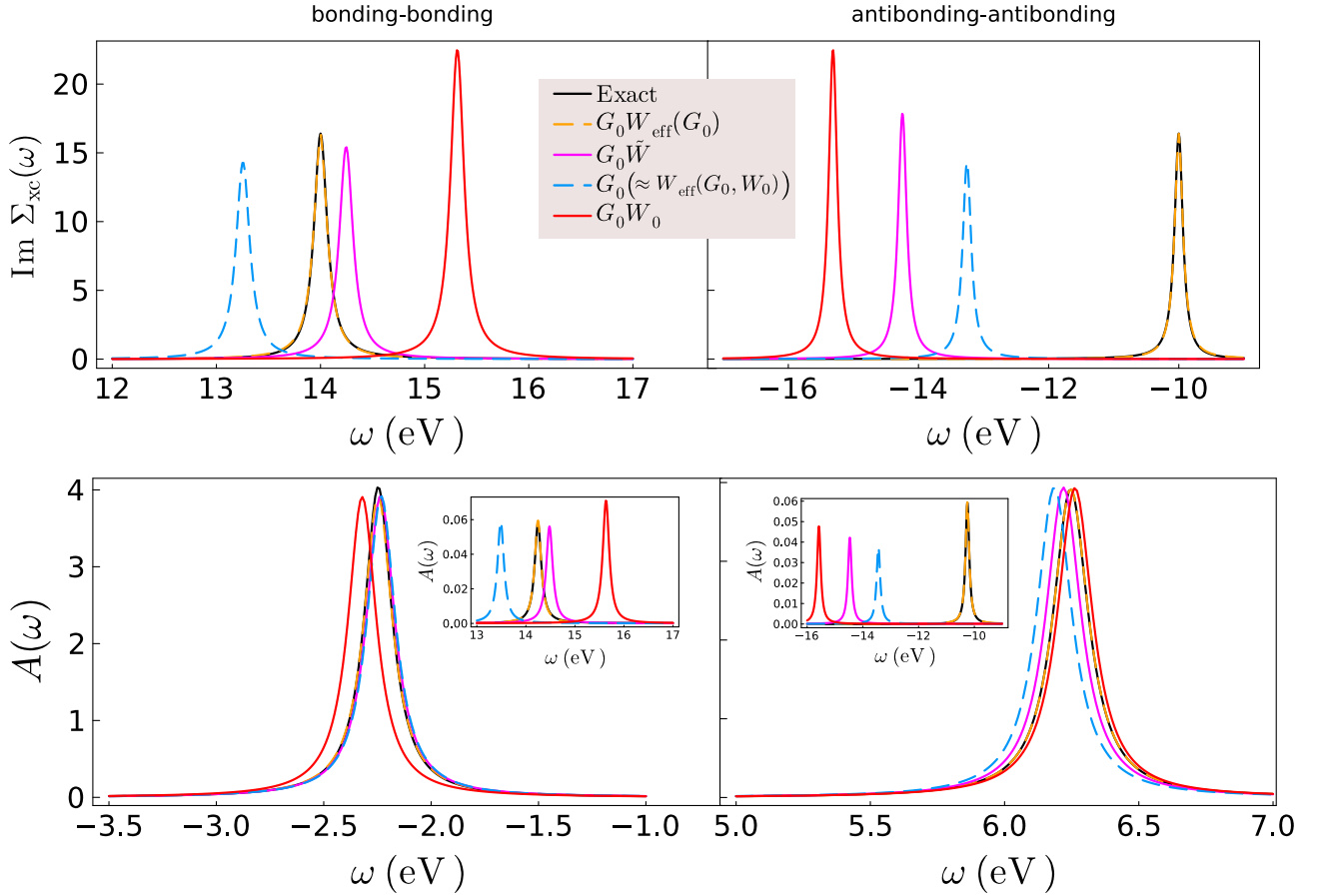
Figure 8.5: Bonding and antibonding components of the imaginary part of Σ_{xc} in the upper panels and of the spectral function in the lower panels for $t = 4$ eV and $U = 4$ eV. Insets in the lower-panels show satellites that appear at higher frequency. In solid black, we represent the exact results. In dashed orange, the $G_0 W_{eff}(G_0)$ results are shown, where $W_{eff}(G_0)$ is the exact effective screened Coulomb interaction. The $G_0 \tilde{W}$ is the self-energy that involves the exact f_{xc} kernel and exact χ in $\tilde{W}$ and its results are shown in solid magenta lines. The $G_0 W_0$, where W_0 is the RPA screening, is shown in solid red. In dashed sky blue lines, we show the $G_0 \big(\approx W_{eff}(G_0, W_0) \big)$ self-energy.

than the $G_0 \tilde{W}$ for the anti-bonding components.

The total energy using the approximate W_{eff} is shown in Fig. 8.6. The Σ_{xc} multiplying G_0 and $\approx W_{eff}(G_0, W_0)$ exhibits the best agreement, and the result is better than $G_0 \tilde{W}$ and $G_0 W_0$ for a wide range of correlation. However, when t decreases, it yields the Hartree-Fock total energy $U/2$ because, the amplitude of $W_{eff}(G_0, W_0)$ for $t \to 0$ goes to zero (see Fig. 8.4). Therefore, there is no screening anymore and the self-energy has simply the exchange contribution.

8.3   Conclusions

In conclusion of this chapter, the ansatz $\Sigma_{xc} = i\bar{G}\bar{W}_{eff}$ seems to be a promising way to go. We have derived a set of simple approximate Dyson equations that could be used in practice. Future work will include more tests on simple models, as well as ab-initio implementation.
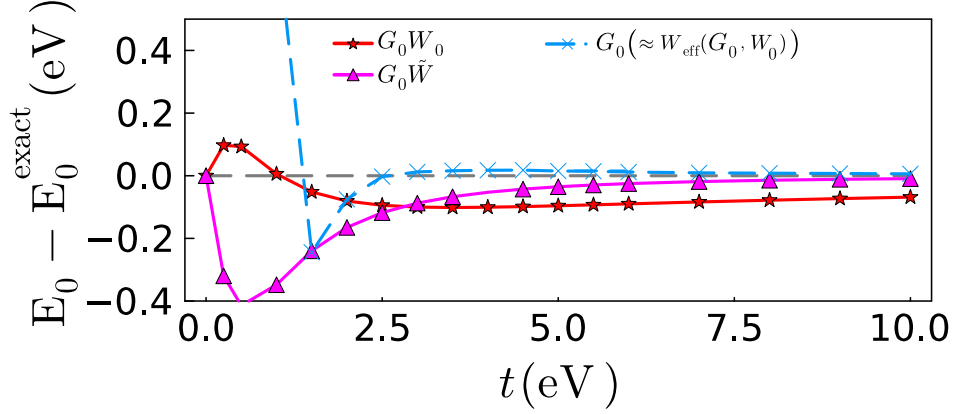
Figure 8.6: Total energy errors as a function of t, where $U = 4$: test of the approximate W_{eff}.

8.4 Supporting informations, analytical and numerical solutions

In the present section, we provide the necessary information about the analytical and numerical calculations of the effective interaction W_{eff}.

8.4.1 The exact self-energy and effective interactions

Having the exact and the non-interacting 1-GF, we calculate the self-energy $\Sigma = v_{\text{H}} + \Sigma_{\text{xc}}$ by inverting the Dyson equation

$$\Sigma_{\text{b-b}}^{\text{exact}}(\omega) = \left(G_{0,\text{b-b}}^{-1}(\omega) - G_{\text{b-b}}^{-1}(\omega) \right)^{-1}. \tag{8.43}$$

In the bonding and anti-bonding basis, this leads to

$$\Sigma_{\text{b-b}}^{\text{exact}}(\omega) = -X_1 - X_1 \times \frac{X_4 - X_2/X_1 - i\eta(X_5 + X_3/X_1)}{\omega - X_4 + iX_5\eta}, \tag{8.44}$$

$$\Sigma_{\text{ab-ab}}^{\text{exact}}(\omega) = -X_1' - X_1' \times \frac{X_4' - X_2'/X_1' - i\eta(X_5' + X_3'/X_1')}{\omega - X_4' - iX_5'\eta}, \tag{8.45}$$

where $X_1 = A\omega_2 + B\omega_1 + (\epsilon_0 - t)(A+B) - \omega_1 - \omega_2 + 2i\eta B$, $X_2 = (\epsilon_0 - t)(A\omega_2 + B\omega_1) - \omega_1\omega_2 - (A-B)(i\eta)^2$, $X_3 = A\omega_2 + B\omega_1 - (A-B)(\epsilon_0 - t) - \omega_2 + \omega_1$, $X_4 = A\omega_2 + B\omega_1$ and $X_5 = A - B$ with $A = \frac{1}{a^2}\left(1 + 4t/(c-U)\right)^2$, $B = \frac{1}{a^2}\left(1 - 4t/(c-U)\right)^2$, $\omega_1 = \epsilon_0 + t - (c-U)/2$ and $\omega_2 = \epsilon_0 + t + (c+U)/2$. $X_1' = A\omega_4 + B\omega_3 + (\epsilon_0 + t)(A+B) - \omega_3 - \omega_4 + 2i\eta B$, $X_2' = (\epsilon_0 + t)(A\omega_4 + B\omega_3) - \omega_3\omega_4 - (A-B)(i\eta)^2$, $X_3 = A\omega_4 + B\omega_3 - (A-B)(\epsilon_0 + t) - \omega_4 + \omega_3$, $X_4' = A\omega_4 + B\omega_3$ and $X_5' = A - B$ with $\omega_3 = \epsilon_0 - t + (c+U)/2$ and $\omega_4 = \epsilon_0 - t - (c-U)/2$.

From this, we calculate the effective screened interaction, which when multiplied by the exact 1-GF, yields the exact self-energy given above from

$$\Sigma_{\text{xc,b-b/ab-ab}}^{\text{exact}}(\omega) = i \int \frac{d\omega'}{2\pi} G_{\text{ab-ab/b-b}}(\omega' + \omega) W_{\text{eff}}^{R/A}(\omega') e^{i\omega'\eta}. \tag{8.46}$$

We obtain

$$W_{\text{eff}}^R(\omega) = \frac{X_1 + U}{B} + \frac{X_1}{A} \times \frac{X_4 - X_2/X_1 - i\eta(X_5 + X_3/X_1)}{\omega + X_4 - \omega_3 - i\eta}, \tag{8.47}$$

and

$$W_{\text{eff}}^A(\omega) = \frac{X_1' + U}{A} - \frac{X_1'}{A} \times \frac{X_4' - X_2'/X_1' - i\eta(X_5' + X_3'/X_1')}{\omega + X_4' - \omega_1 + i\eta}, \tag{8.48}$$

with W_{eff}^R and W_{eff}^A the resonant and anti-resonant parts, respectively.

8.4.2 Different flavors of effective interactions

By changing the 1-GF used in Eq.(8.46), we obtain different W_{eff}. We use G_{KS}, G_{H} and G_0, which differ by a shift Δ in the 1-GF poles. So, we give the solutions as a function of Δ,

$$W_{\text{eff}}^{G^\Delta,R}(\omega) = -(X_1 + U/2)e^{-2i\eta\omega} + \frac{\left(X_1\big(X_4 - X_2/X_1 - i\eta(X_5 + X_3/X_1)\big)\right)}{(\omega + X_4 - (\epsilon_0 + t + \Delta) - i\eta)}, \tag{8.49}$$

$$W_{\text{eff}}^{G^\Delta,A}(\omega) = (X_1' + U/2) - \frac{\left(X_1'\big(X_4' - X_2'/X_1' - i\eta(X_5' + X_3'/X_1')\big)\right)}{(\omega + X_4' - (\epsilon_0 - t + \Delta) + i\eta)}, \tag{8.50}$$

where for $\Delta = 0, U$ and $2t - (c - U)/2$ for $G^\Delta = G_0$, $G^\Delta = G_{\text{H}}$ and $G^\Delta = G_{\text{KS}}$, respectively.

8.4.3 Analytical solutions of the self-energies in the Dyson equation of W_{eff}

As previously explained, solving Eq.(8.41) involves multiplying it by $i\bar{G}(1,2)$, resulting in a $\bar{G}\bar{W}_{\text{eff}}$ self-energy on the left-hand side. The right-hand side contains $\bar{G}W$ and $\bar{G}W\bar{G}W_{\text{eff}}\bar{G}$ terms, where W should ideally be the exact TCTC screened interaction. However, we also aim to include the screened Coulomb interaction within the RPA (W_0), since the exact W might be not known in practice. The calculation of these self-energies involves solving integrals in frequency space, expressed in the Hubbard basis as follows

$$\Sigma_{\text{xc},ij\sigma} = \frac{i}{2\pi} \int d\omega' \, \bar{G}_{ij\sigma}(\omega' + \omega)\bar{W}_{ji}(\omega')e^{i\omega\eta}, \tag{8.51}$$

where $\bar{W}$ is $\bar{W}_{\text{eff}}$ for the left-hand side of Eq.(8.41) and is W (or W_0) for the first term of the right-hand side of the equation. For the second term on the right hand-side, we have

$$\Sigma_{ij\sigma}^{\bar{G}W\bar{G}\bar{W}_{\text{eff}}\bar{G}}(\omega) = -\sum_{kl=1,2} \int \frac{d\omega_1 d\omega_2}{(2\pi)^2} \, G_{0il\sigma}(\omega - \omega_1)\bar{W}_{ik}(\omega_1)G_{0lk\sigma}(\omega - \omega_1 - \omega_2)$$

$$\bar{W}_{\text{eff},lj}(\omega_2)G_{0kj\sigma}(\omega - \omega_2)e^{-i\eta\omega_1}e^{-i\eta\omega_2}. \tag{8.52}$$

In this section, we provide the analytical solutions of these integrals. For $\bar{G}$, we use the non-interacting 1-GFs G_0, G_{H} and G_{KS}.

$$\Sigma_{\text{xc},ij\sigma}^{\bar{G}\bar{W}_{\text{eff}}}(\omega) = -\frac{U}{2}\delta_{ij} + \frac{M}{2}\left(\frac{(-1)^{i-j}}{\omega - (\epsilon_0 + \Delta - t - x) - i\eta} + \frac{1}{\omega - (\epsilon_0 + \Delta + t + x) + i\eta}\right), \tag{8.53}$$

111

where the ansatz that we made for $\bar{W}_{\text{eff}}$ is

$$\bar{W}_{\text{eff},ij}(\omega) = U\delta_{ij} + \frac{M}{2}\left(\frac{1}{\omega - x + i\eta} - \frac{1}{\omega + x - i\eta}\right), \tag{8.54}$$

with M and x the unknown amplitude and pole, respectively. For the right-hand side, when we use the exact W, we have

$$\Sigma^{\bar{G}W}_{\text{xc},ij\sigma}(\omega) = -\frac{U}{2}\delta_{ij} + \frac{U^2}{a^2}\left(\frac{(-1)^{i-j}}{\omega - (\epsilon_0 + \Delta - t - (c+U)/2) - i\eta} + \frac{1}{\omega - (\epsilon_0 + \Delta + t + (c+U)/2) + i\eta}\right), \tag{8.55}$$

and

$$\begin{aligned}
\Sigma^{\bar{G}W\bar{G}\bar{W}_{\text{eff}}\bar{G}}_{\text{c},ij\sigma}(\omega) = &-\left(\frac{(-1)^{i-j}}{\omega - (\epsilon_0 + \Delta - 3t) - i\eta} + \frac{1}{\omega - (\epsilon_0 + \Delta + 3t) + i\eta}\right)\left(\frac{U^2}{8} + \frac{2U^3}{4a^2(2t - (c+U)/2)}\right. \\
&+ \frac{2U^2M}{2a^2(2t-x)(2t-(c+U)/2)} + \frac{UM}{4(2t-x)} - \frac{2U^3}{4a^2(2t+(c+U)/2)} \\
&+ \frac{2U^2M}{2a^2(x+(c+U)/2)(2t+(c+U)/2)} - \frac{2U^2M}{2a^2(x+(c+U)/2)(2t-x)} + \frac{2U^2M}{2a^2(2t+x)(2t+(c+U)/2)} \\
&\left.- \frac{UM}{4(2t+x)} + \frac{2U^2M}{2a^2(2t+x)(x+(c+U)/2)} - \frac{2U^2M}{2a^2(x+(c+U)/2)(2t-(c+U)/2)}\right) \\
&+ \left(\frac{(-1)^{i-j}}{\omega - (\epsilon_0 + \Delta - t - (c+U)/2) - i\eta} + \frac{1}{\omega - (\epsilon_0 + \Delta + t + (c+U)/2) + i\eta}\right)\left(\frac{2U^3}{4a^2(2t-(c+U)/2)}\right. \\
&+ \frac{2U^3}{4a^2(2t+(c+U)/2)} + \frac{2U^2M}{2a^2(2t-x)(2t-(c+U)/2)} + \frac{2U^2M}{2a^2(2t+x)(x+(c+U)/2)} \\
&\left.- \frac{2U^2M}{2a^2(x+(c+U)/2)(2t-(c+U)/2)} + \frac{2U^2M}{2a^2(2t-x)((c+U)/2-x)}\right) \\
&+ \left(\frac{(-1)^{i-j}}{\omega - (\epsilon_0 + \Delta - t - x) - i\eta} + \frac{1}{\omega - (\epsilon_0 + \Delta + t + x) + i\eta}\right)\left(\frac{UM}{4(2t+x)}\right. \\
&+ \frac{UM}{4(2t-x)} + \frac{2U^2M}{2a^2(2t+(c+U)/2)(x+(c+U)/2)} - \frac{2U^2M}{2a^2(x+(c+U)/2)(2t-x)} \\
&\left.- \frac{2U^2M}{2a^2(2t-x)((c+U)/2-x)}\right) + \left(\frac{(-1)^{i-j}}{\omega - (\epsilon_0 + \Delta - t + (c+U)/2) + i\eta} \times \frac{1}{\omega - (\epsilon_0 + \Delta - t + x) + i\eta}\right. \\
&\left.+ \frac{1}{\omega - (\epsilon_0 + \Delta + t - (c+U)/2) - i\eta} \times \frac{1}{\omega - (\epsilon_0 + \Delta + t - x) - i\eta}\right) \\
&\left(\frac{2U^2M}{2a^2(2t+(c+U)/2)} + \frac{2U^2M}{2a^2(2t+x)} - \frac{2U^2M}{a^2(2t+x)}\right) \\
&+ \left(\frac{(-1)^{i-j}}{\omega - (\epsilon_0 + \Delta + t + (c+U)/2 + x) + i\eta} + \frac{1}{\omega - (\epsilon_0 + \Delta - t - (c+U)/2 - x) - i\eta}\right)\frac{2U^2M}{2a^2(2t+x)^2}.
\end{aligned} \tag{8.56}$$

In terms of W_0, we have the following solutions

$$\Sigma^{\bar{G}W_0}_{\text{xc},ij\sigma}(\omega) = -\frac{U}{2}\delta_{ij} + \frac{U^2t}{2h}\left(\frac{(-1)^{i-j}}{\omega - (\epsilon_0 + \Delta - t - h) - i\eta} + \frac{1}{\omega - (\epsilon_0 + \Delta + t + h) + i\eta}\right), \tag{8.57}$$

and

$$\Sigma_{c,ij\sigma}^{\bar{G}W_0\bar{G}\bar{W}_{\text{eff}}\bar{G}}(\omega) = -\left(\frac{(-1)^{i-j}}{\omega - (\epsilon_0 + \Delta - 3t) - i\eta} + \frac{1}{\omega - (\epsilon_0 + \Delta + 3t) + i\eta}\right)\left(\frac{U^2}{8} + \frac{U^3 t}{4h(2t - h)}\right.$$

$$+ \frac{U^2 tM}{2h(2t-x)(2t-h)} + \frac{UM}{4(2t-x)} - \frac{U^3 t}{4h(2t+h)} + \frac{U^2 tM}{2h(x+h)(2t+h)} - \frac{U^2 tM}{2h(x+h)(2t-x)} + \frac{U^2 tM}{2h(2t+x)(2t+h)}$$

$$\left. - \frac{UM}{4(2t+x)} + \frac{U^2 tM}{2h(2t+x)(x+h)} - \frac{U^2 tM}{2h(x+h)(2t-h)}\right)$$

$$+ \left(\frac{(-1)^{i-j}}{\omega - (\epsilon_0 + \Delta - t - h) - i\eta} + \frac{1}{\omega - (\epsilon_0 + \Delta + t + h) + i\eta}\right)\left(\frac{U^3 t}{4h(2t-h)} + \frac{U^3 t}{4h(2t+h)}\right.$$

$$\left. + \frac{U^2 tM}{2h(2t-x)(2t-h)} + \frac{U^2 tM}{2h(2t+x)(x+h)} - \frac{U^2 tM}{2h(x+h)(2t-h)} + \frac{U^2 tM}{2h(2t-x)(h-x)}\right)$$

$$+ \left(\frac{(-1)^{i-j}}{\omega - (\epsilon_0 + \Delta - t - x) - i\eta} + \frac{1}{\omega - (\epsilon_0 + \Delta + t + x) + i\eta}\right)\left(\frac{UM}{4(2t+x)} + \frac{UM}{4(2t-x)} + \frac{U^2 tM}{2h(2t+h)(x+h)}\right.$$

$$\left. - \frac{U^2 tM}{2h(x+h)(2t-x)} - \frac{U^2 tM}{2h(2t-x)(h-x)}\right)$$

$$+ \left(\frac{(-1)^{i-j}}{\omega - (\epsilon_0 + \Delta - t + h) + i\eta} \times \frac{1}{\omega - (\epsilon_0 + \Delta - t + x) + i\eta} + \frac{1}{\omega - (\epsilon_0 + \Delta + t - h) - i\eta}\right.$$

$$\left. \times \frac{1}{\omega - (\epsilon_0 + \Delta + t - x) - i\eta}\right)$$

$$\left(\frac{U^2 tM}{2h(2t+h)} + \frac{U^2 tM}{2h(2t+x)} - \frac{U^2 tM}{h(2t+x)}\right) + \left(\frac{(-1)^{i-j}}{\omega - (\epsilon_0 + \Delta + t + h + x) + i\eta}\right.$$

$$\left. + \frac{1}{\omega - (\epsilon_0 + \Delta - t - h - x) - i\eta}\right)\frac{U^2 tM}{2h(2t+x)^2}\,. \quad (8.58)$$

8.4.4 Solutions of the effective interaction from the approximate Dyson equation

After obtaining the analytical self-energies, from Eq.(8.41), we can write

$$\Sigma_{\text{xc},ij\sigma}^{\bar{G}\bar{W}_{\text{eff}}}(\omega) = \Sigma_{\text{xc},ij\sigma}^{\bar{G}\bar{W}}(\omega) + \Sigma_{\text{c},ij\sigma}^{\bar{G}\bar{W}\bar{G}\bar{W}_{\text{eff}}\bar{G}}(\omega)\,, \quad (8.59)$$

where the two unknowns are M and x, introduced in Sec. 8.4.3. For each frequency, we have an equation for M and x. This forms a set of many equations with only two unknowns. Given the assumption that the pole is the same for both resonant and anti-resonant, which is another approximation, since we have seen that the resonant and anti-resonant poles are not necessarily equivalent, we can simplify the equation to the bonding-bonding or antibonding-antibonding parts of the self-energy, as both will yield the same result. The bonding-bonding elements can be expressed as follows,

$$\Sigma_{\text{xc,bb}}^{\bar{G}\bar{W}_{\text{eff}}}(\omega) = \Sigma_{\text{xc,bb}}^{\bar{G}W}(\omega) + \Sigma_{\text{c,bb}}^{\bar{G}\bar{W}\bar{G}\bar{W}_{\text{eff}}\bar{G}}(\omega)\,. \quad (8.60)$$

It is crucial, before delving into solving this equation, to comprehend and discuss its structure. Initially, choosing random values for the unknowns helps to understand the structure of both sides in Eq.(8.60). This provides insights into the tendencies of the solutions. For instance, we use the coordinates of the exact $W_{\text{eff}}(G_0)$ (amplitude and resonant pole) in Eq.(8.60) in the case where the RPA W_0 is utilized. In Fig. 8.7, we display the imaginary part of both the left-hand and right-hand sides of Eq.(8.60). As

anticipated, numerous peaks are observed in the right-hand side of the equation, with two of them having dominant weights, while the others are small (at least for this value of t). In order to have an equivalent imaginary part for both sides, the weight of the black peak in the red box should vanish, as well as the other small peaks. On the other hand, the weights of both peaks in the green box should be equivalent. This yields two simpler equations, which could be used to determine the unknowns. This is an approximation because there are more peaks whose weights should vanish, but since their weights are small, they can be neglected. If we solve these two equations we obtain approximately the same result as from the solution of the full Eq.(8.60), which will be explained below. Therefore, we directly proceeded to solve the full equations written in Eq.(8.60). Our strategy relies on choosing
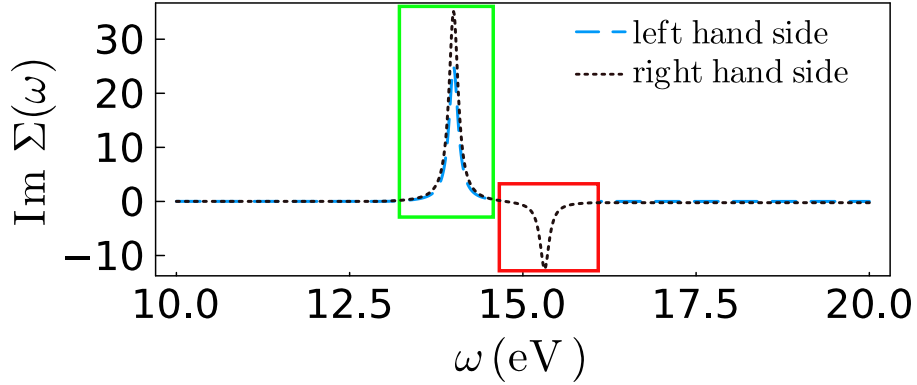
Figure 8.7: Imaginary part of the self-energy as a function of frequency for $t = 4$ and $U = 4$ eV. The left-hand and right-hand sides of Eq.(8.60) are shown in dashed sky blue and dotted black lines, respectively.

two different frequencies. For example we choose $\omega = 0$ and $\omega = \omega_p^{W_{\text{eff}}(G)}$, where $\omega_p^{W_{\text{eff}}(G)}$ is the pole of the exact W_{eff} calculated with $\bar{G} = G$. It is important to note that, if the ansatz is in principle exact, using any couple of frequencies, we should obtain the same result. This yields the following two equations

$$\Sigma_{\text{xc,bb}}^{\bar{G}\bar{W}_{\text{eff}}}(\omega = 0) = \Sigma_{\text{xc,bb}}^{\bar{G}\bar{W}}(\omega = 0) + \Sigma_{\text{c},bb}^{\bar{G}\bar{W}\bar{G}\bar{W}_{\text{eff}}\bar{G}}(\omega = 0) , \tag{8.61}$$

$$\Sigma_{\text{xc,bb}}^{\bar{G}\bar{W}_{\text{eff}}}(\omega = \omega_p^{W_{\text{eff}}(G)}) = \Sigma_{\text{xc,bb}}^{\bar{G}\bar{W}}(\omega = \omega_p^{W_{\text{eff}}(G)}) + \Sigma_{\text{c,bb}}^{\bar{G}\bar{W}\bar{G}\bar{W}_{\text{eff}}\bar{G}}(\omega = \omega_p^{W_{\text{eff}}(G)}) , \tag{8.62}$$

which can be solved numerically in different ways. In practice, we solve Eq.(8.61) and Eq.(8.62) by considering the real part, knowing that in principle if the real part of the correlation part of Σ_{xc} is zero, the imaginary part should be also zero. However, this can be false in this case, since the right-hand side of Eq.(8.60) could violate the Kramers-Kronig relations, since it is approximated. Despite that, we make this assumption and will see a posterio whether the results justify the assumption.

In Fig. 8.8, we present graphical solutions of Eq.(8.61) and Eq.(8.62) (which are called Eq 1 and Eq 2, respectively), using the exact TCTC W and W_0 in the left and right panels, respectively. The intersection of the two curves corresponds to the solutions of the two equations that we are looking for. In both cases (exact and RPA screening), the solutions of the equations are well-behaved and similar, at least for this value of t. When t is small enough, starting from $t = 0.5$ eV, the behavior of the two equations becomes complicated, resulting in many solutions. In that case, one has to select
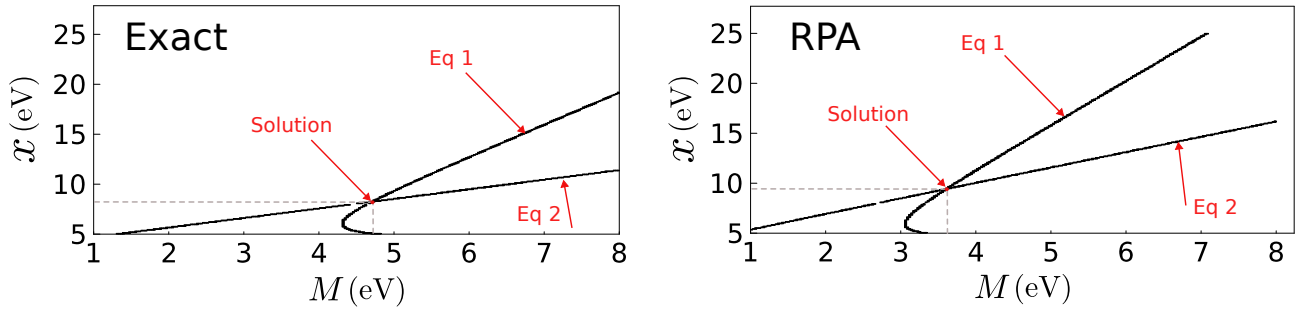
Figure 8.8: Solutions of Eq 1 and Eq 2, respectively given in Eq.(8.61) and Eq.(8.62), representing couples of the pole x and amplitude M. Results using W and W_0 are shown in the left and right panels respectively. In this example, we use $U = 4$ eV and $t = 4$ eV. These results are obtained using the numerical tools: ImplicitEquations in Julia.

the physical solutions, which is not always obvious. *It is important to note that choosing a different frequency couple in Eqs.(8.61) (8.62) leads to a very similar solution, which justifies our procedure.*

Chapter 9

Beyond GW: second-order expansion in terms of W

In Chaps. 7 and 8 we have explored first order expressions for the self-energy, with a TCTE approximation for the effective interaction in Chap. 7, and an in principle exact effective interaction in Chap. 8. In the present chapter we take the more standard route of many-body perturbation theory (MBPT), where the first-order self-energy is corrected by a second-order term. Such an approach suffers in practice from the fact that it is not clear which ingredients to use, and therefore, a lot of flavors exist. We first remind the fact that by using the technique of functional derivatives, various different expansions are possible. Moreover, we show that other possibilities exist, in particular and in the spirit of Ref. [177], we propose a well-defined perturbation series in terms of the screened interaction within the random phase approximation (RPA). In Ref. [177], by using a simple one-point model, evidence was found for the fact that the RPA screened interaction shows a promising route for offering a better expansion for the self-energy. In the present work, by using a more realistic model, namely the Hubbard dimer model at half-filling, we test various flavors of screened Coulomb interactions and confirm to some extent the predictions made on the basis of the simple one-point model. In addition to identifying suitable ingredients for the expansion, our investigation concerns determining whether properties like the spectral function and ground-state total energy exhibit improvements at the second order across various correlation regimes.

9.1   Freedom in the functional derivative approach

In principle, MBPT can be expressed in terms of different effective interactions, since the xc self-energy can be written in terms of an effective interaction starting from the standard definition of Σ_{xc} as

$$\Sigma_{\mathrm{xc}}(1,2) = -i \int d(34)\, G(1,4) v_{\mathrm{c}}(3,1^+) \frac{\delta G^{-1}(4,2)}{\delta v_{\mathrm{ext}}(3)} \tag{9.1}$$

$$= -i \int d(345)\, G(1,4) v_{\mathrm{c}}(3,1^+) \frac{\delta G^{-1}(4,2)}{\delta \bar{v}(5)} \frac{\delta \bar{v}(5)}{\delta v_{\mathrm{ext}}(3)} \tag{9.2}$$

$$= -i \int d(45)\, G(1,4) \bar{W}(5,1^+) \frac{\delta G^{-1}(4,2)}{\delta \bar{v}(5)} \,, \tag{9.3}$$

where $\bar{W}(5,1^+) = \int d3\, v_{\mathrm{c}}(3,1^+) \frac{\delta \bar{v}(5)}{\delta v_{\mathrm{ext}}(3)}$, with $\bar{v}$ an effective potential. For instance, if $\bar{v} = v_{\mathrm{cl}} = v_{\mathrm{ext}} + v_{\mathrm{H}}$, we obtain Σ_{xc} in terms of the test-charge test-charge screened interaction W,

$$\Sigma_{\mathrm{xc}}(1,2) = -i \int d(45)\, G(1,4) W(5,1^+) \frac{\delta G^{-1}(4,2)}{\delta v_{\mathrm{cl}}(5)} \,, \tag{9.4}$$

or if $\bar{v} = v_{\mathrm{KS}} = v_{\mathrm{cl}} + v_{\mathrm{xc}}$, we obtain Σ_{xc} in terms of the test-charge test-electron screened interaction $\tilde{W}$

$$\Sigma_{\mathrm{xc}}(1,2) = -i \int d(45)\, G(1,4) \tilde{W}(5,1^+) \frac{\delta G^{-1}(4,2)}{\delta v_{\mathrm{KS}}(5)} \,. \tag{9.5}$$

In all cases, using

$$G^{-1} = G_0^{-1} - \bar{v} - \left(\Sigma_{\mathrm{xc}} + v_{\mathrm{ext}} + v_{\mathrm{H}} - \bar{v} \right), \tag{9.6}$$

these equations can be iterated, leading to a perturbative expansion in terms of the respective W_{eff}.

9.2 Further freedom in the choice of W

MBPT can be in principle expressed in terms of the bare Coulomb interaction. So, Σ_{xc} is written in terms of v_{c} as

$$\Sigma_{\mathrm{xc}}(1,2) = i G_0(1,2) v_{\mathrm{c}}(2,1^+) + \int d(34)\, G_0(1,2) v_{\mathrm{c}}(3,1^+) v_{\mathrm{c}}(2,4) G_0(4,3^+) G_0(3,4^+)$$

$$+ i^2 \int d(34)\, G_0(1,4) v_{\mathrm{c}}(3,1^+) v_{\mathrm{c}}(2,4^+) G_0(4,3) G_0(3,2^+) + i^2 \int d(34)\, G_0(1,3) G_0(4,4^+) v_{\mathrm{c}}(3,4) G_0(4,2) v_{\mathrm{c}}(2,1^+)$$

$$+ i^2 \int d(34)\, G_0(1,3) G_0(3,4) v_{\mathrm{c}}(3,4^+) G_0(4,2) v_{\mathrm{c}}(2,1^+) + \ldots\ldots, \tag{9.7}$$

where G_0 is the non-interacting (with $v_{\mathrm{c}} = 0$) 1-GF. Eq.(9.7) is illustrated diagrammatically up to the second-order in Fig. 9.1.
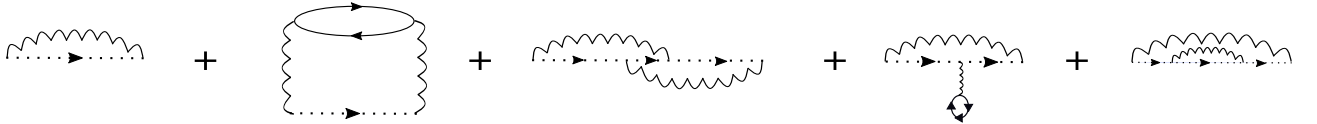

Figure 9.1: Diagrammatic illustration of the exchange-correlation self-energy in terms of the bare Coulomb interaction up to the second-order. The dotted lines and the wiggly lines represent the non-interacting 1-GF and the bare Coulomb interaction, respectively.

G_0 is related to any effective 1-GF, called $\bar{G}$, via the Dyson equation,

$$\bar{G}(1,2) = G_0(1,2) + \int d(34)\, G_0(1,3) \bar{\Sigma}(3,4) \bar{G}(4,2) \,, \tag{9.8}$$

117

where $\bar{\Sigma}$ is the self-energy that depends on the choice of $\bar{G}$. For instance, if $\bar{G} = G_{\mathrm{H}}$ with G_{H} the Hartree 1-GF, $\bar{\Sigma} = \Sigma_{\mathrm{H}}$. Eq.(9.8) can be inverted to

$$G_0(1,2) = \bar{G}(1,2) - \int d(34)\,\bar{G}(1,3)\bar{\Sigma}(3,4)G_0(4,2)\,. \tag{9.9}$$

Similarly, the bare and screened interactions are related via the following Dyson-like equation,

$$\bar{W}(1,2) = v_{\mathrm{c}}(1,2) + \int d(34)\,v_{\mathrm{c}}(1,3)\bar{P}(3,4)\bar{W}(4,2)\,, \tag{9.10}$$

where $\bar{P}$ is the effective polarizability that depends on the choice of $\bar{W}$. For example, if $\bar{W}$ is the exact screened interaction, $\bar{P}$ must be the exact irreducible polarizability. Eq.(9.10) can be inverted to

$$v_{\mathrm{c}}(1,2) = \bar{W}(1,2) - \int d(34)\,\bar{W}(1,3)\bar{P}(3,4)v_{\mathrm{c}}(4,2) \tag{9.11}$$

$$= \bar{W}(1,2) - \int d(34)\,\bar{W}(1,3)\bar{P}(3,4)\bar{W}(4,2) + \int d(3456)\,\bar{W}(1,3)\bar{P}(3,4)\bar{W}(4,5)\bar{P}(5,6)\bar{W}(6,2)$$

$$+ \,...... \,. \tag{9.12}$$

Eq.(9.12) offers an alternative perspective, illustrating the flexibility in the selection of the screened Coulomb interaction within MBPT. Remarkably, Eq.(9.12) highlights a larger range of choices compared to the functional derivative approach. It establishes that, since there is only one v_{c} that can be derived from any $\bar{W}$, as long as $\bar{W}$ and $\bar{P}$ in Eq.(9.12) are mutually consistent, MBPT can be expressed in terms of many different $\bar{W}$. This expands the options for $\bar{W}$ discussed in the preceding section, which introduces the possibility of utilizing the RPA screened interaction. Consequently, in principle, Σ_{xc} can be expressed in terms of the RPA interaction.

Using Eqs.(9.9) and (9.12) in Eq.(9.7), with the RPA choice, i.e, $\bar{P} = \bar{P}^{\mathrm{RPA}} = -i\bar{G}\bar{G}$, we obtain an exact expansion for Σ_{xc} in terms of the RPA interaction $\bar{W}^{\mathrm{RPA}}$

$$\Sigma_{\mathrm{xc}}(1,2) = i\bar{G}(1,2)\bar{W}^{\mathrm{RPA}}(2,1^+) - \int d(34)\,\bar{G}(1,2)\bar{W}^{\mathrm{RPA}}(1,3)\bar{G}(4,3^+)\bar{G}(3,4^+)\bar{W}^{\mathrm{RPA}}(4,2)$$

$$+ \int d(34)\,\bar{G}(1,2)\bar{W}^{\mathrm{RPA}}(1,3)\bar{G}(4,3^+)\bar{G}(3,4^+)\bar{W}^{\mathrm{RPA}}(4,2)$$

$$+ i^2 \int d(34)\,\bar{G}(1,4)\bar{W}^{\mathrm{RPA}}(3,1^+)\bar{W}^{\mathrm{RPA}}(2,4^+)\bar{G}(4,3)\bar{G}(3,2^+) - i^2 \int d(34)\,\bar{G}(13)\bar{\Sigma}(3,4)\bar{G}(4,2)v_{\mathrm{c}}(2,1^+)$$

$$+ i^2 \int d(34)\,\bar{G}(1,4)\bar{G}(4,4^+)v_{\mathrm{c}}(3,4)\bar{G}(4,2)v_{\mathrm{c}}(2,1^+) + i^2 \int d(34)\,\bar{G}(1,3)\bar{G}(3,4)\bar{W}^{\mathrm{RPA}}(3,4^+)\bar{G}(4,2)\bar{W}^{\mathrm{RPA}}(2,1^+)$$

$$+ \,........ \,, \tag{9.13}$$

where the cancellation of the second diagram in Fig. 9.1 occurs due to the emergence of an equivalent diagram with opposite sign, which is a result of the transformation of $v_{\mathrm{c}} \to \bar{W}^{\mathrm{RPA}}$, expressed by Eq.(9.12). Moreover, the choice of $\bar{G}$ in Eq.(9.13) can lead to the cancellation of other diagrams. For

example, if $\bar{G} = G_H$ in Eq.(9.9), resulting in $\bar{\Sigma} = v_H$, then the fourth diagram in Fig. 9.1 is eliminated when substituting $\bar{\Sigma}$ into Eq.(9.13). This illustrates the fact that as corrections are introduced to $\bar{G}$, more diagrams tend to cancel out since they are implicitly accounted for in $\bar{G}$.
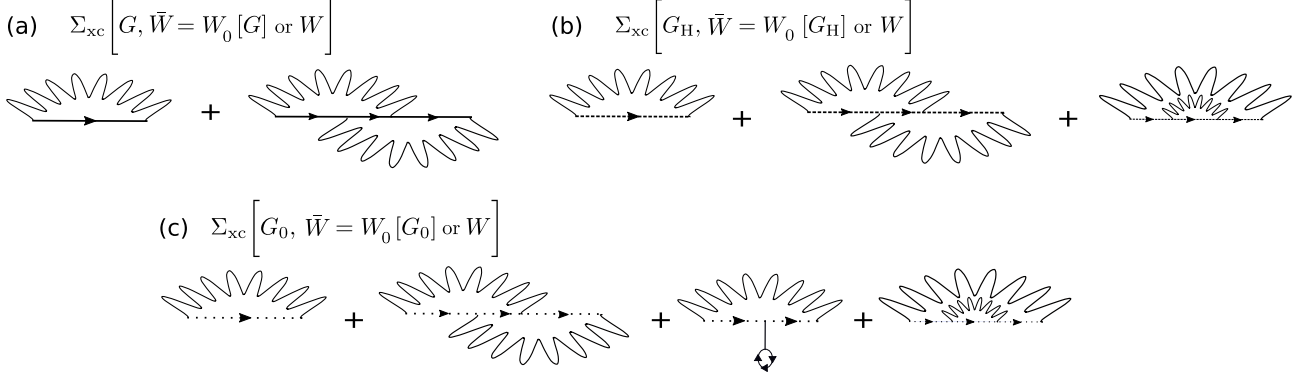
(a) $\Sigma_{\mathrm{xc}}\left[G, \bar{W} = W_0[G] \text{ or } W\right]$ (b) $\Sigma_{\mathrm{xc}}\left[G_H, \bar{W} = W_0[G_H] \text{ or } W\right]$

(c) $\Sigma_{\mathrm{xc}}\left[G_0, \bar{W} = W_0[G_0] \text{ or } W\right]$

Figure 9.2: Second-order expansion of Σ_{xc} in terms of $\bar{W}$: the wiggly lines correspond to the effective screened Coulomb interaction $\bar{W}$. Two differents $\bar{W}$ are used, which are the exact TCTC screened interaction W, and W_0, the RPA screened interaction built with $\bar{P} = -i\bar{G}\bar{G}$. The solid, dashed and dotted lines correspond to the interacting, Hartree and non-interacting ($v_{\mathrm{c}} = 0$) 1-GFs, respectively. When G is employed, there are only two second-order diagrams. When an approximate 1-GF is employed such as G_H and G_0, diagrams at the second-order that include corrections must be added. This is represented by the third diagram and third and fourth diagrams in (b) and (c), respectively. They are called self-consistency diagrams (SCD).

9.3 Optimal choice

After having shown that the self-energy can be obtained exactly by making different expansions in terms of an effective interaction in Sec. 9.1 and in terms of an effective interaction within the RPA in Sec. 9.2, it becomes crucial to address the following question: with such diversity of $\bar{W}$, what can be the optimal choice? Therefore, it is interesting to compare expansions in terms of different $\bar{W}$. A direct, and promising as suggested in Ref. [177], choice for $\bar{W}$ would be the W^{RPA}. Another choice would be the exact TCTC screened interaction $\bar{W}$, that carries vertex corrections in the response function. For comparison, we expand Σ_{xc} to second-order in $\bar{W}$ and $\bar{G}$. It would be also interesting to compare higher orders, but these are complicated to calculate for real materials and we therefore focus on the optimization of the second-order result. In Fig. 9.2, we present the different expansions that will be solved and illustrated using the Hubbard dimer model. For each choice of $\bar{G}$, we make expansions in terms of the RPA and in terms of the exact screened Coulomb interactions, named as W_0 and W, respectively. We recall that the choice of W_0 is always consistent with the choice of $\bar{G}$, i.e, W_0 is obtained using $\bar{P} = -i\bar{G}\bar{G}$. As already discussed, less diagrams will emerge when more corrections are added to the choice of $\bar{G}$. That is why the choice $\bar{G} = G$ in Fig. 9.2 involves the smallest number of diagrams, where G is the interacting 1-GF. The additional diagrams that appear when a non-interacting 1-GF is used, such as G_H and G_0 are called self-consistency diagrams. *It is worth noting that expansions in terms of W_0 and W does not involve the same diagrams when one goes beyond the second-order.*

119

9.4 Recent results in literature

Numerous recent studies have delved into the vertex-corrected self-energy, particularly employing a second-order expansion with respect to the screened Coulomb interaction. While these investigations may not directly align with the specific question about the flavors optimization addressed in this work, they contribute significantly to the understanding of the topic, especially in comparing the first with the second-order performance.

For instance, Shirley in Ref. [73] was adding the second-order diagram in terms of the screened Coulomb interaction (W) on top of the first-order GW one. He concluded that the inclusion of next-order term in W, which is $GWGWG$, restores reduced bandwidths for metals, which agrees well with experiments. He made full and nearly fully self-consistent calculations for the first and second-order self-energies in terms of W, respectively. Moreover, he also discussed the spectral function, highlighting the fact that satellites at the second-order themselves give rise to further satellites.

Grüneis et al. in Ref. [75] emphasized the importance of including vertex corrections in the self-energy based on a second-order expansion in terms of W. The authors highlighted the fact that in GW, not all second-order diagrams in terms of v_c are encompassed. Their study, applied to 21 semiconductors from group IV, III-V and II-VI, demonstrated that incorporating such corrections yields improved agreement with experimental results. Notably, in this study the dynamical screened interaction is substituted with the static one in the first-order (in W) vertex corrections.

Kutepov in Ref. [77] revealed the importance of the frequency dependence of W. He concluded that the inclusion of vertex corrections in the self-energy and the polarizability is important. He highlighted the fact that first-order (in W) corrections are sufficient. Instead, the vertex corrections to the polarizability have to be obtained from the Bethe-Salpeter equation (BSE) [34–39], whereas first-order corrections (in W) to the polarizability yield unphysical results. This conclusion has been obtained by comparing different schemes for different materials (Na, K, Si, and LiF).

In Ref. [78] Kutepov also applied two distinct schemes, the same as in Ref. [77], to calculate the band gap for various semiconductors/insulators. The first scheme involves applying first-order vertex corrections (in terms of W) for both self-energy and polarizability. In the second scheme, vertex corrections derived from BSE are used in the polarizability, while the self-energy still relies on first-order vertex corrections in terms of W. Both schemes outperformed the self-consistent GW (scGW) and quasiparticle GW (QSGW)[31], and a negligeable difference between both schemes have been found.

Similarly, Wang et al. in Ref. [178] conducted an assessment of first-order vertex corrections in terms of the screened Coulomb interaction, introducing an additional second-order diagram termed the full second-order self-energy (FSOS-W) contribution. Their study presented the one-shot $GW+$ FSOS-W, denoted as $G_0W_0(\Gamma_0)^{(1)}$, as benchmarks for the $GW100$ test set and a set of 24 acceptor molecules. The findings indicated that $G_0W_0(\Gamma_0)^{(1)}$ may significantly outperform G_0W_0, depending on the starting point.

In a subsequent work by Wang and Ren in Ref. [81], the $G_0W_0(\Gamma_0)^{(1)}$ approach was applied to a set of first-row transition-metal monoxide anions, yielding similar promising results. However, in a

comparative study by Wen et al. Ref. [179], where the $G_0W_0(\Gamma_0)^{(1)}$ results of Wang et al. [178] were utilized, the accuracy of scGW was observed to be either better or comparable for the $GW100$ set.

By using the Hubbard dimer model at half-filling in Ref. [180], the authors scrutinize the structure of the functional derivative of the self-energy with respect to the 1-Green's function, dissecting it into distinct contributions. One notable contribution corresponds to the first-order vertex corrections in terms of W. Their study involves various insightful comparisons, and their conclusions, particularly relevant to this chapter, indicate that QP energies are barely impacted by the second-order self-energy with respect to the first-order one. However, the overestimation of satellite energies observed in the first-order is mitigated in the second order, resulting in an improved description. It is important to note that their results are based on self-consistent calculations, which differs from our proposed investigations.

In Ref. [115] the authors discuss the importance of vertex corrections in W within the quasiparticle self-consistent GW calculations (QSGW). While the usual QSGW, which does not involve vertex corrections in W, has a tendency to overestimate insulating band gaps, to blueshift plasmon peaks in the imaginary part of the dielectric function, and to underestimate the dielectric constant, the vertex-corrected QS$G\hat{W}$ exhibits improvement. Here, $\hat{W}$ is the screened Coulomb interaction that contains vertex corrections derived from BSE.

Overall, most studies are focused on QP energies, and calculations are often done self-consistently. Our present work is meant to contribute to completing our knowledge of the subject.

9.5 Illustration and analysis

We explore our questions using the symmetric Hubbard dimer model at half-filling. The different results that will be shown are based on the different expansions that we propose in Fig. 9.2.

9.5.1 Tendency of the second-order diagram

Before delving into the comparisons between the different flavors of $\bar{W}$ and $\bar{G}$, it is essential to examine the self-energy, spectral function and total energy at the second-order. To achieve this, we analytically calculate the second-order Σ_{xc}, employing for example $\bar{G} = G_0$ and $\bar{W} = W_0$, (see analytical solutions in 9.7), without taking into account the SCD diagrams for the moment. In Fig. 9.3, we present the imaginary part of the self-energy in the upper panel, the quasi-particle (QP) equation in the middle panel and the spectral function in the lower panel. We choose the bonding-bonding (b-b) element as an example (the same analysis can be obtained for the antibonding-antibonding element) as well as a single value of $U/t = 4$, where $U = 4$ eV and $t = 1$ eV. Comparisons between first and second-order will be discussed next sections for different correlation strenghts, but now let us understand the second-order self-energy tendency. In Fig. 9.3 $G_0W_0\Gamma_0^{(1)}$, which represents Σ_{xc} that includes the second-order diagram, exhibits an intriguing behavior attempting to rectify the first-order error. It introduces a peak at the same energy as the first-order peak but with an opposite sign as shown in the

upper panel. From the analytical solutions, this observation occurs due to a double peak introduced by the second-order at the same energy as the first-order (see Eq.(9.23)). This suggests that the second-order diagram aims to counterbalance the first-order discrepancy by introducing a peak in the opposite direction. Additionally, instead of the partially removed peak, the second-order creates another peak farther away with lower intensity. From Eq.(9.23), it is evident that the added peak corresponds to a double excitation energy, reflecting the double occurrence of the screened Coulomb interaction in the second-order diagram. This peak is absent in the exact result.

This additional peak is responsible for a b-b satellite of $G_0 W_0 \Gamma_0^{(1)}$ (indicated by the sky blue arrow in the lower panel). It appears in the negative frequency, unlike the exact and the first-order b-b satellites, because the self-energy changes its structure at the second-order. However, this should not be the satellite that has to be compared with the exact and first-order ones. For convenient comparisons of satellites, one has to add the ab-ab spectral function elements. These comparisons will be adressed in Fig. 9.4, while here we mainly discuss the tendency of the imaginary and real parts of the $G_0 W_0 \Gamma_0^{(1)}$ self-energy. The QP equation "$\omega - (\epsilon_0 - t) - \text{Re}\Sigma$", whose zero gives rise to the QP components of the spectral function, contains the real part of the self-energy. We show this QP equation, and not the real part of the self-energy to highlight the fact that the real part of the $G_0 W_0 \Gamma_0^{(1)}$ self-energy is completely different from the exact and the first-order ones, as shown in the zoom in the right panel. However, this difference occurs only around the pole, while elsewhere the QP equation of $G_0 W_0 \Gamma_0^{(1)}$ exbibits a promising behavior that yields an accurate QP peak in the spectral function. Moreover, as discussed in detail in Subsec. 5.2.7, in the Hubbard dimer the satellites are created due to the real part of the self-energy and not directly from the imaginary one. This can also be observed in Fig. 9.3, where the satellite of the spectral function is situated where the QP equation crosses zero for the second time. This can be more clearly understood in Subsec. 5.2.7. The second-order result does not exhibit the satellite above 5 eV that is found in the exact result, because the zero-crossing of the double-pole QP equation occurs at the energy of the peak in the imaginary part of Σ_{xc}, which supresses the satellite.

To understand the second-order self-energy behavior, let us introduce the following function that has a double pole at x,

$$f(\omega) = \frac{1}{\left(\omega - x - i\eta\right)^2} \tag{9.14}$$

$$= \frac{1}{(\omega - x)^2 - \eta^2 - 2i\eta(\omega - x)} \tag{9.15}$$

$$= \frac{(\omega - x)^2 - \eta^2 + 2i\eta(\omega - x)}{\left((\omega - x)^2 - \eta^2\right)^2 + 4\eta^2(\omega - x)^2} \, . \tag{9.16}$$

The imaginary part is

$$\text{Im}f(\omega) = \frac{2\eta(\omega - x)}{\left((\omega - x)^2 - \eta^2\right)^2 + 4\eta^2(\omega - x)^2} \, , \tag{9.17}$$

indicating that $\text{Im}f$ has two poles around x at a distance 2η, whose signs are decided by $\omega - x$. This
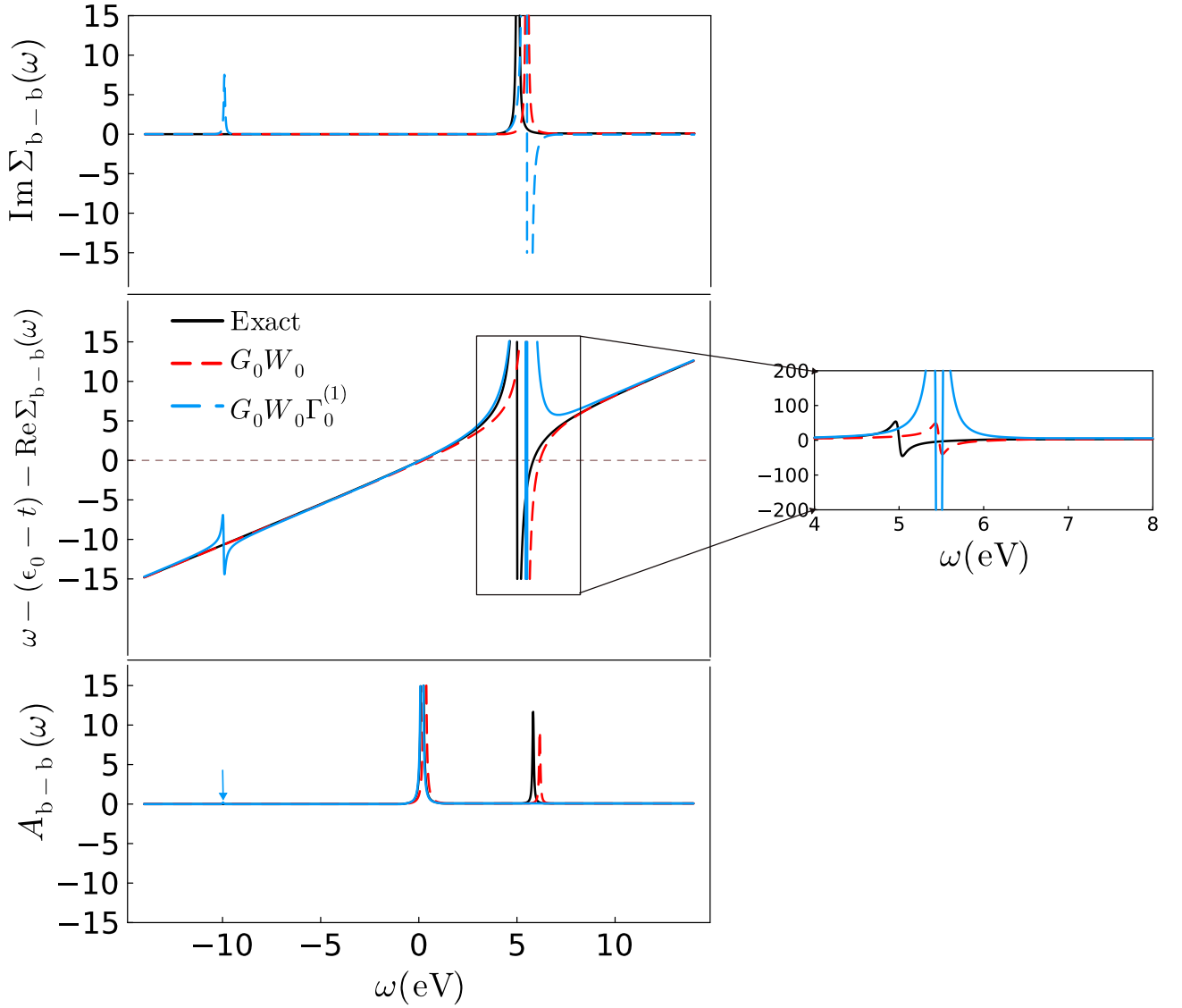
Figure 9.3: Symmetric Hubbard dimer at half-filling, where $U = 4$ eV and $t = 1$ eV. The imaginary part of the bonding-bonding (b-b) element of the self-energy ($v_{\mathrm{H}} + \Sigma_{\mathrm{xc}}$) is shown in the upper panel. The QP equation "$\omega - (\epsilon_0 - t) - \mathrm{Re}\Sigma_{\mathrm{b\text{-}b}}(\omega)$" and the b-b element of the spectral function are shown in the middle and lower panels, respectively. All quantities are shown as a function of frequency. The exact result is represented by the solid black line. The G_0W_0, where G_0 is the non-interacting 1-GF with $U = 0$ and W_0 is the screened Coulomb interaction within the RPA, is shown in dashed red line. The second-order expansion in terms of G_0 and W_0 is shown in the solid sky blue line. $G_0W_0\Gamma_0^{(1)}$ corresponds to the (c) diagrams in Fig. 9.2, where the third and fourth diagrams that represent the SCD are neglected for the moment. $\Gamma_0^{(1)}$ refers to the first-order correction in W_0 beyond G_0W_0.

justifies the observation of Fig. 9.3. The real part of f is

$$\mathrm{Re}f(\omega) = \frac{(\omega - x)^2 - \eta^2}{\left((\omega - x)^2 - \eta^2\right)^2 + 4\eta^2(\omega - x)^2} \tag{9.18}$$

$$= \frac{(\omega - x)^2 - \eta^2}{\left((\omega - x)^2 + \eta^2\right)^2} . \tag{9.19}$$

123

This expression shows two zero-crossings, at $\omega - x = \pm\eta$. To the left and right of these crossings, the function diverges as $\frac{1}{\eta^2}$. Importantly, the function is positive for $|\omega - x > \eta|$, i.e, on both sides of the pole, which does not allow for an additional zero-crossing. This is different than the real part behavior of a single pole: for a given $f'(\omega)$ function that has a single pole at x, the real part is

$$\mathrm{Re}f'(\omega) = \frac{\omega - x}{(\omega - x)^2 + \eta^2} \,, \tag{9.20}$$

with a single zero-crossing next to the $\frac{1}{\eta^2}$ divergencies, and opposite sign on the left and right side of the pole.
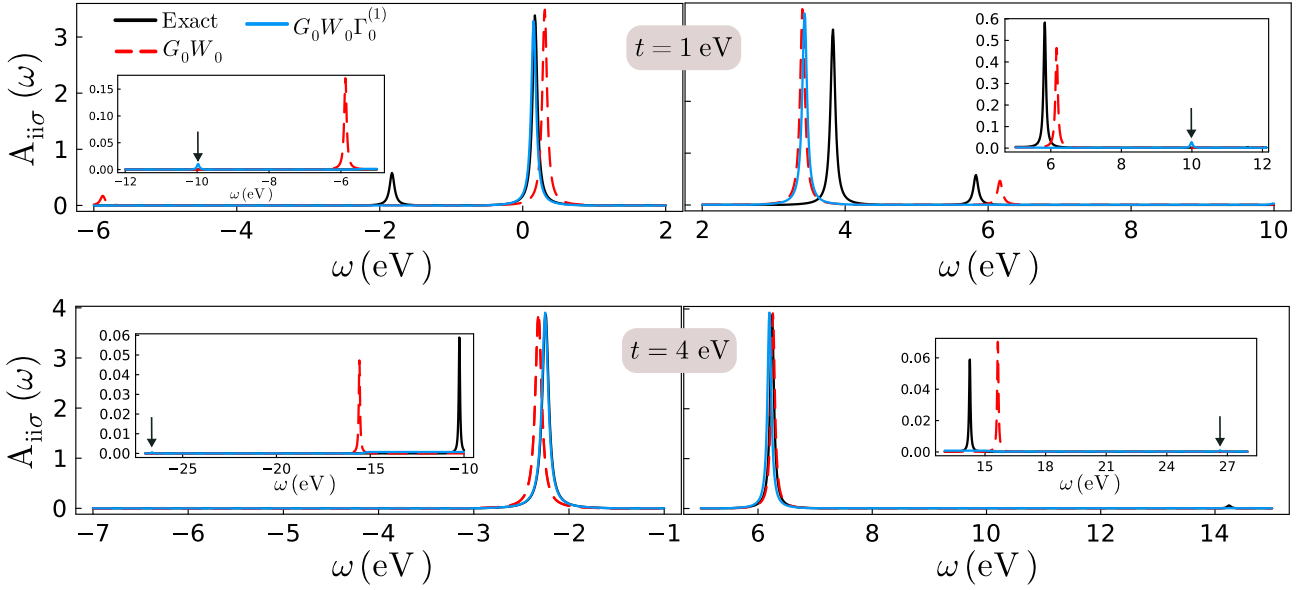
Figure 9.4: Diagonal component of the spectral function in site basis for a given spin σ $A_{ii\sigma}$ ($A_{ii\uparrow} = A_{ii\downarrow}$) as a function of frequency. $t = 1$ eV and $t = 4$ eV in the upper and lower panel, respectively, where $U = 4$ eV. The arrows in the insets indicate the presence of satellite.

After having gained insights into the behavior of the second-order self-energy, let us explore the spectral function, as depicted in Fig. 9.4. From this figure, we observe that $G_0W_0\Gamma_0^{(1)}$ shows significant agreement with the exact result, particularly evident in the highest occupied molecular orbital (HOMO) QP. For the lowest unoccupied molecular orbital (LUMO), G_0W_0 and $G_0W_0\Gamma_0^{(1)}$ exhibit similar outcomes, at least, for these choices of t. The creation of an additional small peak in $\mathrm{Im}\Sigma_{xc}$ farther away from the QP, as discussed in Fig. 9.3, explains the observed little satellites in the insets of Fig. 9.4. We conclude that the second-order self-energy tends to improve the QP energies, particularly the occupied energies, whereas it worsens the satellites.

Finally, we examine the second-order tendencies from the perspective of the ground-state total energy (E_0), which is the primary focus of this thesis. In Fig. 9.5, we present a comparison of total energies between the first and second-order self-energies. From the previous analyses of the self-energy and spectral function for the second-order self-energy, one can anticipate that the total energy at the second-order will be improved in the moderate to large range of correlations. The reason is that the second-order corrections have the tendency to improve the quasi-particle energies and not the satellites (here we refer to the removal peaks only). Consequently, the total energy will be
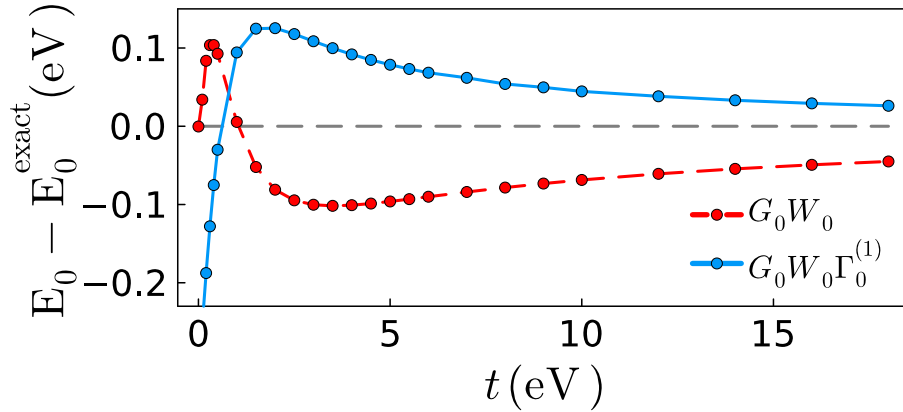
124

Figure 9.5: Total energy errors as a function of t with $U = 4$ eV.

improved in the moderate to weak range of correlations (U/t is not large), where satellites are not dominant. In contrast, when correlations become strong, satellites gain importance with significant weights contributing to the total energy. Since the second-order expansion worsens the description of satellites, it becomes evident that in this range of correlations, the second-order expansion is not the method of choice. This is well demonstrated in Fig. 9.5, where $G_0 W_0 \Gamma_0^{(1)}$ performs better than $G_0 W_0$ in the moderate to weak range of correlations, while it is not the case when correlations are strong. For $t \to 0$, $G_0 W_0 \Gamma_0^{(1)}$ exhibits an error around -0.6 eV.

9.5.2 Optimal choice for $\bar{W}$

After gaining insights into the tendency of the second-order diagram on the top of the first-order one, it is interesting, as mentioned earlier, to compare expansions in terms of different screened Coulomb interactions. Therefore, in this section, while maintaining a fixed choice for $\bar{G}$, we attempt to study expansions using different choices for $\bar{W}$. Two obvious choices are the exact TCTC W and the TCTC within the RPA screened Coulomb interaction W_0. For $\bar{G}$, we use three different Green's function as illustrated in Fig. 9.2, where for the interacting 1-GF, G, we use the G_{QP}, which is the exact 1-GF within the QP approximation (satellites are neglected and QP intensities set to 1). In the following, we provide comparisons between expansions at the first and second-orders in terms of W and W_0 from the perspective of QP energies and ground-state total energy.

In Fig. 9.6, we maintain $\bar{G} = G_0$ while comparing different expansions in terms of W_0 and W at the first and second orders looking at QP energies. Analyzing the left-hand panels at the first-order level, it is evident that the RPA screening outperforms the exact one for both HOMO and LUMO energies. Moving to the middle panels, where we add a second-order diagram on top of the first-order one (analogous to (c) in Fig. 9.2, without SCD), we observe that RPA screening remains superior for HOMO across the entire range of correlation, but it is less clear for LUMO. In the right-hand panels, we present the second-order expansions considering the self-consistency diagrams (SCD), equivalent to (c) in Fig. 9.2. Notably, SCD introduces a variable shift on top of $G_0 \bar{W} \bar{\Gamma}^{(1)}$, making HOMO worse and better with W_0 and W, respectively. In contrast, LUMO becomes slightly better with W_0 and worse with W. It is essential to note that in a small range of t, the second-order self-energy becomes
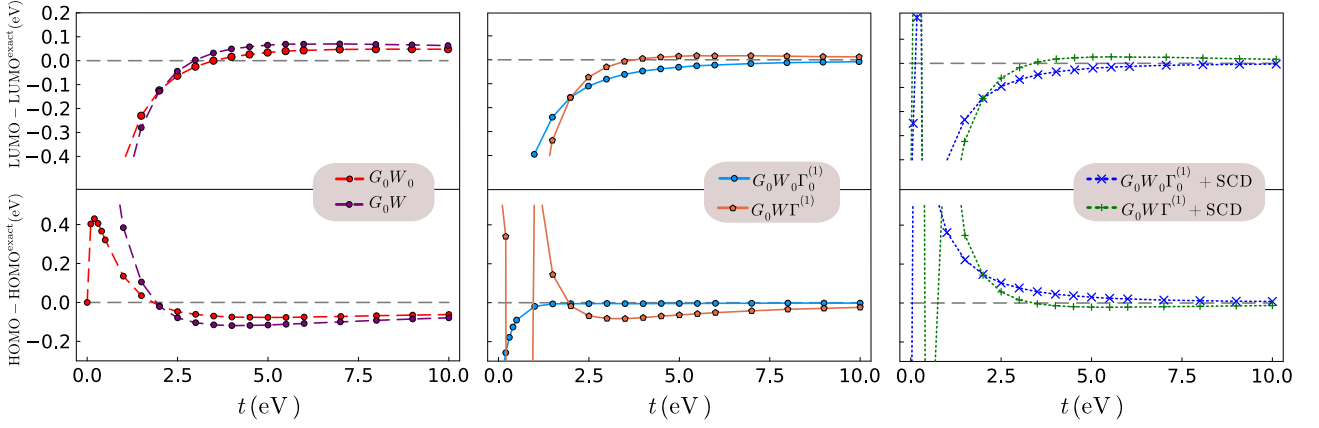
125

Figure 9.6: HOMO (lower panels) and LUMO (upper panels) energy errors as a function of t, where $U = 4$ eV. First, second, and second order plus self-consistency diagrams (SCD) expansions in W_0 and W are presented in the left, middle and right-hand panels, respectively. In dashed red and purple lines with dot markers, the first order in W_0 and W are shown, respectively. In solid sky blue and orange lines with dot and pentagon markers, the second-order (without taking into account the SCD) in W_0 and W are shown, respectively. In dotted blue and green lines with xcross and cross markers, the second-order expansion (where SCD are taken into account) in W_0 and W are shown, respectively. In all cases $\bar{G} = G_0$, and $\bar{W} = W_0$ is the RPA screened interaction built with $\bar{P} = P_0 = -iG_0G_0$.

highly unstable due to multiple peaks, explaining the instability of HOMO and LUMO when t is small.

Comparing first and second-order results for a given $\bar{W}$, we find that HOMO and LUMO are improved by adding second-order corrections, confirming the conclusion in Fig. 9.4. Particularly, $G_0W_0\Gamma_0^{(1)}$ shows high precision for HOMO energies in the moderate to large correlation range.

Overall, the RPA screening demonstrates more efficient outcomes with less instability, obviously observed in the middle panel of Fig. 9.6. By adding SCD, both expansions show instable behavior in the small range of t. The LUMO error of the first-order for both W and W_0 goes to the Hartree-Fock (HF) error, which is $-U/2$. The same holds true for the HOMO when W is employed, whereas with W_0 the HOMO is exact due to a problem of electron number, which was discussed in Subsec. 6.3.3.
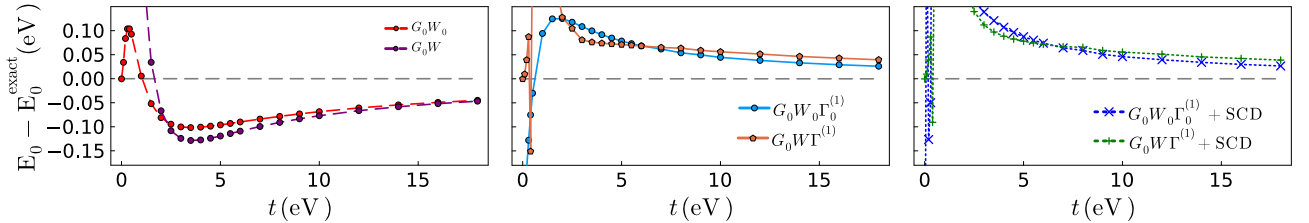
Figure 9.7: Ground-state total energy errors as a function of t with $U = 4$ eV. Labels are explained in Fig. 9.6.

In continuation of the comparisons from the perspective of ground-state total energy E_0, similar conclusions arise. Overall, the RPA screening slightly outperforms the exact one at different orders of expansions. As previously deduced from Fig. 9.5, the second-order expansion, whether using W_0

126

or W, tends to improve the total energy in the moderate to large range of correlations. It is worth mentioning that E_0 for G_0W goes to the HF result when $t \to 0$. $G_0W\Gamma^{(1)}$ exhibits an instable behavior with oscillations in the small range of t ending up with a zero error at $t \to 0$. More severe instability occurs in this range of t when SCD are added, which also impacts the expansion in terms of W_0. This instability occurs due to a problem in the spectral function that is discussed later, where as the QP components are already shown in Fig. 9.6.
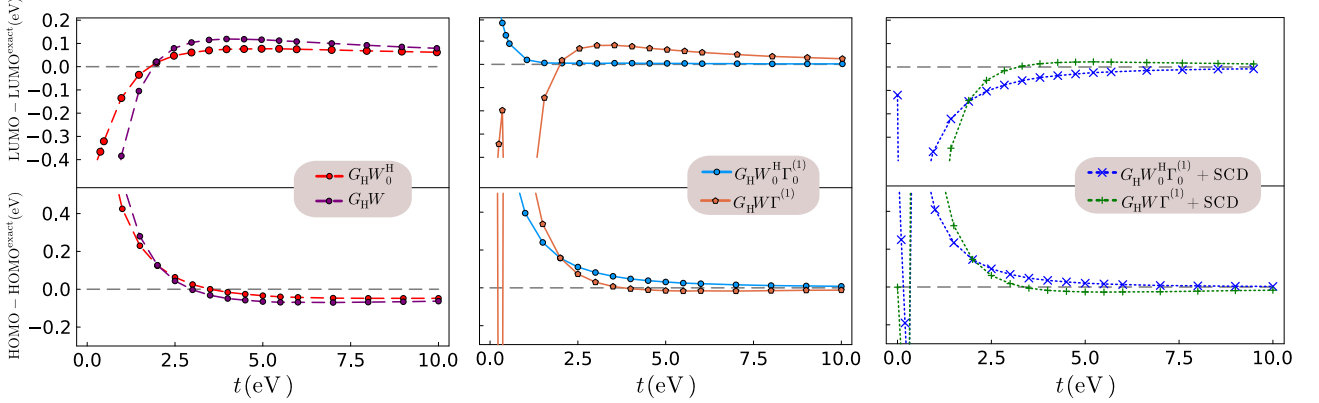
Figure 9.8: HOMO (lower panels) and LUMO (upper panels) energies errors as a function of t, where $U = 4$ eV. In this case, $\bar{G} = G_H$ and $\bar{W} = W_0^H$ or W, with G_H the Hartree 1-GF and where W_0^H is the RPA screened interaction built with $\bar{P} = -iG_HG_H$. Since the energies in G_0 and G_H differ by a constant shift, W_0^H is equal to W_0.

Changing the choice of $\bar{G}$ to $\bar{G} = G_H$, the same comparisons are repeated. At the first-order, for HOMO, LUMO energies, and E_0, W_0 outperforms W, as shown in the left panels of Fig. 9.8 and Fig. 9.9, where for both flavors the results go to the HF ones when $t \to 0$. Introducing a single second-order diagram beyond the first-order one (this is equivalent to (b) in Fig. 9.2, where the SCD diagram is neglected), represented by the middle panels of Fig. 9.8 and Fig. 9.9, again improves the results, especially in the weak to moderate range of correlations. While for HOMO energies, it is not clear which choice of $\bar{W}$ is better, for LUMO energies and E_0, the W_0 choice shows clearly better performance than W. This remains true, especially for HOMO and E_0 when adding SCD, which is equivalent to the diagrammatic expansion in (b) in Fig. 9.2. Interestingly, the W_0 choice shows high precision for E_0, as shown in the right panel of Fig. 9.9. Concerning the small range of t, the HOMO and LUMO show fluctuating errors in the case of $G_0W\Gamma^{(1)}$. Adding the SCD makes things more messy, especially for E_0.
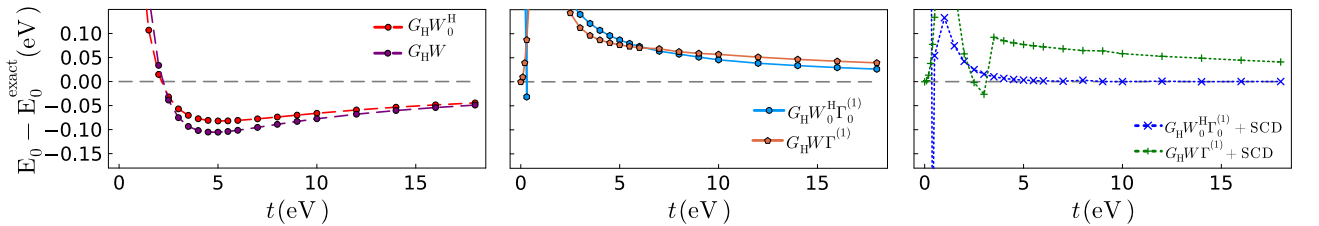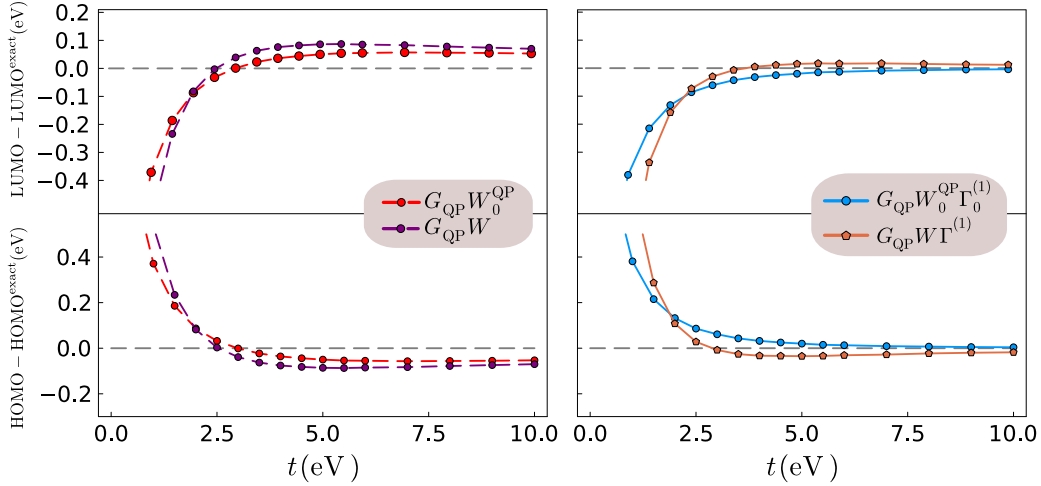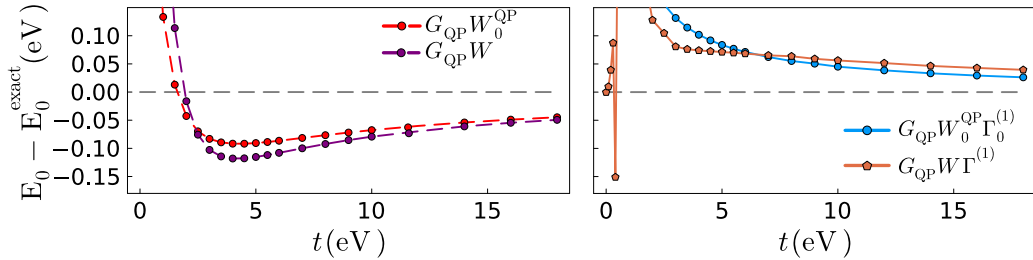

Figure 9.9: Ground-state total energy errors as a function of t with $U = 4$ eV, using $\bar{G} = G_H$ and $\bar{W} = W_0^H$ or W.

Next we utilize $\bar{G} = G_{\mathrm{QP}}$. Here, the SCD should only stem from dynamical corrections to Σ_{xc}, which we neglect here. Results are shown for the QP energies in Fig. 9.10 and for E_0 in Fig. 9.11. Similar to previous scenarios, the conclusions remain consistent. The RPA screening W_0^{QP}, calculated using G_{QP} through $P^{\mathrm{RPA}}(1,2) = -iG_{\mathrm{QP}}(1,2^+)G_{\mathrm{QP}}(2,1^+)$, demonstrates superior results compared to the use of the exact W. This holds true for both the first and second orders concerning QP energies and total energy, as depicted in Fig. 9.10 and Fig. 9.11. It is worth noting that when SCD to all orders are almost implicitly included in the 1-GF, no erratic behavior is observed when W_0 is used, whereas problems in E_0 are observed when W is used as illustrated by Fig. 9.11.

Figure 9.10: HOMO (lower panels) and LUMO (upper panels) energies errors as a function of t, where $U = 4$ eV. $\bar{G} = G_{\mathrm{QP}}$ and $\bar{W} = W_0^{\mathrm{QP}}$ and W, with W_0^{QP} the RPA screening built with $P^{\mathrm{RPA}} = -iG_{\mathrm{QP}}G_{\mathrm{QP}}$.

Figure 9.11: Ground-state total energy errors as a function of t with $U = 4$ eV, where $\bar{G} = G_{\mathrm{QP}}$ and $\bar{W} = W_0$ or W.

Finally, by maintaining the choice of $\bar{W}$ constant and comparing the different flavors of $\bar{G}$ used above, it is noticeable that using G_{H} and the RPA screening is promising for the ground-state total energy calculations as shown in the right-panel of Fig. 9.9. This is the best result among the three flavors of $\bar{G}$ for E_0 calculations. Therefore, it is interesting to examine the spectral function and the self-energy. In Fig. 9.12, we present the spectral features of the $G_{\mathrm{H}}W_{\mathrm{H}}\Gamma_{\mathrm{H}}^{(1)}$+SCD approximation. Comparing the right panel of Fig. 9.8, for example, to the middle one of Fig. 9.6, we can notice that despite the fact that the HOMO energies are more accurate within $G_0W_0\Gamma_0^{(1)}$ than $G_{\mathrm{H}}W_{\mathrm{H}}\Gamma_{\mathrm{H}}^{(1)}$+ SCD, the latter performs better for E_0 as shown in the right-panel of Fig. 9.9. Thus, there should be other
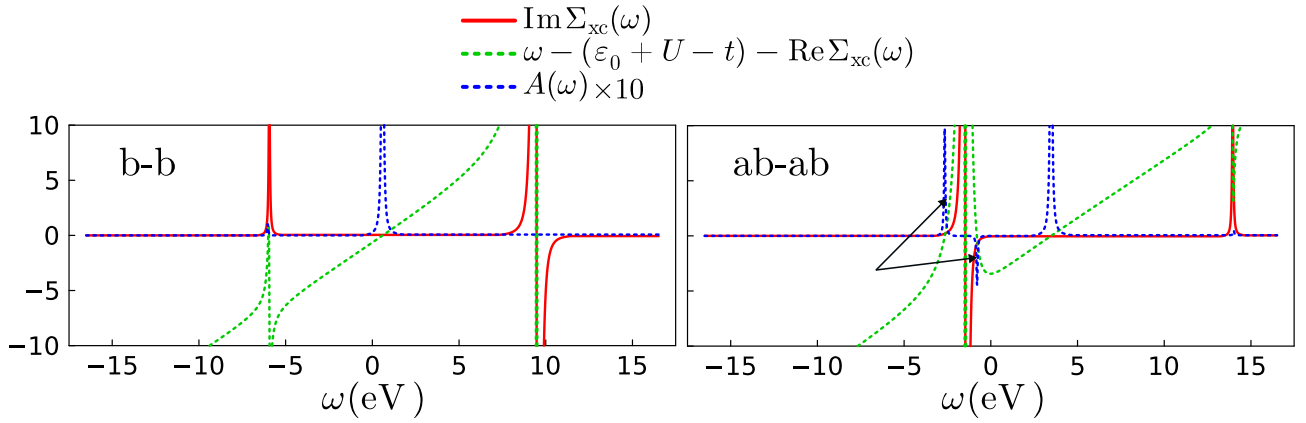
Figure 9.12: Spectral features of the $G_H W_H \Gamma_H^{(1)}+$ SCD approximation. Bonding-bonding and antibonding-antibonding elements are shown in the left and upper panels, respectively. The imaginary part of the xc self-energy is shown in solid red lines. The QP equation and the spectral function are shown in dotted green and blue lines, respectively.

reasons that improve the total energy by employing $G_H W_H \Gamma_H^{(1)}+$ SCD. This can be explained by Fig. 9.12, where emergence of additional two satellites is observed. We have discussed the fact that, for example, $G_0 W_0 \Gamma_0^{(1)}$ has a bad description for satellites since it removes the $G_0 W_0$ ones and adds new ones with higher energies (in absolute value) and very weak intensity. This suggested that the E_0 becomes worse at the second-order when correlations are important. In the case of $G_H W_H \Gamma_H^{(1)}+$ SCD as represented in Fig. 9.12, there are two additional peaks, which are indicated by the arrows, knowing that the spectral function should have only four peaks. The additional peaks, depsite their unfavorable presence, compensate the weak description of the satellites by the second-order self-energies, leading to a better total energy.

9.5.3 Negative spectral function

As mentioned earlier, the behaviors at the second-order were unstable in the small range of t, both for QP energies and total energy, particularly when the exact screening is used. This instability is a result of disturbances in the spectral function, as shown in Fig. 9.13, where negative peaks emerge, notably in the case where W is employed, even at $t = 1$ eV. Furthermore, W induces a more severe instability, causing an erratic behavior in the spectral function as shown for $t = 0.2$ eV in the right-hand panels of Fig. 9.13, where both $G_0 W \Gamma^{(1)}$ and $G_0 W \Gamma^{(1)} +$ SCD exhibit anomalous spectral features. Negative peaks in the spectral functions for MBPT beyond GW is a general feature, extensively discussed in Ref. [181]. It speaks against a straightforward expansion and calls for a careful choice of ingredients and/or combination with ideas such as these presented in Chaps. 7 and 8.

9.6 Conclusions

In summary, this chapter extended beyond the GW approximation by introducing a second-order expansion in terms of different screened Coulomb interactions, which are the exact TCTC and RPA
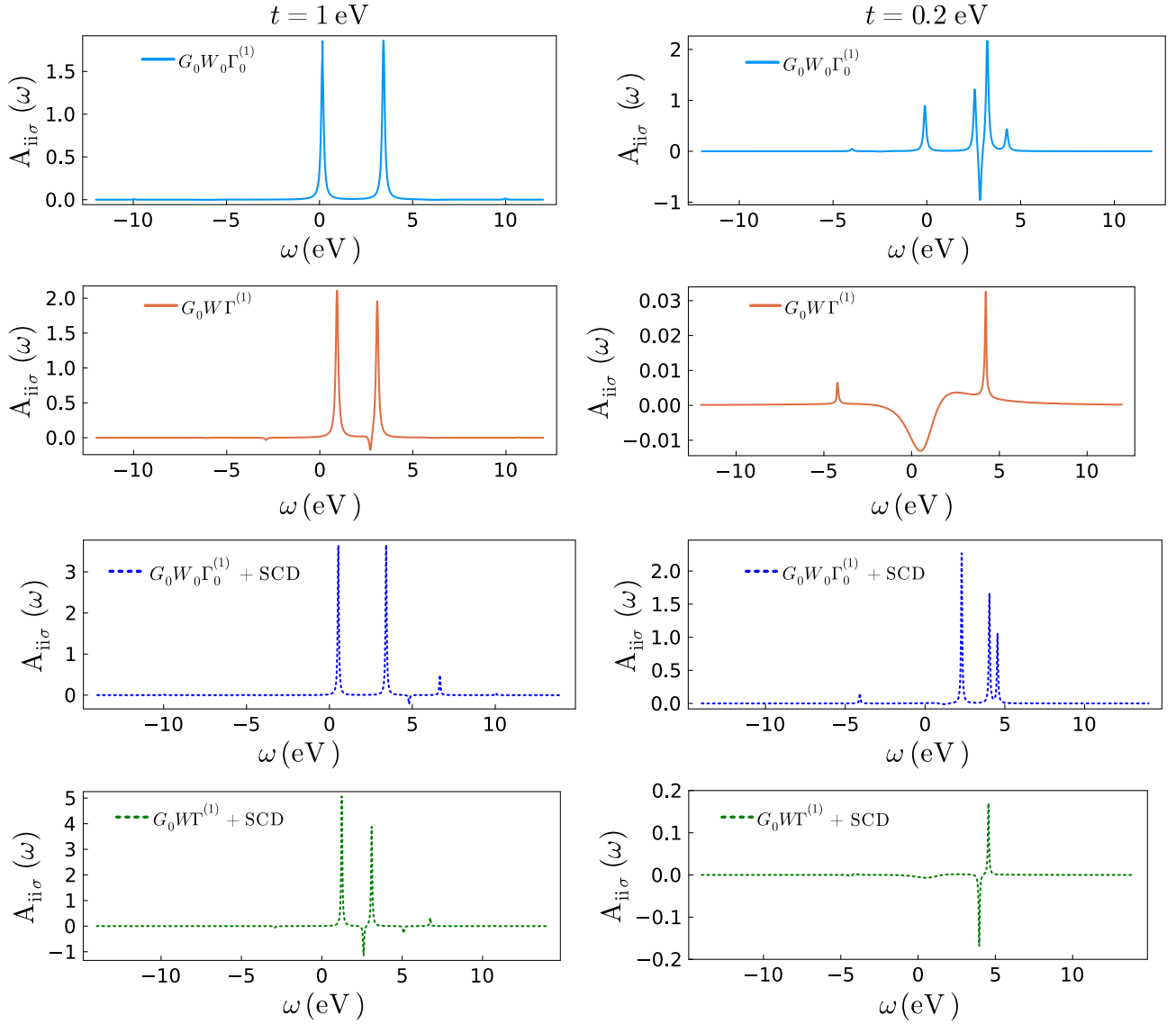
Figure 9.13: Diagonal element for a given spin $\sigma = \uparrow, \downarrow$ of the spectral function matrix as a function of frequency. $t = 1$ eV and $t = 0.2$ eV are shown in the left and right panels, respectively, where $U = 4$ eV. Second-order, with and without SCD, in terms of W_0 and W are shown, where $\bar{G} = G_0$.

interactions. While MBPT can theoretically be formulated with many different screened interactions, one might think that choosing the most realistic screening is crucial for the expansion. In contrast, and for various choice of $\bar{G}$, we demonstrated that the RPA screening outperforms the exact one, at least up to the second-order expansion. The addition of second-order diagrams atop the first-order ones improved QP energies (in agreement with several studies summarized in Sec. 9.4) in the spectral function, but at the expense of degrading satellites. This explains why the ground-state total energy only improves in the weak to moderate correlation range, where satellites have less impact on the total energy due to their weaker intensities. In contrast, as correlations become prominent, satellites play a more significant role, leading to the deterioration of the second-order's performance. Apart from the limitations in capturing satellites and accurately describing E_0 in strong correlations, the second-

order method encounters challenges such as the emergence of negative peaks and spectral function instability, especially notable in the strong correlation regime. Through the different anaylsis made in this chapter, it has been noticeable that this instability was less pronounced when utilizing RPA screening, whereas the exact screened interaction shows an erratic behavior in agreement with the finding (see, e.g, Fig. 6) of Ref. [177]. *In conclusion, the RPA screened Coulomb interaction seems to be a preferable choice for a perturbative expansion, confirming the findings of Ref. [177].*

Besides these findings of the present chapter and Ref. [177] using different models that confirm the advantage of the RPA screening, a theoretical understanding about this superiority is required. In other words, how is it possible to theoretically understand that the RPA screening is a better parameter than the exact one? As demonstrated in this chapter, the RPA screening stands as a valid option for the exact representation of MBPT. This holds true using the exact TCTC screened interaction. On the other hand, as pointed out in Ref. [177], the optimality of the RPA screening can be understood within the context of a one-electron system. In this case, the exact inverse dielectric function that screens the bare Coulomb interaction is given by $\epsilon^{-1} = 1 + v_c\chi_0$, where χ_0 denotes the non-interacting polarizability. Notably, since χ_0 is negative, the screened Coulomb interaction tends to be smaller than v_c. This poses problem for MBPT when χ_0 is significantly negative compared to $1/v_c$, leading to a negative screened interaction that can be very large in absolute value. However, this issue is overcome when employing RPA screening, where the dielectric function, $\epsilon^{RPA} = 1 - v_c\chi_0$, always avoids negativity and $\epsilon^{-1,RPA}$ will be always small. Examining the symmetric Hubbard dimer at quarter-filling provides a practical illustration. Fig. 9.14 demonstrates that the exact TCTC interaction diverges to $-\infty$ under strong correlations (as $t \to 0$). In contrast, the RPA interaction remains consistently non-negative. This observation further supports the notion that RPA screened interaction may be more favorable than using the exact one. Similar suggestions have been made in Ref. [177], where for example, in Fig. 5 the authors show the RPA inverse dielectric function compared to the exact one. Starting from a certain value of correlation, the exact ϵ^{-1} becomes too large making it difficult to suggest the exact screened interaction as a useful parameter in MBPT. However, only looking at the one-point model and at the one-electron case is too simplistic: as one can see from the screened interactions discussed in Chap. 8, in the half-filling case, the exact screened interaction does not diverge, contrary to the case one-electron.

9.7 Supporting informations

In this section, we provide analytical expressions. *We note that in the following, we provide analytical quantities within the time-ordered framework of Green's function, whereas we implement numerically the retarded quantities which are more reliable in the small range of t.*

The second-order self-energy has been obtained by solving analytically, within the time-ordered 1-GF scheme, the following integrals written in frequency space and in the Hubbard basis:
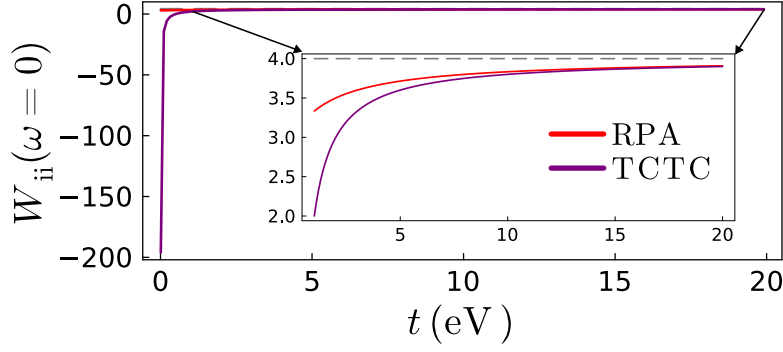
Figure 9.14: Symmetric Hubbard dimer at quarter-filling: diagonal element of the screened Coulomb interaction at $\omega = 0$ as a function of t, where $U = 4$ eV. The RPA is shown in red line. The TCTC interaction that has the exact polarizability is shown in purple.

$$\Sigma_{\mathrm{xc},ij\sigma}(\omega) = \frac{i}{2\pi} \int d\omega' \, \bar{G}_{ij\sigma}(\omega + \omega') \bar{W}_{ji}(\omega') e^{i\eta\omega'}$$
$$- \sum_{kl=1,2} \int \frac{d\omega_1 d\omega_2}{(2\pi)^2} \, \bar{G}_{il\sigma}(\omega - \omega_1) \bar{W}_{ik}(\omega_1) \bar{G}_{lk\sigma}(\omega - \omega_1 - \omega_2) \bar{W}_{lj}(\omega_2) \bar{G}_{kj\sigma}(\omega - \omega_2) e^{-i\eta\omega_1} e^{-i\eta\omega_2} . \quad (9.21)$$

For any $\bar{G}$ and $\bar{W}$, the analytical solution of the first and second orders term are given below.

$$\Sigma_{\mathrm{xc},ij\sigma}^{\bar{G}\bar{W}}(\omega) = -\frac{U}{2} + \frac{AU^2}{2}\left(\frac{1}{\omega - (\epsilon_2 + \omega_p) + i\eta} + \frac{(-1)^{i-j}}{\omega - (\epsilon_1 - \omega_p) - i\eta}\right), \quad (9.22)$$

where A and ω_p are the amplitude and pole of $\bar{W}$, respectively. ϵ_1 and ϵ_2 are the HOMO and LUMO of $\bar{G}$, respectively. Note that, in the case of the half-filling, spin-up and down elements are equivalent.

$$\Sigma_{\mathrm{c},ij\sigma}^{\bar{G}\bar{W}\bar{G}\bar{W}\bar{G}}(\omega) = -\Bigg[\left(\frac{U^2}{8} + \frac{U^3 A}{2((\epsilon_2 - \epsilon_1) - \omega_p)} + \frac{U^4 A^2}{2((\epsilon_2 - \epsilon_1) - \omega_p)^2} - \frac{U^3 A}{2((\epsilon_2 - \epsilon_1) + \omega_p)}\right.$$
$$- \frac{U^4 A^2}{((\epsilon_2 - \epsilon_1) - \omega_p)((\epsilon_2 - \epsilon_1) + \omega_p)} + \frac{U^4 A^2}{2((\epsilon_2 - \epsilon_1) + \omega_p)^2}\Bigg) \times \left(\frac{(-1)^{i-j}}{\omega - (\epsilon_1 - (\epsilon_2 - \epsilon_1)) - i\eta}\right.$$
$$+ \frac{1}{\omega - (\epsilon_2 + (\epsilon_2 - \epsilon_1)) + i\eta}\Bigg) - \left(\frac{(-1)^{i-j}}{\omega - (\epsilon_1 - \omega_p) - i\eta} + \frac{1}{\omega - (\epsilon_2 + \omega_p) + i\eta}\right) \times \left(\frac{U^3 A}{2((\epsilon_2 - \epsilon_1) + \omega_p)}\right.$$
$$+ \frac{U^3 A}{2((\epsilon_2 - \epsilon_1) - \omega_p)} + \frac{U^4 A^2}{2((\epsilon_2 - \epsilon_1) - \omega_p)^2} + \frac{U^4 A^2}{((\epsilon_2 - \epsilon_1) + \omega_p)(2\omega_p)} - \frac{U^4 A^2}{((\epsilon_2 - \epsilon_1) - \omega_p)(2\omega_p)}\Bigg)$$
$$+ \frac{U^4 A^2}{2((\epsilon_2 - \epsilon_1) - \omega_p)}\left(\frac{(-1)^{i-j}}{(\omega - (\epsilon_1 - \omega_p) - i\eta)^2} - \frac{1}{(\omega - (\epsilon_2 + \omega_p) + i\eta)^2}\right)$$
$$- \frac{U^4 A^2}{2((\epsilon_2 - \epsilon_1) + \omega_p)^2}\left(\frac{1}{\omega - (\epsilon_1 - 2\omega_p) - i\eta} + \frac{(-1)^{i-j}}{\omega - (\epsilon_2 + 2\omega_p) + i\eta}\right)\Bigg]. \quad (9.23)$$

The SCD diagrams are originating from the fact that the non-interacting 1-GF is used instead of

the interacting one. So, they are obtained for $\bar{G} = G_0$ as,

$$iG(1,2)\bar{W}(2,1^+) = i\left(G_0(1,2) + \int d(34)\, G_0(1,3)\Sigma(3,4)G(4,2)\right)\bar{W}(2,1^+) \tag{9.24}$$

$$\approx i\left(G_0(1,2) + \int d(34)\, G_0(1,3)\big(\Sigma_{\mathrm{H}}(3,4) + \Sigma_{\mathrm{xc}}(3,4)\big)G_0(4,2)\right)\bar{W}(2,1^+) \tag{9.25}$$

$$\approx i\left(G_0(1,2) + \int d(34)\, G_0(1,3)\big(\Sigma_{\mathrm{H}}(3,4) + iG_0(3,4)\bar{W}(4,3^+)\big)G_0(4,2)\right)\bar{W}(2,1^+) \tag{9.26}$$

$$= iG_0(1,2)\bar{W}(2,1^+) + i\int d(34)\, G_0(1,3)\Sigma_{\mathrm{H}}(3,4)G_0(4,2)\bar{W}(2,1^+) \tag{9.27}$$

$$+ (i)^2 \int d(34)\, G_0(1,3)G_0(3,4)\bar{W}(4,3^+)G_0(4,2)\bar{W}(2,1^+)\,,$$

where the last two terms in Eq.(9.27) are the SCD. For $\bar{G} = G_{\mathrm{H}}$, the second term in Eq.(9.27) does not exist.

In the Hubbard basis and frequency space, the SCD are given as

$$U \sum_{l=1,2,\sigma'=\uparrow,\downarrow} \int \frac{d\omega_1 d\omega_2}{(2\pi)^2}\, G_{0il\sigma}(\omega + \omega_1)G_{0ll\sigma'}(\omega_2)G_{0lj\sigma}(\omega + \omega_1)\bar{W}_{ji}(\omega_1)e^{i\omega_1\eta}e^{i\omega_2\eta}$$

$$- \sum_{ln} \int \frac{d\omega_1 d\omega_2}{(2\pi)^2}\, G_{0il\sigma}(\omega + \omega_2)G_{0ln\sigma}(\omega + \omega_1 + \omega_2)\bar{W}_{nl}(\omega_1)G_{0nj\sigma}(\omega + \omega_2)\bar{W}_{ji}(\omega_2)e^{i\omega_1\eta}e^{i\omega_2\eta}\,. \tag{9.28}$$

So, for $\bar{G} = G_0$, we have

$$\Sigma_{ij\sigma}^{\mathrm{SCD}}(\omega) = \left(\frac{U^3 A}{4} - \frac{U^4 A^2}{2}\right)\left(\frac{(-1)^{i-j}}{\big(\omega - (\epsilon_0 - t - \omega_p) - i\eta\big)^2} + \frac{1}{\big(\omega - (\epsilon_0 + t + \omega_p) + i\eta\big)^2}\right)$$

$$- \frac{U^4 A^2}{2} \times \frac{1}{(2t + \omega_p)^2}\left(\frac{(-1)^{i-j}}{\omega - (\epsilon_0 - t - \omega_p) - i\eta} + \frac{1}{\omega - (\epsilon_0 + t + \omega_p) + i\eta}\right)$$

$$+ \frac{U^4 A^2}{2} \times \frac{1}{(2t + \omega_p)^2} \times \left(\frac{(-1)^{i-j}}{\omega - (\epsilon_0 + t + 2\omega_p) + i\eta} + \frac{1}{\omega - (\epsilon_0 - t - 2\omega_p) - i\eta}\right)\,, \tag{9.29}$$

and for $\bar{G} = G_{\mathrm{H}}$, we have

$$\Sigma_{ij\sigma}^{\mathrm{SCD}}(\omega) = \left(-\frac{U^3 A}{4} - \frac{U^4 A^2}{2}\right)\left(\frac{(-1)^{i-j}}{\big(\omega - (\epsilon_0 - t + U - \omega_p) - i\eta\big)^2} + \frac{1}{\big(\omega - (\epsilon_0 + t + U + \omega_p) + i\eta\big)^2}\right)$$

$$- \frac{U^4 A^2}{2} \times \frac{1}{(2t + \omega_p)^2}\left(\frac{(-1)^{i-j}}{\omega - (\epsilon_0 - t + U - \omega_p) - i\eta} + \frac{1}{\omega - (\epsilon_0 + t + U + \omega_p) + i\eta}\right)$$

$$+ \frac{U^4 A^2}{2} \times \frac{1}{(2t + \omega_p)^2} \times \left(\frac{(-1)^{i-j}}{\omega - (\epsilon_0 + t + U + 2\omega_p) + i\eta} + \frac{1}{\omega - (\epsilon_0 - t + U - 2\omega_p) - i\eta}\right)\,. \tag{9.30}$$

Conclusions

In this thesis, three distinct approaches have been proposed to go beyond the GW approximation (GWA) for the xc self-energy (Σ_{xc}), with a primary focus on improving ground-state total energy calculations. At the same time, we were interested in optimizing spectral properties, for a large range of systems and the whole range of correlation strength. The aim was to investigate and develop methods that are both powerful and relatively cheap, so that their practical applications are feasible.

We have used the exactly solvable Hubbard dimer model, throughout the thesis, to test and benchmark all our results. At the heart of our developments lies the important concept of screened Coulomb interaction W. Screening is often approximated in practice. For example, in GW calculations usually the random phase approximation (RPA) is made, and only static ($\omega = 0$) screening is used in the Bethe-Salpeter equation. Numerous questions regarding the screening remain to be adressed: i) What is the most suitable approximation to be used in simplified expressions for the self-energy? ii) Can we extend the concept of a screened interaction to that of an effective interaction that encompasses additional physical meaning beyond the screening effect? This thesis aimed to address these questions, leading to findings that are not always straightforward, yet suggesting for new lines of research and promising potential for advancements of material science within the framework of the Green's functions formalism of many-body perturbation theory (MBPT).

In Chap. 7, we delved into the $G\tilde{W}$ approximation for Σ_{xc}, which uses ingredients from time-dependent density functional theory (TDDFT) to simulate vertex corrections, specifically the exchange-correlation kernel f_{xc}. It was demonstrated that with the resulting approximate Σ_{xc}, one can derive the exact xc energy contribution to the total energy, provided there is consistency in the combination of ingredients. While in practice the exact f_{xc} is not known and approximations are needed, maintaining consistency in the combination of ingredients permits us to devise powerful approximations for the total energy.

Despite the impressive performance of $G\tilde{W}$, where Σ_{xc} is linear in terms of $\tilde{W}$, while it can still produce the exact xc energy, the fact that $\Sigma_{\text{xc}} = iG\tilde{W}$ is an approximation has important consequences. In particular, the accuracy of the kinetic energy and of spectra falls short of that achieved for the xc energy. In Chap. 8, we take a step further by introducing an effective interaction $\bar{W}_{\text{eff}}$ that, when multiplied by the appropriate 1-GF $\bar{G}$, yields the exact Σ_{xc}. This establishes the existence of an exact Σ_{xc} that is linear in terms of $\bar{W}_{\text{eff}}$, i.e., $\Sigma_{\text{xc}} = i\bar{G}\bar{W}_{\text{eff}}$. We have developed an equation in Chap. 8 that, in principle, provides the exact $\bar{W}_{\text{eff}}$. After gaining insights into the characteristics of these exact $\bar{W}_{\text{eff}}$,

we proposed different approximate equations to determine $\bar{W}_{\text{eff}}$, the solutions of which are feasible in practice. In comparison with the exact and other approximate results, the different approximate $\bar{W}_{\text{eff}}$ demonstrated promising performance, rendering them highly motivating for real-world implementations.

In Chap. 9, with a focus on the test-charge test-charge (TCTC) screened Coulomb interaction calculated at various levels of approximation, we conducted a second-order expansion of Σ_{xc} in the framework of MBPT. We addressed several questions: firstly, what is the optimal choice for $\bar{W}$? This question arises because MBPT can, in principle, be expressed in terms of different flavors of the TCTC interaction $\bar{W}$, especially the exact and the RPA ones. Secondly, how does the second-order correction to Σ_{xc} influence properties such as the ground-state total energy and spectral functions compared to the first-order GW approximation? We have shown that the RPA screened interaction is an advantageous choice for MBPT expansion. We also found that and explained why, ground-state total energy calculations show improvement at the second-order compared to the first-order in the moderate to weak range of correlation. The quasiparticle components of the spectral function are also improved at the second-order, while the description of satellites is relatively less accurate.

This thesis lays the groundwork for several potential avenues of research and practical applications in real systems. The results obtained offer a simpler and alternative approach to complex calculations while providing understanding of interacting electronic systems from new perspectives. In particular, it seems promising to continue research to benchmark and extend approximations for the effective interaction W_{eff}. On one side, the exact equations that we have derived will allow us to introduce a systematic hierarchy of approximations. These approximations should be tested on exactly solvable models such as the Hubbard dimer. On the other side, implementation in an ab initio code seems to be within reach.

At the same time, our results obtained for $G\tilde{W}$ and for the second-order expansion suggest choices for total energy and spectra calculations that require to be validated systematically on real systems.

A major open question concerns self-consistency. In this thesis we were heading for relatively cheap approaches that avoid the need for self-consistency, such as the $G\tilde{W}$ approximation. Nevertheless, a combination with self-consistency might be needed, in particular for a good description of the density and density matrix. Future research is planned to make progress for at least some of these challenges.

List of publications

- Article concerning Chap. 7 is published in Journal of Chemical Theory and Computation (JCTC) (see Ref. [146]). It is also availabe on arXiv in Ref. [145].

Total Energy beyond GW: Exact Results and Guidelines for Approximations

Abdallah El-Sahili,* Francesco Sottile, and Lucia Reining

- Article concerning Chap. 8 is in preparation.

Exact self-energy via an effective interaction

Abdallah El-Sahili,*,†,‡ Francesco Sottile,†,‡ and Lucia Reining†,‡

†LSI, CNRS, CEA/DRF/IRAMIS, École Polytechnique, Institut Polytechnique de Paris, F-91120 Palaiseau, France

‡European Theoretical Spectroscopy Facility (ETSF)

E-mail: abdallah.el-sahili@polytechnique.edu

- Article concerning Chap. 9 is in preparation.

GW and beyond: second-order expansion in terms of screened Coulomb interactions

Abdallah El-Sahili,[*,†,‡] Francesco Sottile,[†,‡] and Lucia Reining[†,‡]

†LSI, CNRS, CEA/DRF/IRAMIS, École Polytechnique, Institut Polytechnique de Paris, F-91120 Palaiseau, France

‡European Theoretical Spectroscopy Facility (ETSF)

E-mail: abdallah.el-sahili@polytechnique.edu

Appendix A

Green's functions in Mathematics

In mathematics, Green's functions are defined as the solutions of linear differential equations with a delta function source, serving as the impulse response of an inhomogeneous linear differential operator defined on a domain with specified boundary conditions. For instance, consider the following simple equation,

$$L_x f(x) = u(x), \tag{A.1}$$

where L is a linear operator, $f(x)$ is the solution and $u(x)$ is a second term. Green's function is defined as

$$L_x G(x - y) = \delta(x - y), \tag{A.2}$$

where $G(x - y)$ is the Green's function and δ is the Dirac delta function. By integrating Eq.(A.2), we obtain

$$\int L_x G(x - y)u(y)\, dy = \int dy\, \delta(x - y)u(y) \tag{A.3}$$

$$L_x \int G(x - y)u(y)\, dy = u(x). \tag{A.4}$$

So, by comparing Eq.(A.4) with Eq.(A.1), the solution of Eq.(A.1) would be dependent on G as

$$f(x) = \int G(x - y)u(y)\, dy. \tag{A.5}$$

Many problems in physics can be formulated in terms of inhomogeneous differential equations as Eq.A.1. Let us now consider a physical problem involving Poisson's equation, which is expressed by the following equation,

$$\nabla_r^2 V(r) = -n(r), \tag{A.6}$$

where $V(r)$ is the electrostatic potential of the electrostatic charges and $n(r)$ is the charge density. By using G, we have

$$\nabla_r^2 G(r - r') = \delta(r - r'), \tag{A.7}$$

and by multiplying Eq.(A.7) by $\int dr' f(r')$, we obtain

$$\nabla_r^2 \int dr'\, G(r - r')f(r') = f(r), \tag{A.8}$$

138

where by considering $f(r) = -n(r)$, the solution of Eq.(A.6) is

$$V(r) = -\int dr'\, G(r - r')n(r')\,. \tag{A.9}$$

Thus, obtaining $V(r)$ relies on $G(r - r')$, which can be obtained by transforming Eq.(A.7) to Fourier space as

$$\int d^3r\, \nabla_r^2 G(r)e^{-i\vec{k}\cdot\vec{r}} = \int d^3r\, e^{-i\vec{k}\cdot\vec{r}}\delta(r) \tag{A.10}$$

$$-k^2\tilde{G} = 1\,, \tag{A.11}$$

where $\tilde{G}$ is the Green's function in Fourier space. So,

$$\tilde{G} = -\frac{1}{k^2}\,. \tag{A.12}$$

Then, to find G in real space, we will make the inverse Fourier transform as follows,

$$G(r) = -\int d^3k\, \frac{e^{i\vec{k}\cdot\vec{r}}}{(2\pi)^3 k^2} \tag{A.13}$$

$$= -\int_0^{2\pi} d\phi \int_0^\pi d\theta \int_0^\infty dk\, k^2 \sin\theta e^{ik\,r\cos\theta}\frac{1}{k^2} \tag{A.14}$$

$$= -\frac{1}{2\pi^2 r}\int_0^\infty dk\, r\frac{\sin k\, r}{k\, r} \tag{A.15}$$

$$= -\frac{1}{4\pi|r - r'|}\,. \tag{A.16}$$

Finally, the electrostatic potential is

$$V(r) = \int dr'\, G(r - r')f(r') = \int dr'\, \frac{n(r')}{|r - r'|}\,. \tag{A.17}$$

This demonstrates how useful Green's functions are in solving linear differential equations.

Appendix B

Basis transformations

In order to ensure clarity when making basis transformations, it is necessary to establish specific definitions.

B.1   From real space to discrete orbital basis

First and foremost, we define the single-particle "spin orbital" as follows,

$$\phi_{i\sigma}(x) = \varphi_{i\sigma}(r)\chi_\sigma(s), \tag{B.1}$$

where φ is the space orbital part and χ is the spin part, where i denotes the quantum number (for examle, in the case of atom $i = n, l, m_l$) and σ is the quantum number of the spin projection, $\sigma = \pm\frac{1}{2}$ for its z-component. The orbital part may depend on σ in spin-polarized systems (Magnetic systems where there is a net magnetization). Each part of the single-particle spin orbital form, an orthonormalized and complete set,

$$\int dx\, \phi_{i\sigma}^*(x)\phi_{j\sigma'}(x) = \int dr\varphi_{i\sigma}^*(r)\varphi_{j\sigma'}(r)\sum_s \chi_\sigma^*(s)\chi_{\sigma'}(s) = \delta_{ij}\delta_{\sigma\sigma'}. \tag{B.2}$$

Taking advantage of the orthonormal basis of single-particle spin orbitals, we can define the following transformations. For a one-body function,

$$f(x) = \sum_{i\sigma} \phi_{i\sigma}(x)f_{i\sigma}, \tag{B.3}$$

which is when multiplied by $\phi_{j\sigma'}^*(x)$ and integrated, it becomes

$$\int dx\, \phi_{j\sigma'}^*(x)f(x) = \sum_{i\sigma} \int dx\, \phi_{j\sigma'}^*(x)\phi_{i\sigma}(x)f_{i\sigma}, \tag{B.4}$$

thus, we obtain in the discrete basis,

$$f_{j\sigma'} = \int dx\, \phi_{j\sigma'}^*(x)f(x). \tag{B.5}$$

The basis transformation for a two body-function proceeds as follows,

$$f(x, x') = \sum_{ij\sigma\sigma'} \phi_{i\sigma}(x)f_{ij\sigma\sigma'}\phi_{j\sigma'}^*(x'), \tag{B.6}$$

where, by integrating Eq.(B.6) we obtain

$$\iint dx dx' \, \phi^*_{k\sigma_1}(x) f(x, x') \phi_{l\sigma_2}(x') = f_{kl\sigma_1\sigma_2} \,. \tag{B.7}$$

The four-point function would, therefore, be in the discrete space written as,

$$f(x_1, x_2, x_3, x_4) = \sum_{ijkl} \sum_{\sigma_1\sigma_2\sigma_3\sigma_4} \phi_{j\sigma_2}(x_2)\phi_{i\sigma_1}(x_1) f_{ijkl\sigma_1\sigma_2\sigma_3\sigma_4} \phi^*_{k\sigma_4}(x_3)\phi^*_{l\sigma_4}(x_4) \,. \tag{B.8}$$

For instance, by applying the transformation of Eq.(B.7) to the 1-GF, we obtain the 1-GF expression in the discrete basis as,

$$G(x, t, x', t') = -i \langle N_0| \hat{T} \big[\hat{\Psi}(x, t)\hat{\Psi}^\dagger(x', t') \big] |N_0\rangle \,, \tag{B.9}$$

$$= -i \langle N_0| \hat{T} \big[\sum_{i\sigma} \phi_{i\sigma}(x)\hat{c}_{i\sigma}(t) \sum_{j\sigma'} \phi^*_{j\sigma'}(x')\hat{c}^\dagger_{j\sigma'}(t') \big] |N_0\rangle \,, \tag{B.10}$$

$$= -i \langle N_0| \hat{T} \big[\sum_{i\sigma} \varphi_{i\sigma}(r)\chi_\sigma(s)\hat{c}_{i\sigma}(t) \sum_{j\sigma'} \varphi^*_{j\sigma'}(r')\chi^*_{\sigma'}(s')\hat{c}^\dagger_{j\sigma'}(t') \big] |N_0\rangle \,, \tag{B.11}$$

$$= \sum_{ij\sigma\sigma'} \phi_{i\sigma}(x) \bigg(-i \langle N_0| \hat{T} \big[\hat{c}_{i\sigma}(t)\hat{c}^\dagger_{j\sigma'}(t') \big] |N_0\rangle \bigg) \phi^*_{j\sigma'}(x') \,. \tag{B.12}$$

Thus, we obtain the 1-GF definition in the discrete basis,

$$G_{kl\sigma_1\sigma_2}(t, t') = -i \langle N_0| \hat{T} \big[\hat{c}_{k\sigma_1}(t)\hat{c}^\dagger_{l\sigma_2}(t') \big] |N_0\rangle \,. \tag{B.13}$$

B.2 Fourier transform

To move from real time space to the frequency one and vice versa, we use the Fourier and inverse Fourier transforms. For a given time-dependent function $f(t)$, we define the following Fourier transform,

$$f(\omega) = \int dt \, f(t) e^{i\omega t} \,, \tag{B.14}$$

and the inverse Fourier transform,

$$f(t) = \int \frac{d\omega}{2\pi} \, f(\omega) e^{-i\omega t} \,. \tag{B.15}$$

Appendix C

Ground-state total energy in terms of the Green's function

C.1 The Galitskii-Migdal formula

Many observables can be written explicitly in terms of the 1-GF such as the one-body density, one-body density-matrix, spectral function and total energy. We derive in the following the Galitskii-Migdal [94] formula that provides the total energy expression in terms of the 1-GF. Any one-body operator as can be written in terms of the field operators as,

$$\hat{O} = \int dx \, \hat{\Psi}^\dagger(x) O(x) \hat{\Psi}(x) \,, \tag{C.1}$$

whose expectation value is

$$\langle \hat{O} \rangle = \lim_{x' \to x} \int dx \, O(x) \, \langle \hat{\Psi}^\dagger(x) \hat{\Psi}(x) \rangle \,. \tag{C.2}$$

The time-ordered 1-GF is already defined in Eq.(4.9). By considering $x = x'$ and $t' = t^+$, we obtain

$$G(x, t; x, t^+) = i \, \langle N | \hat{\Psi}^\dagger(x) \hat{\Psi}(x) | N \rangle \,, \tag{C.3}$$

so,

$$\langle \hat{\Psi}^\dagger(x') \hat{\Psi}(x) \rangle = -i G(x, t; x', t^+) \,. \tag{C.4}$$

Therefore, the expectation value of a one-body operator can be written in terms of the 1-GF as,

$$\langle \hat{O} \rangle = -i \int dx \, O(x) \lim_{t' \to t^+, x' \to x} G(x, t; x', t') \,. \tag{C.5}$$

With this, we can write the one-body part of the the electronic hamiltonian, defined in Eq.(4.14), in terms of the 1-GF,

$$\langle \hat{H}_0 \rangle = -i \int dx \lim_{t' \to t^+, x' \to x} h(x) G(x, t, x', t') = -i \int dx \lim_{t' \to t^+, x' \to x} \left[\left(-\frac{\nabla_r^2}{2} + v_{\text{ext}}(x, x') \right) G(x, x'; t, t') \right] . \tag{C.6}$$

For the two-body part of the hamiltonian Eq.(4.14), which requires four field operators, we need the 2-GF that is defined in Eq.(4.31). Using the 2-GF, we can express the field operators of the two-body operator as,

$$\langle \hat{\Psi}^\dagger(x)\hat{\Psi}^\dagger(x')\hat{\Psi}(x')\hat{\Psi}(x)\rangle = -G_2(x,t,x',t^+;x,t^{+++},x',t^{++}). \tag{C.7}$$

Then, the Coulomb interaction expectation value becomes

$$\langle \hat{v}_{\mathrm{c}}\rangle = -\frac{1}{2}\int dx \int dx'\, v_{\mathrm{c}}(x,x')G_2(x,t,x',t^+;x,t^{+++},x',t^{++}). \tag{C.8}$$

To express $\langle \hat{v}_{\mathrm{c}}\rangle$ in terms of G instead of G_2, we use the equation of motion for the 1-GF, given in Eq.(4.32). Hence, we obtain

$$\langle \hat{v}_{\mathrm{c}}\rangle = \frac{1}{2}\int dx \lim_{t'\to t^+, x'\to x}\left[\frac{\partial}{\partial t} + ih(x)\right]G(x,t;x',t'). \tag{C.9}$$

So, finally the ground-state total energy in terms of the 1-GF, represented by the Galitskii-Migdal formula, is

$$E_0 = \frac{1}{2}\int dx \lim_{t'\to t^+, x'\to x}\left[\frac{\partial}{\partial t} - ih(x)\right]G(x,t;x',t'). \tag{C.10}$$

C.2 Total energy in terms of the Green's function and the self-energy

In order to explicitly make the self-energy appear in the ground-state total energy formula Eq.(C.10), one can use the equation of motion for the 1-GF, where the self-energy appears. So, by using Eq.(4.32) in Eq.(C.10), we obtain

$$E_0 = -i\lim_{t_2\to t_1^+}\int dx_1\left[-\frac{\nabla_{r_1}^2}{2} + v_{\mathrm{ext}}(x_1)\right]G(x_1,x_1;t_1 - t_2) - \frac{i}{2}\lim_{t_2\to t_1^+}\int dx_1\, v_{\mathrm{H}}(x_1)G(x_1,x_1;t_1 - t_2)$$
$$-\frac{i}{2}\lim_{t_2\to t_1^+}\int dx_1 dx_3 dt_3\, \Sigma_{\mathrm{xc}}(x_1,x_3;t_1 - t_3)G(x_3,x_1;t_3 - t_2). \tag{C.11}$$

The two Eqs.(C.10) and (C.11) are important and have been used in this thesis.

C.3 The Galitskii-Migdal formulas for the Hubbard model

In the discrete Hubbard basis and frequency spaces, the two different expressions of the GM formula are

$$E_0 = -\frac{i}{4\pi}\sum_{i\sigma}\int_{-\infty}^{+\infty}d\omega\,\omega\,G_{ii\sigma}(\omega)e^{i\omega\eta} + \frac{it}{4\pi}\sum_{<i=1,j=1>,i\neq j,\sigma}\int_{-\infty}^{+\infty}d\omega\,G_{ij\sigma}(\omega)e^{i\omega\eta} - \frac{i\epsilon_0}{4\pi}\sum_{i\sigma}\int_{-\infty}^{+\infty}d\omega\,G_{ii\sigma}(\omega)e^{i\omega\eta},$$
$$\tag{C.12}$$

and

$$E_0 = it \sum_{<i,j>=1,2,\sigma} \int \frac{d\omega}{2\pi} G_{ij\sigma}(\omega) e^{i\eta\omega} - i \sum_{i=1,2,\sigma} v_{\text{ext},ii\sigma} \int \frac{d\omega}{2\pi} G_{ii\sigma}(\omega) e^{i\eta\omega} - i \sum_{i=1,2,\sigma} \frac{v_{\text{H},ii\sigma}}{2} \int \frac{d\omega}{2\pi} G_{ii\sigma}(\omega) e^{i\eta\omega}$$

$$- \frac{i}{2} \sum_{ij=1,2,\sigma} \int \frac{d\omega}{2\pi} \Sigma_{\text{xc},ji\sigma}(\omega) G_{ij\sigma}(\omega) e^{i\omega\eta} . \quad \text{(C.13)}$$

144

Appendix D

The retarded Green's function

Let us recall the time-ordered Green's function definition,

$$G(x_1, t_1; x_2, t_2) = -i \langle N_0 | \hat{T} [\hat{\psi}(x_1, t_1) \hat{\psi}^\dagger(x_2, t_2)] | N_0 \rangle \tag{D.1}$$
$$= -i \langle N_0 | \hat{\psi}(x_1, t_1) \hat{\psi}^\dagger(x_2, t_2) | N_0 \rangle \, \theta(t_1 - t_2) + i \langle N_0 | \hat{\psi}^\dagger(x_2, t_2) \hat{\psi}(x_1, t_1) | N_0 \rangle \, \theta(t_2 - t_1) \,. \tag{D.2}$$

First, we introduce the greater and lesser 1-GFs,

$$G^>(x_1, t_1; x_2, t_2) = -i \langle N_0 | \hat{\psi}(x_1, t_1) \hat{\psi}^\dagger(x_2, t_2) | N_0 \rangle \,, \tag{D.3}$$

and

$$G^<(x_1, t_1; x_2, t_2) = +i \langle N_0 | \hat{\psi}^\dagger(x_2, t_2) \hat{\psi}(x_1, t_1) | N_0 \rangle \,. \tag{D.4}$$

We also define

$$\tilde{G}(x_1, t_1; x_2, t_2) = G^>(x_1, t_1; x_2, t_2) - G^<(x_1, t_1; x_2, t_2) \tag{D.5}$$
$$= -i \langle N_0 | [\hat{\psi}(x_1, t_1), \hat{\psi}^\dagger(x_2, t_2)] | N_0 \rangle \,. \tag{D.6}$$

Finally, we introduce the retarded and advanced 1-GFs,

$$G^R(x_1, t_1; x_2, t_2) = -i \langle N_0 | [\hat{\psi}(x_1, t_1), \hat{\psi}^\dagger(x_2, t_2)] | N_0 \rangle \, \theta(t_1 - t_2) \,, \tag{D.7}$$

$$G^A(x_1, t_1; x_2, t_2) = +i \langle N_0 | [\hat{\psi}(x_1, t_1), \hat{\psi}^\dagger(x_2, t_2)] | N_0 \rangle \, \theta(t_2 - t_1) \,. \tag{D.8}$$

D.1 Retarded GW self-energy

The retarded Σ_{xc} is defined as follows [159, 160],

$$\Sigma_{\mathrm{xc}}^R(x_1, t_1; x_2, t_2) = i \left[G^<(x_1, t_1; x_2, t_2) W^A(x_2, t_2; x_1, t_1) + G^R(x_1, t_1; x_2, t_2) W^<(x_2, t_2; x_1, t_1^+) \right], \tag{D.9}$$

where W^A and $W^<$ are the advanced and less TCTC screened Coulomb interactions. In frequency space, we have

$$\Sigma_{\text{xc}}^R(x_1, x_2; \omega) = i\left[\int \frac{d\omega_1}{2\pi} G^<(x_1, x_2; \omega_1 + \omega) W^A(x_2, x_1; \omega_1) e^{i\omega_1 \eta} \right.$$
$$\left. + \int \frac{d\omega_1}{2\pi} G^R(x_1, x_2; \omega_1 + \omega) W^<(x_2, x_1; \omega_1) e^{i\omega_1 \eta} \right]. \quad \text{(D.10)}$$

$G^<$, $G^>$, G^R and G^A are written in frequency space, respectively as

$$G^<(x_1, x_2; \omega) = \int dt\, G(x_1, x_2; t_1 - t_2) e^{i\omega t} \quad \text{(D.11)}$$

$$= i \sum_s \langle N_0 | \hat{\psi}^\dagger(x_2) | N-1 \rangle_s \langle N-1 |_s \hat{\psi}(x_1) | N_0 \rangle \int dt\, e^{it(\text{E}_s^{N-1} - \text{E}_0^N)} e^{i\omega t} \quad \text{(D.12)}$$

$$= 2\pi i \sum_s \langle N_0 | \hat{\psi}^\dagger(x_2) | N-1 \rangle_s \langle N-1 |_s \hat{\psi}(x_1) | N_0 \rangle\, \delta\left(\omega - (\text{E}_0^N - \text{E}_s^{N-1})\right), \quad \text{(D.13)}$$

$$G^>(x_1, x_2; \omega) = -2\pi i \sum_s \langle N_0 | \hat{\psi}(x_1) | N+1 \rangle_s \langle N+1 |_s \hat{\psi}^\dagger(x_2) | N_0 \rangle\, \delta\left(\omega - (\text{E}_s^{N+1} - \text{E}_0^N)\right), \quad \text{(D.14)}$$

$$G^R(x_1, x_2; \omega) = \sum_s \left[\frac{\langle N_0 | \hat{\psi}^\dagger(x_2) | N-1 \rangle_s \langle N-1 |_s \hat{\psi}(x_1) | N_0 \rangle}{\omega - (\text{E}_0^N - \text{E}_s^{N-1}) + i\eta} + \frac{\langle N_0 | \hat{\psi}(x_1) | N+1 \rangle_s \langle N+1 |_s \hat{\psi}^\dagger(x_2) | N_0 |\rangle}{\omega - (\text{E}_s^{N+1} - \text{E}_0^N) + i\eta} \right]$$
$$\text{(D.15)}$$

and

$$G^R(x_1, x_2; \omega) = \sum_s \left[\frac{\langle N_0 | \hat{\psi}^\dagger(x_2) | N-1 \rangle_s \langle N-1 |_s \hat{\psi}(x_1) | N_0 \rangle}{\omega - (\text{E}_0^N - \text{E}_s^{N-1}) - i\eta} + \frac{\langle N_0 | \hat{\psi}(x_1) | N+1 \rangle_s \langle N+1 |_s \hat{\psi}^\dagger(x_2) | N_0 |\rangle}{\omega - (\text{E}_s^{N+1} - \text{E}_0^N) - i\eta} \right].$$
$$\text{(D.16)}$$

Then, in order to calculate Σ_{xc} from Eq.(D.10), we need to find W^R and $W^>$ in frequency space. This relies on the polarizability, which has the following components,

$$P_0^>(x_1, t_1; x_2, t_2) = -iG^>(x_1, t_1; x_2, t_2) G^<(x_2, t_2; x_1, t_1^+), \quad \text{(D.17)}$$

$$P_0^<(x_1, t_1; x_2, t_2) = -iG^<(x_1, t_1; x_2, t_2) G^>(x_2, t_2; x_1, t_1^+), \quad \text{(D.18)}$$

$$P_0^R(x_1, t_1; x_2, t_2) = -iG^<(x_1, t_1; x_2, t_2) G^A(x_2, t_2; x_1, t_1^+) - iG^R(x_1, t_1; x_2, t_2) G^<(x_2, t_2; x_1, t_1^+), \quad \text{(D.19)}$$

and

$$P_0^A(x_1, t_1; x_2, t_2) = -iG^<(x_1, t_1; x_2, t_2) G^R(x_2, t_2; x_1, t_1^+) - iG^A(x_1, t_1; x_2, t_2) G^<(x_2, t_2; x_1, t_1^+). \quad \text{(D.20)}$$

146

In frequency space, these components become

$$P_0^>(x_1, x_2; \omega) = -i \int \frac{d\omega_1}{2\pi} G^>(x_1, x_2; \omega + \omega_1) G^<(x_2, x_1; \omega_1) e^{i\omega_1 \eta}, \tag{D.21}$$

$$P_0^<(x_1, x_2; \omega) = -i \int \frac{d\omega_1}{2\pi} G^<(x_1, x_2; \omega + \omega_1) G^>(x_2, x_1; \omega_1) e^{i\omega_1 \eta}, \tag{D.22}$$

$$P_0^R(x_1, x_2; \omega) = -i \int \frac{d\omega_1}{2\pi} G^<(x_1, x_2; \omega + \omega_1) G^A(x_2, x_1; \omega_1) e^{i\omega_1 \eta}$$
$$- i \int \frac{d\omega_1}{2\pi} G^R(x_1, x_2; \omega + \omega_1) G^<(x_2, x_1; \omega_1) e^{i\omega_1 \eta}, \tag{D.23}$$

and

$$P_0^A(x_1, x_2; \omega) = -i \int \frac{d\omega_1}{2\pi} G^<(x_1, x_2; \omega + \omega_1) G^R(x_2, x_1; \omega_1) e^{i\omega_1 \eta}$$
$$- i \int \frac{d\omega_1}{2\pi} G^A(x_1, x_2; \omega + \omega_1) G^<(x_2, x_1; \omega_1) e^{i\omega_1 \eta}. \tag{D.24}$$

D.2 The Hubbard dimer model

Using Eq.(D.10), we aim to calculate the retarded GW Σ_{xc} for the Hubbard dimer, e.g at half-filling. To do so, we provide the neccessary ingredients in the ij basis of the Hubbard model.

$$P_{0ij\sigma}^>(\omega) = -i \int \frac{d\omega_1}{2\pi} G_{0ij\sigma}^>(\omega_1 + \omega) G_{0ji\sigma}^<(\omega_1) e^{i\omega_1 \eta}, \tag{D.25}$$

with

$$G_{0ij\sigma}^<(\omega_1) = 2\pi i \times \frac{1}{2} \times \delta(\omega_1 - (\epsilon_0 - t)), \tag{D.26}$$

and

$$G_{0ij\sigma}^>(\omega_1 + \omega) = -2\pi i \times \frac{(-1)^{i-j}}{2} \times \delta(\omega_1 + \omega - (\epsilon_0 + t)). \tag{D.27}$$

So,

$$P_{0ij\sigma}^>(\omega) = -i(2\pi)^2 \frac{(-1)^{i-j}}{4} \int \frac{d\omega}{2\pi} \delta(\omega_1 + \omega - (\epsilon_0 + t)) \delta(\omega_1 - (\epsilon_0 - t)) e^{i\omega_1 \eta} \tag{D.28}$$

$$= -2\pi i \frac{(-1)^{i-j}}{4} \delta(\omega - 2t). \tag{D.29}$$

The lesser component is obtained as

$$P_{0ij\sigma}^<(\omega) = -i \int \frac{d\omega_1}{2\pi} G_{0ij\sigma}^<(\omega_1 + \omega) G_{0ji\sigma}^>(\omega_1) e^{i\omega_1 \eta} \tag{D.30}$$

$$= -2\pi i \frac{(-1)^{i-j}}{4} \int \frac{d\omega}{2\pi} \delta(\omega_1 + \omega - (\epsilon_0 - t)) \delta(\omega_1 - (\epsilon_0 + t)) e^{i\omega_1 \eta} \tag{D.31}$$

$$= -2\pi i \frac{(-1)^{i-j}}{4} \delta(\omega + 2t). \tag{D.32}$$

Then, the advanced component of P in the ij basis is

$$P_{0ij\sigma}^A(\omega) = -i \int \frac{d\omega_1}{2\pi} G_{0ij\sigma}^<(\omega+\omega_1) G_{0ji\sigma}^R(\omega_1) e^{i\omega_1\eta} - i \int \frac{d\omega_1}{2\pi} G_{0ij\sigma}^A(\omega+\omega_1) G_{0ji\sigma}^<(\omega_1) e^{i\omega_1\eta}, \quad \text{(D.33)}$$

where

$$G_{0ij\sigma}^R(\omega_1) = \frac{1}{2}\left(\frac{1}{\omega-(\epsilon_0-t)+i\eta} + \frac{(-1)^{i-j}}{\omega-(\epsilon_0+t)+i\eta}\right), \quad \text{(D.34)}$$

$$G_{0ij\sigma}^A(\omega_1) = \frac{1}{2}\left(\frac{1}{\omega-(\epsilon_0-t)-i\eta} + \frac{(-1)^{i-j}}{\omega-(\epsilon_0+t)-i\eta}\right). \quad \text{(D.35)}$$

Thus, we obtain

$$P_{0ij\sigma}^A(\omega) = \frac{(-1)^{i-j}}{4} \times \left(\frac{1}{\omega-2t-i\eta} - \frac{1}{\omega+2t-i\eta}\right), \quad \text{(D.36)}$$

$$P_{0ij\sigma}^R(\omega) = \frac{(-1)^{i-j}}{4} \times \left(\frac{1}{\omega-2t+i\eta} - \frac{1}{\omega+2t+i\eta}\right). \quad \text{(D.37)}$$

The random phase approximation (RPA) screened interaction components can be then obtained using the Dyson equation

$$W_{0ij}^{R/A}(\omega) = U\delta_{ij} + U \sum_{k=1,2\sigma=\uparrow,\downarrow} P_{0ik\sigma}^{R/A}(\omega) W_{0kj}^{R/A}(\omega). \quad \text{(D.38)}$$

So, we obtain

$$W_{ij}^R(\omega) = U\delta_{ij} + (-1)^{i-j}\frac{U^2 t}{h'} \times \left(\frac{1}{\omega-h'+i\eta} - \frac{1}{\omega+h'+i\eta}\right), \quad \text{(D.39)}$$

and

$$W_{ij}^A(\omega) = U\delta_{ij} + (-1)^{i-j}\frac{U^2 t}{h'} \times \left(\frac{1}{\omega-h'-i\eta} - \frac{1}{\omega+h'-i\eta}\right). \quad \text{(D.40)}$$

$W^<$ and $W^>$ are defined, respectively, as follows,

$$W^<(\omega) = if_{BE}(\omega-\mu)Im(W^R(\omega)), \quad \text{(D.41)}$$

and

$$W^>(\omega) = i\big(f_{BE}(\omega-\mu) - 1\big)Im(W^A(\omega)), \quad \text{(D.42)}$$

where $f_{BE}(\omega-\mu)$ is the Bose-Einstein distribution. So, we have

$$W_{ij}^<(\omega) = -i(-1)^{i-j}\frac{U^2 t}{h'}\delta(\omega+h'), \quad \text{(D.43)}$$

and

$$W_{ij}^>(\omega) = i(-1)^{i-j}\frac{U^2 t}{h'}\delta(\omega-h'). \quad \text{(D.44)}$$

Finally, using the previous ingredients, we calculate the retarded Σ_{xc}

$$\Sigma_{\text{xc}ij\sigma}^R(\omega) = i \int \frac{d\omega}{2\pi} G_{ij\sigma}^<(\omega_1+\omega) W_{ji}^A(\omega) + i \int \frac{d\omega}{2\pi} G_{ij\sigma}^R(\omega_1+\omega) W_{ji}^<(\omega). \quad \text{(D.45)}$$

The first integration in Eq.(D.45) yields

$$-\frac{U}{2}\delta_{ij} + \frac{(-1)^{i-j}U^2 t}{2h'}\left(\frac{1}{\omega - (\epsilon_0 - t - h') + i\eta} - \frac{1}{\omega - (\epsilon_0 - t + h') + i\eta}\right), \qquad \text{(D.46)}$$

and the second one yields

$$\frac{U^2 t}{2h'}\left(\frac{(-1)^{i-j}}{\omega - (\epsilon_0 - t + h') + i\eta} + \frac{1}{\omega - (\epsilon_0 + t + h') + i\eta}\right). \qquad \text{(D.47)}$$

So, we obtain

$$\Sigma^R_{\text{xc},ij\sigma}(\omega) = -\frac{U}{2}\delta_{ij} + \frac{U^2 t}{2h'}\left(\frac{1}{\omega - (\epsilon_0 + t + h') + i\eta} + \frac{(-1)^{i-j}}{\omega - (\epsilon_0 - t - h') + i\eta}\right), \qquad \text{(D.48)}$$

which only differs from the retarded quantity by a sign in the broadening of the removal part.

Appendix E

Functionals in terms of the Green's function with time non-local potentials

In the following, based on Ref. [101], we show more general derivation of Green's functions functionals using a time non-local external potential, and therefore, a generalized 4-times Coulomb interaction. We start with the self-energy definition in terms of four-point Coulomb interaction,

$$\Sigma(1,5) = -\frac{i}{2} \int d(1'234) V(1,2,3,4) G_2(4,3,1',2) G^{-1}(1',5), \tag{E.1}$$

where

$$V(1,2,3,4) = v_c(1,2^+) \Big(\delta(2,3^+)\delta(1,4^{+++}) - \delta(1,3^{++})\delta(2,4^{++}) \Big). \tag{E.2}$$

For the definition of G_2, we keep using our notations, which is slightly different from the one used in Ref. [101]. So, G_2 is

$$G_2(4,3,1',2) = G(4,1')G(3,2) - L(4,3,1',2). \tag{E.3}$$

E.1 Hartree potential and exchange self-energy expressions

By approximating G_2 as follows,

$$G_2(4,3,1',2) \approx G(4,1')G(3,2) - L_0(4,3,1',2) \tag{E.4}$$

$$= G(4,1')G(3,2) - G(4,2)G(3,1'), \tag{E.5}$$

we can get the Hartree potential and the exchange self-energy expressions.

$$\Sigma_{\mathrm{Hx}}(1,5) = -\frac{i}{2} \int d(1'234) V(1,2,3,4) \Big(G(4,1')G(3,2) - G(4,2)G(3,1') \Big) G^{-1}(1',5) \tag{E.6}$$

$$= -\frac{i}{2} \int d(234) V(1,2,3,4) \Big(G(3,2)\delta(4,5) - G(4,2)\delta(3,5) \Big) \tag{E.7}$$

$$= -\frac{i}{2} \int d(23) V(1,2,3,5) G(3,2) + \frac{i}{2} \int d(23) V(1,2,5,3) G(3,2), \tag{E.8}$$

so, in terms of the 4-point Coulomb interaction, we have

$$\Sigma_{\text{Hx}}(1,4) = -\frac{i}{2}\int d(23)V(1,2,3,4)G(3,2) + \frac{i}{2}\int d(23)V(1,2,4,3)G(3,2)\,, \tag{E.9}$$

where by writing V in terms of v_{c}, we obtain v_{H} and Σ_{x} written separately and respectively as

$$v_{\text{H}}(1,4) = -\frac{i}{2}\int d2v_{\text{c}}(1,2^+)\Big(\delta(1,4^{+++})G(2^-,2) + \delta(1,4^{++})G(2^{--},2)\Big)\,, \tag{E.10}$$

and

$$\Sigma_{\text{x}}(1,4) = \frac{i}{2}\int d2\,v_{\text{c}}(1,2^+)\Big(\delta(1,4^{++})G(1^{--},2) + \delta(2,4^+)G(1^{---},2)\Big)\,, \tag{E.11}$$

where v_{H}, besides the fact that it is non-local as we already discussed in the main text, it is also taken as a mean value of two terms, which is also the case for Σ_{x}.

E.2 The Bethe-Salpeter Equation for the polarizability

We go beyond the Hartree-Fock approximation, by writing the Bethe-Salpeter equation for L at the random phase approximation (RPA),

$$L(1,2,3,4) = -\int d(56)\,G(1,5)\frac{\delta G^{-1}(5,6)}{\delta v_{\text{ext}}(4,2)}G(6,3)\,, \tag{E.12}$$

where $G^{-1}(5,6) = G_0^{-1}(5,6) - v_{\text{ext}}(5,6) - v_{\text{H}}(5,6) - \Sigma_{\text{xc}}(5,6)$. So

$$L^{\text{RPA}}(1,2,3,4) = L_0(1,2,3,4) + \int d(56)\,G(1,5)\frac{\delta v_{\text{H}}(5,6)}{\delta v_{\text{ext}}(4,2)}G(6,3) \tag{E.13}$$

$$= L_0(1,2,3,4) - \frac{i}{2}\int d(567)\,G(1,5)v_{\text{c}}(5,7^+)\frac{\delta}{\delta v_{\text{ext}}(4,2)}\Big(\delta(5,6^{+++})G(7^-,7) \tag{E.14}$$

$$+ \delta(5,6^{++})G(7^{--},7)\Big)G(6,3)$$

$$= L_0(1,2,3,4) - \frac{i}{2}\int d(57)\,L_0(1,5^{---},3,5)v_{\text{c}}(5,7^+)L^{\text{RPA}}(7^-,2,7,4) \tag{E.15}$$

$$- \frac{i}{2}\int d(57)\,L_0(1,5^{--},3,5)v_{\text{c}}(5,7^+)L^{\text{RPA}}(7^{--},2,7,4)\,.$$

From L, we can get the two-point polarizability χ,

$$\chi^{\text{RPA}}(1,2) = -iL(1,2,1^+,2^+) = \chi_0(1,2) + \frac{1}{2}\int d(57)\,v_{\text{c}}(5,7^+)\Big(\chi_0(1,5^{--})\chi(7,2) \tag{E.16}$$

$$+ \chi_0(1,5^-)v_{\text{c}}(5,7^+)\chi^{\text{RPA}}(7^-,2)\Big)\,, \tag{E.16}$$

which in frequency space can be written as

$$\chi^{\text{RPA}}(x_1,x_2;\omega) = \chi_0(x_1,x_2;\omega) + \int dx_5 dx_7\,\chi_0(x_1,x_5;\omega)v_{\text{c}}(x_5,x_7)\chi^{\text{RPA}}(x_7,x_2;\omega)\Big(e^{i\omega\eta} + e^{-i\omega\eta}\Big) \tag{E.17}$$

$$= \chi_0(x_1,x_2;\omega) + \int dx_5 dx_7\,\chi_0(x_1,x_5;\omega)v_{\text{c}}(x_5,x_7)\chi^{\text{RPA}}(x_7,x_2;\omega)\,. \tag{E.18}$$

E.3   *GW* self-energy

Using the L^{RPA} in the self-energy E.1, a part of v_{H} and Σ_{x}, we obtain the GW correlation contribution

$$\Sigma_{\text{c}}^{GW}(1,5) = -\frac{1}{4}\int d(1'234)\, V(1,2,3,4)\left(\int d(57)G(4,5)G(5^{---},1')v_{\text{c}}(5,7^+)L^{\text{RPA}}(7^-,3,7,2)\right.$$

$$\left. +\int d(57)\, G(4,5)G(5^{--},1')v_{\text{c}}(5,7^+)L^{\text{RPA}}(7^{--},3,7,2)\right)G^{-1}(1',5)$$

(E.19)

$$= -\frac{1}{4}\int d(2347)\, V(1,2,3,4)\Big(G(4,5^{---})v_{\text{c}}(5^{---},7^+)L^{\text{RPA}}(7^-,3,7,2)$$

(E.20)

$$+ G(4,5^{--})v_{\text{c}}(5^{--},7^+)L^{\text{RPA}}(7^{--},3,7,2)\Big)$$

$$= -\frac{1}{4}\int d(2347)\, v_{\text{c}}(1,2^+)\Big(\delta(2,3^+)\delta(1,4^{+++}) - \delta(1,3^{++})\delta(2,4^{++})\Big)$$

$$\Big(G(4,5^{---})v_{\text{c}}(5^{---},7^+)L^{\text{RPA}}(7^-,3,7,2) + G(4,5^{--})v_{\text{c}}(5^{--},7^+)L^{\text{RPA}}(7^{--},3,7,2)\Big)$$

(E.21)

$$= -\frac{1}{4}\int d(2347)\, v_{\text{c}}(1,2^+)\delta(2,3^+)\delta(1,4^{+++})G(4,5^{---})v_{\text{c}}(5^{---},7^+)L^{\text{RPA}}(7^-,3,7,2)$$

$$+ \frac{1}{4}\int d(2347)\, v_{\text{c}}(1,2^+)\delta(1,3^{++})\delta(2,4^{++})G(4,5^{---})v_{\text{c}}(5^{---},7^+)L^{\text{RPA}}(7^-,3,7,2)$$

$$- \frac{1}{4}\int d(2347)\, v_{\text{c}}(1,2^+)\delta(2,3^+)\delta(1,4^{+++})G(4,5^{--})v_{\text{c}}(5^{--},7^+)L^{\text{RPA}}(7^{--},3,7,2)$$

$$+ \frac{1}{4}\int d(2347)\, v_{\text{c}}(1,2^+)\delta(1,3^{++})\delta(2,4^{++})G(4,5^{--})v_{\text{c}}(5^{--},7^+)L^{\text{RPA}}(7^{--},3,7,2)$$

(E.22)

$$= -\frac{1}{4}\int d(27)\, v_{\text{c}}(1,2^+)G(1^{---},5^{---})v_{\text{c}}(5^{---},7^+)L^{\text{RPA}}(7^-,2^-,7,2)$$

(E.23)

$$+ \frac{1}{4}\int d(27)\, v_{\text{c}}(1,2^+)G(2^{--},5^{---})v_{\text{c}}(5^{---},7^+)L^{\text{RPA}}(7^-,1^{--},7,2)$$

$$- \frac{1}{4}\int d(27)\, v_{\text{c}}(1,2^+)G(1^{---},5^{--})v_{\text{c}}(5^{--},7^+)L^{\text{RPA}}(7^{--},2^-,7,2)$$

$$+ \frac{1}{4}\int d(27)\, G(2^{--},5^{--})v_{\text{c}}(5^{--},7^+)L^{\text{RPA}}(7^{--},1^-,7,2)\,.$$

(E.24)

Résumé

Dans cette thèse, trois approches distinctes ont été proposées pour aller au-delà de l'approximation GW (GWA) pour l'auto-énergie xc (Σ_{xc}), en mettant principalement l'accent sur l'amélioration des calculs d'énergie totale à l'état fondamental. En même temps, nous nous sommes intéressés à l'optimisation des propriétés spectrales, pour une large gamme de systèmes et sur l'ensemble de la plage de force de corrélation. L'objectif était d'investiguer et de développer des méthodes à la fois puissantes et relativement peu coûteuses, de sorte que leurs applications pratiques soient réalisables.

Nous avons utilisé le modèle de dimère de Hubbard exactement soluble, tout au long de la thèse, pour tester et évaluer tous nos résultats. Au cœur de nos développements se trouve le concept important d'interaction de Coulomb écrantée W. L'écrantage est souvent approximé en pratique. Par exemple, dans les calculs GW, généralement l'approximation de phase aléatoire (RPA) est utilisée, et seul l'écrantage statique ($\omega = 0$) est utilisé dans l'équation de Bethe-Salpeter. De nombreuses questions concernant l'écrantage restent à adresser : i) Quelle est l'approximation la plus adaptée à utiliser dans des expressions simplifiées pour l'auto-énergie ? ii) Pouvons-nous étendre le concept d'interaction écrantée à celui d'interaction effective qui englobe un sens physique supplémentaire au-delà de l'effet d'écrantage ? Cette thèse visait à répondre à ces questions, conduisant à des conclusions qui ne sont pas toujours simples, mais suggérant de nouvelles pistes de recherche et un potentiel prometteur pour les avancées de la science des matériaux dans le cadre du formalisme des fonctions de Green de la théorie de la perturbation à plusieurs corps (MBPT).

Dans le chapitre 7, nous avons exploré l'approximation $G\tilde{W}$ pour Σ_{xc}, qui utilise des éléments de la théorie de la fonctionnelle de la densité dépendant du temps (TDDFT) pour simuler des corrections de sommet, en particulier le noyau d'échange-corrélation f_{xc}. Il a été démontré qu'avec l'approximation résultante de Σ_{xc}, on peut dériver la contribution exacte d'énergie xc à l'énergie totale, à condition qu'il y ait une cohérence dans la combinaison des éléments. Bien que, en pratique, le f_{xc} exact ne soit pas connu et que des approximations soient nécessaires, maintenir une cohérence dans la combinaison des éléments nous permet de concevoir des approximations puissantes pour l'énergie totale.

Malgré les performances impressionnantes de $G\tilde{W}$, où Σ_{xc} est linéaire en termes de $\tilde{W}$, tout en pouvant toujours produire l'énergie xc exacte, le fait que $\Sigma_{\mathrm{xc}} = iG\tilde{W}$ soit une approximation a des conséquences importantes. En particulier, la précision de l'énergie cinétique et des spectres est inférieure à celle atteinte pour l'énergie xc. Dans le chapitre 8, nous allons plus loin en introduisant une interaction efficace $\bar{W}_{\mathrm{eff}}$ qui, lorsqu'elle est multipliée par le 1-GF approprié $\bar{G}$, donne le Σ_{xc} exact. Cela établit l'existence d'un Σ_{xc} exact qui est linéaire en termes de $\bar{W}_{\mathrm{eff}}$, c'est-à-dire $\Sigma_{\mathrm{xc}} = iG\bar{W}_{\mathrm{eff}}$. Nous avons développé une équation dans le chapitre 8 qui, en principe, fournit le $\bar{W}_{\mathrm{eff}}$ exact. Après avoir obtenu des informations sur les caractéristiques de ces $\bar{W}_{\mathrm{eff}}$ exacts, nous avons proposé différentes équations approximatives pour déterminer $\bar{W}_{\mathrm{eff}}$, dont les solutions sont réalisables en pratique. En comparaison avec les résultats exacts et autres approximations, les différentes $\bar{W}_{\mathrm{eff}}$ approximatives ont démontré des performances prometteuses, les rendant très motivantes pour des implémentations réelles.

Dans le chapitre 9, en mettant l'accent sur l'interaction de Coulomb écrantée de test-charge à test-

charge (TCTC) calculée à différents niveaux d'approximation, nous avons réalisé une expansion du second ordre de Σ_{xc} dans le cadre de la MBPT. Nous avons abordé plusieurs questions : premièrement, quel est le choix optimal pour $\bar{W}$? Cette question se pose car la MBPT peut, en principe, être exprimée en termes de différentes variantes de l'interaction TCTC $\bar{W}$, en particulier les exactes et celles de la RPA. Deuxièmement, comment la correction du second ordre à Σ_{xc} influence-t-elle des propriétés telles que l'énergie totale à l'état fondamental et les fonctions spectrales par rapport à l'approximation GW du premier ordre ? Nous avons montré que l'interaction écrantée de la RPA est un choix avantageux pour l'expansion de la MBPT. Nous avons également constaté et expliqué pourquoi, les calculs d'énergie totale à l'état fondamental montrent une amélioration au second ordre par rapport au premier ordre dans la plage de corrélation modérée à faible. Les composantes quasiparticulaires de la fonction spectrale sont également améliorées au second ordre, tandis que la description des satellites est relativement moins précise.

Cette thèse pose les bases pour plusieurs avenues potentielles de recherche et d'applications pratiques dans des systèmes réels. Les résultats obtenus offrent une approche plus simple et alternative aux calculs complexes tout en fournissant une compréhension des systèmes électroniques en interaction sous de nouveaux angles. En particulier, il semble prometteur de poursuivre la recherche pour évaluer et étendre les approximations pour l'interaction efficace W_{eff}. D'un côté, les équations exactes que nous avons dérivées nous permettront d'introduire une hiérarchie systématique d'approximations. Ces approximations devraient être testées sur des modèles exactement solubles

Bibliography

[1] G. Bacciagaluppi and A. Valentini, "The proceedings of the 1927 solvay conference", in *Quantum theory at the crossroads: reconsidering the 1927 solvay conference* (Cambridge University Press, 2009), pp. 251–258 (cit. on p. 3).

[2] G. Bacciagaluppi and A. Valentini, *Quantum theory at the crossroads: reconsidering the 1927 solvay conference*, 2009 (cit. on p. 3).

[3] M. Born and R. Oppenheimer, "Zur quantentheorie der molekeln", Annalen der Physik **389**, 457–484 (1927) https://doi.org/10.1002/andp.19273892002 (cit. on p. 4).

[4] R. M. Martin, L. Reining, and D. M. Ceperley, *Interacting electrons: theory and computational approaches* (Cambridge University Press, 2016), 10.1017/CBO9781139050807 (cit. on pp. 4, 7, 25, 38, 44, 58, 71, 72).

[5] X. Gonze, J.-M. Beuken, R. Caracas, F. Detraux, M. Fuchs, G.-M. Rignanese, L. Sindic, M. Verstraete, G. Zerah, F. Jollet, M. Torrent, A. Roy, M. Mikami, P. Ghosez, J.-Y. Raty, and D. Allan, "First-principles computation of material properties: The ABINIT software project", Computational Materials Science **25**, 478–492 (2002) 10.1016/s0927-0256(02)00325-7 (cit. on p. 6).

[6] X. Gonze, B. Amadon, G. Antonius, F. Arnardi, L. Baguet, J.-M. Beuken, J. Bieder, F. Bottin, J. Bouchet, E. Bousquet, N. Brouwer, F. Bruneval, G. Brunin, T. Cavignac, J.-B. Charraud, W. Chen, M. Côté, S. Cottenier, J. Denier, G. Geneste, P. Ghosez, M. Giantomassi, Y. Gillet, O. Gingras, D. R. Hamann, G. Hautier, X. He, N. Helbig, N. Holzwarth, Y. Jia, F. Jollet, W. Lafargue-Dit-Hauret, K. Lejaeghere, M. A. L. Marques, A. Martin, C. Martins, H. P. C. Miranda, F. Naccarato, K. Persson, G. Petretto, V. Planes, Y. Pouillon, S. Prokhorenko, F. Ricci, G.-M. Rignanese, A. H. Romero, M. M. Schmitt, M. Torrent, M. J. van Setten, B. V. Troeye, M. J. Verstraete, G. Zérah, and J. W. Zwanziger, "The abinit project: impact, environment and recent developments", Comput. Phys. Commun. **248**, 107042 (2020) (cit. on p. 6).

[7] P. Hohenberg and W. Kohn, "Inhomogeneous electron gas", Phys. Rev. **136**, B864–B871 (1964) 10.1103/PhysRev.136.B864 (cit. on pp. 6, 14, 71).

[8] W. Kohn and L. J. Sham, "Self-consistent equations including exchange and correlation effects", Phys. Rev. **140**, A1133–A1138 (1965) 10.1103/PhysRev.140.A1133 (cit. on pp. 6, 18, 19, 71).

[9] A. Szabo and N. S. Ostlund, *Modern quantum chemistry: introduction to advanced electronic structure theory*, First (Dover Publications, Inc., Mineola, 1996) (cit. on p. 6).

[10] N. Metropolis and S. Ulam, "The monte carlo method", Journal of the American Statistical Association **44**, PMID: 18139350, 335–341 (1949) 10.1080/01621459.1949.10483310 (cit. on p. 6).

[11] R. G. Parr, "Density functional theory of atoms and molecules", in Horizons of quantum chemistry, edited by K. Fukui and B. Pullman (1980), pp. 5–15 (cit. on p. 6).

[12] R. M. Martin, *Electronic structure: basic theory and practical methods* (Cambridge University Press, 2004), 10.1017/CBO9780511805769 (cit. on p. 6).

[13] R. Dreizler and E. Gross, *Density functional theory: an approach to the quantum many-body problem* (Springer Berlin Heidelberg, 2012) (cit. on p. 6).

[14] D. M. Ceperley and B. J. Alder, "Ground state of the electron gas by a stochastic method", Phys. Rev. Lett. **45**, 566–569 (1980) 10.1103/PhysRevLett.45.566 (cit. on pp. 6, 20).

[15] F. Furche and T. Van Voorhis, "Fluctuation-dissipation theorem density-functional theory", The Journal of Chemical Physics **122**, 164106 (2005) 10.1063/1.1884112 (cit. on p. 6).

[16] M. Fuchs and X. Gonze, "Accurate density functionals: approaches using the adiabatic-connection fluctuation-dissipation theorem", Phys. Rev. B **65**, 235109 (2002) 10.1103/PhysRevB.65.235109 (cit. on p. 6).

[17] J. F. Dobson, A. White, and A. Rubio, "Asymptotics of the dispersion interaction: analytic benchmarks for van der waals energy functionals", Phys. Rev. Lett. **96**, 073201 (2006) 10.1103/PhysRevLett.96.073201 (cit. on p. 6).

[18] F. Bruneval, "Range-separated approach to the rpa correlation applied to the van der waals bond and to diffusion of defects", Phys. Rev. Lett. **108**, 256403 (2012) 10.1103/PhysRevLett.108.256403 (cit. on p. 6).

[19] X. Ren, P. Rinke, and M. Scheffler, "Exploring the random phase approximation: application to co adsorbed on cu(111)", Phys. Rev. B **80**, 045402 (2009) 10.1103/PhysRevB.80.045402 (cit. on p. 6).

[20] S. Lebègue, J. Harl, T. Gould, J. G. Ángyán, G. Kresse, and J. F. Dobson, "Cohesive properties and asymptotics of the dispersion interaction in graphite by the random phase approximation", Phys. Rev. Lett. **105**, 196401 (2010) 10.1103/PhysRevLett.105.196401 (cit. on p. 6).

[21] S. Ismail-Beigi, "Correlation energy functional within the GW-rpa: exact forms, approximate forms, and challenges", Phys. Rev. B **81**, 195126 (2010) 10.1103/PhysRevB.81.195126 (cit. on p. 6).

[22] L. Schimka, J. Harl, A. Stroppa, A. Grüneis, M. Marsman, F. Mittendorfer, and G. Kresse, "Accurate surface and adsorption energies from many-body perturbation theory", Nature Materials **9**, 741–744 (2010) 10.1038/nmat2806 (cit. on p. 6).

[23] J. Harl and G. Kresse, "Cohesive energy curves for noble gas solids calculated by adiabatic connection fluctuation-dissipation theory", Phys. Rev. B **77**, 045136 (2008) 10.1103/PhysRevB.77.045136 (cit. on p. 6).

[24] L. Hedin, "New method for calculating the one-particle green's function with application to the electron-gas problem", Phys. Rev. **139**, A796–A823 (1965) 10.1103/PhysRev.139.A796 (cit. on pp. 7, 40, 42–44, 72).

[25] R. Godby, M. Schlüter, and L. Sham, Phys. Rev. B **35**, 4170 (1987) (cit. on pp. 7, 44).

[26] M. S. Hybertsen and S. G. Louie, "First-principles theory of quasiparticles: calculation of band gaps in semiconductors and insulators", Phys. Rev. Lett. **55**, 1418–1421 (1985) 10.1103/PhysRevLett.55.1418 (cit. on pp. 7, 44, 58, 72).

[27] R. W. Godby, M. Schlüter, and L. J. Sham, "Trends in self-energy operators and their corresponding exchange-correlation potentials", Phys. Rev. B **36**, 6497–6500 (1987) 10.1103/PhysRevB.36.6497 (cit. on pp. 7, 72).

[28] R. W. Godby, M. Schlüter, and L. J. Sham, "Self-energy operators and exchange-correlation potentials in semiconductors", Phys. Rev. B **37**, 10159–10175 (1988) 10.1103/PhysRevB.37.10159 (cit. on pp. 7, 72).

[29] X. Blase, A. Rubio, S. G. Louie, and M. L. Cohen, "Quasiparticle band structure of bulk hexagonal boron nitride and related systems", Phys. Rev. B **51**, 6868–6875 (1995) 10.1103/PhysRevB.51.6868 (cit. on pp. 7, 72).

[30] M. van Schilfgaarde, T. Kotani, and S. V. Faleev, "Adequacy of approximations in *GW* theory", Phys. Rev. B **74**, 245125 (2006) 10.1103/PhysRevB.74.245125 (cit. on pp. 7, 72).

[31] T. Kotani, M. van Schilfgaarde, and S. V. Faleev, "Quasiparticle self-consistent *GW* method: a basis for the independent-particle approximation", Phys. Rev. B **76**, 165106 (2007) 10.1103/PhysRevB.76.165106 (cit. on pp. 7, 72, 120).

[32] L. Reining, "The gw approximation: content, successes and limitations", WIREs Computational Molecular Science **8**, e1344 (2018) https://doi.org/10.1002/wcms.1344 (cit. on pp. 7, 72).

[33] F. Bruneval, N. Dattani, and M. J. van Setten, "The gw miracle in many-body perturbation theory for the ionization potential of molecules", Frontiers in Chemistry **9**, 10.3389/fchem.2021.749779 (2021) 10.3389/fchem.2021.749779 (cit. on pp. 7, 72).

[34] E. E. Salpeter and H. A. Bethe, "A relativistic equation for bound-state problems", Phys. Rev. **84**, 1232–1242 (1951) 10.1103/PhysRev.84.1232 (cit. on pp. 7, 39, 100, 120).

[35] G. Strinati, "Application of the green's functions method to the study of the optical properties of semiconductors", La Rivista del Nuovo Cimento **11**, 1–86 (1988) 10.1007/BF02725962 (cit. on pp. 7, 41, 100, 120).

[36] G. Onida, L. Reining, R. W. Godby, R. Del Sole, and W. Andreoni, "Ab initio calculations of the quasiparticle and absorption spectra of clusters: the sodium tetramer", Phys. Rev. Lett. **75**, 818–821 (1995) 10.1103/PhysRevLett.75.818 (cit. on pp. 7, 100, 120).

[37] E. Salpeter, "Bethe-salpeter equation (origins)", Scholarpedia **3**, 7483– (2008) 10.4249/scholarpedia.7483 (cit. on pp. 7, 39, 100, 120).

[38] L. X. Benedict, E. L. Shirley, and R. B. Bohn, "Optical absorption of insulators and the electron-hole interaction: an ab initio calculation", Phys. Rev. Lett. **80**, 4514–4517 (1998) 10.1103/PhysRevLett.80.4514 (cit. on pp. 7, 100, 120).

[39] S. Albrecht, L. Reining, R. Del Sole, and G. Onida, "*Ab Initio* calculation of excitonic effects in the optical spectra of semiconductors", Phys. Rev. Lett. **80**, 4510–4513 (1998) 10.1103/PhysRevLett.80.4510 (cit. on pp. 7, 100, 120).

[40] W. Hanke and L. J. Sham, "Many-particle effects in the optical excitations of a semiconductor", Phys. Rev. Lett. **43**, 387–390 (1979) 10.1103/PhysRevLett.43.387 (cit. on pp. 7, 100).

[41] F. Bruneval, S. M. Hamed, and J. B. Neaton, "A systematic benchmark of the ab initio Bethe-Salpeter equation approach for low-lying optical excitations of small organic molecules", The Journal of Chemical Physics **142**, 244101 (2015) 10.1063/1.4922489 (cit. on pp. 7, 100).

[42] P. Cudazzo, C. Attaccalite, I. V. Tokatly, and A. Rubio, "Strong charge-transfer excitonic effects and the bose-einstein exciton condensate in graphane", Phys. Rev. Lett. **104**, 226804 (2010) 10.1103/PhysRevLett.104.226804 (cit. on pp. 7, 100).

[43] P. Cudazzo, M. Gatti, A. Rubio, and F. Sottile, "Frenkel versus charge-transfer exciton dispersion in molecular crystals", Phys. Rev. B **88**, 195152 (2013) 10.1103/PhysRevB.88.195152 (cit. on pp. 7, 100).

[44] A. R. Kshirsagar, C. Attaccalite, X. Blase, J. Li, and R. Poloni, "Bethe–salpeter study of the optical absorption of trans and cis azobenzene-functionalized metal–organic frameworks using molecular and periodic models", The Journal of Physical Chemistry C **125**, 7401–7412 (2021) 10.1021/acs.jpcc.1c00367 (cit. on pp. 7, 100).

[45] A. R. Kshirsagar, X. Blase, C. Attaccalite, and R. Poloni, "Strongly bound excitons in metal–organic framework mof-5: a many-body perturbation theory study", The Journal of Physical Chemistry Letters **12**, 4045–4051 (2021) 10.1021/acs.jpclett.1c00543 (cit. on pp. 7, 100).

[46] L. X. Benedict, E. L. Shirley, and R. B. Bohn, "Theory of optical absorption in diamond, si, ge, and gaas", Phys. Rev. B **57**, R9385–R9387 (1998) 10.1103/PhysRevB.57.R9385 (cit. on pp. 7, 100).

[47] M. Rohlfing and S. G. Louie, "Electron-hole excitations in semiconductors and insulators", Phys. Rev. Lett. **81**, 2312–2315 (1998) 10.1103/PhysRevLett.81.2312 (cit. on pp. 7, 100).

[48] M. Rohlfing and S. G. Louie, "Electron-hole excitations and optical spectra from first principles", Phys. Rev. B **62**, 4927–4944 (2000) 10.1103/PhysRevB.62.4927 (cit. on pp. 7, 100).

[49] G. Onida, L. Reining, and A. Rubio, "Electronic excitations: density-functional versus many-body green's-function approaches", Rev. Mod. Phys. **74**, 601–659 (2002) 10.1103/RevModPhys.74.601 (cit. on pp. 7, 26, 100).

[50] X. Blase, I. Duchemin, and D. Jacquemin, "The bethe-salpeter equation in chemistry: relations with td-dft, applications and challenges", Chem. Soc. Rev. **47**, 1022–1043 (2018) 10.1039/C7CS00049A (cit. on pp. 7, 100).

^{51}F. Bruneval, M. Rodriguez-Mayorga, P. Rinke, and M. Dvorak, "Improved one-shot total energies from the linearized gw density matrix", Journal of Chemical Theory and Computation **17**, PMID: 33705127, 2126–2136 (2021) `10.1021/acs.jctc.0c01264` (cit. on pp. 7, 71, 72, 78, 88).

^{52}A. Stan, N. E. Dahlen, and R. van Leeuwen, "Levels of self-consistency in the GW approximation", The Journal of Chemical Physics **130**, 114105 (2009) `10.1063/1.3089567` (cit. on pp. 7, 44, 72).

^{53}F. Caruso, P. Rinke, X. Ren, M. Scheffler, and A. Rubio, "Unified description of ground and excited states of finite systems: the self-consistent *GW* approach", Phys. Rev. B **86**, 081102 (2012) `10.1103/PhysRevB.86.081102` (cit. on pp. 7, 44, 71–73).

^{54}P. Romaniello, S. Guyot, and L. Reining, "The self-energy beyond gw: local and nonlocal vertex corrections", The Journal of Chemical Physics **131**, 154111 (2009) `10.1063/1.3249965` (cit. on pp. 7, 44, 47, 72, 79, 85).

^{55}P. Romaniello, F. Bechstedt, and L. Reining, "Beyond the *GW* approximation: combining correlation channels", Phys. Rev. B **85**, 155131 (2012) `10.1103/PhysRevB.85.155131` (cit. on pp. 7, 47, 49, 57, 65).

^{56}D. J. Carrascal, J. Ferrer, J. C. Smith, and K. Burke, "The hubbard dimer: a density functional case study of a many-body problem", Journal of Physics: Condensed Matter **27**, 393001 (2015) `10.1088/0953-8984/27/39/393001` (cit. on pp. 7, 47).

^{57}F. Aryasetiawan and O. Gunnarsson, "Exchange-correlation kernel in time-dependent density functional theory", Phys. Rev. B **66**, 165119 (2002) `10.1103/PhysRevB.66.165119` (cit. on pp. 7, 47, 80).

^{58}C. J. N. Coveney and D. P. Tew, "A regularized second-order correlation method from green's function theory", Journal of Chemical Theory and Computation **19**, 3915–3928 (2023) `10.1021/acs.jctc.3c00246` (cit. on pp. 7, 47).

^{59}R. Del Sole, L. Reining, and R. W. Godby, "Gwgamma approximation for electron self-energies in semiconductors and insulators", Phys. Rev. B **49**, 8024–8028 (1994) `10.1103/PhysRevB.49.8024` (cit. on pp. 7, 72, 77).

^{60}L. Reining, V. Olevano, A. Rubio, and G. Onida, "Excitonic effects in solids described by time-dependent density-functional theory", Phys. Rev. Lett. **88**, 066404 (2002) `10.1103/PhysRevLett.88.066404` (cit. on pp. 7, 72, 77).

^{61}A. W. Overhauser, "Simplified theory of electron correlations in metals", Phys. Rev. B **3**, 1888–1898 (1971) `10.1103/PhysRevB.3.1888` (cit. on pp. 7, 72).

^{62}C. Petrillo and F. Sacchetti, "Electron-gas self-energy at metallic density", Phys. Rev. B **38**, 3834–3840 (1988) `10.1103/PhysRevB.38.3834` (cit. on pp. 7, 72).

^{63}G. D. Mahan and B. E. Sernelius, "Electron-electron interactions and the bandwidth of metals", Phys. Rev. Lett. **62**, 2718–2720 (1989) `10.1103/PhysRevLett.62.2718` (cit. on pp. 7, 71, 72, 87).

^{64}M. S. Hybertsen and S. G. Louie, "Electron correlation in semiconductors and insulators: band gaps and quasiparticle energies", Phys. Rev. B **34**, 5390–5413 (1986) `10.1103/PhysRevB.34.5390` (cit. on pp. 7, 58, 72).

[65] M. Hindgren and C.-O. Almbladh, "Improved local-field corrections to the g0w approximation in jellium: importance of consistency relations", Phys. Rev. B **56**, 12832–12839 (1997) 10.1103/PhysRevB.56.12832 (cit. on pp. 7, 72).

[66] P. S. Schmidt, C. E. Patrick, and K. S. Thygesen, "Simple vertex correction improves gw band energies of bulk and two-dimensional crystals", Phys. Rev. B **96**, 205206 (2017) 10.1103/PhysRevB.96.205206 (cit. on pp. 7, 72).

[67] L. Hung, F. H. da Jornada, J. Souto-Casares, J. R. Chelikowsky, S. G. Louie, and S. Ö ğüt, "Excitation spectra of aromatic molecules within a real-space GW-bse formalism: role of self-consistency and vertex corrections", Phys. Rev. B **94**, 085125 (2016) 10.1103/PhysRevB.94.085125 (cit. on p. 7).

[68] T. Olsen, C. E. Patrick, J. E. Bates, A. Ruzsinszky, and K. S. Thygesen, "Beyond the rpa and gw methods with adiabatic xc-kernels for accurate ground state and quasiparticle energies", npj Computational Materials **5**, 106 (2019) 10.1038/s41524-019-0242-8 (cit. on pp. 7, 72).

[69] W. Chen and A. Pasquarello, "Accurate band gaps of extended systems via efficient vertex corrections in gw", Phys. Rev. B **92**, 041115 (2015) 10.1103/PhysRevB.92.041115 (cit. on p. 7).

[70] A. Tal, W. Chen, and A. Pasquarello, "Vertex function compliant with the ward identity for quasiparticle self-consistent calculations beyond GW", Phys. Rev. B **103**, L161104 (2021) 10.1103/PhysRevB.103.L161104 (cit. on pp. 7, 72).

[71] P. Minnhagen, "Aspects on diagrammatic expansion for models related to a homogeneous electron gas", J. Phys. C: Solid State Phys. **8**, 1535 (1975) (cit. on pp. 7, 72).

[72] P. A. Bobbert and W. van Haeringen, "Lowest-order vertex-correction contribution to the direct gap of silicon", Phys. Rev. B **49**, 10326–10331 (1994) 10.1103/PhysRevB.49.10326 (cit. on pp. 7, 72).

[73] E. L. Shirley, "Self-consistent gw and higher-order calculations of electron states in metals", Phys. Rev. B **54**, 7758–7764 (1996) 10.1103/PhysRevB.54.7758 (cit. on pp. 7, 72, 120).

[74] A. Grüneis, G. Kresse, Y. Hinuma, and F. Oba, "Ionization potentials of solids: the importance of vertex corrections", Phys. Rev. Lett. **112**, 096401 (2014) 10.1103/PhysRevLett.112.096401 (cit. on pp. 7, 72).

[75] Y. Hinuma, A. Grüneis, G. Kresse, and F. Oba, "Band alignment of semiconductors from density-functional theory and many-body perturbation theory", Phys. Rev. B **90**, 155405 (2014) 10.1103/PhysRevB.90.155405 (cit. on pp. 7, 72, 120).

[76] X. Ren, N. Marom, F. Caruso, M. Scheffler, and P. Rinke, "Beyond the GW approximation: a second-order screened exchange correction", Phys. Rev. B **92**, 081104 (2015) 10.1103/PhysRevB.92.081104 (cit. on pp. 7, 72).

[77] A. L. Kutepov, "Electronic structure of na, k, si, and lif from self-consistent solution of hedin's equations including vertex corrections", Phys. Rev. B **94**, 155101 (2016) 10.1103/PhysRevB.94.155101 (cit. on pp. 7, 72, 120).

[78] A. L. Kutepov, "Self-consistent solution of hedin's equations: semiconductors and insulators", Phys. Rev. B **95**, 195120 (2017) 10.1103/PhysRevB.95.195120 (cit. on pp. 7, 72, 120).

[79] Y. Pavlyukh, A.-M. Uimonen, G. Stefanucci, and R. van Leeuwen, "Vertex corrections for positive-definite spectral functions of simple metals", Phys. Rev. Lett. **117**, 206402 (2016) 10.1103/PhysRevLett.117.206402 (cit. on pp. 7, 72).

[80] E. Maggio and G. Kresse, "Gw vertex corrected calculations for molecular systems", Journal of Chemical Theory and Computation **13**, PMID: 28873298, 4765–4778 (2017) 10.1021/acs.jctc.7b00586 (cit. on pp. 7, 72, 79).

[81] Y. Wang and X. Ren, "Vertex effects in describing the ionization energies of the first-row transition-metal monoxide molecules", The Journal of Chemical Physics **157**, 214115 (2022) 10.1063/5.0122425 (cit. on pp. 7, 72, 120).

[82] D. R. Hartree, "The wave mechanics of an atom with a non-coulomb central field. part i. theory and methods", Mathematical Proceedings of the Cambridge Philosophical Society **24**, 89–110 (1928) 10.1017/S0305004100011919 (cit. on p. 9).

[83] D. R. H. F. R. S, "The calculation of atomic structures", Reports on Progress in Physics **11**, 113 (1947) 10.1088/0034-4885/11/1/305 (cit. on p. 9).

[84] D. R. H. F. R. S, "Näherungsmethode zur lösung des quantenmechanischen mehrkörperproblems", Zeitschrift für Physik **61**, 148 (1930) 10.1007/BF01340294 (cit. on p. 10).

[85] J. C. Slater, "Note on hartree's method", Phys. Rev. **35**, 210–211 (1930) 10.1103/PhysRev.35.210.2 (cit. on p. 10).

[86] K. Capelle, C. A. Ullrich, and G. Vignale, "Degenerate ground states and nonunique potentials: breakdown and restoration of density functionals", Phys. Rev. A **76**, 012508 (2007) 10.1103/PhysRevA.76.012508 (cit. on p. 16).

[87] J. P. Perdew, K. Burke, and M. Ernzerhof, "Generalized gradient approximation made simple", Phys. Rev. Lett. **77**, 3865–3868 (1996) 10.1103/PhysRevLett.77.3865 (cit. on p. 20).

[88] E. K. U. Gross, L. N. Oliveira, and W. Kohn, "Density-functional theory for ensembles of fractionally occupied states. i. basic formalism", Phys. Rev. A **37**, 2809–2820 (1988) 10.1103/PhysRevA.37.2809 (cit. on p. 20).

[89] E. Runge and E. K. U. Gross, "Density-functional theory for time-dependent systems", Phys. Rev. Lett. **52**, 997–1000 (1984) 10.1103/PhysRevLett.52.997 (cit. on pp. 21, 72).

[90] C. Ullrich, *Time-dependent density-functional theory: concepts and applications*, Oxford Graduate Texts (OUP Oxford, 2012) (cit. on pp. 23, 24).

[91] A. Zangwill and P. Soven, "Density-functional approach to local-field effects in finite systems: photoabsorption in the rare gases", Phys. Rev. A **21**, 1561–1572 (1980) 10.1103/PhysRevA.21.1561 (cit. on p. 25).

[92] W. Kohn, "Nobel lecture: electronic structure of matter—wave functions and density functionals", Rev. Mod. Phys. **71**, 1253–1266 (1999) 10.1103/RevModPhys.71.1253 (cit. on p. 27).

[93] L. Reining, "The gw approximation: content, successes and limitations", WIREs Computational Molecular Science **8**, e1344 (2018) `https://doi.org/10.1002/wcms.1344` (cit. on pp. 29, 44).

[94] A. M. V.M. Galitskii, "Application of quantum field theory methods to the many body problem", JETP **7**, 96 (1950) (cit. on pp. 29, 71, 73, 142).

[95] P. C. Martin and J. Schwinger, "Theory of many-particle systems. i", Phys. Rev. **115**, 1342–1373 (1959) `10.1103/PhysRev.115.1342` (cit. on pp. 31, 33).

[96] D. M. Ceperley and B. Bernu, "The calculation of excited state properties with quantum Monte Carlo", The Journal of Chemical Physics **89**, 6316–6328 (1988) `10.1063/1.455398` (cit. on p. 32).

[97] A. Georges, G. Kotliar, W. Krauth, and M. J. Rozenberg, "Dynamical mean-field theory of strongly correlated fermion systems and the limit of infinite dimensions", Rev. Mod. Phys. **68**, 13–125 (1996) `10.1103/RevModPhys.68.13` (cit. on p. 32).

[98] J. Schwinger, "On the green's functions of quantized fields. i", Proceedings of the National Academy of Sciences of the United States of America **37**, 452–455 (1951) (cit. on p. 33).

[99] G. Baym, "Self-consistent approximations in many-body systems", Phys. Rev. **127**, 1391–1401 (1962) `10.1103/PhysRev.127.1391` (cit. on p. 33).

[100] G. Stefanucci and R. van Leeuwen, *Nonequilibrium many-body theory of quantum systems: a modern introduction* (Cambridge University Press, 2013) (cit. on p. 33).

[101] R. van Leeuwen, N. E. Dahlen, and A. Stan, "Total energies from variational functionals of the green function and the renormalized four-point vertex", Phys. Rev. B **74**, 195105 (2006) `10.1103/PhysRevB.74.195105` (cit. on pp. 34, 38, 150).

[102] W. G. Aulbur, L. Jönsson, and J. W. Wilkins, "Quasiparticle calculations in solids", Journal of Physics C: Solid State Physics **54**, 1–218 (2000) (cit. on pp. 44, 58).

[103] F. Aryasetiawan and O. Gunnarsson, "Thegwmethod", Reports on Progress in Physics **61**, 237–312 (1998) `10.1088/0034-4885/61/3/002` (cit. on pp. 44, 58).

[104] F. Kaplan, M. E. Harding, C. Seiler, F. Weigend, F. Evers, and M. J. van Setten, "Quasi-particle self-consistent gw for molecules", Journal of Chemical Theory and Computation **12**, 2528–2541 (2016) `10.1021/acs.jctc.5b01238` (cit. on p. 44).

[105] F. Kaplan, F. Weigend, F. Evers, and M. J. van Setten, "Off-diagonal self-energy terms and partially self-consistency in gw calculations for single molecules: efficient implementation and quantitative effects on ionization potentials", Journal of Chemical Theory and Computation **11**, 5152–5160 (2015) `10.1021/acs.jctc.5b00394` (cit. on p. 44).

[106] F. Bruneval and M. A. L. Marques, "Benchmarking the starting points of the gw approximation for molecules", Journal of Chemical Theory and Computation **9**, 324–329 (2013) `10.1021/ct300835h` (cit. on p. 44).

[107] F. Bruneval, "Optimized virtual orbital subspace for faster GW calculations in localized basis", The Journal of Chemical Physics **145**, 234110 (2016) `10.1063/1.4972003` (cit. on p. 44).

[108]F. Bruneval, T. Rangel, S. M. Hamed, M. Shao, C. Yang, and J. B. Neaton, "Molgw 1: many-body perturbation theory software for atoms, molecules, and clusters", Computer Physics Communications **208**, 149–161 (2016) https://doi.org/10.1016/j.cpc.2016.06.019 (cit. on p. 44).

[109]F. Bruneval, "Ionization energy of atoms obtained from GW self-energy or from random phase approximation total energies", The Journal of Chemical Physics **136**, 194107 (2012) 10.1063/1.4718428 (cit. on p. 44).

[110]F. Caruso, D. R. Rohr, M. Hellgren, X. Ren, P. Rinke, A. Rubio, and M. Scheffler, "Bond breaking and bond formation: how electron correlation is captured in many-body perturbation theory and density-functional theory", Phys. Rev. Lett. **110**, 146403 (2013) 10.1103/PhysRevLett.110.146403 (cit. on p. 44).

[111]M. J. van Setten, F. Weigend, and F. Evers, "The gw-method for quantum chemistry applications: theory and implementation", Journal of Chemical Theory and Computation **9**, 232–246 (2013) 10.1021/ct300648t (cit. on p. 44).

[112]S. V. Faleev, M. van Schilfgaarde, and T. Kotani, "All-electron self-consistent GW approximation: Application to Si, MnO, and NiO", Phys. Rev. Lett. **93**, 126406 (2004) 10.1103/PhysRevLett.93.126406 (cit. on p. 44).

[113]M. van Schilfgaarde, T. Kotani, and S. Faleev, "Quasiparticle self-consistent GW theory", Phys. Rev. Lett. **96**, 226402–226402 (2006) 10.1103/PhysRevLett.96.226402 (cit. on p. 44).

[114]O. Dernek, D. Skachkov, W. R. L. Lambrecht, and M. van Schilfgaarde, "Real-space representation of the quasiparticle self-consistent GW self-energy and its application to defect calculations", Phys. Rev. B **105**, 205136 (2022) 10.1103/PhysRevB.105.205136 (cit. on p. 44).

[115]B. Cunningham, M. Grüning, D. Pashov, and M. van Schilfgaarde, "Qsgw: quasiparticle self-consistent gw with ladder diagrams in w", Phys. Rev. B **108**, 165104 (2023) 10.1103/PhysRevB.108.165104 (cit. on pp. 44, 121).

[116]U. von Barth and B. Holm, "Self-consistent GW_0 results for the electron gas: fixed screened potential W_0 within the random-phase approximation", Phys. Rev. B **54**, 8411–8419 (1996) 10.1103/PhysRevB.54.8411 (cit. on p. 44).

[117]"Self-consistent calculation of total energies of the electron gas using many-body perturbation theory", Phys. Rev. B **63**, 075112 (2001) 10.1103/PhysRevB.63.075112 (cit. on pp. 44, 71).

[118]M. Shishkin and G. Kresse, "Self-consistent GW calculations for semiconductors and insulators", Phys. Rev. B **75**, 235102 (2007) 10.1103/PhysRevB.75.235102 (cit. on p. 44).

[119]N. Marom, F. Caruso, X. Ren, O. T. Hofmann, T. Körzdörfer, J. R. Chelikowsky, A. Rubio, M. Scheffler, and P. Rinke, "Benchmark of GW methods for azabenzenes", Phys. Rev. B **86**, 245127 (2012) 10.1103/PhysRevB.86.245127 (cit. on p. 44).

[120]J. Wetherell, M. J. P. Hodgson, and R. W. Godby, "Gw self-screening error and its correction using a local density functional", Physical Review B **97**, 10.1103/physrevb.97.121102 (2018) 10.1103/physrevb.97.121102 (cit. on p. 44).

[121] J.Hubbard, "Electron correlations in narrow energy bands", Proc. R. Soc. Lond. A **276**, 238 (1963) https://doi.org/10.1098/rspa.1963.0204 (cit. on p. 47).

[122] J.Hubbard, "Electron correlations in narrow energy bands", Proc. R. Soc. Lond. A **277**, 237 (1964) https://doi/10.1098/rspa.1964.0019 (cit. on p. 47).

[123] A. Schindlmayr, "Violation of particle number conservation in the GW approximation", Phys. Rev. B **56**, 3528–3531 (1997) 10.1103/PhysRevB.56.3528 (cit. on pp. 57, 78).

[124] G. Strinati, H. J. Mattausch, and W. Hanke, "Dynamical correlation effects on the quasiparticle bloch states of a covalent crystal", Phys. Rev. Lett. **45**, 290–294 (1980) 10.1103/PhysRevLett. 45.290 (cit. on p. 58).

[125] G. Strinati, H. J. Mattausch, and W. Hanke, "Dynamical aspects of correlation corrections in a covalent crystal", Phys. Rev. B **25**, 2867–2888 (1982) 10.1103/PhysRevB.25.2867 (cit. on p. 58).

[126] C. Rödl, F. Fuchs, J. Furthmüller, and F. Bechstedt, "Quasiparticle band structures of the antiferromagnetic transition-metal oxides mno, feo, coo, and nio", Phys. Rev. B **79**, 235114 (2009) 10.1103/PhysRevB.79.235114 (cit. on p. 58).

[127] T. L. Gilbert, "Hohenberg-kohn theorem for nonlocal external potentials", Phys. Rev. B **12**, 2111–2120 (1975) 10.1103/PhysRevB.12.2111 (cit. on p. 71).

[128] R. A. Donnelly and R. G. Parr, "Elementary properties of an energy functional of the first-order reduced density matrix", The Journal of Chemical Physics **69**, 4431–4439 (2008) 10.1063/1.436433 (cit. on p. 71).

[129] M. Levy, "Universal variational functionals of electron densities, first-order density matrices, and natural spin-orbitals and solution of the ¡i¿v¡/i¿-representability problem", Proceedings of the National Academy of Sciences **76**, 6062–6065 (1979) 10.1073/pnas.76.12.6062 (cit. on p. 71).

[130] J. M. Luttinger and J. C. Ward, "Ground-state energy of a many-fermion system. II", Phys. Rev. **118**, 1417–1427 (1960) 10.1103/PhysRev.118.1417 (cit. on p. 71).

[131] A. Klein, "Perturbation theory for an infinite medium of fermions. II", Phys. Rev. **121**, 950–956 (1961) (cit. on p. 71).

[132] B. Holm, "Total energies from gw calculations", Phys. Rev. Lett. **83**, 788–791 (1999) 10.1103/PhysRevLett.83.788 (cit. on p. 71).

[133] P. Garcı´a-González and R. W. Godby, "Many-body GW calculations of ground-state properties: quasi-2d electron systems and van der waals forces", Phys. Rev. Lett. **88**, 056406 (2002) 10.1103/PhysRevLett.88.056406 (cit. on p. 72).

[134] F. Aryasetiawan, L. Hedin, and K. Karlsson, "Multiple plasmon satellites in na and al spectral functions from ab initio cumulant expansion", Phys. Rev. Lett. **77**, 2268–2271 (1996) 10.1103/PhysRevLett.77.2268 (cit. on p. 72).

[135] M. Guzzo, G. Lani, F. Sottile, P. Romaniello, M. Gatti, J. J. Kas, J. J. Rehr, M. G. Silly, F. Sirotti, and L. Reining, "Valence electron photoemission spectrum of semiconductors: ab initio description of multiple satellites", Phys. Rev. Lett. **107**, 166401 (2011) `10.1103/PhysRevLett.107.166401` (cit. on p. 72).

[136] D. Langreth and J. Perdew, "The exchange-correlation energy of a metallic surface", Solid State Communications **17**, 1425–1429 (1975) `https://doi.org/10.1016/0038-1098(75)90618-3` (cit. on pp. 72, 78).

[137] D. C. Langreth and J. P. Perdew, "Exchange-correlation energy of a metallic surface: wave-vector analysis", Phys. Rev. B **15**, 2884–2901 (1977) `10.1103/PhysRevB.15.2884` (cit. on pp. 72, 78).

[138] E. K. U. Gross and W. Kohn, "Local density-functional theory of frequency-dependent linear response", Phys. Rev. Lett. **55**, 2850–2852 (1985) `10.1103/PhysRevLett.55.2850` (cit. on pp. 72, 76).

[139] I. V. Tokatly and O. Pankratov, "Many-body diagrammatic expansion in a kohn-sham basis: implications for time-dependent density functional theory of excited states", Phys. Rev. Lett. **86**, 2078–2081 (2001) `10.1103/PhysRevLett.86.2078` (cit. on pp. 72, 77).

[140] F. Bruneval, F. Sottile, V. Olevano, R. Del Sole, and L. Reining, "Many-body perturbation theory using the density-functional concept: beyond the GW approximation", Phys. Rev. Lett. **94**, 186402 (2005) `10.1103/PhysRevLett.94.186402` (cit. on pp. 72, 77).

[141] M. Gatti, V. Olevano, L. Reining, and I. V. Tokatly, "Transforming nonlocality into a frequency dependence: a shortcut to spectroscopy", Phys. Rev. Lett. **99**, 057401 (2007) `10.1103/PhysRevLett.99.057401` (cit. on pp. 72, 77).

[142] S. Botti, A. Schindlmayr, R. D. Sole, and L. Reining, "Time-dependent density-functional theory for extended systems", Reports on Progress in Physics **70**, 357 (2007) `10.1088/0034-4885/70/3/R02` (cit. on pp. 72, 77).

[143] S. P. Singhal and J. Callaway, "Exchange correction to the dielectric function in the local exchange approximation", Phys. Rev. B **14**, 2347–2351 (1976) `10.1103/PhysRevB.14.2347` (cit. on p. 72).

[144] M. S. Hybertsen and S. G. Louie, "Ab initio static dielectric matrices from the density-functional approach. i. formulation and application to semiconductors and insulators", Phys. Rev. B **35**, 5585–5601 (1987) `10.1103/PhysRevB.35.5585` (cit. on p. 72).

[145] A. El-Sahili, F. Sottile, and L. Reining, *Total energy beyond gw : exact results and guidelines for approximations*, 2023 (cit. on pp. 73, 136).

[146] A. El-Sahili, F. Sottile, and L. Reining, "Total energy beyond gw: exact results and guidelines for approximations", Journal of Chemical Theory and Computation **0**, PMID: 38324673, null (0) `10.1021/acs.jctc.3c01200` (cit. on pp. 73, 136).

[147] M. Hellgren and L. Baguet, "Strengths and limitations of the adiabatic exact-exchange kernel for total energy calculations", The Journal of Chemical Physics **158**, 184107 (2023) `10.1063/5.0146423` (cit. on p. 74).

[148] F. Sottile, V. Olevano, and L. Reining, **91**, 056402 (2003) (cit. on p. 77).

[149] S. Sharma, J. K. Dewhurst, A. Sanna, and E. K. U. Gross, "Bootstrap approximation for the exchange-correlation kernel of time-dependent density-functional theory", English, **107**, 10.1103/PhysRevLett.107.186401 (2011) 10.1103/PhysRevLett.107.186401 (cit. on p. 77).

[150] G. Adragna, R. Del Sole, and A. Marini, **68**, 165108 (2003) (cit. on p. 77).

[151] A. Marini, R. Del Sole, and A. Rubio, **91**, 256402 (2003) (cit. on p. 77).

[152] S. Rigamonti, S. Botti, V. Veniard, C. Draxl, L. Reining, and F. Sottile, "Estimating excitonic effects in the absorption spectra of solids: problems and insight from a guided iteration scheme", Phys. Rev. Lett. **114**, 146402 (2015) 10.1103/PhysRevLett.114.146402 (cit. on p. 77).

[153] M. Levy and J. P. Perdew, "Hellmann-feynman, virial, and scaling requisites for the exact universal density functionals. shape of the correlation potential and diamagnetic susceptibility for atoms", Phys. Rev. A **32**, 2010–2021 (1985) 10.1103/PhysRevA.32.2010 (cit. on p. 77).

[154] K. Jiang, M. A. Mosquera, Y. Oueis, and A. Wasserman, "Virial relations in density embedding", International Journal of Quantum Chemistry **120**, e26204 (2020) https://doi.org/10.1002/qua.26204 (cit. on p. 77).

[155] M.-C. Kim, E. Sim, and K. Burke, "Understanding and reducing errors in density functional calculations", Phys. Rev. Lett. **111**, 073003 (2013) 10.1103/PhysRevLett.111.073003 (cit. on p. 77).

[156] S. Di Sabatino, "Reduced density-matrix functional theory: correlation and spectroscopy", PhD thesis (Université Paul Sabatier, Toulouse (France), Nov. 2015) (cit. on p. 78).

[157] X. Ren, P. Rinke, C. Joas, and M. Scheffler, "Random-phase approximation and its applications in computational chemistry and materials science", Journal of Materials Science **47**, 7447 (2012) 10.1007/s10853-012-6570-4 (cit. on p. 78).

[158] A. Savin, F. Colonna, and M. Allavena, "Analysis of the linear response function along the adiabatic connection from the Kohn–Sham to the correlated system", The Journal of Chemical Physics **115**, 6827–6833 (2001) 10.1063/1.1405011 (cit. on p. 79).

[159] C. D. Spataru, L. X. Benedict, and S. G. Louie, "Ab initio calculation of band-gap renormalization in highly excited gaas", Phys. Rev. B **69**, 205204 (2004) 10.1103/PhysRevB.69.205204 (cit. on pp. 80, 96, 145).

[160] A. Honet, L. Henrard, and V. Meunier, "Exact and many-body perturbation solutions of the Hubbard model applied to linear chains", AIP Advances **12**, 035238 (2022) 10.1063/5.0082681 (cit. on pp. 80, 96, 145).

[161] B. Holm and U. von Barth, "Fully self-consistent gw self-energy of the electron gas", Phys. Rev. B **57**, 2108–2117 (1998) 10.1103/PhysRevB.57.2108 (cit. on p. 81).

[162] J. Heyd, G. E. Scuseria, and M. Ernzerhof, "Hybrid functionals based on a screened coulomb potential", The Journal of Chemical Physics **118**, 8207–8215 (2003) 10.1063/1.1564060 (cit. on p. 81).

[163] F. Aryasetiawan, R. Sakuma, and K. Karlsson, "Gw approximation with self-screening correction", Phys. Rev. B **85**, 035106 (2012) `10.1103/PhysRevB.85.035106` (cit. on p. 84).

[164] L. Hedin, B. Lundqvist, and S. Lundqvist, "New structure in the single-particle spectrum of an electron gas", Solid State Communications **5**, 237–239 (1967) `10.1016/0038-1098(67)90264-5` (cit. on p. 84).

[165] Bergerse.B, F. W. Kus, and C. Blomberg, "Single-particle Greens function in electron-plasmon approximation", Canadian J. Phys. **51**, 102–110 (1973) (cit. on p. 84).

[166] M. Guzzo, J. J. Kas, L. Sponza, C. Giorgetti, F. Sottile, D. Pierucci, M. G. Silly, F. Sirotti, J. J. Rehr, and L. Reining, "Multiple satellites in materials with complex plasmon spectra: from graphite to graphene", Phys. Rev. B **89**, 085425 (2014) `10.1103/PhysRevB.89.085425` (cit. on p. 84).

[167] W. Nelson, P. Bokes, P. Rinke, and R. W. Godby, "Self-interaction in green's-function theory of the hydrogen atom", Phys. Rev. A **75**, 032505 (2007) `10.1103/PhysRevA.75.032505` (cit. on p. 85).

[168] J. J. Fernandez, "Gw calculations in an exactly solvable model system at different dilution regimes: the problem of the self-interaction in the correlation part", Phys. Rev. A **79**, 052513 (2009) `10.1103/PhysRevA.79.052513` (cit. on p. 85).

[169] S. Botti, A. Fourreau, F. ç. Nguyen, Y.-O. Renault, F. Sottile, and L. Reining, "Energy dependence of the exchange-correlation kernel of time-dependent density functional theory: a simple model for solids", Phys. Rev. B **72**, 125203 (2005) `10.1103/PhysRevB.72.125203` (cit. on p. 86).

[170] P. Minnhagen, "Vertex correction calculations for an electron gas", Journal of Physics C: Solid State Physics **7**, 3013 (1974) `10.1088/0022-3719/7/17/011` (cit. on p. 87).

[171] A. M. Lewis and T. C. Berkelbach, "Vertex corrections to the polarizability do not improve the gw approximation for the ionization potential of molecules", Journal of Chemical Theory and Computation **15**, 2925–2932 (2019) `10.1021/acs.jctc.8b00995` (cit. on p. 88).

[172] G. Baym and L. P. Kadanoff, "Conservation laws and correlation functions", Phys. Rev. **124**, 287–299 (1961) `10.1103/PhysRev.124.287` (cit. on p. 89).

[173] J. P. Perdew and M. R. Norman, "Electron removal energies in kohn-sham density-functional theory", Phys. Rev. B **26**, 5445–5450 (1982) `10.1103/PhysRevB.26.5445` (cit. on p. 91).

[174] J. Bezanson, A. Edelman, S. Karpinski, and V. B. Shah, "Julia: a fresh approach to numerical computing", SIAM Review **59**, 65–98 (2017) `10.1137/141000671` (cit. on p. 96).

[175] D. P. Laurie, "Calculation of gauss-kronrod quadrature rules", Mathematics of Computation **66**, 1133–1145 (1997) (cit. on p. 96).

[176] S. Christ, D. Schwabeneder, C. Rackauckas, M. K. Borregaard, and T. Breloff, "Plots.jl – a user extendable plotting api for the julia programming language", **11**, 5 (2023) `https://doi.org/10.5334/jors.431` (cit. on p. 96).

[177] W. Tarantino, B. S. Mendoza, P. Romaniello, J. A. Berger, and L. Reining, "Many-body perturbation theory and non-perturbative approaches: screened interaction as the key ingredient", Journal of Physics: Condensed Matter **30**, 135602 (2018) 10.1088/1361-648X/aaaeab (cit. on pp. 116, 119, 131).

[178] Y. Wang, P. Rinke, and X. Ren, 2021 (cit. on pp. 120, 121).

[179] M. Wen, V. Abraham, G. Harsha, A. Shee, B. Whaley, and D. Zgid, 2023 (cit. on p. 121).

[180] C. Mejuto-Zaera and V. ě. Vl ček, Phys. Rev. B **106**, 165129 (2022) 10.1103/PhysRevB.106.165129 (cit. on p. 121).

[181] Y. Pavlyukh, G. Stefanucci, and R. van Leeuwen, "Dynamically screened vertex correction to gw", Phys. Rev. B **102**, 045121 (2020) 10.1103/PhysRevB.102.045121 (cit. on p. 129).

Titre : Des spectres à l'énergie totale: au-delà de l'approximation GW pour concevoir des interactions effectives.

Mots clés : Énergie totale, théorie de perturbation à plusieurs corps, fonction de Green.

Résumé : L'énergie totale et les spectres d'ajout et de retrait d'électrons peuvent en principe être calculés exactement à partir de la fonction de Green à un corps (GF). En pratique, la GF est le plus souvent obtenue à partir d'une self-énergie approximée. Pour la structure de bandes des solides et pour les niveaux d'énergie des molécules, l'approximation GW est devenue l'approche la plus courante. Cette approximation est une expression au premier ordre de la self-énergie en termes de l'interaction de Coulomb écrantée. Cependant, le choix du meilleur cadre pour accéder à l'énergie totale de l'état fondamental demeure flou. En effet, la plupart des calculs d'énergie totale sont aujourd'hui effectués à l'aide de la théorie de la fonctionnelle de la densité (DFT), et non en utilisant des fonctions de Green. Ceci est dû au fait que les calculs GF ont généralement un coût de calcul plus élevé que les calculs DFT, mais aussi au fait qu'il n'y a pas aujourd'hui d'approximation bien établie pour l'énergie totale de l'état fondamental dans le cadre des fonctions de Green. Néanmoins, il y a de bonnes raisons d'étudier comment utiliser les fonctions de Green pour calculer l'énergie totale. Premièrement, des expressions exactes pour l'énergie totale en tant que fonctionnelle de la fonction de Green et/ou de la self-énergie sont connues en principe. Deuxièmement, le cadre des fonctions de Green suggère des approximations efficaces et systématiques. L'approximation GW, bien qu'adaptée aux spectres, n'est en pratique pas satisfaisante pour l'énergie totale, pour laquelle une grande précision est généralement requise. En outre, la validité de l'approximation GW est limitée aux systèmes faiblement ou modérément corrélés. Dans cette thèse, nous entreprenons une exploration pour surmonter les limitations de l'approximation GW. Nous procédons d'abord à une étude approfondie pour comprendre ses échecs et ses contraintes. Ensuite, nous présentons des développements théoriques généraux et suggérons de nouvelles approximations basées sur l'utilisation d'interactions effectives afin d'améliorer les calculs d'énergie totale fondés sur les fonctions de Green. Les développements théoriques et la qualité des approximations sont illustrés par des applications à un modèle exactement soluble, le dimère de Hubbard. Les résultats confirment nos conjectures et motivent les applications futures à des matériaux réels.

Title : From spectra to total energy: beyond the GW approximation designing effective interactions.

Keywords : Total energy, many-body perturbation theory, Green's function.

Abstract : The total energy and electron addition and removal spectra can in principle be calculated exactly from the one-body Green's function (GF). In practice, the GF is most often obtained from an approximate self-energy. For the band structure of solids and energy levels of molecules, the GW approximation has become the state-of-the-art approach. This approximation is a first-order expression of the self-energy in terms of the screened Coulomb interaction. By the way of contrast, it is not clear what is the best framework to access the ground state total energy. Indeed, most total energy calculations are today performed using density-functional theory (DFT), not Green's functions. This is due both to the fact that GF calculations have usually a higher computational cost than DFT calculations, and to the fact that there is today no well established approximation for the total energy in the GF framework. Still, there are good reasons to investigate ways to use Green's functions to calculate the total energy. First, exact expressions for the total energy as functional of GF and/or the self-energy are known in principle. Second, the GF framework suggests powerful and systematic approximations. However, the GW approximation, while suitable for spectra, is in practice not satisfactory for the total energy, where usually a high precision is required. Moreover, the validity of the GW approximation is limited to weakly to moderately correlated systems. In this thesis, we embark on a journey to overcome the limitations of GW. We first make a comprehensive exploration to understand the failures and constraints of GW. Subsequently, we present general theoretical developments and suggest new approximations based on the use of effective interactions in order to improve total energy calculations based on Green's functions. The theoretical developments and the quality of the approximations are illustrated through applications to an exactly solvable model, the Hubbard dimer. The results confirm our conjectures and motivate future applications to real materials.